2005 Annual Progress Report

HIGH STRENGTH WEIGHT REDUCTION MATERIALS

Less dependence on foreign oil, and eventual transition to an emissions-free, petroleum-free vehicle

FreedomCAR and Vehicle Technologies Program

U.S. Department of Energy
Energy Efficiency and Renewable Energy
Bringing you a prosperous future where energy is clean, abundant, reliable, and affordable

FreedomCAR & Fuel Partnership

21st CENTURY TRUCK PARTNERSHIP

Acknowledgement

We would like to express our sincere appreciation to QSS Group, Inc., Oak Ridge National Laboratory, and Argonne National Laboratory for their technical and artistic contributions in preparing and publishing this report.

In addition, we would like to thank all the participants for their contributions to the programs and all the authors who prepared the project abstracts that comprise this report.

U.S. Department of Energy
Office of FreedomCAR and Vehicle Technologies
1000 Independence Avenue S.W.
Washington, DC 20585-0121

FY 2005

Progress Report for High Strength Weight Reduction Materials

Energy Efficiency and Renewable Energy
Office of FreedomCAR and Vehicle Technologies
Advanced Materials Technologies

Edward Wall	**Program Manager, OFCVT**
Rogelio Sullivan	**Advanced Materials Technologies Team Leader**
James Eberhardt	**Chief Scientist**

August 2006

CONTENTS

CONTENTS (CONT.)

1. INTRODUCTION

The energy consumption of on-road heavy trucks has been increasing due to the growth in demand for freight delivery as the U.S. economy continues to expand. The recent rapid rise in fuel prices has raised fuel costs to be the number one concern of the trucking industry. Owners and operators of trucks and truck fleets have been operating on “razor thin” margins and increasing the fuel economy of their vehicles is one way of reducing their fuel costs to remain viable as a business. One way of achieving heavy vehicle fuel economy improvements without sacrificing revenue earnings limited by maximum allowable vehicle weight or volume is through the use of high strength weight reduction materials for either or both the tractor and trailer. Vehicle weight reduction results in reduced parasitic energy losses and improved overall vehicle fuel efficiency by enabling more ton-miles per gallon of fuel consumed. In addition, it is recognized that improved materials may enable the implementation of other technologies that can further improve the fuel efficiency of heavy vehicles.

The High-Strength Weight Reduction (HSWR) Materials Technology activity of the U.S. Department of Energy’s (DOE’s) Office of FreedomCAR and Vehicle Technologies (OFCVT) Program seeks to reduce the weight of heavy vehicles without reducing vehicle functionality, durability, reliability, or safety and to do so cost-effectively. Work has been focused on developing advanced materials and materials processing technologies that can be applied to a wide array of heavy vehicle body, chassis, and suspension components to achieve weight reduction. Research is focused on overcoming barriers to the widespread introduction of lightweight materials in the heavy vehicle industry. Major barriers include: cost; design and simulation technologies; manufacturability; prototyping and tooling; joining and assembly; and maintenance, repair, durability, and recycling. Priority materials include advanced high-strength steels, aluminum, magnesium, titanium, and composites such as metal matrix materials and glass- and carbon-fiber-reinforced thermosets and thermoplastics. The research required to develop these technologies is too high-risk to be pursued independently by the heavy vehicle industry because of substantial return-on-investment uncertainties. In addition, the relatively low volume of truck components makes it difficult for any individual truck manufacturer to develop on its own a new production/fabrication process utilizing new kinds of materials such as composites.

Research and development (R&D) activities were conducted through a variety of contractual Mechanisms. These include cooperative research and development agreements (CRADAs), university grants, R&D subcontracts, and directed research. Research partners include heavy vehicle manufacturers (including member companies of the government/industry 21st Century Truck Partnership), first-tier component manufacturers and materials suppliers, national laboratories, and other non-profit technology organizations. Laboratories include Argonne National Laboratory (ANL), Idaho National Engineering and Environmental Laboratory (INEEL), Los Alamos National Laboratory (LANL), Oak Ridge National Laboratory (ORNL), and Pacific Northwest National Laboratory (PNNL).

Among the several goals established for this development area, one is to enable at least a 22 percent reduction in the weight of an unloaded tractor-trailer combination and about a 10-33 percent reduction in the weight of other classes of heavy vehicles, depending on performance requirements and duty cycles. With the completion and issuance of this final High Strength Weight Reduction Materials report, most of these goals have been accomplished. Technology research and development results have been made available to industry for further development and commercialization. Some of these results are discussed in this final annual report.

2. MATERIALS DEVELOPMENT

A. Advanced Materials for Friction Brakes

Principal Investigator: P. J. Blau
Oak Ridge National Laboratory
P.O. Box 2008, Oak Ridge, TN 37831-6063
(865) 574-5377; fax: (865) 574-6918; e-mail:blaupj@ornl.gov

Chief Scientist: James J. Eberhardt
(202)586-9837; fax: (202)587-2476; e-mail: james.eberhardt@ee.doe.gov
Field Technical Manager: Philip S. Sklad
(865) 574-5069; fax: (865) 576-4963; e-mail: skladps@ornl.gov

---

Contractor: Oak Ridge National Laboratory
Contract No.: DE-AC05-00OR22725

Objectives

- Identify candidate materials for the next generation of high-performance, light-weight truck brakes; investigate their friction and wear characteristics; and provide data to support their introduction into the trucking industry.

Approach

- Design and build a subscale brake material testing apparatus to investigate the friction and frictional heating characteristics of advanced materials at speeds and contact pressures similar to those in full-sized brakes.
- Evaluate and understand the friction and thermal characteristics of candidate materials including titanium alloys, metal matrix composites, and ceramic matrix composites. Down-select the more promising materials, select appropriate linings to go with them, and focus on obtaining data to support their implementation on vehicles.
- Develop metrics for analyzing the dissipation of frictional energy in various braking material combinations, and apply that knowledge to the selection of brake material pairs.

Accomplishments

- Working the Dynamet Inc, obtained and evaluated the friction and frictional-heating characteristics of three experimental Ti-based, high-strength composites.
- Published a summary compilation of friction and thermo-physical properties data for all materials tested to-date.
- Working with Red Devil Brakes Company, obtained a set of full-sized, ceramic-coated titanium alloy truck brake rotors for dynamometer testing during FY 2006.

Future Direction

- Work with a leading truck brake system manufacturer to plan a testing program for ceramic-coated titanium brake rotors that were obtained during FY 2005.
- Continue to investigate novel methods to surface-engineer titanium-based rotor materials.
- Investigate carbon-based composite materials for possible use as rotors and/or pads.
- Identify lining materials that are frictionally compatible with advanced disc materials and develop a more fundamentals-based rationale for rotor/pad selection.

Introduction

Advanced aerodynamic designs and tires with lower rolling-resistance can improve the fuel efficiency of trucks. However, as these developments decrease the drag forces on trucks, the demands on braking systems increase. Brake engineering involves design, instrumentation and controls, and materials development. This project specifically addresses the latter. Brake materials must exhibit a balance of properties including frictional stability over a wide temperature range, appropriate thermal properties, dimensional stability, corrosion resistance to road deicers, and wear resistance. They must also be cost-competitive. Using non-traditional brake materials it may be possible to create lighter-weight braking systems that will enable improved fuel-efficiency without compromising vehicle safety and reliability.

This project concerns the selection and use of advanced structural materials and surface treatments that show potential as truck brake friction materials. Testing such new materials is made more cost-effective by using small specimens to screen the most promising candidates. To this end, a subscale brake tester (SSBT) was designed and built. It was instrumented to measure normal force, friction force, surface temperature and vibrations during braking. An attachable water spray system has enabled the effects of wet and dry braking to be studied. Analysis of SSBT results is supplemented by optical microscopy, scanning electron microscopy, and transmission electron microscopy of friction-induced surface films.

Prompted by stricter Department of Trans-portation regulations on stopping distances for trucks, air-disc brakes are beginning to replace drum brakes on new Class 8 trucks sold in the United States. Air disc brakes can achieve shorter stopping distances and are less likely to fade from overheating. With this trend in mind, the focus in this project has been on rotor materials for disc-brakes and the appropriate friction linings to mate with them.

Titanium-Based Candidate Rotor Materials

After evaluating the physical properties of candidate materials those with low-softening-points, brittle behavior, corrosion sensitivity, and environmentally unacceptable wear by-products were eliminated from consideration. A list of materials and the rationale for their selection were presented in the FY 2003 and FY 2004 Annual Reports.

During FY 2005, it was decided to focus on titanium (Ti)-based rotor materials, in metal matrix composites and as the structural material over which thermally-sprayed ceramic coatings were applied. Ti offers approximately 38% in weight savings compared to a comparably-sized cast iron rotor.

Titanium-based metal matrix composites (Ti-MMC) were selected and purchased from Dynamet, Inc. The Massachusetts firm has developed a proprietary cold and hot isostatic pressing (CHIP) process to manufacture Ti-based composites that can be produced with a variety of hard particles.

The surface-coated Ti samples were prepared by Red Devil Brakes Company, a Pennsylvania firm that developed a ceramic-based thermal spray process for coating Ti alloy brake rotors for high-performance racing applications. Coatings were typically about 1-2 mm thick.

Table 1 lists the Ti-alloy material combinations that were investigated. As in the past, pad materials were selected based on factors like the performance of similar linings against cast iron, recommendations from suppliers, and materials

Table 1. Ti-Based Friction Material Combinations.

Disc Specimen Material	Mating Material(s)
Titanium alloys (Ti-6Al-4V, and Ti-6Al-2Sn-4Zr-2Mo)	Jurid 539 disc brake lining
Ti-MMC with 10% TiC particles (CermeTi™ C-10) (Two thicknesses to evaluate thermal behavior)	Jurid 539 disc brake lining Performance FrictionCarbon-Metallic Pad (type 10)
Ti-MMC with 5% TiB2, balance: Ti-6Al-4V	Jurid 539 disc brake lining
Ti-MMC with 7.5% W, 7.5% TiC, balance: Ti-6Al-4V	Jurid 539 disc brake lining
Thermally-sprayed Titanium – Red Devil Brakes Co.	Metallic and semi-metallic pads materials supplied by Red Devil Brakes

whose thermo-physical properties made them likely partners. The pad materials may not necessarily be the optimum partners for the new rotor materials but they served as a means to compare friction characteristics in the SSBT relative to cast iron. For example, Jurid 539 is a semi-metallic disc brake lining material that is well known in the industry.

Experiments were conducted to characterize the effects of speed and contact pressure on the friction coefficient and frictional temperature rise for these Ti-MMC disc materials. Their thermo-physical properties were also measured at Oak Ridge National Laboratory (ORNL--H. Wang). Results are summarized in the following sections.

Studies of Titanium-Based Disc Materials

Table 2 lists the measured densities and thermophysical properties of the friction tested, candidate rotor materials. Symbols: kth is the thermal conductivity, □th is the thermal diffusivity, and Cp is the heat capacity.

Table 2. Property Data for Experimental Ti Materials Relative to that for Typical Gray Cast Iron.

Disc Material	Density (g/cm^3)	K_{th} (W/m-K)	□$_{th}$ (cm^2/s)	C_P (MJ/m^3-K)
Cast iron	7.2	42.-62.	-	-
Ti-6Al-4V	4.40	6.6	-	-
Ti -5TiB2	4.34	7.99	0.044	1.82
Ti-(7.5W, 7.5TiC)	4.68	6.57	0.028	2.36
Ti–10 TiC	4.37	6.89	0.029	2.41

Friction data were obtained on the materials listed in Table 1 under a variety of applied pressures and sliding velocities. A several step process is used to distill the 28,800 data values from each sliding test into a form that will reveal general trends in friction and temperature rise. For example, Figure 1 illustrates the effects of sliding speed on the friction of the Ti-based 5%TiB2 MMC slid against Jurid 539 pad material. Friction coefficients for typical brake linings against gray cast iron tend to fall within the range of 0.35 to 0.55, so the Ti-MMC data fall on the low end of conventional values. However, as pointed out earlier, use of an alternative lining material could likely improve this performance.

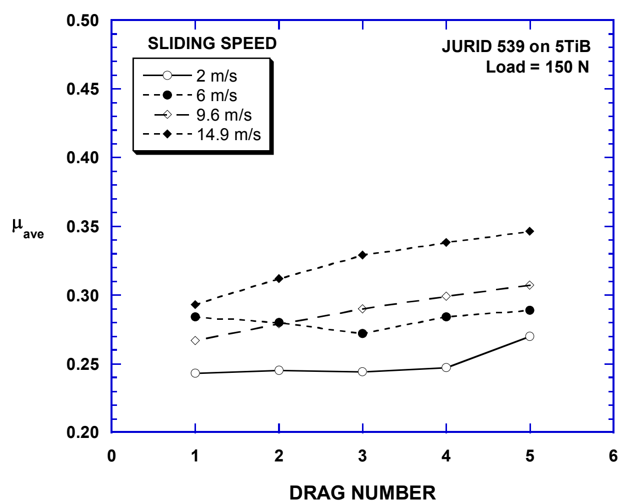

Figure 1. Effect of sliding speed on the friction of a TiB2 reinforced Ti-MMC (150N applied force).

Conversion of Friction into Heat

One convenient measure of the efficiency by which the frictional energy generated during braking is converted into heat is what is here called the 'thermal conversion parameter' (Qf) and is defined as follows:

$$Q_f = c\ (\Delta T / F x)$$

where ΔT is the temperature rise of the disc specimen surface during a constant speed drag, F is the average friction force, and x is the distance slid during the drag. The constant c is a function of the testing geometry and recognizes the fact that only the heating of the disc is considered, not the heating of the pad as well. Q_f can be thought of as the efficiency of a given rotor material in coverting frictional work (the product F x) into an observed surface temperature rise (ΔT). The higher Q_f, the more readily frictional work of braking translates into the heating of the disc surface.

Table 3 lists experimentally-measured values for several material combinations involving the Jurid 539 pad material and Ti-based materials. Cast iron, with its relatively high thermal conductivity, dissipates heat and has a lower Q_f, but the Ti-MMCs tend to run somewhat hotter. Adding thermally-conductive ceramic particles like TiB_2 tends to moderate that effect. Consequently, Ti-MMCs do not run quite as hot as the matrix alloy Ti-6Al-4V. Note that some of the previously tested ceramic composites, especially those with anisotropic microstructures, had Q_f values approaching 21. x 10^{-3} °C/N-m. Higher frictional heating behavior is acceptable as long as the high temperature strength and resistance to thermal distortion are adequate, but it also suggests that the use of materials like Ti will require more attention to designing rotors with cooling vents and heat control passages.

Future Plans

Plans to scale up and test thermal spray-coated Ti alloy discs are underway, and the results will be reported during FY 2006.

Table 3. Thermal Conversion Parameter (Q_f) for Various Discs against Jurid 539 (300 N test load).

Disc Material	Q_f (°C/N-m)
Gray Cast Iron	1.18 x 10^{-3}
Ti-6Al-4V* alloy disc	7.30 x 10^{-3}
CermeTi C10*	6.33 x 10^{-3}
Ti-MMC with 5TiB2	3.12 x 10^{-3}
Ti-MMC with (7.5W, 7.5TiC)	3.12 x 10^{-3}
Ti–MMC 10 TiC**	3.75 x 10^{-3}
Red Devil spray-coated Ti*	9 - 10 x 10^{-3}

*Results from FY 2004 studies.
**Similar to C10 but tested with a thinner disc backed by aluminum alloy 3003.

Two new candidate materials, not previously available for friction brake studies, will be evaluated in FY 2006. Both are under development at ORNL. One is an infrared-processed Ti-MMC and the other is a high thermal conductivity, carbon-based composite that is being developed by a novel low-cost processing route.

Publications

P. J. Blau (2000) "Energy Efficiency in Heavy Vehicle Tires, Drivetrains, and Braking Systems – A Multi-year Program Plan," ORNL Technical Report, ORNL/TM-2000/177, 10 pp.

P. J. Blau (2001) "Compositions, Functions, and Testing of Friction Brake Materials and Their Additives," Technical Report, ORNL/TM-2001/64, 29 pp.

P. J. Blau (2003) "Microstructure and Detachment Mechanism of Friction Layers on the Surface of Brake Shoes," *J. of Materials Engr. and Performance*, Vol. 12(1), pp 56-60.

P. J. Blau and J. C. McLaughlin (2003) "Effects of Water Films and Sliding Speed on the Frictional Behavior of Truck Disc Brake Materials," *Tribology International*, Vol. 36 (10), pp. 709-715.

P. J. Blau and H. M. Meyer III (2003) "Characteristics of Wear Particles Produced during Friction Tests of Conventional and Non-Conventional Disc Brake Materials," *Wear*, Vol. 255, 1261-1269.

M. Mosleh, P. J. Blau, and D. Dumitrescu (2004) “Characteristics and morphology of wear particles from laboratory testing of disk brake materials,” *Wear*, Vol. 256, pp. 1128-34

J. Qu, P. J. Blau, T. R. Watkins, O. B. Cavin, and N.S. Kulkarni (2004) “Friction and Wear of Titanium Alloys Sliding against Metal, Ceramic, and Polymer Counterfaces,” Wear, Vol. 258, pp. 1348-1356.

P. J. Blau and B. C. Jolly (2005) “Wear of truck brake lining materials using three different test methods,” Wear, Vol. 259, pp.1022-1030.

P. J. Blau (2005) Research on Non-Traditional Materials for Friction Surfaces in Heavy Vehicle Disc Brakes, ORNL, Tech. Report. ORNL/TM-2004/265, 32 pp.

Conclusions

Studies have been conducted on a wide range of candidate friction brake materials for use in energy-efficient vehicles.

An ORNL technical report has been prepared and distributed to summarize most of the past work on candidate material evaluations.

Research in FY 2005 has revealed the potential of strong, heat-resistant Ti-based metal matrix composites to provide reasonable friction levels. These disc materials tend to run hotter, but the pad material has yet to be optimized to enhance their performance.

Plans are being made to conduct full-scale dynamometer tests on a set of coated Ti-based rotors.

Research in FY 2006 will include two new materials: an IR thermally-processed, in situ formed Ti MMC and a novel carbon composite material, both under development at ORNL.

B. Integrated Approach for Development of Energy-Efficient Steel Components for Heavy Vehicle and Transportation Applications

Co-Principal Investigator: Leo Chuzhoy
Caterpillar, Inc.
P.O. Box 1875, Peoria, IL 61656-1875
(309) 578-6621; fax: (309) 578-2953; email: Chuzhoy_Leo@cat.com

Co-Principal Investigator: Gerard Ludtka
Oak Ridge National Laboratory
P.O. Box 2008, Oak Ridge, TN 37831-6064
(865) 574-5098; fax: (865) 574-3940; email: ludtkagm1@ornl.gov

Co-Principal Investigator: Clyde Briant
Brown University
Box D, Brown University, Providence, RI 02912-D
(401) 863-1422; fax: 401-863-1157; email: Clyde_Briant@Brown.EDU

Chief Scientist: James J. Eberhardt
(202) 586-9837; fax: (202) 587-2476; e-mail: James.Eberhardt@ee.doe.gov
Field Technical Manager: Philip S. Sklad
(865) 574-5069; fax:(865) 576-4963; e-mail:skladps@ornl.gov

Contractor: Caterpillar Corp.
Contract No.: DE-AC05-00OR22726

Objective

This project focuses on development of methods and tools to achieve energy-efficient and environmentally benign steel components. The primary objective of this four-year project is to develop microstructure-level (often called mesoscale) simulation tools (MLS) to capture the formation and influence of nonhomogeneous (real life) microstructures in steel processing. The tools will be used to understand and predict microstructure evolution during processing and ultimately to predict the resultant component performance. This information will then be used to design steel microstructures and develop process roadmaps. The developed techniques will be demonstrated on a pilot project at Caterpillar involving a defined structural component, namely a track roller shaft, which represents a steel component with high production volume that can potentially benefit from microstructure-level improvements. These goals will be achieved through the four tasks described in the technical task section.

Approach

To apply an integrated approach to development of energy-efficient steel components, three major areas of research needs will be pursued:

- Development of microstructure-level models to accurately predict the evolution and behavior of steel microstructures during component processing and performance.
- Characterization of thermo-mechanical properties of microstructural constituents as a function of temperature and composition for exact chemistries.
- Development and integration into the modeling simulation endeavor of the tools to assess required environmental resources.

Accomplishments

Specific MLS modules have been developed and validated for at least one experimental case for the prediction of:

- Solidification microstructures capturing solute segregation;
- Machining damage for each constituent phase as a function of high strain, strain rate, temperature, tool geometry, and loading path;
- The decomposition of austenite during heat treatment for eutectoid and hypoeutectoid steels;
- Accurate stress states and damage in individual phases during heat treatment;
- Microcrack propagation at the fracture initiation stage for the martensite as part of a steel toughness prediction model.

Future Direction

The accomplished MLS machining and casting tasks from the first and second year of this project will be refined during this third year to integrate with the current version of the heat treatment simulation module developed this past year. The phase transformation kinetic model of this heat treatment module developed during year 2 of this project will be also expanded to account for chemical and microstructural inhomogeneities. Likewise, the MLS casting solidification model will be enhanced to predict microporosity along with its current capability to explicitly simulate dendrite growth and alloy segregation. In addition, MLS material strength and fracture resistance models will be developed to explicitly account for inclusions, precipitates, and grain boundaries. Finally, ambient temperature and elevated temperature magnetic processing will be investigated as a material processing approach to tailor microstructures with enhanced performance. Therefore, magneto-thermodynamic processing will be incorporated into the integrated simulation tool as part of the heat treatment considerations for material performance optimization. More specifically, our third year deliverables will be the following:

- A microstructure-level model incorporating phase transformation kinetics that accounts for chemical and microstructural inhomogeneities will be developed and demonstrated for the heat treatment processes used by Caterpillar for the SAE 1045 and SAE 15V45 steel alloys (9/2006).
- Microporosity prediction capability will be incorporated into the casting solidification model (3/2006).
- Experimental failure strain data for individual phases under compressive and tensile loading will be generated for inputs and validation of the damage initiation and failure predictions that will be part of the material strength and fracture resistance model (4/2006).
- The material strength and fracture resistance models will be developed to explicitly account for inclusions, precipitates, and grain boundaries. (8/2006).
- Magnetic processing experiments will be conducted on the ORNL 9-T superconducting magnet to investigate this processing approach for enhancing performance in ferrous alloys of interest to Caterpillar (6/2006).

Introduction

Product cost and performance are two major pressures influencing the acceptance of energy savings technologies by the manufacturers, suppliers, and users in the heavy vehicle and transportation industries. Energy cost has become a significant portion of total product cost for steel applications. Major reductions in energy use are potentially achievable for the transportation and heavy vehicle industries through development and optimization of cost-effective fabrication processes and enhanced product performance.

The key enabling technologies to achieve these benefits are improved materials and realistic, microstructure-level simulations to predict manufacturability and life-cycle performance. Over the past two decades, steel mills and forge shops have successfully implemented numerous energy-efficient processes. The next logical step is to focus on the development of steel microstructures that are produced in such a way that they are energy efficient and environmentally benign over the entire manufacturing cycle.

Structural materials used in critical steel components of machines have evolved to the point where further improvements in the performance can be achieved only through a fundamental understanding of the mechanisms driving material behavior during processing and service. Microstructural elements such as grain size, inclusion and precipitate distributions, and chemistry control the performance of engineering materials. Variation in these microstructural elements leads to variation in such critical properties as fatigue life, toughness, and wear resistance. Therefore, understanding and developing the capability to control the formation of steel microstructures and predicting the functional and environmental performance is critical to moving the industry closer to its energy-efficiency, resource-efficiency, and pollution-prevention goals. The full realization of these benefits, however, requires a design tool that optimizes the microstructure with respect to the mechanical and environmental performance throughout the life cycle of a particular steel component.

To apply an integrated approach to development of energy-efficient steel components, the development of three major areas of research needs to be completed:

- microstructure-level models to accurately predict evolution and behavior of steel microstructures during component processing and performance,
- thermomechanical properties of microstructural constituents as a function of temperature and composition for exact chemistries, and
- tools to assess required environmental resources.

This project addresses activities required for the first of these three areas. The second and third tasks are either supported by current funding through the National Science Foundation or are expected to be funded through the DOE Initiative for Proliferation Prevention. Through these integrated efforts, a design tool will be developed that optimizes the microstructure, manufacturability, and performance of components with respect to the mechanical and environmental performance required throughout the components' life cycles. The overall benefit of this research will be the development and demonstration of a design methodology that will enable the domestic transportation and heavy vehicle industries to compete effectively in future worldwide markets through improved product performance and energy savings. Furthermore, the proposed design tool can be extended to other materials, i.e., cast iron, aluminum, titanium, magnesium, nickel-based alloys, ceramics, and composites, thus impacting virtually all industries.

In addition to the transportation and steel industries receiving significant energy and cost savings benefit through microstructure-level modeling, virtually all industries will be impacted. Examples of such industries include aerospace (engines, transmissions, structural), marine (engines and drives), agricultural and construction equipment, oil and chemical processing (pumps and gear boxes), military vehicles, mining machinery, appliances (compressors, motors, gear boxes, shafts), power tools, and automotive aftermarket.

Project-end Deliverables

The deliverables for the project will be the following:

- Microstructure-level methods for simulating the manufacturing cycle of steel products coupled with material performance computations (Tasks 1, 2, and 3).
- A specific chemical composition and processing map for a 1500-series steel and a micro-alloyed steel suitable for the application under consideration (Task 4).
- Energy and environmental resources required to produce the selected steel component using at least two steels and processing schemes (Task 4).

The project tasks will focus on three critical areas in the development of these models: heat treatment processing, machining, and materials performance in specific applications. These three processes have been chosen because they are critical steps in reaching the goal of being able to develop a specific steel for a particular application with a heavy reliance on modeling and with energy requirements optimized as an integral part of the development process. Modeling of casting and forming processing has been performed under other programs, and Caterpillar has shown successful application and commercialization of these models. These existing models will be used along with the heat treatment, machining, and specific applications models described below to complete a suite of models for the manufacture of micro-alloyed steels.

To accomplish the project objectives, a multidisciplinary team consisting of a national laboratory, a university, and a steel end user has been assembled. The team will be supported by an international research institute for material characterization and by experts in environmental impact assessment. The section below describes each of the technical tasks to be performed.

Semi-annual Period Report Topics

Model development and results for the following two topics were reported in detail in the 2005 semiannual report and therefore will not be duplicated in this annual report:

- Solidification microstructures capturing solute segregation
- Machining damage for each constituent phase as a function of high strain, strain rate, temperature, tool geometry, and loading path.

Current Period Progress

Multistage Heat Treat Simulation

Background: Caterpillar started to develop a heat treat simulation package called QSIM in the late 1980s. This predictive tool has gradually become an integral part of heat treat process development, trouble shooting, and material selection in Caterpillar. Recently, an explicit microstructure-based Representative Volume Element (RVE) model was used to capture the mechanical response of steel for different stages of phase transformation. The material response is then used as input for a global model to simulate the quenching process and obtain residual stress during phase transformations. This microstructure level-based simulation approach provided an accurate prediction of material response during heat treat processing. In the current study, the QSIM heat treat simulation is being further integrated into component failure analysis under a multi-scale microstructure based integration model. Microstructure transformations during manufacturing are simulated and are used for material property determination and input to failure analysis. Simulation techniques are being used from initial concept design, through manufacturing process development to failure analysis in a large steel component. The current state of heat treat process simulation and material failure simulation techniques make it possible to accurately predict material behavior and the impact on possible component failure. A combined effect with design, manufacturing simulation and failure simulation will help to address critical issues in the early design stage.

Heat treatment simulation

QSIM contains four modules: (1) a pre-processor for solid model and FEM mesh generation, (2) a quench, carburizing, induction heating, and material database, (3) FEM engines based on ABAQUS, and (4) a post-processor. The database interacts with every major phase of the FEM engines to insure that actual description of the material and quench characteristics are captured. This includes thermodynamics data, transient behavior, phase transformation, related transformation strain and plasticity data, and each individual constituent stress-strain curve under a defined temperature range.

1. Heat transfer model

The temperature field is governed by a standard Laplace equation:

$$\nabla \bullet (k\nabla T) + \dot{q} = \rho c_p \dot{T} \quad (1)$$

where ρ, c_p, k and $\dot{q}$ are density, heat capacity, heat conductivity and rate of internal heat generation, respectively. The latent heat associated with phase transformations is considered in the model by an enhanced specific heat method. All the material properties are defined as functions of temperature and microstructure.

The most significant factor in transient thermal analysis during steel heat treatment is heat extraction rate at a part boundary. This heat extraction rate is taken into form as:

$$\left(\frac{dQ}{dt}\right)\bigg|_{\Gamma} = h[T(t,x)_s - T_\infty] \quad (2)$$

where Γ is the part boundary, T_∞ is the equivalent ambient temperature, *h* is the effective heat transfer coefficient, and $T(t,x)_s$ is the time and location dependent surface temperature.

During the quench process, three stages of cooling occur: vapor blanket, boiling, and convection. The three stages of cooling make the heat extraction rate a strong function of part surface temperature, quenchant properties, and the relative velocity of the steel part and the quenchant. Caterpillar has developed a reliable quench characterization method based on measured microstructure and hardness either on a quench characterization bar or on a real quenched component. A genetic algorithm is integrated into the QSIM heat treat simulator to inverse calculate the heat transfer coefficient as illustrated in Figure 1.

The effective heat transfer coefficient is determined by the described quench characterization scheme for the given quenchant and part geometry. It is stored in the quench characterization database and is selected during pre-processing.

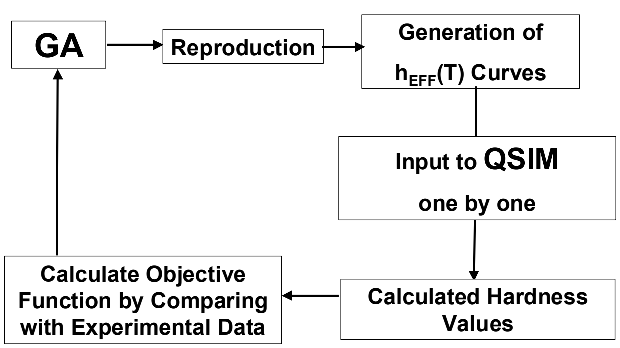

Figure 1. Genetic algorithm (GA) and QSIM inverse heat transfer calculation procedure.

2. Microstructural model

Austenite decomposition is a key element in modeling microstructure formation during the quenching of steel. Many research efforts have been made in describing austenite decomposition kinetics. There are two types of phase transformation involved during heat treatment: diffusion and diffusionless transformations. For diffusion-based transformations, the fraction of the transformed constituent, f_T, is a function of time *t*, nucleation rate *N*, and growth rate *G*. It can be expressed as:

$$f_T(t) = 1 - \exp[-(\pi/3)NG^3t^4] \quad (3)$$

where nucleation rate and growth rate are dependent on temperature, diffusion coefficient of carbon in austenite, free energy barrier and austenite grain size.

For diffusionless transformations, that is when austenite transforms into martensite, martensite-start temperature is first calculated as a function of chemistry. The percentage of martensite is then calculated according to the transformation database deducted from the measured dilatometric curve for each alloy.

3. Stress model

Small deformation theory is applied to heat treat simulation. The total strain in this quasi-static elastic-plastic stress model can generally be expressed as:

$$\dot{\varepsilon}_{ij} = \dot{\varepsilon}_{ij}^{e} + \dot{\varepsilon}_{ij}^{p} + \dot{\varepsilon}_{ij}^{tp} + \dot{\varepsilon}_{ij}^{tr} + \dot{\varepsilon}_{ij}^{th} \quad (4)$$

where the superscripts *e, p, tp, tr,* and *th* represent the strain caused by elastic, plastic, transformation plasticity, transformation strain and thermal strain. For multiphase mechanical response, behavior of each individual pure micro-constituent was evaluated from uniaxial tensile tests under various temperatures. An explicit description of microstructure according to volume percentage of each constituent on a normal grain size was used in the micro-scale local model to capture material responses for the global model. Grain boundaries were neglected in this study. For each material within the QSIM database, dilatometric data was also measured for each material to determine transformation strain.

Failure models

1. Material model

The most frequently encoutered mode of failure for heat-treated components is mainly due to void growth and coalescence types of ductile damage processes. Figure 2 shows the ductile dimple type of the fracture surface. This type of fracture normally proceeds in three stages: (1) *void nucleation* by cracking of the particles or decohesion of the inclusions, (2) *void growth* developed by plastic deformation, (3) *void coalescence* by strain localization, void sheet or plastic instability. Different types of models based on micromechanics and damage mechanics have been developed to model these processes. Compared with classical fracture mechanics based approaches, these so-called local approaches do not have geometry dependence and all have certain independency to stress triaxiality. Thus failure parameters can be transferred from lab identification to component level simulation with different geometry and boundary conditions. More important, these models can capture actual mechanisms of failure and supply in-depth understanding of the failure process. Among these void growth models, the Gurson model, which has been modified by Tvergaard and Needleman (GTN), has been proved successful in several studies of lab size failure problems. This modified GTN model can also be combined with other void nucleation and coalescence models.

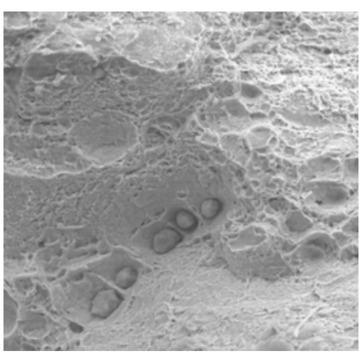

Figure 2. Ductile fracture surface of component. Particles are MnS.

Modifications with considerations like void shape, relative void spacing and strain hardening are also available. Thus, it is chosen for the current study on failure simulation. Due to the element size limitation, the Gurson model has rarely been applied to large component failure simulation. In the current study, the GTN model is used in a submodel manner for failure analysis of a large part.

In the GTN model, flow potential of porous material is given as:

$$\Phi = \left(\frac{\sigma_e}{\sigma_0}\right) + 2 f^* q_1 \cosh\left(q_2 \frac{3\sigma_h}{2\sigma_0}\right) - 1 - q_3 f^{*2} \qquad (5)$$

Here, σ_0 is the flow stress of non-porous material; σ_e and σ_h are macro-effective stress and hydrostatic stress, respectively; and q_1, q_2, q_3 are parameters to account for void shape and hardening effects. These final three parameters were first introduced by Tvergaard to better fit the curve of a void growth cell model. Interaction of voids near the stage of coalescence can be counted by introducing an effective void volume fraction f^*, which can be expressed as:

$$f^* = \begin{cases} f & f < f_c \\ f_c + \dfrac{f_u - f_c}{f_F - f_c}(f - f_c) & f_F > f > f_c \end{cases} \qquad (6)$$

and

$$f_u = \frac{q_1 + \sqrt{q_1^2 - q_3}}{q_3} \qquad (7)$$

where, f is void volume fraction, f_c is the critical void volume fraction, and f_F is the void volume fraction at failure. A fixed critical void volume fraction, f_F, at failure is assumed in the model. As the majority of voids formed in the current material are directly from gas porosity, shrinkage porosity and MnS inclusions, voids would form or exist at the beginning of the loading history. Thus, a nucleation stage can be ignored. The increment of f is:

$$\dot{f} = (1 - f)\dot{\varepsilon}_{ii}^p \qquad (8)$$

where, $\dot{\varepsilon}_{ii}^p$ is plastic strain increment and follows the summation convention. For Matrix material, an actual hardening curve from mechanical testing has been used.

2. Model parameter calibration

A full Gurson model with consideration of growth and coalescence involves six model parameters. These parameters can be identified with a full curve fit or by combination of micromechanics models and experiment. However, the phenomenological parameters occur in the model regardless of the micromechanics approach. A combined micromechanics and experiment approach was adopted here. q_1, q_2, q_3 are parameters mainly related to void growth, which can be identified by micromechanics study of a cell model by a curve fit manner. Notched bar tests can be used to identify the void coalescence parameters f_c and f_F. Initial porosity volume fraction f_0 is sometimes considered as an adjustable parameter to take the void shape effect into account. In the current study, since most voids and inclusions are spherical, f_0 could be directly identified as the initial porosity volume fraction in the porous material.

Multiscale model integration and failure load identification

To determine the failure load of a component, part assembly structures with applied load need to be analyzed using non-linear contact structure FEM analysis. As discussed in the previous section, part loading capability greatly depends on the residual stress pattern, local material properties, and local material defects. In this study, material properties due to the microstructure difference from heat treatment were mapped into the simulation model. Residual stress was also mapped into the structure assembly. Due to element size restriction, it is difficult and time consuming to directly apply failure models to the global assembly structure.

In the current study, a submodeling technique has been used to identify the global failure load and failure location. First, from global structure simulation, several critical locations were identified as candidates for further submodel micro-scale failure simulation. This can be accomplished by using several criteria based on effective stress, which identifies the plastic deformation, maximum principal stress and a damage stress criterion:

$$\sigma_D = \sigma_e + h\sigma_h \tag{9}$$

where, h is set as 0.4.

Occasionally, large defects might be present in the part due to up-stream manufacturing processes, such as casting. To eliminate those defects can often be very costly and might be unnecessary if not in the critical load carrying locations in the component. It is very crucial to understand how those large defects influence part load carrying capability in order to have confidence in product reliability. These large material defects act like voids normally in the 'mm' size range. Those large material voids could either be predicted using quantitative process simulation tools, or determined by metallurgical investigations. For those locations where large material voids exist in the modeled components, the voids were directly built into the explicitly described micro-scale level local sub-models. Boundary nodes of the sub-model were driven by the global model that carry out the part assembly non-linear calculation. Boundary node reaction force was used to identify global failure load. Small porosity, such as material inclusions, can be treated in the material damage model through initial void volume fraction. Figure 3 illustrated the integration multi-scale modeling scheme used in this study.

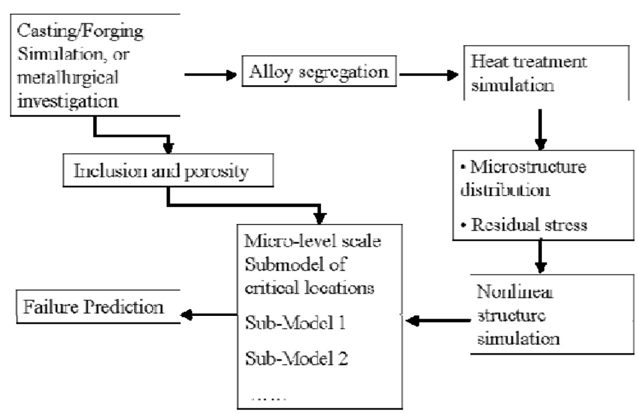

Figure 3. Multi-scale heat-treated component failure analysis scheme.

Application to a Large Steel Casting

A large steel casting weighing 240 pounds and made from low alloy steel was selected to exercise the new model. The part is direct hardened and tempered. Basing cooling rates on previously developed quench characterization techniques, Figure 4 gives the predicted material hardness profile achieved through the direct hardening process. Hardness at surface reached HRC 49 with a fully martensitic structure, while hardness at core only reached HRC 32 with only 30% martensite. The predicted hardness profile was compared with several measured hardness profiles from production parts and is shown in Figure 4. The hardness profile predicted after tempering is also presented in the same plot. The predicted hardness agreed well with the measured curves. As expected, dramatically different material mechanical properties would be formed at those locations due to different microstructure.

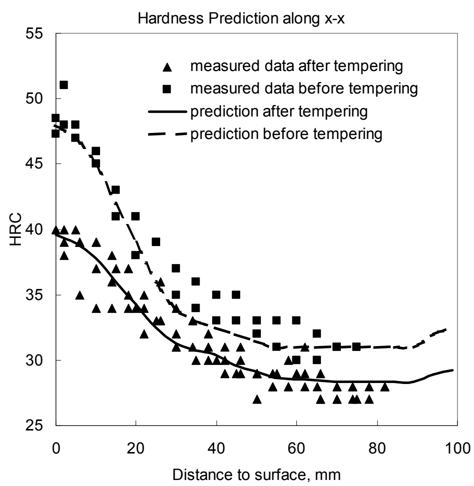

Figure 4. Predicted hardness plot for the large steel casting.

Conclusions

An integrated microstructure level approach has been used for large steel component failure prediction. Simulation started from heat treatment, then results were ported into nonlinear structure simulation and finally to submodeling failure analysis. Final failure load was directly predicted based on heat treat simulation and microstructure porosity inputs. The simulation predictions agreed well with test results. This approach demonstrated that a microstructure-level manufacturing simulation procedure can be used to predict large component loading capacity during the component design validation stage. It can be futher integrated with quantitative material defect prediction models of the various up stream processes to provide a reliable virtual product development and testing platform.

Presentations/Publications/Patents

L. Chuzhoy, C. Briant, A. Needleman, G. Ludtka, "Application of Microstructure-Level Simulation to Life Cycle of Steel Components", presented at MRS Fall 2005 meeting Nov. 28 – Dec. 2, 2005, Boston, MA.

C. Development of Technologies for the Application of Magnesium Metal Matrix Composites for Heavy Vehicles

Principal Investigator: Adam R. Loukus
GS Engineering, Inc.
101 West Lakeshore Drive
(906) 482-1235; fax: 906-482-1236; e-mail: adam.loukus@gsengineering.com

Chief Scientist: James J. Eberhardt
(202) 586-9837; fax: (202) 587-2476; e-mail: James.Eberhardt@ee.doe.gov
Field Technical Manager: Philip S. Sklad
(865) 574-5069; fax: (865) 576-4963; e-mail: skladps@ornl.gov

Participants:
Glen Simula, GS Engineering, Inc.
Andrew Halonen, GS Engineering, Inc.
Josh Loukus, REL Machine, Inc.
Robert Hathaway, Oshkosh Truck Corp.
Chad Johnson, Oshkosh Truck Corp.
Dave Weiss, Eck Industries
Bob Coleman, Engineered Fiber Solutions

Contractor: GS Engineering, Inc.
Contract No.: WR10637

Objective

- Successfully cast magnesium metal matrix composites in an effort to replace low specific strength primary structural components. Implement a selectively reinforced Mg MMC component into a class 8 vehicle.

Approach

- Infiltrate liquid AZ91 magnesium into a variety of readily available ceramic preforms. Evaluate the resulting mechanical and physical characteristics of the samples. The characteristics obtained from an optimum material and process selection shall be used to select and design a primary structural class 8 vehicle component. Once the component is selected, prototypes shall be cast and durability tested. Iterations in design, process, and testing are anticipated prior to successful integration of component on production vehicles. The systematic isolation and control of process parameters is crucial to the success of this project. The team has worked with production squeeze casting and pressureless infiltration processes and found them inadequate from a process control standpoint. This has resulted in an effort to design a state of the art process-controlled squeeze casting press.

Accomplishments

- Accomplishment 1 – Cast samples exhibiting elastic moduli three times that of as-cast AZ91D (from 6.5 to ~20 Mpsi).

- Accomplishment 2 – Acquired extensive knowledge in casting magnesium composites through hands on trials and literature search.
- Accomplishment 3 - Developed in-house casting capability with the focus of extensive process control.

Future Direction

- Milestone 1 – Refine material, i.e. matrix/reinforcement, and process parameters for production capable system.
- Milestone 2 – Select, design, cast, test, implement component(s) for heavy duty specialty trucks.

Introduction

Metal matrix composites (MMCs) have been the focus of numerous studies based on the promise of high specific strength and modulus. Weight savings, without loss in performance, has provided a driving force to develop MMCs using various reinforcements. Preforms of silicon carbide particles and/or whiskers, (SiCp and SiCw), Al_2O_3 particles and/or fibers, carbon fibers, and hybrid combinations of these when used in conjunction with high pressure casting processes that infiltrate the perform with molten metal have specific component design and production advantages. The incorporation of a hard, high modulus reinforcement into a malleable metal matrix provides an end product with properties predictable through the rule of mixtures. Preforms in conjunction with squeeze casting offer selective reinforcement versus a random distribution common in stir casting. Squeeze casting densifies the casting to reduce porosity and grain size thereby maximizing ductility and toughness for a given strength and stiffness. Squeeze casting, powder metallurgy, spray deposition and stir casting methods are commonly used in industry to produce MMC materials. (Gui et al 2004,Kaneko et al 2000, Chmelik et al 2000)

The use of magnesium alloys in the production of MMCs is of interest for researchers and industrial professionals due to the low density of the material and a relatively high stiffness to weight ratio. For example, a common magnesium alloy, AZ91 has a density of 1.81g/cc, whereas aluminum alloys and steel densities are 2.7 and 7.8g/cc respectively.

The focus of this work investigates the potential of using magnesium MMCs in stiffness, strength, and wear driven applications. There have been numerous investigations into this area especially with aluminum alloys. Magnesium composite studies, while not so thoroughly researched as aluminum, have been performed and have provided the impetus and direction to the current investigation. The goal of the first portion of the work is to quantify and reproduce material properties to understand strength mechanisms and matrix/reinforcement interactions in magnesium composites. In the larger scope of the work, components of Mg MMCs could be implemented into Class 8 vehicle components.

Figure 1 illustrates the constraints, variables and goals of the projects. The funding, time and resources are fixed to reach the high strength, weight reduction (HSWR) goals. The design, mechanical properties, quality, cycle time and cost of the resulting component are affected by the process. The selection of an optimized process with control of as many process parameters as possible will result in consistent high quality components. As consistency increases, the overall yield of a given melt will increase resulting in lower overall product cost. In the final analysis cost is the driver in whether a material/technology is introduced on a vehicle platform.

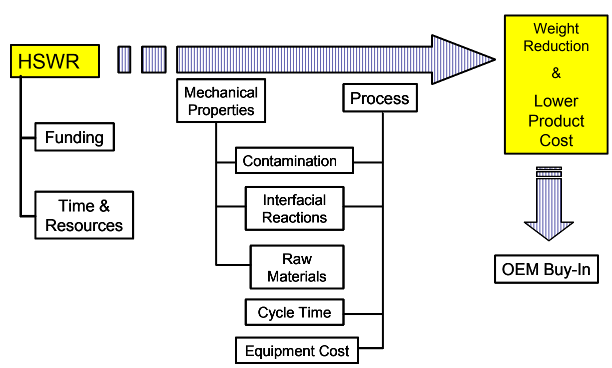

Figure 1. Flow chart of objectives and variables affecting mechanical properties and outcomes.

Carbon fiber work, performed by Schultz et al 1999, demonstrates the effect of pressure during the infiltration of a preform. A pressure-tight inert autoclave is used in the experiment as the casting press. The pure magnesium (99.95%) matrix material and the preform are heated in a vacuum until the melting point of the matrix is achieved. The vacuum is then broken and Argon (Ar) gas is allowed to flow into the chamber to prevent oxidation. The autoclave produces the pressure needed for the molten metal to infiltrate the space within the permeable carbon fiber preform and the densifying force needed to minimize shrinkage porosity. For a given carbon fiber perform, both aluminum and magnesium trials showed the resulting flexural strength and flexural modulus of the MMC were directly related to applied pressure (up to 40 MPa) during infiltration.

Alumina, Al_2O_3, is a widely used preform material and has been utilized extensively in aluminum and magnesium work. Creep tests performed on magnesium reinforced with Saffil fiber at a 20% volume fraction (vf) showed increases in creep resistance, strength and stiffness over the monolithic alloys in the study. (Sklenicka et al 2000).

Perhaps the most prevalent preform material in the literature is silicon carbide. Silicon carbide particles promote higher modulus and wear resistance with moderate increases in strength (Zheng et al 2000, Svoboda et al 2000, Gui et al 2004). Silicon Carbide whiskers have also been used for similar mechanical property enhancements (Kaneko et al 2000, Zheng et al 2004). Typical whisker aspect ratios are from 10 to 100. The prior art shows that the volume fraction of reinforcement is directly related to elastic modulus, wear resistance and ultimate tensile strength. This is true for both the particulate and whisker reinforcement morphologies.

As in the case of common engineering materials, increases in strength and stiffness come at a cost to the ductility and toughness of the material. The higher the strength and the stiffness, the lower the failure strain for a given composite. The successful integration of MMCs in vehicle component design requires a thorough understanding of this mechanical property tradeoff. On the other hand this tradeoff can be tailored through modifications in the interfacial reactions that take place between the fiber and matrix materials. (Kaneko et al 2000, Zheng et al 2004). The preform binders that coat the material react to produce by-products that can be favorable or unfavorable for load transfer between the matrix and the reinforcing material. Kaneko performed tests with whiskers that were uncoated and observed fracture along the whisker matrix interface due to the lack of interfacial reactions. When a silica binder was used to coat the whiskers the magnesium wetted the reinforcement enabling the formation of interfacial MgO which bonded the matrix to the whisker. Different types of binders such as $Al(PO_3)_3$ are available and offer different reactions for binding the composite constituents (Zheng et al 2001, Zheng et al 2003).

<u>Background</u>

AZ91D Precipitation Behavior:

Theory states that AZ91D contains a nominal 9% Al and 1% Zn and a small amount of Mn (0.15%). Based on the binary Mg-Al phase diagram, under equilibrium conditions, this alloy will solidify as a single phase α-Mg solid solution and subsequent cooling will lead to the precipitation of an intermetallic $Mg_{17}Al_{12}$ (β-phase) within the α-Mg grains.

In reality, in commercial casting operations, faster cooling rates will cause non-equilibrium cooling conditions which will lead to the formation of eutectic consisting of α-Mg solid solution and $Mg_{17}Al_{12}$ (β-phase). As the temperature cools below the liquidus, the α-Mg (primary) will begin to solidify and grow. As the temperature decreases toward the eutectic temperature, the liquid becomes enriched in aluminum because the solid that forms will contain a lower amount of Al than the nominal composition since there is not enough time for diffusion to take place in the solid. As the remaining liquid reaches the eutectic temperature, it solidifies as two phases: supersaturated α-Mg and $Mg_{17}Al_{12}$. Therefore, at room temperature, the alloy will contain three phases: Primary α-Mg, eutectic α-Mg and $Mg_{17}Al_{12}$.

Solution heat treated (T4)

Solutionizing requires bringing the solidified alloy to a temperature above the solvus line and holding there until the $Mg_{17}Al_{12}$ phase is dissolved and a homogeneous α-Mg solid solution is formed. Subsequent quenching retains the single α-Mg phase, but now the phase is super-saturated i.e., there is excess aluminum in a non-equilibrium state.

The ASTM (ASTM B 661) recommended heat treatment for AZ91 casting alloy is 775°F for 16 to 24 hours. ASTM also suggests an alternate treatment to minimize grain growth; a) 775°F for 6 hrs.; b) 665°F for 2 hrs.; or c) 775°F for 10 hrs. It is possible that the optimum solution treatment for squeeze cast composites will have a shorter time because the $Mg_{17}Al_{12}$ will be more broken up and therefore require less time to dissolve into the matrix.

Aging treatment (T6)

Aging the T4 structure at a temperature below the solvus will allow the excess aluminum to diffuse to nucleation sites and form $Mg_{17}Al_{12}$ precipitates. Since these precipitates are formed at a lower temperature compared to the eutectic $Mg_{17}Al_{12}$ formed during solidification, they will be finer and more evenly dispersed and therefore more effective at strengthening the alloy.

The ASTM recommended aging treatment for an AZ91 casting is a) 335°F for 16 hrs. or b) 420°F for 5-6 hrs. It is likely that the optimum aging treatment will be different for a composite. Jayalakshmi et al., found that the presence of ceramic reinforcements significantly decreases the peak aging time for an AM100/Saffil short fiber composite. It is suggested that the presence of the fiber-metal interface provides nucleation sites and enhances the precipitation.

Effect of the preform

Table 1 summarizes the reactions that can take place between the matrix and the ceramic/preform binder. The interfacial reactions that take place can enhance or degrade the desired mechanical and physical characteristics of the composite. The goal is to form a strong bond between the ceramic and matrix without forming detrimental reaction products at the interface. Although the interface reactions can increase the ability of the matrix to wet the ceramic, the reaction products or a chemical degradation of the ceramic can adversely affect the mechanical properties of the composite. A method that minimizes reaction product but achieves matrix to fiber load transfer under stress is the balance that must be achieved in the production of a quality engineering material. This is the approach taken by the Lo et al patent. By forming a coating of magnesium fluoride on the surface of the ceramic, the interfacial reactions are avoided.

Table 1. Possible interfacial reactions that can form with an Mg + Al alloy:

Ceramic or binder	Possible Interfacial Reactions:
C	$4Al + 3C \rightarrow Al_4C_3$
Si	$Si + 2Mg \rightarrow Mg_2Si$
SiC	$4Al + 3SiC \rightarrow Al_4C_3 + 3Si$
Al_2O_3	$3Mg + 4\ Al_2O_3 \rightarrow 3Mg\ Al_2O_4 + 2Al$ $3Mg + Al_2O_3 \rightarrow 3MgO + 2Al$
SiO_2	$Mg + 2SiO2 + 2Al \rightarrow MgAl_2O_4 + 2Si$ $2MgAl_2O_4 + 3Si \rightarrow 2MgO + 3SiO_2 + 4Al$ $2Mg + SiO_2 \rightarrow 2MgO + Si$

Procedure

Squeeze Casting

A vertical squeeze cast press was utilized in this work. The machine specifically was a 400 ton model with an H-bar die. Figure 2 shows pictures of this equipment. In this method the material can be injected and held at 100 MPa in order to reduce both the infiltration porosity and the shrinkage porosity. This is a commercially viable process with potential for high volume production quantities. The following is the procedure for infiltration and Table 2 shows the process parameters.

1. Shot Sleeve Charged with Liquid Magnesium.
2. Preforms were preheated to 1292°F and placed into the die cavity.
3. Die is slid into position.
4. The die is closed and clamped together with 400 tons of closing force.
5. Shot piston moves up, forcing material into the die and preforms at a predetermined speed.
6. Pressure is held until solidification of the casting.
7. Die opens and the part is taken out.

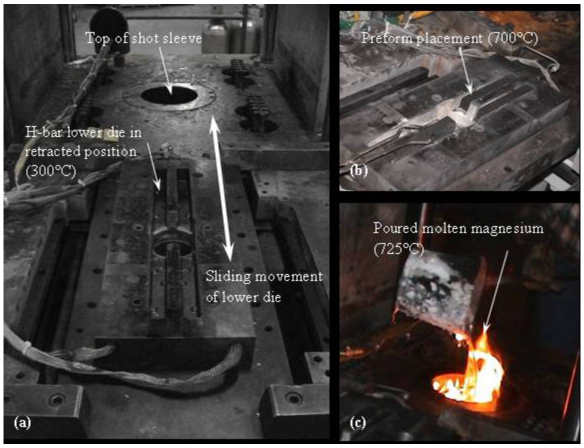

Figure 2. (a) Squeeze casting equipment with an H-bar die with (b) preforms inserted. (c) molten magnesium poured into shot sleeve.

Table 2. The process parameters set for these tests.

Process parameters	Value
Molten Magnesium Temperature (°C)	725
Die Temperature (°C)	300
Shot Speed (in/sec)	1
Shot Time (sec)	4.5
Pressure (psi)	3000
Dwell (hold) Time (sec)	100
Reload Time (sec) (approx.)	150
Total Cycle Time (sec)(approx.)	255

The squeeze casting trials with the H-Bar die resulted in samples contaminated with MgO inclusions. As a result, it was imperative to eliminate the opportunity for MgO inclusion formation. It was felt the majority of the oxidation took place during transfer of the liquid magnesium to the shot sleeve. The liquid must be protected during this step to provide consistent properties within a given Mg MMC system.

Pressureless Infiltration

A comparative study was performed on similar materials using a pressureless infiltration method. The pressureless infiltration furnace enables the process to take place within a specialized casting atmospheres. The inert cover gas allows the liquid to infiltrate the preform without competing with oxidation reactions. This process eliminates the need for an expensive die because the preform is infiltrated largely by capillary action. The preform is placed on top of the magnesium in the furnace as it melts. Figure 3 illustrates this pressureless infiltration process.

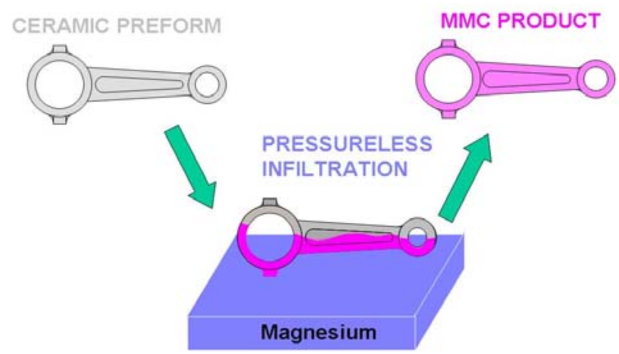

Figure 3. Schematic of the pressureless infiltration process.

This process is effective for near net shaped reinforcements involving complicated geometry and better melt flow. The disadvantage of this casting method is that it is slow and difficult to achieve high cooling rates needed for solid solution strengthening (Polmear, 1995).

A simplified procedure follows:

1. Set preform down in graphite bedding material
2. Magnesium billet placed on top
3. Argon purges chamber
4. Ramp furnace to desired temperature with argon flow through furnace
5. Alloy melts and completely infiltrates preform
6. Furnace cooled to 400ºC ***(Units)*** with argon flow
7. Break away bedding material and extract finished part.

Preforms of various types were cast using this method. AZ91D and AZ91E alloys were used for these trials. The resulting mechanical properties are discussed in the following results section.

PIVAC Method

The PIVAC (Pressure Infiltrated, Vacuum Assisted Casting) method was specifically designed for infiltrating preforms with liquids. Experiments conducted were well instrumented to monitor the temperature and pressure inside the die. Two thermocouples were placed in the region where the magnesium billet sits and three thermocouples were placed along the length in the preform region shown in Figure 4.

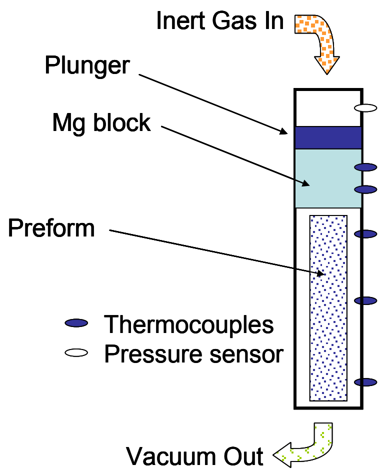

Figure 4. PIVAC method schematic.

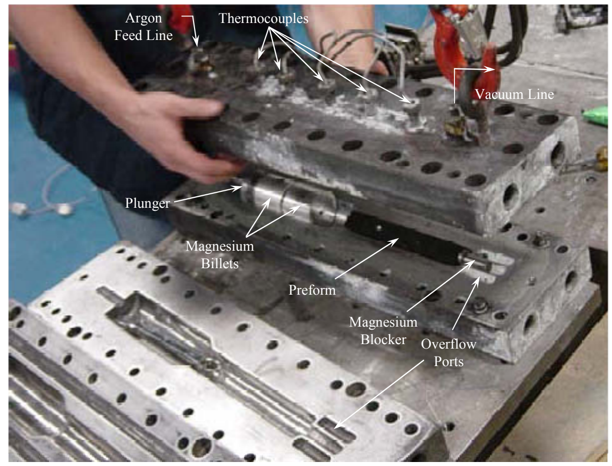

Figure 5. Experimental setup of the PIVAC method.

The temperature is monitored during the critical stages of the process. The method is similar to the carbon fiber work performed by Schultz et al 1999, which demonstrated the affect of pressure during the infiltration of a preform. A pressure-tight inert autoclave is used in the experiment as the casting press. The pure magnesium (99.95%) matrix material and the preform are heated in a vacuum until the melting point of the matrix is achieved. The vacuum is then broken and Argon (Ar) gas is allowed to flow into the chamber to apply pressure to the matrix material. This pressure, combined with the vacuum forces the molten metal to infiltrate the carbon fiber preform and minimize shrinkage porosity. The flexural strength and the modulus both increased as a function of pressure (up to 40 MPa) during the casting trial for both magnesium and aluminum for a given carbon fiber preform material (Shultz, et al. 1999). The experimental lab setup used for this work is shown in Figure 5.

The experimental procedure is as follows:

1. Place preform and 2” diameter magnesium billets in die cavity with plunger. Close die.
2. Bolt together top and bottom die.
3. Attach thermocouples, vacuum and argon pressure lines to die.
4. Place die in furnace and bring temperature up to 1200°F (monitor thermocouples with data acquisition system. Vacuum die chamber simultaneously.
5. Once temperature is reached in the die. Apply argon pressure to specified value.
6. Open furnace, force air cool to 900°F, quench in water to room temperature.
7. Unbolt dies and remove infiltrated preform.

Results and Discussion

There are several data sets that could be compared from the three different processes, Squeeze Casting, Pressureless and PIVAC. In the current study, the tensile strength, elastic modulus and strain to failure were measured. The data from the different processes is tabulated below.

Squeeze casting gave good results when filters were incorporated to limit MgO inclusion contamination. Results from the trial are tabulated below.

The non reinforced AZ91D squeeze cast control run results provided properties consistent with published data. Squeeze casting with single constituent preforms and hybrids of mixed fibers and particulate placed in the H-Die prior to infiltration was performed. The results from these tests showed various degrees of success. With the exception of O influence affecting repeatability, the data below indicates the promise of using a squeeze cast machine in producing composite components, specifically those with hybrid preforms.

Table 3. AZ91D Squeeze Cast Material Properties

Condition	Ultimate Tensile Strength (UTS)	Strain at UTS (%)
As Cast	21100 psi (145 MPa)*	1.2*
T6	29850 psi (206 MPa)*	2.7*
	*average of 5 tests	

The hybrid preforms were the most successful under the process conditions chosen for these studies. These showed great gains in elastic modulus when compared to the non reinforced control. Figure 6 demonstrates the production potential of this process for composite material manufacturing. However, there are negative attributes in the composite material properties due to lack of complete infiltration, compaction and fracture of preforms and the deleterious effects of MgO formation.

The squeeze cast trials were run on a production caster which did not have access to monitor and control the parameters that were felt necessary for the production of a consistent quality composite material. A more in depth understanding of the fluid dynamics and chemical reactions is essential. More controlled infiltration studies to understand the reactionary chemistry of the process was undertaken.

Pressureless infiltration studies were performed at GOM Technologies in order to understand the infiltration potential of various preform materials. Using the pressureless process would also provide evidence on the effects of infiltration velocity and cooling rate on material properties. The controllable casting atmosphere in the process eliminates rapid oxide formation prevalent with the squeeze casting process. The matrix material in the pressureless infiltration studies and the PIVAC process showed much lower matrix strengths as shown in Table 4 below. It is felt that the lower cooling rates contributed to large grain size (Figure 7).

Although the grain size has an adverse affect on the mechanical properties of the castings, the strength of carbon fiber Mg MMC more than doubled the matrix material strength. The strain to failure increased as well. This indicates that there is good

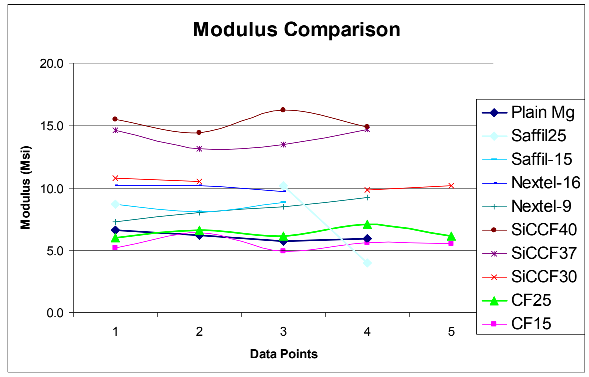

Figure 6. Squeeze Cast composite modulus data

Table 4. Pressureless Infiltration Data

Material	Elastic Modulus (Mpsi)	Elastic Modulus (GPa)	UTS (psi)	UTS (MPa)	Strain at Failure
33% SiC - 4% Carbon Fiber	19.5	134.4	29000	199.9	0.0021
33% SiC - 4% Carbon Fiber	17.9	123.4	24900	171.7	0.0019
33% SiC - 4% Carbon Fiber	14.2	97.9	27400	188.9	0.003
33% SiC - 4% Carbon Fiber	22.3	153.8	34900	240.6	0.003
Saffil - 15	15.7	108.2	11500	79.3	0.007
Saffil - 15	12.9	88.9	13300	91.7	0.0015
Saffil - 15	10.5	72.4	15200	104.8	0.0019
Nextel - 9	7.95	54.8	14200	97.9	0.0028
Saffil - 15	8.75	60.3	14900	102.7	0.0034
Nextel - 9	8.25	56.9	10500	72.4	0.0017
54% alumina	15.31	105.6	10450	72.1	0.00213
54% alumina	N/A	N/A	10550	72.7	N/A
54% alumina	16.3	112.4	14950	103.1	0.00092
CF - 25 AZ91E	N/A	N/A	19050	131.3	0.00415
CF - 25 AZ91D	N/A	N/A	21700	149.6	0.00361
CF - 25 AZ91D-1	N/A	N/A	25885	178.5	0.0086
CF - 25 AZ91D-2b	9.8	67.6	31107	214.5	0.0089
CF - 25 AZ91D-3	N/A	N/A	32189	221.9	0.0049
CF - 25 AZ91E-4b	N/A	N/A	27708	191.0	0.0063
CF - 25 AZ91D-5b	11.2	77.2	34353	236.9	0.009
CF - 25 AZ91E-6	3.86	26.6	11812	81.4	0.0048

Figure 7. AZ91D fracture surface - PIVAC method.

Table 5. PIVAC experimental data

Material	Elastic Modulus (Mpsi)	Elastic Modulus (GPa)	UTS (ksi)	UTS (MPa)	Strain at Failure
CF 15 - 1	5.67	39.1	31.6	217.9	0.0110
CF 15 - 2a	6.96	48.0	35.2	242.7	0.0084
CF 15 - 2b	5.16	35.6	16.7	115.1	0.0045
CF 15 - 3a	7.51	51.8	27.4	188.9	0.0096
CF 15 - 3b	6.01	41.4	27	186.2	0.0071
CF 15 - 4a	6.31	43.5	25.9	178.6	0.0086
CF 15 - 4b	6.17	42.5	23.5	162.0	0.0068
CF 15 - 5	5.51	38.0	25.6	176.5	0.0093
CF 15 - 6	5.05	34.8	22.3	153.8	0.0085
Pure AZ91E - 7	N/A	N/A	12.7	87.6	N/A
CF 15 - 8a	N/A	N/A	26.03	179.5	N/A
CF 15 - 8b	N/A	N/A	25.96	179.0	N/A
CF 15 - 9_1	6.8	46.9	24.54	169.2	0.0088
CF 15 - 9_2	6.11	42.1	14.48	99.8	0.0031
CF 15 -10	9.29	64.1	24.4	168.2	0.0073
CF 25_1	7.65	52.7	11.79	81.3	0.0022
CF25_1b	12.1	83.4	20.1	138.6	0.0038
CF25_2	7.96	54.9	17.32	119.4	0.0031
CF25_3	13	89.6	23.07	159.1	0.0045
CF25_4	7.55	52.1	20.98	144.7	0.0049
CF25_4b	5.31	36.6	20.24	139.6	0.0031
AZ91E_1	5.82	40.1	12.06	83.2	0.0035
AZ91E_2	3.03	20.9	6.4	44.1	0.004
CF25_1	5.19	35.8	27.05	186.5	0.0061
CF25_3	9.28	64.0	26.99	186.1	0.0056
CF25_4	6.57	45.3	26.13	180.2	0.0054

CF 15 - Averages	6.41	44.17	23.97	165.28	0.0074
CF 25 - Averages	8.29	57.16	21.52	148.37	0.0043
AZ91E - Averages	4.43	30.51	10.39	71.61	0.0038

adhesion and load transfer between the matrix and the carbon fiber reinforcement

The PIVAC elastic modulus for the Mg MMC with the SiC_p-C_f hybrid preform is similar to that observed with the squeeze cast trial. This suggests that casting in an inert environment can bolster the mechanical properties without the implementation of high pressures (in a dense preform).

The effects of pressure on the results from the PIVAC method were not able to be delineated in the study due to leakage problems in the die. The pressure was then reduced in order to keep the molten magnesium contained to minimize collateral damage. However, calculations of material infiltration based on weight show that the preform was fully infiltrated. This pressure affect and effects of heat treatment will be further pursued in future work to set process parameters in future squeeze cast trails. Also, metallographic, SEM-EDS, and TEM characterization of matrix-reinforcement interfacial reactions are ongoing.

Microstructural Analysis

Due to the reactive behavior of the magnesium melt, the reactions between the molten metal and the reinforcement need to be analyzed. Extensive work was done analyzing the preform-metal interface. The microstructural features affect the macroscopic response (yield strength and UTS) and therefore it is important to control the reactions at this interface. The following SEM micrograph (Figure 8) of a fracture surface from a squeeze casting sample shows the fiber-matrix interface. It can be observed that the bond strength in this sample is poor as there are areas of fiber pullout. This is reflected in the poor mechanical properties of the material as the fibers are pulling out of the matrix and the load transfer is poor due to this adhesive failure.

SEM observations from the samples cast in an inert environment during pressureless infiltration show a different behavior. It is shown in Figure 9 that the fibers are cracking and the fracture of the material is shearing through the fibers rather than pulling them out. This is an example of cohesive failure. This is the mode in which increases in strength and moduli are seen.

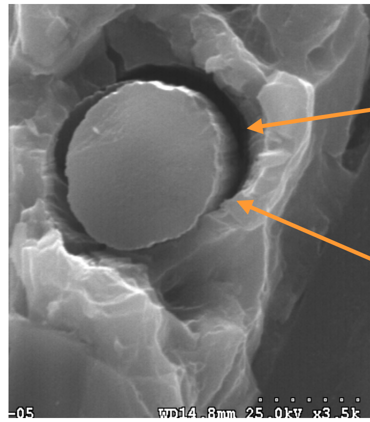

Figure 8. Adhesive failure between the fiber and the surrounding magnesium matrix.

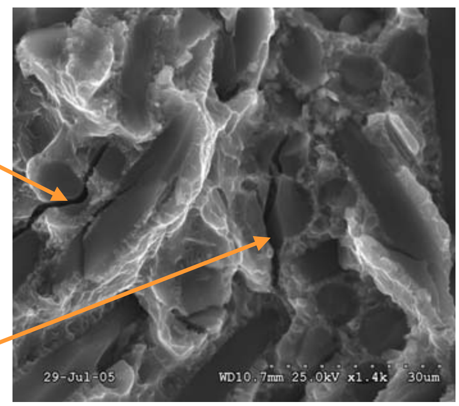

Figure 9. Cohesive failure of the material showing an excellent bond between the fibers and matrix.

Squeeze Casting Press Development

From the above casting iterations, it is clear that there is a distinct need for process control and the correct process selection. Each process brings its own set of variables, advantages and disadvantages. Figure 10 shows how each affects the end goal of achieving excellent metallurgical and mechanical properties.

It is well known that a fine grain structure leads to improved mechanical properties. Therefore, the squeeze casting process looks favorable due to the inherent fast solidification rates leading to fine grains. Squeeze casting also reduces the casting cycle times, and therefore, reduces part cost. The inert environment seen by the pressureless infiltration process shows that casting without MgO

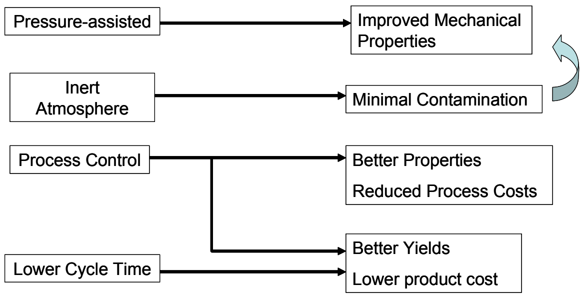

Figure 10. Positive attributes of each process.

contamination can dramatically improve the mechanical properties of the Mg MMC. If the process parameters are carefully controlled, the mechanical properties are favorable. The detrimental affects of pressureless infiltration are seen when the fibers degrade due to long reaction times between the magnesium alloy and the reinforcing fibers.

It is of great scientific and commercial interest to combine the positive attributes of each of these processes to cast components. Therefore, the intent of the PIVAC method was to prove this concept. The results have shown that there is promise in this ideology, and therefore a squeeze casting press is being built specifically with these factors considered.

Most commercial squeeze casting presses available today have some exposure of the melt to the air. The intent of this press is to control the environment completely throughout the casting process. Other improvements are extensive process control. Careful monitoring and control of melt temperature, preform temperature and shot sleeve temperature; shot velocity, profiles and pressure are very important to control to avoid damage to the preforms, yet obtain complete infiltration.

The press (Figure 11) has a 400 ton capacity with the potential of providing ~15000 psi (~100MPa) of pressure to the molten metal. Process control and melt protection are crucial design criteria.

Preliminary casting trials will commence in early December 2005.

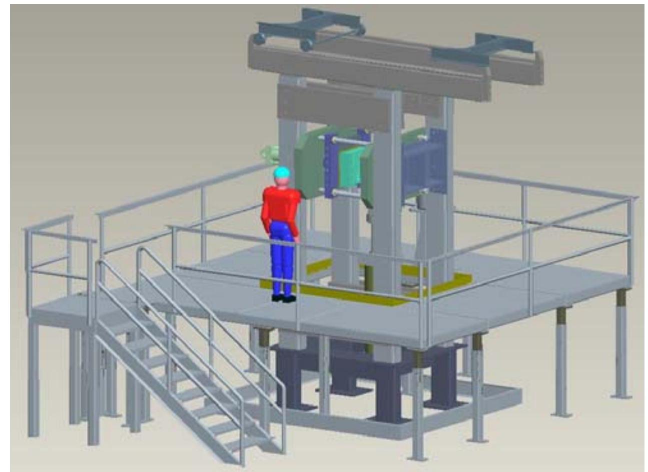

Figure 11. 400 ton squeeze casting press.

Conclusions

Process control in magnesium metal matrix composites is complicated by the reactive nature of the molten metal. Interactions between the metal and the preforms can be positive for good fiber-matrix bonding, but too much of these reaction products can produce intermetallics and oxides that are unwanted in the matrix.

New process development is underway to cast selectively reinforced magnesium composites. Component casting and testing will occur in the early part of 2006.

Presentations/Publications/Patents

1. ORNL – Heavy Truck Peer Review. Status of "Development of Technologies for the Application of Magnesium Metal Matrix Composites for Heavy Vehicles" Sept. 13, 2005.
2. AFS International Conference on High Integrity Light Metal Castings. "The Effects of Processing Methods on the Mechanical Properties of Cast Magnesium Metal Matrix Composites." Oct. 31 – Nov. 1, 2005. Indianapolis, IN.
3. TMS – Rohatgi Honorary Solidification Symposium of Metal Matrix Composites; "Solidification Rate Effects on Microstructural and Mechanical Properties in Pressure Cast Magnesium Metal Matrix Composites." March 12-16, 2006 in San Antonio, TX.
4. NADCA, 110th Metal Casting Congress, April 18-21, 2006. Mg MMC topic. Columbus, OH.

D. Lightweight Functional Composite Materials

Principal Investigator: Nidia C. Gallego
Oak Ridge National Laboratory
P.O. Box 2008, Oak Ridge, TN 37831-6087
(865) 241-9459; fax: (865) 576-8424; e-mail:gallegonc@ornl.gov

Chief Scientist: James J. Eberhardt
(202) 586-9837; fax: (202) 587-2476; e-mail: James.Eberhardt@ee.doe.gov
Field Technical Manager: Philip S. Sklad
(865) 574-5069; fax:(865) 576-4963; e-mail: skladps@ornl.gov

Participants:
Dan D. Edie, Clemson University
Edwin H. Kraft, EHK Technologies

Contractor: Oak Ridge National Laboratory
Contract No.: DE-AC05-00OR22725

Objectives

- To develop an economic evaluation of the cost of providing fuel to internal combustion engines using ORNL's carbon fiber monoliths as a medium for storing adsorbed natural gas for use in vehicular applications.
- To investigate and develop methodologies to disperse metal nanoparticles in a carbon fiber substrate and, to determine the appropriate heat treating (stabilization and carbonization) and activation conditions for metal-containing fibers.

Approach

- Prepare process flow diagrams for monolith and storage system manufacture.
- Create an economic model for the methane storage and delivery (tank to engine, including injection) system.
- Determine cost of vehicular methane pressure storage and gasoline storage and delivery systems.
- Determine operating fuel cost of gasoline and methane systems in comparable vehicles.
- Mix metal salts with isotropic pitch, the precursor for carbon fibers; initial run will evaluate palladium additions.
- Melt-spin metal-containing pitch into fiber form. Stabilize, carbonize, and activate metal-containing fibers.
- Characterize surface area and pore size distribution of metal-containing carbon fibers.

Accomplishments

- Economical model showing that high cost of precursor carbon fiber, makes ORNL's monolith an extremely expensive material for storing adsorbed natural gas.
- Successfully melt-spun carbon fibers containing approximately 1 wt % of the following metals: silver, palladium, and silver/palladium mixtures. These samples were heat-treated (stabilized and carbonized) and activated to developed porosity.

Future Direction

- The development of low cost carbon fiber is a critical step towards reducing the cost of carbon fiber monoliths. The low cost carbon fibers could increase the potential of carbon fiber monolith as a medium for storing adsorbed natural gas at low pressure.
- Metal-containing carbon fibers have potential application for enhanced gas storage and catalysis applications, however, the evaluation of these applications are not part of the scope of this program and will not be pursued further here.

Introduction

During this fiscal year, we undertook two main tasks in this project: The first one was to conduct an economic analysis of the cost of using ORNL's carbon fiber monoliths for storing adsorbed natural gas for vehicular applications; this task was carried out by EHK Technologies under contract with ORNL. A summary of the findings is presented below. A more detailed report of this economic evaluation is available upon request.

The second task was to investigate methodologies for the production and processing of metal-containing activated carbon fibers. This task was conducted in collaboration with Clemson University.

Cost Model - Introduction

Natural gas is currently used as an alternative fuel in vehicles such as taxicabs, buses and some medium duty trucks. The method of fuel storage in each of these cases is as a compressed gas in what is essentially a pressure vessel. This gas is stored in most cases at 250 bar (3,600psi). An alternative storage concept consists of using ORNL's carbon fiber monolith, capable of adsorbing natural gas in large volumes at considerably lower pressure. In concept, this new method would have the advantages of lower cost and lighter weight for the storage equipment.

The present study was conducted to assess the cost and weight of this Adsorbed Natural Gas (ANG) system compared to the conventional Compressed Natural Gas (CNG) system. The intended application for this ANG system is medium duty trucks at a rate of 50,000 units per year.

Approach and Results

The cost of manufacture of an ANG storage system was estimated by creation of a mass production concept and economic model of that production. The concept was based on the limited data available from laboratory material, process and application experiments conducted at ORNL. Laboratory data on material composition, processing and methane storage capacity was necessary to calculate material volume requirements and process parameters. Early in this study, it became apparent that the method of producing ANG storage material used in the lab efforts would not be suitable for production of the large quantities required by the intended application. A high volume production methodology was therefore conceived based on discussion with both ORNL personnel and manufacturers of process equipment applicable to several potential methodologies.

The essential difference in use of ANG vs. CNG as a fuel system for vehicles is only in the storage tank and media. Vehicles would use natural gas at the same pressure, and with the same delivery and carburetion system regardless of how the gas was stored, and would require pressure and flow regulators of approximately the same cost regardless of the storage pressure. The essential difference in cost is therefore the cost of tank and storage media. The amount (mass and volume) of ANG storage media therefore became a critical study parameter. A key issue in determining this requirement is the storage capacity of the media at a reasonable pressure.

Previous work at ORNL showed that the "deliverable capacity" of the media with an average density of 0.65 g/cc, was 120 (V/V). V/V is the volume of gas at 500 psi per unit volume of media. This means that for this study, we assume that at 500 psi, the media will store 120 times its gross volume of methane.

Using the data collected and reasonable assumptions, the cost of an ANG storage device would be approximately $10,000, and the device would weigh approximately 1,100 lbs. The breakdown of cost and sale price is shown in Figure 1. Obviously, the carbon and resin raw materials at 60%, and the steel shell of the container at 20%, constitute the majority of expected price of this device.

Conclusions

The results of the technical and economic analysis provided an estimate of the production cost of an ANG storage system and comparison to a CNG system. A CNG storage tank for a 20 gallon gasoline equivalent is about 60 gallons in volume, and would cost from ~$250 for Type 1 all steel weighing ~200lbs, to over $2,000 for a Type 4 all composite tank weighing only about 100lbs. Thus, saving around 100lbs of weight costs close to $2,000. The penalty in space of using CNG vs. gasoline is a factor of 3X. An ANG storage system for the same fuel value was estimated in this analysis to cost approximately $10,000, to weigh ~1,100lbs, and require a tank of ~130gallon volume (6.5X space penalty). Therefore, even with the uncertainties in materials and processing inherent in a study of this nature, it is not likely that an ANG system would have significant probability of success in this market.

The search for a low-cost carbon fiber might make this monolithic material more reasonable in cost and a viable material for a variety of applications.

Metal-containing Activated Carbon Fibers - Introduction

The purpose of this task was to investigate and develop techniques to disperse metal nanoparticles in activated carbon fibers. The project is to determine the appropriate heating and activation conditions and to evaluate the catalytic and absorption properties of activated carbon fibers doped with metal.

Metal-containing activated carbon fibers offer several advantages. First, the isotropic pitch precursors are inexpensive and conventional melt spinning techniques can be used to produce fibers with diameters of from 10 to 15 microns, resulting in a high surface-to-volume ratio and facilitating mass transfer to and from the fiber. Also, because of the high surface-to-volume ratio, activation is extremely effective. As a result, the specific surface area of the activated carbon fibers is two to three times that of conventional activated carbon particles. Finally, the fibers can be inexpensively converted into a monolith form using slurry molding techniques.

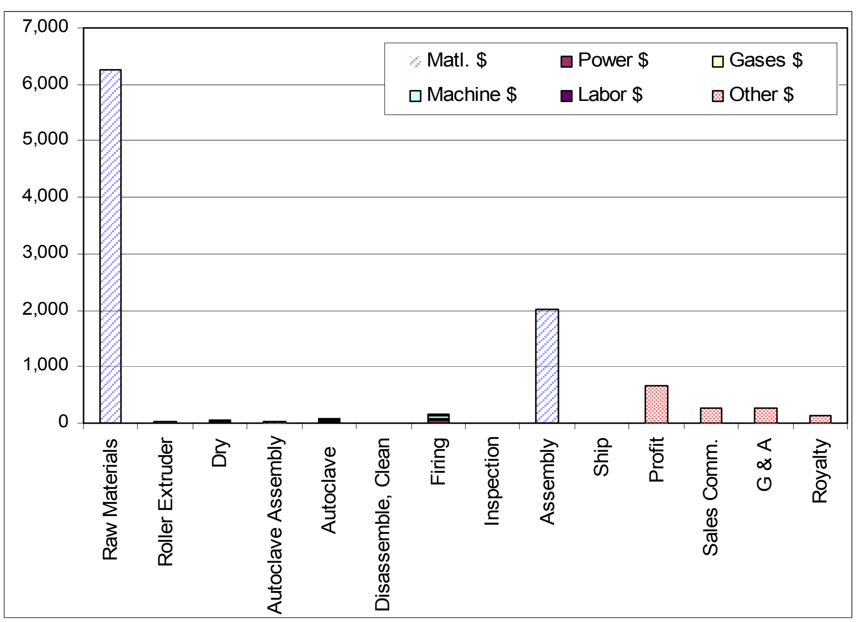

Figure 1. Cost / Price Factors for a 20 Gal. Gasoline Equivalent ANG Storage Device

Fiber Preparation

Figure 2 shows a flow diagram for the production of metal-containing activated carbon fibers. The process involves the mixing of a metal precursor (typically a metal salt) with an isotropic pitch. The mixture is then melt-spun into fibers using a bench-scale melt spinning apparatus. As-spun pitch-based fibers are stabilized in air in a conventional oven and carbonized at 1000°C in a helium atmosphere. Once stabilized and carbonized, the fibers are activated by exposing them to either CO_2 or steam and then heat-treated in a reducing or an inert atmosphere at elevated temperature. Activated, metal-containing carbon fibers are then characterized.

We have produced fibers from unmixed pitch (KU) and fibers containing silver (KAn), palladium (KPa), and mixtures of silver/palladium (KAP).

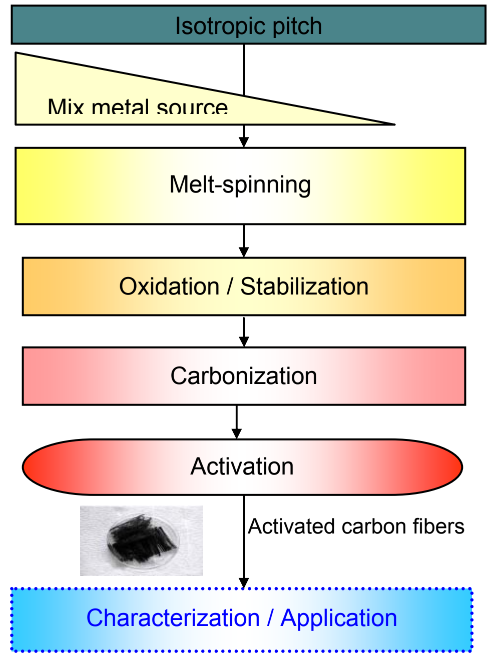

Figure 2. low process for the production of metal-containing activated carbon fibers.

Fiber Characterization

The surface properties of the metal-containing activated carbon fibers were determined from nitrogen adsorption-desorption isotherms obtained at -196°C using a Micromeritics ASAP 2020 surface analyzer. All fibers were outgassed at 290°C overnight prior to each adsorption experiment. The Brunauer, Emmett, and Teller (BET) method was used to calculate the total surface area and pore volume. The Barrett-Joyner-Halenda (BJH) method was applied to the desorption branch of nitrogen adsorption-desorption isotherms to calculate the surface area and pore volume, the pore size distribution and average pore size (4V/S) in the meso-/macropore range. The micropore size distribution was calculated from the nitrogen adsorption-desorption isotherms measured at relative pressures ranging from 5×10^{-5} to 1 using Horvath-Kawazoe (H-K) method.

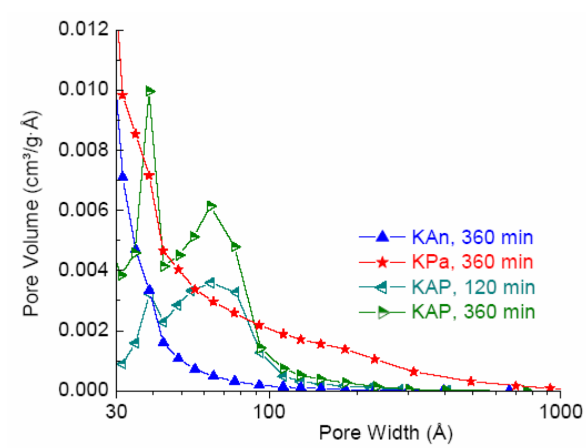

Figure 3. JH Desorption dV/dw pore volume plot of Ag-, Pd- and Ag/Pd-containing activated carbon fibers.

Figure 3 shows the pore size distribution for a selected set of activated carbon fibers. The pore size distribution curves for the Ag/Pd-containing activated carbon fibers exhibit a more pronounced peak at ~39 Å than that detected for the Pd-containing samples, even at their higher burnoff. An additional peak appears between 60 and 70 Å; this peak is not observed for the fibers containing the individual metals. Such peculiarities are most likely attributable to the formation of Ag/Pd alloy during the heat treatment, and they illustrate the synergistic effect of combining these two metals. These peculiarities of Ag-Pd pore structure formation may be useful for production of fibers with defined pore sizes.

Conclusions

We have successfully produced Pd- Ag- and Ag/Pd-containing activated carbon fibers. It was shown that the pore size distribution of these fibers is highly dependent on the type of metal contained in the fibers.

Additionally, the surface characteristics of the activated fibers will also be highly dependent on the type of metal present in the fibers.

Next steps will be the evaluation of these metal-containing carbon fibers for enhanced gas storage and for applications as catalyst. However, these applications are outside the scope of this program and will not be pursued here.

3. MATERIALS PROCESSING TECHNOLOGIES

A. Laser Glazing and Friction Stir Processing of Materials to Reduce Friction

Principal Investigator: George Fenske
Argonne National Laboratory
9700 S. Cass Avenue
Argonne, Illinois 60439
630-252-5190; fax: 630-252-4798; gfenske@anl.gov

Chief Scientist: James J. Eberhardt
(202) 586-9837; fax: (202) 587-2476; e-mail: James.Eberhardt@ee.doe.gov
Field Technical Manager: Philip S. Sklad
(865) 574-5069; fax:(865) 576-4963; e-mail:skladps@ornl.gov

Participants
Layo Ajayi, Argonne National Laboratory
Ron DiMelfi, Materials Research Development
Stan David, Oak Ridge National Laboratory

Contractor: Argonne National Laboratory
Contract No.: W-31-109-ENG-38

Objective

- Determine the potential of laser glazing to lower parasitic energy losses between the flange and rail in rail transport.
- Develop a fundamental understanding of the metallurgy associated with the formation of low-friction. surface layers during laser glazing processing, and how these layers reduce friction between rail and wheel.
- Determine the potential of laser glazing to improve fuel efficiency and component durability/reliability of critical engine/powertrain components.
- Evaluate the impact of friction stir processing techniques on the friction and wear of steel.

Approach

- Develop advanced laser glazing processes to form glazed regions on carbon steels.
- Perform benchtop tests, full-scale rig tests, and field tests of glazed steels and rails to quantify the impact of glazing and friction stir processing on parasitic friction losses.
- Characterize glazed and non-glazed steels to elucidate the impact of glazing and friction stir processing on the microstructure of steel (1080 steel).

Accomplishments

- Optimized laser processing conditions under which uniform glazed surfaces form on carbon steels
- Evaluated friction and wear performance of glazed (and unglazed) rail steel by using benchtop and wheel/rail rig tests.
- Evaluated friction and wear performance of friction stir processed steel using benchtop rig tests.
- Characterized the microstructure and hardness of glazed and friction stir processed steels.
- Developed a deformation theory for nanocrystalline materials to model friction in glazed steel.
- Demonstrated efficacy of laser glazing to reduce friction on a full-scale test rig using prototype wheels, loads, and speeds.
- Glazed a 40 foot long section of rail steel for high-tonnage rail tests.
- Evaluated the friction and wear performance of friction stir processed steel using benchtop test rigs.

Future Direction

- Perform high-tonnage field tests at the Association of American Railroads/Transportation Technology Center, Inc., Facility for Accelerated Service Testing (AAR/TTCI FAST) in Pueblo, Colorado.
- Characterize the microstructure of glazed rail subjected to AAR/TTCI FAST tests.
- Make go/no-go decision to proceed with development of rail glazing technology.
- If go/no-go decision is to proceed, establish project with a railroad track maintenance equipment and service organization.
- Identify critical engine and powertrain components that if treated by advanced laser-based processes would lower parasitic energy losses.

Introduction

Wheel/Rail interactions account for a significant fraction of the energy consumed in rail transport. Past studies have indicated that energy savings could be as high as 24% when friction at the wheel/rail interface is properly managed. The key aspect is control of the friction forces. At the locomotive, high friction between the rail (specifically the top of the rail) and the wheel is desired to ensure adequate traction to keep wheels from slipping and sliding when power is applied. Friction is also required under braking conditions to control the speed of downhill-bound trains or to bring a train to a safe stop. The trailing cars, however, require much lower friction levels under normal train operations. For these cars, a low, controllable friction is desirable and can significantly reduce the energy required to pull a train. Two regions account for most of the frictional losses between the wheel and the rail: the region between the top of the rail and the wheel tread, and the region between the wheel flange and the gage face of the rail. Current wheel/rail lubrication (e.g., application of degradable greases and lubricants) is inconsistently applied and often disengaged by train crews. The research described herein focuses on the development of a laser glazing technique that imparts a durable, low-friction surface to the gage face of the rails to reduce parasitic frictional losses between the flange and rail gage.

Recent changes within the portfolio of activities supported by DOE's Office of FreedomCAR and Vehicle Technologies have re-focused this project on applications to reduce parasitic energy losses in engine and powertrain components. Approximately 10 % of the energy consumed in an engine can be attributed to asperity and viscous friction. Furthermore, advanced concepts (low-sulfur fuels, exhaust gas recirculation (EGR), and aftertreatment devices) under consideration to reduce emissions will have significant impacts on the tribological system. Concerns over low-lubricity fuels, higher soot and acid loading of engine lubes, and lower levels of sulfur and phosphorous containing additives have been raised regarding their impact on component durability and reliability. Efforts are currently under way to evaluate the potential of laser-based technologies to improve the durability and reliability of critical engine components operating under more demanding tribological environments imposed by the advent of new fuels and lubricant formulations. Efforts are also in progress to evaluate the tribological potential of friction-stir processing (FSP). Traditionally FSP was developed to join components – e.g., friction stir joining of aluminum. However, FSP may also have potential to modify surfaces – e.g., harden near surface regions, or introduce alloying elements into near surface regions. To this end, preliminary studies were initiated to evaluate the impact of FSP on the tribological properties of steel.

Approach

The objective of this activity was to develop an advanced laser modification process to form a glaze on the gage face of the rail. Initial results and models predicted the formation of a nanocrystalline surface layer that would impart low-friction properties at the interface. The tasks associated with this project involve:

- Process development (laser glazing)
- Microstructural characterization of laser-modified surfaces
- Development of a model (of surface deformation)
- Lab-scale friction and wear testing of laser-modified surfaces (glazed and shot-peened)
- Full-scale friction testing of laser glazed steel
- Glazing of full-scale rail segments for field tests, and
- For, friction-stir-processing, lab-scale friction and wear testing under dry and lubricated conditions.

Results

The development [1,2] of the laser glazing processes used in these studies was documented in the FY03 Annual Report. Several approaches were investigated: two involved laser glazing, while a third approach investigated a laser shock-peening technique. Parametric studies were performed to optimize the conditions under which a glazed layer forms on 1080 steel. For this purpose, an Electrox 1.6-kW pulsed neodymium doped yttrium aluminium garnet (ND:YAG) laser with fiber-optic beam delivery and special beam shaping optics was used in Argonne National Laboratory's (ANL's) Laser Applications Laboratory. Two approaches were developed: one involved a single pass of the laser over a given area, and the other involved multiple overlapping passes. The Knoop hardness of the martensitic glazed regions was 2-3 times greater than that of the substrate, depending on whether a single-pass (factor of 3 times harder) or multipass (slightly over 2 times harder) process was employed. A commercial laser glazing process that utilized high-power diode laser technology was also investigated. In this case, bars of 1080 steel were processed by a commercial vendor (NuVonyx) and subsequently tested at ANL.

Friction and wear studies were performed using a number of lab-scale systems. Block-on-ring tests performed by Falex Corp. showed static friction coefficients of ≈0.35-0.45 for untreated 1080 steel that dropped to values ranging from 0.2 to 0.4 for differing glazing conditions. Large-scale (using a glazed segment of rail and a full-size wheel) "block-on-ring" tests performed at the AAR/TTCI Pueblo facility showed the static friction coefficient of the untreated 1080 rail varied from 0.2 to 0.5, depending on the applied load, whereas the friction coefficient of the glazed regions varied from 0.1 to 0.25. Dynamic friction coefficients for the glazed regions varied from 0.2 to 0.35, depending on load, compared to 0.2 to 0.55 for unglazed regions.

Benchtop pin-on-disc tests at ANL used flats of 1080 steel, glazed and unglazed, that rubbed against stationary balls or pins (52100 steel, 1080 steel, 440C steel, or alumina). The tests revealed that the composition of the pin/ball had a significant impact on the friction coefficient. The general trend was that the glazing reduced the friction coefficient by 3-35%, depending on the material. The greatest reduction was for the alumina ball sliding against the 1080 steel, suggesting that a strong chemical adhesion mechanism may be active with the metallic counterparts.

Twin roller tests were conducted at ANL with 1045 steel rail and wheel discs that were through-hardened (Rc 40) or glazed. The glazing effectively reduced the friction coefficient from roughly 0.4 for the unglazed condition to 0.3 for the glazed rail rotating against an unglazed 1045 steel counterpart.

Results of tests performed in a twin-roller test rig at the Canadian National Research Center WBB (Wheel, Bearing, and Brake) facility in Ottawa, Ontario were reported in the FY 2004 Annual Report. More detailed results can be found in reference 2. The WBB Facility uses conventional and instrumented full-scale wheelsets loaded against large 63-in. diameter rims that simulate the track. The system is designed to operate at prototypical speeds and loads (30 mph and 33,000 lb in these tests). The instrumented wheelset allowed continuous monitoring of the lateral, longitudinal and vertical forces during the tests – a feature that was used to measure differences between glazed and non glazed regions.

The WBB tests were performed to confirm the friction reductions observed in the lab-scale tests and to evaluate the durability of the glazed regions prior to installing glazed rail segments in the FAST loop at the AAR/TTCI facilities. A 180^{o} segment of the lower WBB wheel was sent to NuVonyx where two, 10-12 mm wide tracks were glazed along the circumference of the rim – one track along the gage face, and the second track on the top of the rail approximately 5 mm from the gage point.

A series of runs was performed over a 5-day period to evaluate the efficacy of the glazing to reduce lateral and longitudinal forces (e.g., reduce friction), and to evaluate the durability of the glazing after moderate tonnage. The friction measurements were performed with an instrumented wheelset that permitted direct measurement of the forces using strain gauges applied to the rotating wheels. These provided a continuous measurement of the lateral, longitudinal, and vertical forces.

The WBB tests showed friction reductions ranging from 8 to 50% depending on the angle of attack. After 1 million gross tons (MGT) exposure, the friction reduction ranged from 4 to 45%. Based on these encouraging results, efforts were initiated to treat a 40 foot long segment of track and to test it on the FAST loop facility in Pueblo, Colorado. The results presented below describe the effort to glaze the rail which was recently installed in the FAST loop.

Glazing of the 40 foot long segment of rail was performed by NuVonyx Inc. using protocols previously established for the WBB tests in Ottawa. Two segments of rail were provided by the TTCI: one segment, 4 foot in length, which was used to optimize glazing conditions to produce a glazing depth of 1-1/2 mm, and the second segment, 40 feet in length that was glazed and returned to TTCI for installation in the FAST loop facility. The 40-foot length had been cut in half and then rejoined (welded) to evaluate the impact of the glazing process on welded sections.

Results from the optimization studies on the 4 foot long segment indicated the optimum speed required using a 3800 watt beam was 0.5m/s. Two overlapping passes were used to produce a 1" wide glazed track along the gauge face of the rail. Figure 1 shows a dye-penetrant image of a portion of the 4 foot long rail that had been treated with overlapping tracks. The image shows no evidence of cracking that occurred (and subsequently resolved) in prior development efforts at NuVonyx for the Ottawa tests.

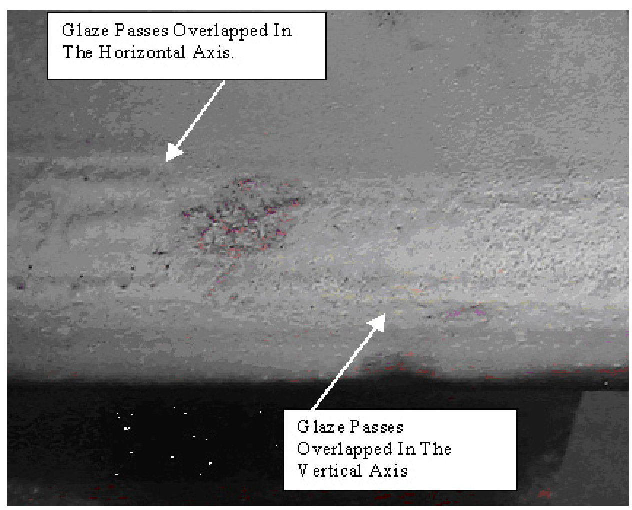

Figure 1. Dye-penetrant photograph of overlapped laser glazed tracks on 4-foot long trial rail.

With this assurance, effort proceeded to treat the 40 foot long segment. The entire 40 foot long segment was treated with two overlapping passes. Figure 2 shows a photograph of the rail during the glazing operation at NuVonyx. Post glazing dye-penetrant analysis was performed on the 40-foot long segment. Figure 3 shows a section of the 40 foot long segment – in this case significant cracking was observed. The impact of the 'hockey-stick' cracks is not definitively known – these cracks were observed in optimization studies for the Ottawa tests, and great care was taken to optimize the spacing between the overlapping tracks to avoid the hockey-stick cracks. The Ottawa test optimization studies revealed the cracks occurred while the second overlapping track was applied and that it occurred in the overlap region on the first track. This is a concern that needs to be addressed in future development efforts and may involve the development of a single-pass glazing treatment.

The current status of the glazed rail project is that the glazed rail was returned to the TTCI where it was installed in the FAST loop for the next cycle of runs. Friction measurements will be made at periodic intervals during the FAST loop test period. After the runs are complete, sections of the glazed rail will be returned to ANL for microstructural characterization. Materials Research Development will prepare a proposal to the Transportation Research Board for follow-on research with NuVonyx, Harsco, and ANL to commercialize the process.

Investigation of the tribological properties of FSP'd steel was initiated in FY05 in collaboration with Oak Ridge National Laboratory (Dr. Stan David). Several plates of 1080 steel were prepared for FSP'ing at ORNL. Figure 4 shows a photograph of the plate in the as-treated condition. Two FSP'd tracks/regions were produced: one with a single pass treatment, and the second with multiple overlapping tracks.

Microstructural examination of the plate revealed the base material was fully pearlitic with a Knoop hardness of 300 to 350. The FSP'd regions were martensitic with Knoop hardnesses ranging from 700 to 750. The depth of the hardened region was 4 to 6 mm.

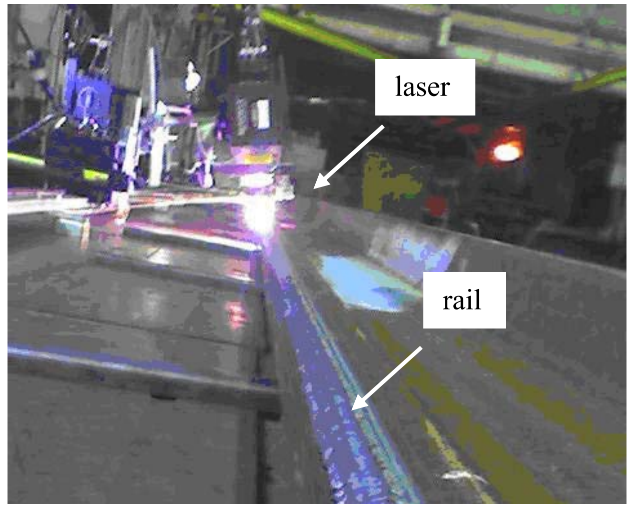

Figure 2. Photograph of the laser set-up used to glaze the 40 foot long rail.

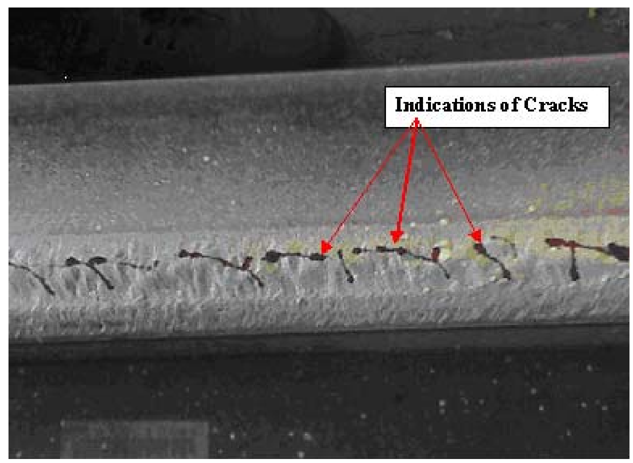

Figure 3. Dye-penetrant image of 40-foot long rail segment showing the presence of 'hockey-stick' cracks after overlapping tracks were applied.

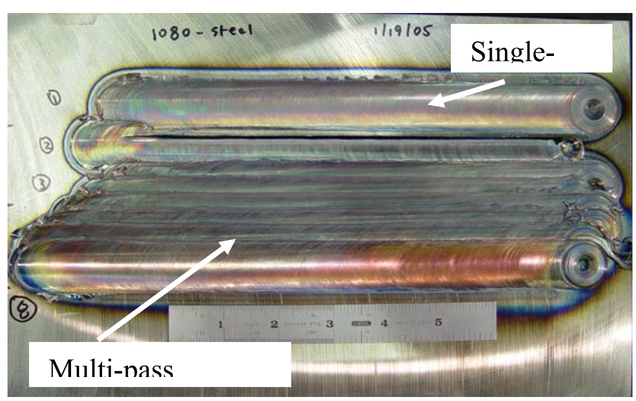

Figure 4. Photograph of a 1080 steel plate after single-pass and multi-pass friction stir processing.

Tribological tests were performed under dry and lubricated conditions using a pin-on-disc configuration on single and multi-pass test coupons. Prior to testing the rough surfaces were ground flat with a final grind using 320 grit SiC paper. The tribo tests were performed using a ½" diameter alumina ball sliding against the FSP'd coupons under a 10N load. The test duration was 1 hour at a sliding speed of 0.05 m/s. All tests were performed at room temperature in normal lab air (RH approximately 30 to 40 %). Tests were performed on single pass FSP steel, multi-pass FSP steel, and untreated steel under dry and lubricated (Mobil 1 10W-30 oil) conditions.

Results of the dry (open-air) and lubricated (Mobil 1 10W-30) tests are shown in figure 5 for the three different treatments. The untreated/reference coupon exhibited a friction coefficient of approximately 0.9, while the single or multi-pass surfaces exhibited friction coefficients of 0.7 – a significant reduction. Under lubricated conditions, all three surfaces appear to have similar friction coefficients close to 0.11, however, under closer examination (shown in the insert in figure 5, the multipass treatment appears to have a friction coefficient about 5 % lower than the single pass, or untreated surfaces.

The wear rates were also quantified after the tests. A 3-D optical microscope was used to measure the wear volume at multiple locations on the wear track. Under dry sliding conditions, the FSP'd coupons had wear rates approximately 1 order of magnitude lower than the untreated steel. Under lubricated conditions, no measurable wear was detected for the FSP's runs (1 hour in duration).

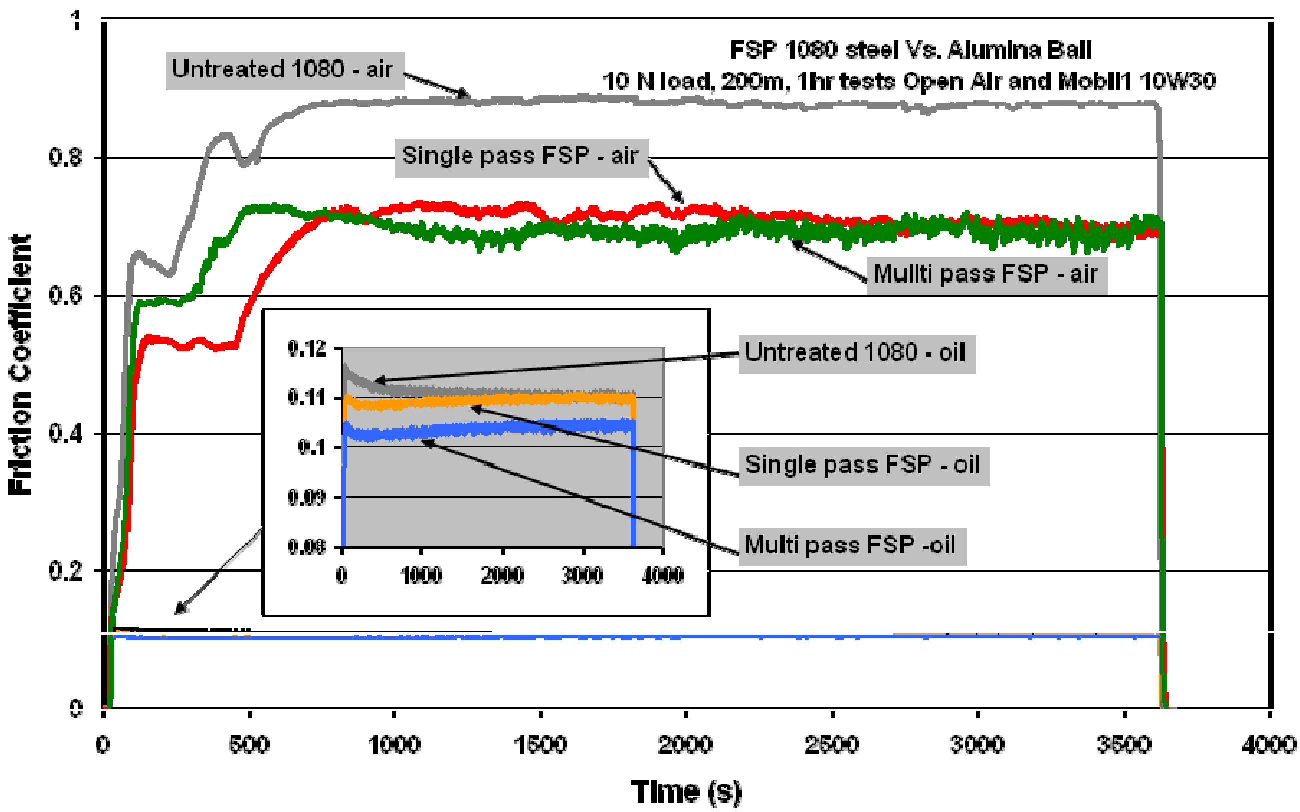

Figure 5. Graph of the friction coefficient of friction stir processed (and non-processed) 1080 steel as a function of time under dry and lubricated conditions.

Conclusions

Testing of laser glazing to improve the friction (and wear) performance of steels continues to progress. Initial lab-scale tests showed significant friction reductions and the more recent studies at Canadian National Research Council (CNRC), Ottawa have confirmed the friction reductions using full-scale wheels under high loads and prototypical speeds. Friction reductions in the range of 10 to 40 % have been observed – the magnitude of the reduction being dependent on the yaw and side loading. Efforts are in progress to establish a team to commercialize this technology with a rail maintenance firm. A 40-foot long track segment was glazed and installed in the FAST loop at the AAR/TTCI facility in Pueblo. The FAST loop tests are designed to put significant levels of tonnage on the treated track (upwards of 100 MGT). If successful, arrangements are being made to incorporate a laser-glazing system on a rail maintenance vehicle.

Efforts have also been initiated to explore the use of laser-glazing processing to treat engine and powertrain components. The increased hardness of near surface regions produced with laser-based processing may have significant impact on improving the durability of critical components (e.g., cylinder liners) that will be prone to accelerated wear with high levels of EGR.

Preliminary lab tests were performed on friction stir processed 1080 steel. The FSP produced a relatively thick, hard martensitic region that lowered friction under dry and lubricated conditions. Wear was lowered by at least one-order of magnitude.

References

1. S. H. Aldajah, O.O. Ajayi, G. R. Fenske, C. Reed, and Z. Xu, "Effect of Laser Surface Modifications on Tribological Performances of 1080 Carbon Steel", submitted to ASME Journal of Tribology, October, 2004.
2. Laser Glazing of Rails WBB/IWS Tests (CNRC-Ottawa), Saud Aldajah, George Fenske, and Layo Ajayi (Energy Technology Division - ANL), Claude Reed and Zach Xu (Technology Development Division – ANL), and Ron DiMelfi (Materials Research Development), ANL Report ANL-05/03, January 2005.

B. Development of an Advanced Squeeze Casting (ASC) Process for the Production of High-Integrity Truck Components

Principal Investigator: David C. Weiss
Eck Industries, Incorporated
1602 North 8th Street, Manitowoc, WI 54221-0967
(920) 682-4618; fax: (920) 682-9298; e-mail: dweiss@eckindustries.com

Chief Scientist: James J. Eberhardt
(202) 586-9837; fax: (202) 587-2476; e-mail: James.Eberhardt@ee.doe.gov
Field Technical Manager: Philip S. Sklad
(865) 574-5069; fax:(865) 576-4963; e-mail:skladps@ornl.gov

Contractor: Eck Industries, Inc.
Contract No.: 4000022893

Objective

- Develop the equipment and process technology for an advanced squeeze casting (ASC) process to enable production of high-integrity cast metal components.
  - Integrate the advantages of two casting methods – low-pressure permanent mold and direct squeeze casting – to attain non-turbulent fill of the die, high solidification rates to refine microstructural features, and solidification under pressure to minimize microporosity.
  - Design and build a new kind of casting machine and develop process technologies needed to cast high-integrity truck components from nonferrous alloys.

Approach

- Design and construct a casting machine that integrates a low-pressure metal delivery system suitable for either aluminum or magnesium alloys, reliable gate shut-off technology, and direct application of squeeze pressures up to 103 MPa (15,000 psi). This machine is intended for production.
- Develop a gate shut-off mechanism that will operate reliably in a production environment.
- Select a casting that will be produced in the casting machine built for this project.
- Use fluid-flow and solidification analysis to predict optimum flow conditions for metal entering the mold and differential squeeze pressure requirements.
- Design and build cast tooling.
- Develop process technologies for the low-pressure/squeeze casting of aluminum alloys and evaluate the effect of various process parameters on casting integrity.
- Apply developed technologies to the production of a selected automotive component.

Accomplishments

- Fabrication of ASC machine has been completed and the machine installed at Eck Industries, Inc., Manitowoc, WI.
- Squeeze cast tooling designed and fabricated.

Future Direction

- Develop ASC process parameters for prototype production of B356-T6 connecting rods.

- Determine static and dynamic properties of ASC processed B356-T6.
- Demonstrate production viability of ASC casting machine and process.

Introduction

Squeeze casting is the solidification of liquid metal under pressure in a closed metal die. The resultant casting has improved properties and a more uniform microstructure as compared to those produced by traditional molten metal fabrication techniques. The higher properties are achieved through controlled entry of the metal into the die through large gates, which reduces turbulence, and high solidification rates with resultant refinement of microstructural features.

There are two squeeze casting methods--direct and indirect. The method and efficiency of pressure application distinguish the two processes. Direct squeeze casting applies pressure directly on the casting. This contrasts with indirect squeeze casting where pressure is applied via the gating system. The length of the gating system and any partial solidification prior to complete solidification of the part reduces the magnitude of the pressure applied and may result in casting porosity. For the indirect squeeze cast method the dimensions of the die cavity control part dimensions. For the direct squeeze cast method, the part dimensions are controlled by the die cavity dimensions and the finish position of the top die. Thus, the direct squeeze cast method requires precise machine control to attain the desired part dimensions. In addition, the direct method requires in-gate shut-off technology to control pressure during cavity pressurization. Both methods suffer from poor metal handling from the furnace into the mold or gating system. Inadequate control of pouring speed generates turbulence and casting defects such as oxide inclusions that reduce fatigue properties.

Earlier attempts to improve the squeeze casting process by combining the advantages of low-pressure die fill with those of squeeze casting demonstrated substantial mechanical property improvement and reduced component porosity. However, continuous production operation of the equipment was not achieved. The machines used were not specifically designed to meet the needs of the process.

Technical Approach

The results of this project will provide (1) a production viable ASC machine, (2) process technology that will improve the strength and reliability of cast automotive components, and (3) demonstrated production viability of the equipment and process.

Machine Design. Previous efforts had demonstrated that modification of current cast machine designs would not provide a production capable ASC machine. An assessment of the capabilities and limitations of current machine designs demonstrated that:

- Low-pressure cast equipment typically does not have the structural rigidity needed to withstand the high pressures required of squeeze casting.
- Die-casting and currently available squeeze casting machines are not designed for proper (non-turbulent) molten metal entry into the die cavity.
- Neither type of equipment is typically available with the hydraulic and electronic controls necessary to attain the die cavity motions required for the direct squeeze casting process.

After much consideration, the project team decided it was easier and more cost effective to build a machine from the “ground up” than to modify an existing cast machine design. To facilitate this design and construction, the team partnered with Empire Castings, Inc., an experienced producer of low-pressure casting equipment.

Process Development. Bendix, Inc. is an industrial manufacturer of truck components with an interest in reducing manufacturing cost by the use of high quality castings. Consultation with them led to the selection of an air compressor connecting rod for prototype production in the ASC machine. This component has a level of complexity that can demonstrate the production capability of the ASC machine and process, the need for mechanical properties higher than those attainable with commercially available castings, and provides an opportunity for production with the ASC process.

The cast part was modeled for fluid flow and solidification. This work was done in parallel with equipment design. Simulation provided an understanding of optimum metal flow conditions and squeeze requirements, if any, to contend with solidification shrinkage. This is very important to the success of the program and, potentially, to the details of the machine design. The ASC machine has two mechanisms to feed the casting—low-pressure, nonturbulent fill of the die cavity and high-pressure, direct squeeze to minimize solidification shrinkage. Modeling experiments were used to explore the interaction of the two feed mechanisms and select process parameters that lead to process optimization. Modeling results were used to refine the die design and select initial casting process parameters.

After tooling construction and ASC machine delivery, castings will be made under the range of process conditions anticipated during modeling. A variety of both cast and wrought alloys (Table 1) will be used. Evaluation of those castings will include radiography, die penetrant inspection, tensile testing, and functional component testing at Bendix. It is anticipated that this part of the program will require multiple iterations to produce the desired product quality. Some equipment and tooling modification may be required during this part of the program.

Table 1. Aluminum alloys to be used for casting trials

AA 380	AA 206
AA 356	AA 6061
AA 357	AA 535
AA 319	AA 388

After successful production of development castings, the production viability of the equipment and process will be demonstrated. This will be done by:

- Production of a connecting rod with reduced porosity and improved mechanical properties as compared to the current die-cast connecting rod used by Bendix.
- Continuous production with the ASC machine and connecting rod tooling to include at least one 5-h continuous run with the equipment running at least three days in a week.

The goal of the project team is to implement part production on an ongoing basis. The production phase of the project will include detailed cost analysis of part production, determination of die-life parameters, and ongoing equipment and tooling development for maximum uptime.

Program Schedule

The revised scheduled start and end dates for the various program tasks are listed in Table 2.

Table 2. Overall program schedule (revised).

Program Task	Start Date	Finish Date
Machine design	June 2003	Feb. 2004
Machine build	Mar. 2004	Nov. 2004
Tooling design	July 2003	Oct. 2003
Tooling build	Nov. 2003	Mar. 2004
Process Model	Oct. 2004	Dec. 2004
In-gate S.O. development	Nov. 2003	Dec. 2003
Machine install	Nov. 2004	Nov. 2004
Casting development	Dec. 2004	Dec. 2005
Evaluation & Testing	Jan. 2006	Mar. 2006
Final Report	Jan. 2006	Mar. 2006

Program Status

ASC Machine. The design (Figure 1) for the 600-ton capacity ASC machine has been completed. Positioning of the top die is accomplished independently of the squeeze-cast cylinder. To

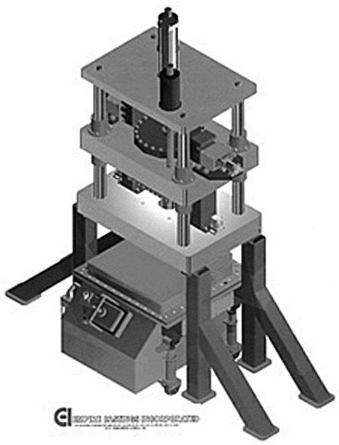

Figure 1. Design for 600-ton ASC machine.

maximize machine capability, the melting vessel is equipped with a crucible furnace. This facilitates the melting of both cast and wrought aluminum and magnesium alloys as well as aluminum and magnesium metal matrix composite alloys.

To match the dimensional capabilities of the die-cast process, a closely controlled volume of liquid metal must be fed into the die cavity. Conventional low-pressure fill technology does not have the capability to accurately meter a fixed amount of liquid metal into the die. Therefore, we will accurately position (± 0.13 mm) the top die to obtain the desired fill volume and use a fill sensor and an independently controlled gate shut-off to control metal volume. Development of a reliable gate shut-off technology is a key part of the experimental program. Gate shut-off system components are shown in Figure 2.

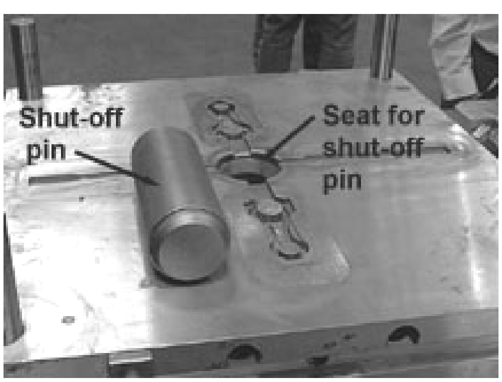

Figure 2. Components of in-gate shut-off system.

The machine (Figure 3) has been installed at Eck Industries, Inc., Manitowoc, WI.

Data Acquisition System. A computerized data acquisition system has been designed to interface with the displacement, pressure and temperature sensors located on the ASC press and cast tooling. Analysis of these data will be critical in understanding the operation of the ASC process. A plot of a typical data set is shown in Figure 4.

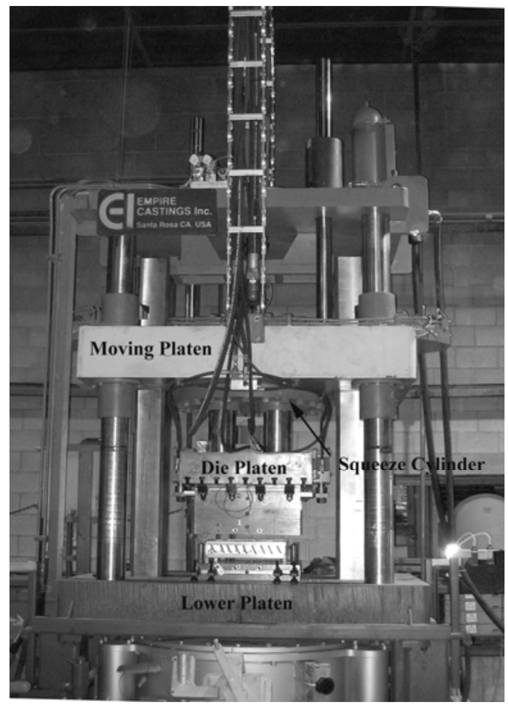

Figure 3. ASC Machine installed at Eck Industries, Manitowoc, WI

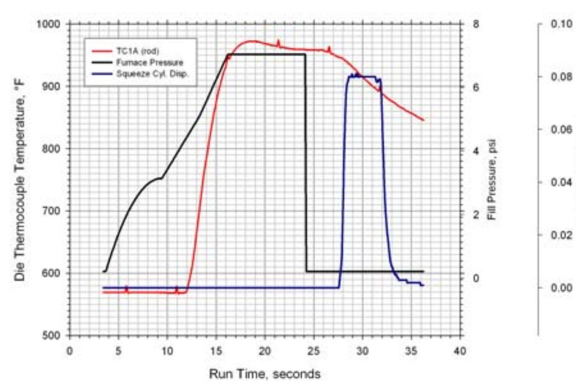

Figure 4. Typical data obtained from data collection system during casting runs.

Cast Tooling. The die for casting air-compressor connecting rods and tensile test bars has been completed. As shown in Figure 5, the tooling consists of a die holder and individual die inserts for the particular part being cast. This tooling will be used for process development and the machine run-off trials.

Process Development. Early development trials demonstrated that the use of temperature data from the thermocouples installed in the tooling does not provide consistent operation of the ASC machine. Therefore, the PLC program was modified to control sequencing of the machine operations by a combination of adjustable timers and thermocouple inputs from the tooling. Thermocouple inputs are used to initiate the sequence and determine when the die is opened after the squeeze pressure application has been completed. All other functions are controlled by timers.

This modification to the machine's PLC program was proven successful by the sequential accomplishment of 40 castings. A typical casting is shown in Figure 6. A few connecting rod castings have been machined to determine if the as-cast dimensions meet Bendix's requirements. Figure 7 shows a machined connecting rod and an as-cast part after the gating has been removed. The connecting rod castings meet the part dimensional requirements.

Preliminary tensile data (see Table 3) show the ASC processed alloy to have about the same properties permanent mold cast material of the same chemistry but the elongation values are significantly higher. The higher elongation value may be the result of either smaller grain size because of the higher solidification rates or lower porosity levels.

Figure 5. View of cast tooling.

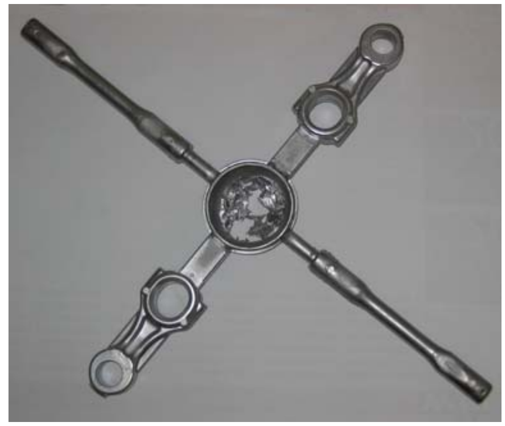

Figure 6. Typical casting from 40 shot run.

Figure 7. Machined (left) and as-cast (right) connecting rod parts.

Table 3. Preliminary mechanical property results.

B356-T6	LPPM Cast	ASC Cast
Ultimate Strength, ksi	39.0	41.8
Yield Strength, ksi	26.6	25.7
Percent Elongation	5.8	15.5

Conclusions

Good progress has been made on the project. Consistent operation of the ASC machine has been obtained. Casting trials are in progress to develop the specific parameters needed to produce test bars and connecting rods from which mechanical properties and performance data may be obtained. As shown in Table 2, the schedule has been revised to reflect expected completion dates.

C. Wrought Magnesium Alloy/Process Development

Principal Investigator: J. A. Horton
Oak Ridge National Laboratory
P.O. Box 2008, Oak Ridge, TN 37831-6115
(865) 574-5575; fax: (865) 574-7659; hortonja@ornl.gov

Principal Investigator: S. R. Agnew
University of Virginia
116 Engineer's Way
P.O. Box 400745, Charlottesville, VA 22904-4745
(434) 924-0605; e-mail: agnew@virginia.edu

Chief Scientist: James J. Eberhardt
(202) 586-9837; fax: (202) 586-1600; e-mail: james.eberhardt@ee.doe.gov
Field Technical Manager: Philip S. Sklad
(865) 574-5069; fax: (865) 576-4963; e-mail: skladps@ornl.gov

---

Contractor: Oak Ridge National Laboratory
Contract No.: DE-AC05-00OR22725

Objectives

- Develop wrought magnesium alloys with better formability than current magnesium alloys.
- Investigate new processing techniques for cost reduction and formability improvement.
- Contribute to basic understanding of deformation, processing, and alloy behavior for this lightweight metal.

Approach

Explore new processing schemes for magnesium alloy sheets; evaluate the practical formability of new alloys and after new processes; determine deformation mechanisms using experimentation and simulation.

Accomplishments

- Devised a new approach to substantially reduce texture development utilizing rare earth additions and a recrystallization step during hot rolling processing.
- Completed infrared rolling study on narrow strips of Mg sheet removed at various points during a commercial processor's rolling schedule.
- Found significant 0002 texture formation after hot rolling at temperatures from RT to 450°C.
- Demonstrated roll bonding as a technique to reduce grain size. Good metallurgical bonds were produced.
- Demonstrated feasibility of infrared processing of twin roll cast Mg sheet in collaboration with Norsk Hydro.
- Performed a study of the effect of grain size on deformation mechanism in alloy AZ31B. Found surprising result that mechanical twinning contributes significantly to tensile behavior of coarse-grain sheet.

Future Direction

- Interact with an industrial partner to advance commercialization of infrared processing for cost reductions.
- Define further correlations of microstructure, mechanisms, and anisotropy. In particular, define the kinetics and crystallography of recrystallization in magnesium alloys.
- Further explore superplastic-type behavior observed at warm forming temperatures.
- Investigate fundamental parameters affecting castability of the more creep-resistant alloys.

Introduction

Magnesium, with a density 66% of aluminum, has obvious advantages for use as a structural material in the transportation industry. Magnesium castings are steadily growing in use in autos and trucks. However, wrought applications are held back by the high cost of sheet due to the large number of processing steps. This project is currently focusing on processing techniques and issues to reduce the cost of sheet magnesium. In addition, we are continuing to investigate formability issues of sheet magnesium.

Infrared Processing Study of Magnesium Strip

Strips of magnesium sheet were extracted from midway thru the processing route from a commercial magnesium producer, Magnesium Elektron Corp (MEL). These strips were readily processed using infrared lamps and subsequent rolls in a lab table top setup. Grain size and properties were tracked. However, it was concluded that the widths used, ~50 mm, was insufficient to replicate commercial practice. A scale up to strips approximately 30 cm is planned.

0002 texture formation after hot rolling

Texture in hexagonal magnesium is unfortunately easily developed during thermomechanical processing thereby reducing fabricability. Many processing routes have been investigated to produce material with reduced texture. The following experiment was performed to find out if there was an optimum rolling temperature. AM60 was cast into a rectangular mold and then annealed 24 hr at 413°C. Three mm thick slabs were cut from this casting. This starting material had no 0002 texture. The slabs were then pack rolled one time sandwiched in stainless steel to retain the heat. The conditions were either 34% at 250°C, 42% at 350°C, or 54% at 450°C. Texture determinations were then performed, see Figure 1.

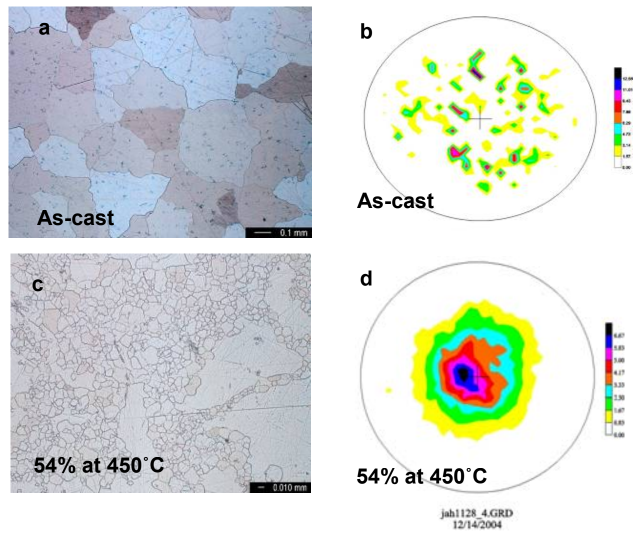

Figure 1. Optical micrographs and 0002 pole figures showing the degree of texture developed in just one pass at 450°C.

The intensity is approximately half of that of rolled commercial sheet after many trips through the rolling mill. The results from 250, 350 and 450°C were nearly identical. Just one pass through a rolling mill produces a substantial amount of 0002 texture. 450°C is a practical limit for such processing in air without running a risk of a runaway exothermic reaction.

Accumulative Roll Bonding

Commercial AZ31 sheets were roll bonded together (see Figure 2). This process results in severe plastic deformation which leads to a refinement of the microstructure and improvements in the mechanical properties. This technique is relatively simple and can be applied to large sheets. A maximum of 6 passes; resulting in a 64 layer bond was successfully achieved with approximately 60% reduction per pass. AZ31 was also roll clad with Al-alloy 6061 and good bonding was achieved.

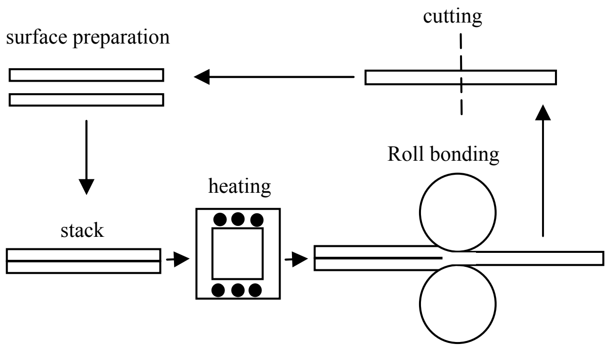

Figure 2. Schematic diagram of the accumulative roll bonding process

Roll bonding resulted in dynamic recrystallization (DRX) and a fine equiaxed grain size (down to 1 µm), see Figure 3. The bonding line is a very thin non-continuous oxide film in the Mg only bonds, in some areas grains appear to have grown across the bonding line. In tensile testing no delimitation of the bonds was observed. In the roll clad Mg-AL sample an intermetallic layer appears on the bonding line (Figure 3b); from EDS analysis it is likely that this is $Mg_{17}Al_{12}$. In tensile loading no delimitation resulting from the brittle intermetallic layer was observed.

The mechanical properties of the roll bonded/clad specimens are given in Table 1. The high temperature mechanical properties of the roll bonded specimens shows a remarkable improvement over the original material. Improvements in the roll bonding process shows potential to improve the mechanical properties and formability of magnesium alloys. Roll cladding of magnesium alloys should also be further investigated; this process may be used to improve the mechanical, physical and chemical properties of the alloys.

Twin Roll Cast Mg rolled to sheet using infrared heating

Direct twin roll cast Mg sheet with dimensions approximately 30 cm wide and 6 mm thick was obtained from Norsk Hydro. This material was further rolled down to 1 mm thickness using quick infrared lamp anneals and heating to 415°C between 20% reduction passes. Figure 4 shows the optical microstructure after the 7th pass and a 1 mm in thickness. Use of twin roll casting and infrared heating could together substantially reduce the cost of Mg alloy sheet.

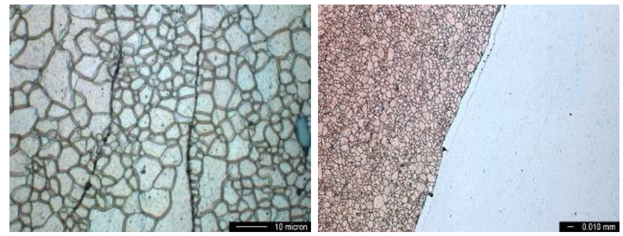

(a) (b)

Figure 3. Optical micrographs of (a) AZ31 64 layer roll bond. Three layers can be seen in the figure; the layer thickness is 20-50 µm. and (b) cross section of Al-Mg-Al roll clad sample, the etched microstructure is AZ31 and Al-alloy 6061 is unetched.

Table 1. Tensile properties of the roll bonded samples at room temperature (RT) and at 400°C tested parallel to the rolling direction at a strain rate of 1x10-3 s-1.

	RT		400°C	
	ε_f (%)	UTS (MPa)	ε_f (%)	UTS (MPa)
AZ31-H24 (original material)	12.2	294.5	37.9	20.5
AZ31-64 layers	9.0	234.0	137.9	22.6
Al-Mg-Al	15.2	199.5	64.8	29.5

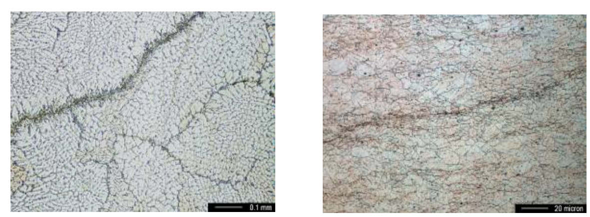

(a) (b)

Figure 4. Optical micrographs of twin roll cast as cast (a) and after rolling 7 times with infrared anneals (b) to 1 mm thickness.

Equal channel angular extrusion (ECAE)

At the University of Virginia, we have been completing our examination of equal channel angular extrusion of magnesium alloys to close two studies. One is a close examination of the texture evolution enforced by ECAE upon 5 different wrought magnesium alloys (AZ31, AZ80, ZK60, WE43, and Mg-4wt%Li.) The texture evolution of these alloys was modeled using a polycrystal plasticity code, enabling inferences regarding the deformation mechanism activity of the different alloys to be made. In terms of their texture evolutions, the alloys may be classified into three groups, the zirconium-, the aluminum-, and the lithium-containing. Based upon the modeling, these appear to be connected with a preference for slip of <c+a>, balanced non-basal <a> and <c+a>, and non-basal <a> dislocations, respectively. It is also mentioned that the texture evolution of the WE alloy is particularly unique, in that it possesses a rather weak texture throughout its processing history. (This latter result was an important finding that went unnoticed until recently and corroborates other findings reported below.) These studies have resulted in two journal publications listed at the end of this report.

In addition to examining the structure of magnesium alloys subjected to ECAE, we have continued to examine the mechanical properties, as a follow-up to our previously published work on the ductility enhancement of alloy AZ31. We have elected to examine the ductility enhancement of a heat-treatable magnesium alloy, AZ80. Although the highest magnitude of the obtained ductility is less impressive in this alloy (~28% vs. ~40%), the magnitude of the improvement over conventional processing (~2.5 times) is similarly impressive. Again, there appears to be a strong connection between the ductility enhancement and an unusual texture which results from ECAE processing. Age-hardening of the ECAE processed material succeeds in improving its strength; however, the combined property set (strength and ductility) is not superior to that obtained by conventional processing methods. This study has been submitted for publication and is presently in revision.

Effect of Grain Size Deformation Mechanisms of Magnesium Alloy AZ31

Beginning with the relatively small grain size of recrystallized AZ31 sheet (~13 μm), samples were annealed at high temperatures (up to 525°C) for a range of times to produce grain sizes up to 220 μm. Not surprisingly, the increase in grain size led to a decrease in both strength and ductility. Figure 5 shows that the data obey traditional expectations for the grain size dependence of yield strength, albeit with the effect of anisotropy superimposed.

Our study focused on the effect of grain size on the strain anisotropy, since our earlier investigations of sheet anisotropy had shown a link between strain anisotropy and deformation mechanism activity.

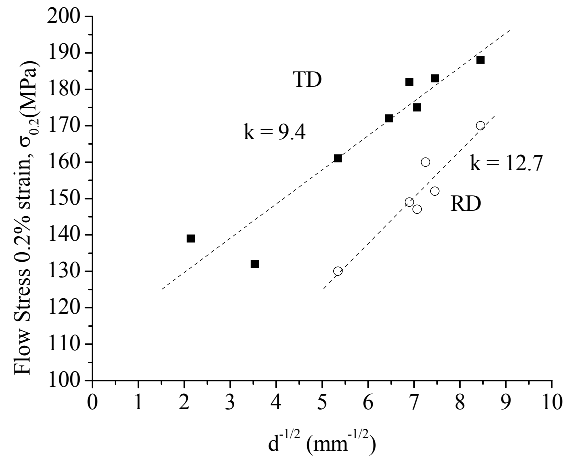

Figure 5. Hall-Petch plot of AZ31B strengths along the rolling (RD) and transverse directions (TD).

As a measure of anisotropy, we have relied on measurements of r-value, the ratio between Poisson strains along the sheet thickness direction and the sample width directions during a tensile test. Initially, it was found that the strain anisotropy after 11% tensile strain was virtually unaffected by grain size. We instituted the capability to measure the r-value evolution *in-situ*, and this provided a completely different picture (Figure 6). The instantaneous r-values increase with increasing grain size. Interestingly, {10.2} tensile twinning appears to be responsible, despite the fact that the texture and imposed stress direction would appear to preclude activation of this mechanism during these tensile tests.

The observations of this study, as well as those of a parallel study sponsored by the National Science Foundation, suggest that certain types of mechanical twinning are potential aides to ductility (note ECAE results above) while other types of twinning may serve as failure mechanisms. Control of the texture and grain size has been a consistent theme of our research program and the present results further emphasize the need to pursue this goal to control the influence of mechanical twinning mechanisms.

Neutron Diffraction Studies of Deformation Mechanisms of Magnesium

In-situ neutron diffraction techniques have been used to determine the internal stresses that develop within magnesium alloy AZ31 under load. Using an

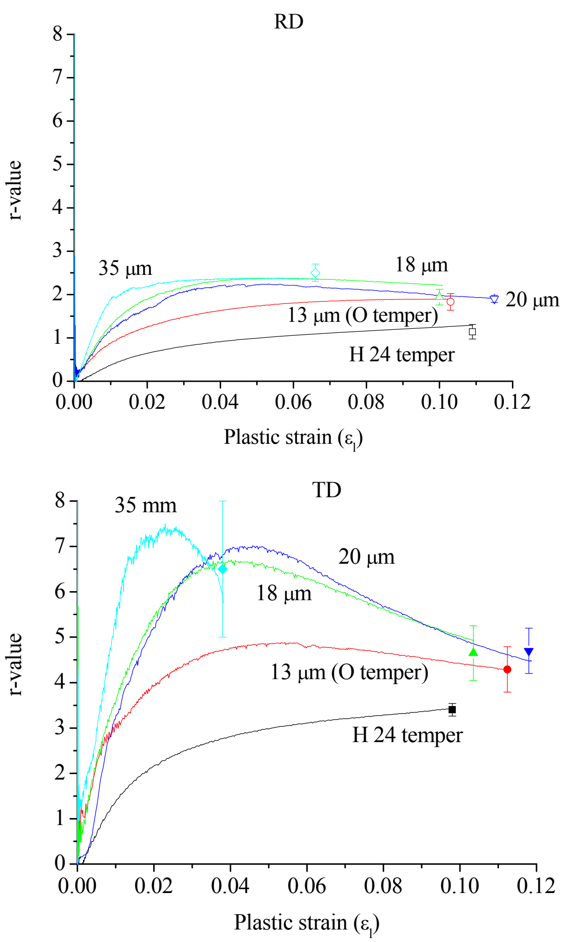

Figure 6. Measured r-value evolution with strain for samples tested along the (RD) rolling direction and (TD) transverse direction with different grain sizes.

inverse method involving an internal stress data have been used to assess the critical stresses and activities of the various deformation mechanisms with magnesium alloys. Specifically, we have used neutron diffraction to compare conventional and ECAE processed material. These experiments provided further evidence in support of the hypothesis which we published previously, that due to the unusual ECAE texture, the soft mechanisms (basal slip and mechanical twinning) are able to accommodate the imposed strain. Because this keeps the flow stress low, it helps to explain why the ductility is enhanced in this material which appears to fail at a critical stress level. Not only have these results been useful for developing a greater understanding of magnesium, the data have also served an important role of validating a modeling code (EPSC) which is of use for many materials.

Figure 7 shows results obtained from a larger grained sample of AZ31 sheet from the grain size study described above. The ex-situ (00.2) pole-figure data indicate that mechanical twinning has taken place (Figure 7a); however, it was initially unclear if the twinning happened during the deformation or during unloading. The in-situ measurement of the (00.2) diffraction peak intensity shows that the twinning was indeed happening during the deformation. As discussed above, this is a much unexpected result, given the crystallography of twinning and the stressing direction. However, they will provide a basis for determining why twinning is so pervasive in magnesium alloys under straining conditions where twinning is unexpected (i.e., during rolling of sheet, during tensile deformation of rolled sheets, extrusions, etc.).

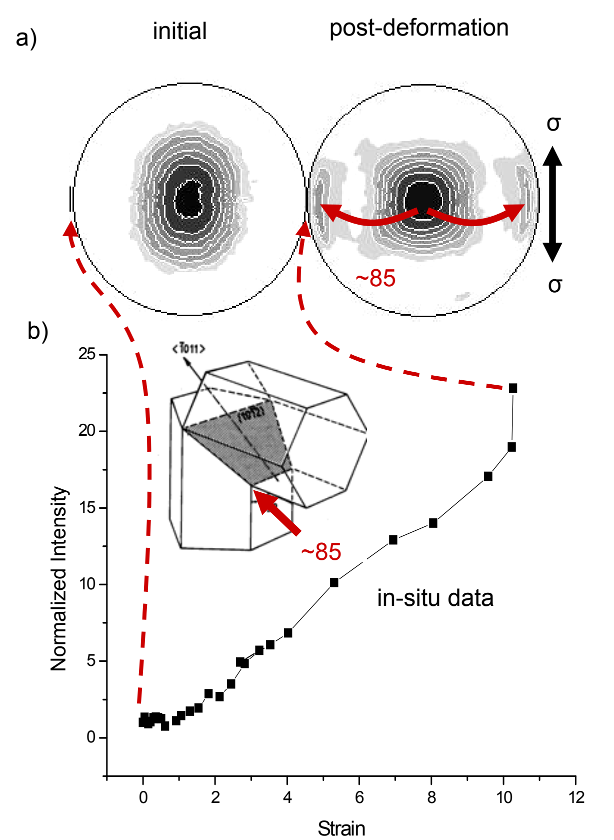

Figure 7. a) Initial and post-deformation basal (00.2) pole figures from tensile tests show evidence that twinning has occurred within grains of the dominant texture component. b) (00.2) diffraction peak intensities obtained using in-situ neutron diffraction show that the anomalous twinning occurs during the deformation, not after.

Wrought Alloy Development

Our work in past years has demonstrated that the mechanical behavior of magnesium alloys is strongly affected by crystallographic texture because of the intrinsic plastic anisotropy of the hexagonal close packed crystal structure. Indeed, conventional Mg alloy sheets exhibit strong textures (with basal planes parallel to the sheet plane) with little variation from one alloy to another. We have used this fact to our advantage to selectively study the mechanisms of plastic deformation, such as the study of twinning described above. However, it is certain to affect a positive change in the performance if the texture could be qualitatively altered. In fact, Dow Magnesium offered "special bending sheet" in years past, which was nothing more than a texture-altered alloy AZ31-O temper that had much better forming characteristics than conventional sheet (e.g., critical bending radius of 5 times the sheet thickness, versus 3 times.)

Until recently we had not devised a practical scheme to alter the strong textures that evolve during deformation processing. As described earlier in this report, we recently explored the effect of hot rolling at various temperatures and various recrystallization treatments at Oak Ridge National Laboratory (ORNL). Although there was some quantitative variation in the texture, the textures were all qualitatively the same, and did not promise to quantitatively alter the forming behavior.

It has been reported that alloy WE54 containing significant additions of expensive alloying additions, yttrium (W) and rare earth (E) elements, develop much weaker textures during extrusion than conventional alloys, and that the undesirable tension-compression strength asymmetry which plagues most magnesium extrusions was effectively eliminated [E.A. Ball and P. B. Prangnell, "Tensile-compressive yield asymmetries in high strength wrought magnesium alloys," Scripta Metall. Mater., 31 (1994) pp. 111-116, 1994]. The authors suggested that the result might be related to particle-stimulated nucleation of randomly oriented grains during recrystallization. More recent doctoral research of Luke Mackenzie at the University of Manchester on similar alloys provided more evidence that recrystallization phenomena were responsible for the texture randomization [G.W. Lorimer, L.W.F. Mackenzie, F.J. Humphreys, and T. Wilks, "The Recrystallization Behavior of AZ31 and WE43," Mater. Sci. Forum, 488-489 (2005) 99-102]. A new member of the project team, Jeremy Senn, has devised a plane strain compression fixture for enforcing rolling type deformation under controlled temperature and strain rate conditions. His recent results from WE53 confirm strong texture development during hot-rolling conditions and a very weak texture after recrystallization (Figure 8). These results suggest an avenue to improve the formability of Mg sheets by through careful alloying and thermomechanical treatment.

Finally, we have begun collaborating with researchers at the GKSS, Geestacht who provided us with a number of experimental alloys, which had been warm rolled in their facilities or by an industrial partner. These alloys are very different in composition from the ones mentioned above, yet have very weak textures, in comparison with conventional alloys, ZM21 containing Zn and Mn (or AZ31). Their mechanical behavior is very distinct from AZ31 on which we have focused in the past (some alloys are more ductile, and all exhibit much lower strain anisotropy.) Similarly, a press release from Primo Metal in Korea boasted the best warm forming behavior of any wrought magnesium alloy. They have sent us sheet samples and we have verified that this alloy has a very weak texture, and

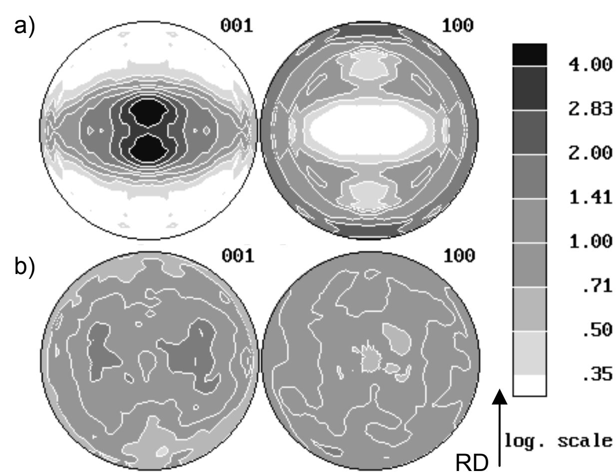

Figure 8. Textures measured in alloy WE53 produced at ORNL show a) strong texture after hot-rolling type deformation and b) very weak texture after recrystallization annealing of the same.

low strain anisotropy. Again, there does seem to be a path towards a sheet alloy with better forming characteristics.

Publications and Presentations

A. L. Bowles, Q. Han, J. A. Horton, "Castability of Magnesium Alloys" *Magnesium Technology 2005,* ed. by N. R. Neelameggham, H.I. Kaplan, and B.R. Powell, TMS (2005) 99-104.

J.A. Horton, C.A. Blue, T. Muth, A.L. Bowles, S.R. Agnew, "Infrared Processing of Magnesium Wrought Alloys" i*bid.,* 155-158.

S.R. Agnew and O. Duygulu, "Plastic Anisotropy and the Role of Non-basal Slip in Magnesium Alloy AZ31," *Inter. J. Plasticity*, 21 (2005) 1161-1193.

S.R. Agnew, D.W. Brown, and C.N. Tomé, "Validating a Polycrystal Model for the Elasto-Plastic Response of Magnesium Alloy AZ31 Using In-situ Neutron Diffraction," *submitted to Acta Mater.*

S.R. Agnew, P. Mehrotra, and T.M. Lillo, "Equal Channel Angular Extrusion of a Heat Treatable Magnesium Alloy," *Scripta Mater.*, *in revision*.

S.R. Agnew, P. Mehrotra, T.M. Lillo, G.M. Stoica, and P.K. Liaw, "Crystallographic Texture Evolution of Three Wrought Magnesium Alloys During Equal Channel Angular Extrusion," *Mat. Sci. Eng. A*, **408** (2005) 72-78.

S.R. Agnew, P. Mehrotra, T.M. Lillo, G.M. Stoica, and P.K. Liaw, "Texture Evolution of Five Wrought Magnesium Alloys During Route A Equal Channel Angular Extrusion: Experiments and Simulations" *Acta Mater.,* **53** (2005) 3135-3146.

D.W. Brown, S.R. Agnew, M.A.M. Bourke, T.M. Holden, S.C. Vogel and C.N. Tomé, "Internal Strain and Texture Evolution During Deformation Twinning in Magnesium," *Mat. Sci. Eng. A*., **399** (2005) 1-12.

D.W. Brown, S.R. Agnew, S. Abeln, W. Blumenthal, M.A.M. Burke, M. Mataya, C.N.Tome, and S.C.Vogel, "The role of texture, temperature and strain-rate in the activity of deformation twinning," *Mat. Sci. Eng. A,* **495-497**, (2005) 1037-1042.

Presentations w/o Publication

S.R. Agnew, O. Duygulu, and A. Jain, "Using Polycrystal Plasticity Simulation to Explore the Behavior of Wrought Magnesium Alloys," presented at "Plasticity 2005", Kauai, Jan. '05.

S.R. Agnew, O. Duygulu, and A. Jain, "Developing Mechanism-Based Models of the Mechanical Behavior of Wrought Magnesium Alloys" U. of Michigan, Dept. MSE Seminar Series, Ann Arbor, Feb. '05.

O. Duygulu and S.R. Agnew, "Grain Size Effects on Deformation Mechanism Activity in Magnesium Alloy AZ31B", presented in the Magnesium Technology 2005 Symposium, TMS Annual Meeting, San Francisco, CA, Feb '05.

S.R. Agnew, D.W. Brown, and C.N. Tomé, "Neutron Diffraction Study of Deformation Mechanisms in Magnesium Alloy AZ31B," presented in the Symposium on Neutron Diffraction Characterization of Mechanical Behavior, ibid.

S.R. Agnew, A. Jain, and O. Duygulu, "Modeling the Temperature Dependent Effect of Twinning on Mechanical Behavior of Magnesium", 10th International Symposium on the Physics of Materials, Prague, Czech Republic, Aug '05.

D. Thermomechanical Processing of Ti and Ti-6Al-4V Sheet and Plate from Low Cost Powders

Principal Investigator: Craig A. Blue
Oak Ridge National Laboratory
Oak Ridge, TN 37831-8063
(865) 574-4351; fax (865) 574-4357; e-mail: blueca@ornl.gov

Field Project Manager: William H. Peter
Oak Ridge National Laboratory
Oak Ridge, TN 37831-8063
(865) 241-8113; fax (865) 574-4357; e-mail: rivardjd@ornl.gov

Chief Scientist: James J. Eberhardt
(202) 586-9837; fax: (202) 587-2476; e-mail: James.Eberhardt@ee.doe.gov
Field Technical Manager: Philip S. Sklad
(865) 574-5069; fax:(865) 576-4963; e-mail:skladps@ornl.gov

Participants:
Evan K. Ohriner, Oak Ridge National Laboratory
David C. Harper, Oak Ridge National Laboratory
Jim O. Kiggins, Oak Ridge National Laboratory
Paul A. Menchhofer, Oak Ridge National Laboratory
Lance Jacobsen, International Titanium Powder, L.L.C.
Dariusz Kogut, International Titanium Powder, L.L.C.

Contractor: Oak Ridge National Laboratory
Contract No.: DE-AC05-00OR22725

Objective

- Investigate and develop vacuum hot pressing (VHP) methods for the production of titanium (Ti) and Ti-6Al-4V plate from Ti and Ti-6Al-4V powder provided by International Titanium Powder, LLC (ITP).
- Demonstrate the ability to extrude rod using powder Ti precursor.
- Mechanically test Oak Ridge National Laboratory (ORNL) – consolidated materials.
- Optically and chemically analyze ORNL-produced materials.

Approach

- Conduct parametric studies using VHP to consolidate ITP Ti and Ti-6Al-4V powder to demonstrate the feasibility of powder use for automotive applications.
- Develop extrusion techniques for the production of Ti and Ti-6Al-4V from ITP powder.
- Characterize ORNL-produced material properties.
- Develop approach to scaling processing techniques for large-scale automotive production applications.

Accomplishments

- A preliminary parametric study of VHP was completed looking at the effect of temperature, stress, and time. Developed minimum limits of stress for the full consolidation of Ti plates.
- CP Ti plates as large as 270 mm in diameter and roughly 9 mm thick were pressed at temperatures between 550°C and 1500°C, and low pressure levels between 0.9 MPa and 5 MPa. These results were compared with previously reported VHP samples [1, 2].
- Ti and Ti-6Al-4V powders were successfully extruded.
- Evaluated physical, microstructural, and chemical properties of ORNL-produced materials.

Future Direction

- Partner with ITP and Ametek to scale process to produce Ti and Ti-6Al-4V sheet and plate at substantially reduced cost using pneumatic isostatic forging and extrusion processes as a basis for commercial processing.
- Partner with Universal Alloy Corporation to extrude ITP Ti and Ti-6Al-4V rod and plates up to 40 in. wide.

Introduction

The aircraft industry is currently the single largest market for Ti and Ti alloy products primarily because of the exceptional strength-to-weight ratio, elevated temperature performance, and corrosion resistance.

Titanium usage, however, is strongly limited outside the aerospace industry by its higher cost relative to competing materials, primarily aluminum alloys and steels. Although Ti possesses an attractive set of properties, including high specific strength and corrosion resistance, and allows for damage-tolerant design, cost limits applications to selected markets. Many automotive systems would benefit from the use of Ti products. Automotive exhaust systems could save as much as 50% of their current weight by integrating Ti parts. Titanium valves and valve springs, connecting rods, suspension springs, wheels, drive shafts, underbody panels, side impact bars, and half shafts are just some of the automotive applications that could benefit from the use of Ti.

The present market comparison for the use of engineering materials shows that steel is the most widely used material, with 800 million tons used each year. Aluminum, stainless steel, and copper are used at a rate of 22 million tons, 16 million tons, and 12 million tons, respectively. Titanium is much less widely used at 0.05 millions tons per year.

Potential technical problems preventing the integration of Ti, apart from cost of manufacturing, include wear resistance, a lower modulus than steel, and machining difficulties. Wear resistance can be addressed by coatings/reinforcements; the modulus can be increased by reinforcing the part with a second material; and the machining difficulties can be reduced by the production of near-net-shape parts. The major problem is that Ti costs substantially more than competing materials.

Although the cost of Ti ore is significantly more than that of other competing materials, the difference in the cost of sheet is a result of processing. Processing of Ti from ingot to plate accounts for 47% of the total cost of the material.

Current melting techniques include vacuum arc remelting (VAR), electron beam melting, and plasma arc single-melt processes. VAR is used to consolidate feedstocks, improve homogeneity and refine grain size. To VAR-cast an ingot, a dc arc is struck between a Ti electrode and a base plate. The intense heat melts the electrode, and the Ti is cast into an ingot. VAR requires 20 hours and large-scale equipment.

Electron beam and plasma arc single-melt processes have the advantage over VAR in increased use of low cost scrap and improved removal of high density and low density inclusions. In these two processes, ingots are cast directly from melted feed sponge, alloy additions and scrap. But the cast ingot still requires post-processing, which accounts for 47% of the total cost.

Alternative processing methods such as casting, laser forming, and spray forming have also been explored. Casting is best suited for complex shape forming and is not economical for sheet processing. The process requires extensive tooling and frequent inspections. A post–hot isostatic pressing (HIP) is needed to eliminate porosity. Laser forming uses a raw powder stream injected into a rastered laser beam to melt, form, and build up sheet. Spray forming operates similarly, although a plasma torch melts the powder. Laser forming and spray forming have the advantages of using less material, requiring minimal tooling, and needing short cycle times. But it is difficult to control the thermal history of laser forming, and both methods suffer from residual porosity. In addition, both of these methods require conventionally produced and atomized powder, which is very costly.

Although much time and effort has been invested in the development of these processing techniques, the cost of Ti still remains high because of the cost of raw materials, cost of post-processing, and yield losses. Previous work performed at the Infrared Processing Center at ORNL, focused on the consolidation of low-cost Ti powder via preliminary VHP studies, high-density infrared (HDI) processing, and simulated roll compaction processing [1,2]. Recently, the Materials Processing Group at ORNL has investigated VHP of moderately sized parts at low pressures and extrusion of CP Ti and Ti alloys. Both processing methods used powder provided by ITP. ITP has developed a new low-cost method of powder production and is currently running a pilot processing facility.

Experimental Procedure

ITP Ti powder was processed into rod, flat stock, and plate using two methods, extrusion and VHP techniques. An off-stoichiometry alpha-beta ITP Ti alloy (used to establish processing parameters) and limited Ti-6Al-4V were processed into rods using extrusion techniques. Metallography, chemical analysis, and mechanical evaluation of the CP Ti extrusion followed. Metallography was performed on the Ti-6Al-4V extrusion sample, but limited powder prevented sufficient material for mechanical evaluation.

VHP, a batch process, was used to make Ti plates for the prototype production of Ti-brake rotors. VHP was used to make nine - 267 mm diameter Ti discs, 9 mm in thickness. Each sample was pressed under vacuum in a graphite element radiant furnace. For each of the pressing operations, the die was lined with Grafoil and around 1900 grams of Ti powder was poured into the die. Two independent production batches of low cost Ti from International Titanium Powder were used for the VHP evaluation. These runs were also separate from powder previously mentioned in the FY04 annual report [2]. To prevent mechanical interaction between air and the powder, no pre-pressing was applied until after a vacuum was pulled. A special collar was placed under the die to keep it in place while the powder was being pressed. When the rams were jogged into place, the furnace was closed, sealed, and evacuated. The furnace was back-filled with argon gas and evacuated three times in order to ensure a clean processing environment. The Ti samples were pressed at low pressures, between 0.8 and 4.9 MPa, and temperatures between 580 and 1500 ^{o}C. All samples were allowed to furnace cool after the heating cycle was completed. After the samples were removed from the furnace, the sample surfaces were sand blasted, and the densities were measured by immersion in ethanol (Archimedes method). Tensile specimens were machined out of several of the VHP discs. Mechanical testing, chemical analysis, and optical microscopy were performed. Mechanical testing was performed on plate specimens with a testing gauge section of ~1.47 mm in width and ~0.74 mm in thickness. The test gauge length was 20.32 mm. The monotonic tensile testing was performed with a strain rate of ~0.05 in/in·min based on constant cross head speed.

Four CP-Ti samples, one Ti-6Al-4V sample, and three off-stoichiometry alpha-beta Ti alloy samples were extruded. The powder for each extrusion was cold pressed in a 5.1 or 8.9 cm diameter steel can to a green density of approximately 20% of theoretical density. The cans were then electron-beam welded in a vacuum chamber. All samples were extruded on ORNL material processing group's 1250 ton extrusion press. The Ti samples were preheated between 850°C and 950°C for 1.5 hours and then extruded up to a maximum load of 640 tons. The Ti-6Al-4V sample was preheated at 950°C for 2 hours and then extruded at a maximum load of 380 tons. The off-stoichiometry Ti alpha beta alloy cans were preheated at 925°C for 1.5 hours and then extruded up to a maximum load of 410 tons. Table 1 contains the preheat temperature and the die size for all Ti extrusions. Samples were de-canned. Tensile and metallography specimens were made from selected extruded samples. Figure 1 is an image of round and flat bar extrusion stock and tensile specimens made from the CP-Ti extrusions.

Results and Discussion

Successful production of low-cost Ti powder could be beneficial for promoting new, innovative applications that were not realized due to the high cost of Ti. Several of these applications could use the high strength to weight ratios. Brake rotors are one particular application that utilizes titanium for weight reduction. Particularly, vehicular racing, such as sprint car and midget car, utilizes Ti brake rotors to reduce the weight of conventional gray cast iron rotors. In this application, good ductility and corrosion resistance are not necessary. However, moderate plate diameters and strengths are necessary for the service conditions. Wear is a large concern for automotive brake rotors, but common practice is to coat the Ti rotor with a ceramic coating, such as alumina. Therefore, ORNL evaluated the consolidation of low-cost CP Ti powder into 267. mm Ti brake rotors for sprint car application.

A 64 mm and 178 mm fully consolidated plate had previously been produced with low-cost Ti, and was reported in last year's annual report [2]. Furthermore, the 64 mm plate exhibited mechanical properties and metallography comparable to grade 2 CP Ti specimens [1,2,3]. The purpose of this VHP parametric study was to obtain the lowest pressure and temperature required to consolidate large components with strengths comparable to CP grade 2 Ti.

The maximum pressure used in this parametric study, 4.8 MPa, was only approximately 10% of the pressure used to produce the 64 mm sample exhibiting textbook strengths and ductility.

The density of each plate was measured by the Archimedes method, and is listed in table 2, along with any mechanical results obtained and the processing parameters. All of the plates from the first Ti powder production batch were consolidated to 90% of the theoretical density of Ti with the exceptions of trials 1 and 2. Trial 1 was pressed at considerably low pressure, 0.9 MPa; trial 2 was pressed at low temperatures, 580°C. The processing pressure for satisfactory consolidation and strength seems to be a minimum of 1.8 MPa for this batch of

Table 1. Extrusion Parameters for Ti and Ti Alloy Low Cost Powder

Extrusion	Material	Preheat Temperature (°C)	Preheat Time (min.)	Can Diameter (cm)	Die Shape	Die Size (cm)	Extrusio n Ratio	Max. Load (tons)
1-1	CP Ti	885	90	5.1	Round	2.0	6.3	380
2-1	CP Ti	950	90	8.9	Round	4.45	4.0	440
2-2	CP Ti	950	90	8.9	Round	3.25	7.5	490
2-3	CP Ti	850	90	8.9	Round	3.25	7.5	640
3-1	Ti-6Al-4V	950	120	5.1	Round	2.0	6.3	380
4-1	Off Stoich. α-β Ti	925	90	8.9	Round	3.25	7.5	410
4-2	Off Stoich. α-β Ti	925	90	8.9	Round	4.45	4.0	340
4-3	Off Stoich. α-β Ti	925	90	8.9	Rectangular	5.08x1.91	6.4	405

Figure 1. Extruded bars and flat stock after removing the can material and machined tensile specimens.

low-cost Ti powder. Low alpha phase temperatures, e.g., 580°C, are not sufficient for consolidation at low to moderate pressures. Temperatures ranging from near alpha transus temperatures (the alpha transus is around 890°C [3]) to beta phase temperatures seemed to be the best range for consolidation. However, temperatures in the range between 600°C and 850°C were not tested.

The chemistry of the low-cost Ti seems to play a role in the minimum pressure required for consolidation. A second batch of powder was consolidated; this powder would only consolidate to 86% of the theoretical density under similar VHP parameters as the first batch. The results can be seen as trials 8-9. Chemical analysis is being conducted on the two batches to understand the deviation, but a conclusion could not be made before submission of the annual report. Preliminary analysis of the two powders before consolidation did not show any outstanding quantities of oxygen, nitrogen, carbon, and/or iron compared to CP Ti grade 2 ASTM specifications. However, a broader evaluation is being conducted. Powder morphology may also play a significant role, and will be investigated.

The VHP plates showed excellent tensile strength, 545 MPa to 595 MPa. Elongation measured after failure was considerably low for Ti, between 1 to 5%. Once again, high ductility does not seem to be a necessary characteristic for brake rotor application; 1 to 5% is higher than most gray cast iron alloys. The Ti plates pressed from the second batch of powder had lower tensile strengths as would be expected for material consolidated only to 86% of the theoretical density; this material was still close to CP Ti grade 2 strength limitations.

Microstructural investigations were performed on the VHP Ti plates. Samples were cut from the as-pressed plates, mounted, polished, and etched with Kroll's reagent. Figure 2 is an optical micrograph of the VHP trial #3 sample using polarized light. This micrograph was representative of most of the samples where a standard equiaxed alpha Ti microstructure was present. However, porosity is visible throughout the cross section. An increase in the pressing load should eliminate this porosity, and increase the density to the theoretical density of Ti. The porosity could also be affecting the observed elongation.

Table 2. Consolidation results of 267 mm-diameter VHP Ti plates.

Description	Diameter (mm)	Pressure (MPa)	Temperature (ºC)	Time (Hr)	Bulk Density (%)	Alcohol Density (%)	UTS (MPa)	Elongation (%)	Batch
Trial 1 – Low Pressure	267	0.9	865	1	71%	NM[1]	NM[1]	NM[1]	Batch 1
Trial 2 – Low Temperature	267	2.9	580	2.5	85%	NM[1]	NM[1]	NM[1]	Batch 1
Trials 3-7	267	1.7-4.5	885-1250	1-2	90-94%	92-94%	545-595	1-5	Batch 1
Trials 8-9 – Secondary Batch of Powder	267	2.8-4.8	900-1500	1	82-89%	87-88%	338	< 1	Batch 2
ORNL VHP Results of 64 mm Disc [1,2]	64	55.3	900	0.5	100%	100%	614	21	Previous Batch
ORNL VHP Results of 178 mm Disc [1,2]	178	11.7	900	1	100%	100%	614	21	Previous Batch
ASTM Grade 2 [3]	N/A	N/A	N/A	N/A	100%	100%	345	20	N/A

[1] NM = Not Measured.

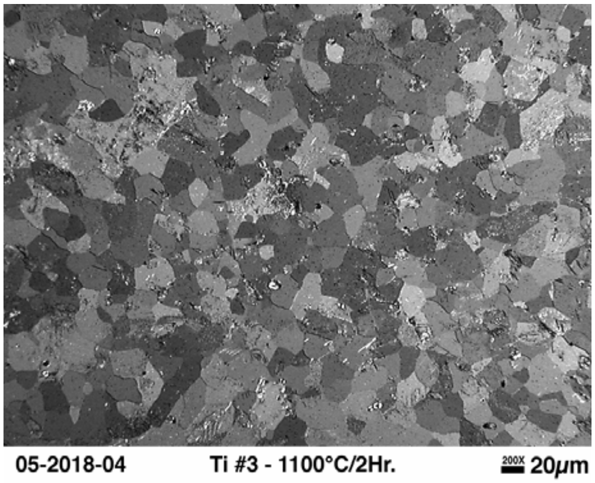

Figure 2. Microstructure for a Ti VHP sample #3.

After pressing, a few of the Ti plates were machined into sprint car brake rotors for demo components. Figure 3 shows an example of one of the plates machined into a disc rotor for sprint car application. The consolidated low-cost Ti powder did not cause any noticeable problems or changes to machining of the Ti components. Future VHP components may be pressed to near net shape, eliminating a great extent of the machining.

The cans with the Ti and Ti-6Al-4V powder were successfully extruded. Microstructural investigations were performed on the as-extruded Ti and Ti-6Al-4V bars. Samples were etched with Kroll's reagent. Figure 4 is an optical micrograph of one of the Ti extruded samples (left) and the Ti-6Al-4V sample (right). Table 2 contains the mechanical properties of the CP Ti sample extruded at 885°C. Other CP Ti samples are in the processes of being tested, but seem to have similar strength and ductility. The extruded low-cost Ti seems to have mechanical properties similar to Grade 2 CP Ti. The Ti-6Al-4V properties were inconclusive due to extremely small amounts of powder utilized and the machining of specimens from the can. Further investigation is being conducted. These results show a strong potential for the extrusion of ITP Ti powder.

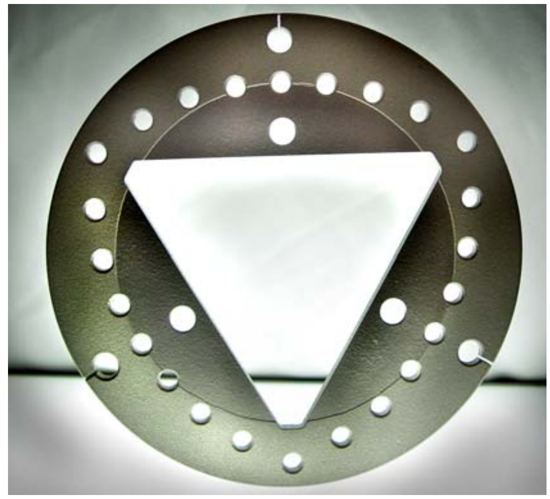

Figure 3. Machined Ti break rotor from 267 mm diameter VHP plate pressed at ORNL.

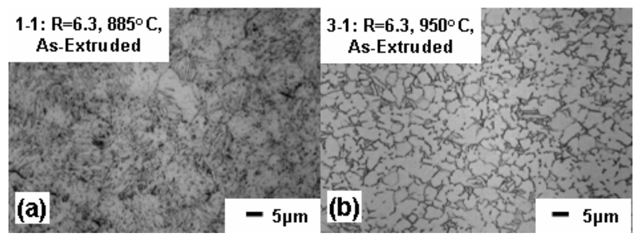

Figure 4. Microstructures for extruded (a) CP Ti and (b) Ti-6Al-4V, both had extrusion ratios, R, of 6.3.

Table 2. Mechanical testing results of as-extruded Ti samples.

Sample	Yield strength [MPa]	Tensile strength [MPa]	Elongation [%]
Extruded Ti 885°C R = 6.3	407	552	17.0
Ti Grade 2	345	448	20.0

Summary

These are the highlights of progress in FY 2005:

1. Production of VHP Ti plates up to 267 mm and the potential to be made into commercial parts.
2. Preliminary results indicate plates consolidated at low pressures can obtain tensile strengths within allowable limits. However, elongation is low compared to fully consolidate CP Ti.

3. Extrusion of Ti and Ti-6Al-4V rod was performed.
4. CP Ti extrusions had similar strength and ductility to Grade 2 CP Ti.

Conclusions

Although Ti and Ti-6Al-4V have attractive properties that would benefit a great number of engineering applications, their use is limited by the cost of the raw material and the processing that is necessary to make a usable product. But with the recent advancements in low-cost powder production at ITP, in conjunction with processing techniques developed at ORNL in collaboration with industry, the cost of Ti products could be drastically reduced. While VHP on a large scale may not be an economical method of plate production, it does demonstrate that ITP powder can produce a viable product, and make substantial parts. On the other hand, the extrusion processing of Ti powder could easily be adapted to industry with already existing equipment. The preliminary study of CP-Ti extrusions seems to produce mechanical properties similar to cast Ti. The ductility and strength of the Ti-6Al-4V was inconclusive due to minimal powder utilized; full investigation of Ti-6Al-4V with sufficient material may result in production of materials with commercial properties. Results suggest that the extrusion and pneumatic isostatic forging of low cost Ti based materials for automotive applications are highly feasible and will be further explored.

References

1. J.D.K. Rivard, C.A. Blue, D.C. Harper, J.O. Kiggans, P.A. Menchhofer, J.R. Mayotte, L. Jacobsen, and D. Kogut. "The Thermomechanical Processing of Titanium and Ti-6Al-4V Thin Gage Sheet and Plate," *JOM*, 57(11), 2005.
2. FY 2004 Progress Report for High Strength Weight Reduction Materials.
3. R. Boyer, G. Welsch, and E.W. Colligs (Eds). Materials Properties Handbook: Titanium Alloys. ASM International. pgs. 165-260, 1994.

E. Counter Gravity (Hitchiner) and Pressure Assisted Lost Foam Magnesium Casting

Principal Investigator: Qingyou Han
Oak Ridge National Laboratory
Oak Ridge, TN 37831-6083
(865) 574-4352; fax (865) 574-4357; e-mail:hanq@ornl.gov

Chief Scientist: James J. Eberhardt
(202) 586-9837; fax: (202) 587-2476; e-mail: James.Eberhardt@ee.doe.gov
Field Technical Manager: Philip S. Sklad
(865) 574-5069; fax: (865) 576-4963; e-mail:skladps@ornl.gov

Participants:
Ralph B. Dinwiddie, Oak Ridge National Laboratory
Pete Angelini, Oak Ridge National Laboratory
Graham V. Walford, Walford Technologies
Ken Currie, Tennessee Technological University
Mohamed Abdelrahman, Tennessee Technological University
Fred Vondra, Tennessee Technological University

Contractor: Oak Ridge National Laboratory
Contract No.: DE-AC05-00OR22725

Objective

The objective of this project is to evaluate the Hitchiner process and pressure assisted lost foam casting of magnesium alloys, in particular, the project will

- Develop the casting system
- Develop low density foams and appropriate coatings
- Establish casting parameters for selected magnesium alloys
- Conduct computer simulations of the process to be used to generate design guidelines
- Validate the process by characterizing microstructure and properties of castings

Approach

- Compare lost foam casting characteristics of magnesium and aluminum at 1 atmosphere
  - Plate casting
    - Flow, mold filling, metal/mold/coating interactions
    - Integrity: porosity, oxide content, microstructure, and mechanical properties
  - Complex casting
    - Castability/integrity/mechanical properties
- Compare lost foam Mg casting with Hitchiner lost foam Mg casting (pressure assistant)
  - Castability/integrity/mechanical properties

- Document the features of the Hitchiner lost foam Mg casting
  - Possible applications, typical features of casting that are suitable for the Hitchiner process, and limitations of the Hitchiner process

Accomplishments

- Melting and casting capabilities have been developed at Tennessee Technological University and Oak Ridge National Laboratory
- Simulation tools have been prepared for the prediction of lost foam castings
- A system has been developed for the selection of foam materials and coatings
- Experiments have been carried out to develop baseline data and to evaluate the lost foam process

Future Direction

- Select/develop coatings and foams for lost foam magnesium casting
- Complete the design of parametric study of the parameters affecting the castability of magnesium alloys
- Start the simulation of the Hitchiner/lost foam process
- Analyze mold filling and molten metal/foam interactions.

Introduction

The last 10 years have seen a dramatic increase in the production and utilization of magnesium. This demand is primarily due to an increase of 20% annually in the use of magnesium in the automobile industry driven by the desire to increase vehicle fuel efficiency by reducing vehicle weight. Magnesium has found uses in several automotive components because of its low density and high strength-to-weight ratio as compared to conventional automotive materials. More recently, magnesium castings have been introduced into pick-up trucks and vans such as the standard size Ford F-150. Additional opportunities exist for the use of magnesium casting in these vehicles, as well as, in heavier trucks. Even with these successes, however, magnesium has not been so widely accepted as it might have been for the following reasons: the cost of the alloys, the lack of long-term field validation or controlled fleet testing data for powertrain components, and lack of a technological base for foundry casting of magnesium alloys.

Magnesium castings are traditionally produced by die casting or precision sand casting. Each of these processes has its advantages and disadvantages for producing components. The major disadvantage of the conventional processes is that certain geometries cannot be produced using steel die sections and are limited by moving cores. In addition, die casting often results in unacceptable levels of porosity. On the other hand, precision sand casting can produce a wide range of shapes with high levels of soundness, but at an unacceptable cost. While successful castings can be manufactured, continuing problems experienced during the casting of the magnesium alloys include porosity formation, oxidation, and hot tearing/crack formation.

In order to take greater advantage of the attractive properties of magnesium, alternative approaches that promise to be more robust and lead to the development and fabrication of larger thinner wall castings must be considered. Lost foam castings can be competitive with other casting techniques for applications with complex internal passages (coring) that can reduce machining, save space, and/or integrate multiple complex features or components into a single casting.

Previous studies at Oak Ridge National Laboratory on gravity lost foam casting of aluminum have determined that many factors affect the quality of the casting outcome. In particular, the metals filling process of the lost foam pattern is greatly influenced by the pattern properties. The advancing metal front decomposes the foam into gaseous and liquid decomposition products that must be eliminated from the casting volume to complete the process.

Pattern density and the pattern gas permeability arising from the combination of the foam and ceramic coating are critical factors in the process, yet are not measured on any commercial process line. Variances in these properties are difficult to control and result in variance in the metal filling behavior. The physical properties of magnesium would increase this problem further. In particular, the low density and latent heat, and the high reactivity of the molten magnesium alloy are serious issues for its castability under lost foam casting conditions.

The problems described above can be overcome by making use of pressure/vacuum assisted mold filling together with closed loop process control. The Hitchiner process, which uses vacuum as a driving force for mold filling, is a logical choice for lost foam casting of magnesium alloys. The change of pressure across the advancing metal front can then be used to accommodate variances in the gas permeability of the foam and coating for the whole pattern and for local variations in the pattern. Pressure can also be used to assist in mold filling.

The challenges of using the Hitchiner process and pressure assisted lost foam Mg casting are in the areas of setting up the experimental equipment for the research, a parametric study of the parameters affecting the processes, development of low density foams for the casting of magnesium alloys, control of permeability of the sand, foam and foam coatings, and the use of controlled atmospheres for reducing metals reactance chemistry and the thermal profile of the pattern to be cast. This article is the first year report of the project. The goal of the first year research was to develop the casting system and to evaluate the existing lost foam casting process for magnesium and aluminum alloys.

The Casting Systems

The existing metalcasting facilities at TTU have been modified for handling molten magnesium alloys and for counter gravity lost foam casting of magnesium alloys. A Thermtronix Solid State Aluminum/Magnesium Electric Resistance Furnace has been purchased and is currently being facilitated for use. It has a 200-300 pound charge capability (depending on whether it is used for magnesium or aluminum) and a special purpose cover made from mild steel has been added to the furnace to allow for introduction of a cover gas to prevent the molten magnesium alloys from reacting with the atmosphere. The cover also has a hinged lid on the very top to facilitate direct insertion of the counter gravity sprue. The Hitchiner counter gravity casting system, shown in Figure 1, has also been successfully tested for aluminum castings. Both a simple flat plate pattern (GM provided) and widget pattern (Foseco Morval provided) were successfully cast using aluminum alloy 319. A 1% Sulfur Hexafluoride – 99% Carbon Dioxide cover gas will be used over the molten magnesium either in the crucible or the furnace. A set of safe operating procedures have been adopted to safely handle and cast magnesium alloys in the current casting facility. However, to better facilitate a safer work environment, an additional 1,200 sq. ft. of foundry space is in the process of being specified and built directly behind the current TTU Foundry facility. An additional $20,000 has been committed from the local AFS Tennessee chapter and the Foundrymen's Education Foundation for supplementing the construction costs. Expected completion of the facility is expected within the next several months. Until the new facility comes on-line, additional safety procedures within the existing foundry are being undertaken to ensure that project deliverables can be met.

Figure 1. The Hitchiner casting system located at TTU.

Foam Development and Selection

A broader study of foam decomposition has been undertaken that seeks to develop a kinetic and thermo-chemical model that describes polystyrene foam decomposition for a broad range of heating rates for oxidizing and non-oxidizing environments. Understanding the foam decomposition processes under different process conditions including foam decomposition in the presence of molten magnesium served as the motivation behind this work. This might help in improving casting quality such as reducing residue entrainment.

A thorough literature search was conducted to find an appropriate kinetic model applicable to the polystyrene foam decomposition phenomena encountered in the lost foam casting process. Results of this investigation indicate that the process conditions in which the available models were developed were very different from the casting process conditions, and hence no one model could be suitably employed for the LFC process. A more rigorous and intrinsic kinetic experiment, depicting the actual foundry conditions, is necessary to develop a model that describes the foam degradation kinetics.

The main purpose of this experimentation is to obtain data on the composition of polystyrene foam degradation products as a function of melt temperatures and processing times. The challenge lies in developing a technique and apparatus for a small-scale kinetic study, which simulates the LFC process conditions and also which eliminates or minimizes the gas phase transients experienced on the commercial scale.

Initially a simple burn chamber using an Infra-red heat source was constructed for these experiments but a more precise reactor concept was conceived. Figure 2 shows the burn chamber to be used. The reactor consists of a heater maintained at a constant surface temperature, an automatic feeder that feeds the foam at a velocity ‘v’ from the automatic feeder, which simulates the actual metal temperature and melt flow rate respectively in the commercial casting process. When the foam impinges on the heater surface, it decomposes and forms various products. These liquid and gaseous products are

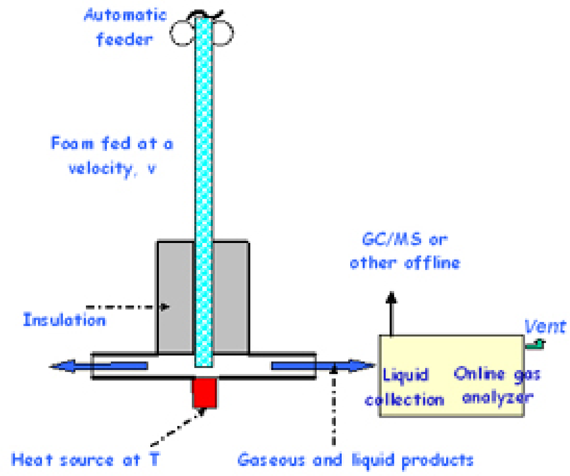

Figure2. The burn chamber for characterizing foam decomposition.

collected and analyzed for their composition. Decomposition data could be collected as a function of both foam push rate and metal temperature. A schematic of the proposed reactor is shown in the figure.

The Reactor heater design considerations include a uniform surface temperature profile on the heater surface, which is very important to carry out this kinetic study. Also, the surface has to be maintained at a steady temperature throughout the process. A “huge” melt (metal anvil) is needed to withstand the high heat of degradation. The heating anvil was modeled in FEMLAB to determine the total power required for the process. A simple anvil geometry was constructed and byusing FEMLAB’s built-in heat transfer modules, a detailed parametric study was performed and the anvil sizing determined. Design of the exit ports of the reactor is currently in progress. Careful attention is paid to reduce the backpressure/pressure inside the reactor by suitably sizing the exit ports. Provisions for the gas inlet are also being considered so that the kinetic study could be performed under different oxidizing and non-oxidizing environments. The effect of materials used for the construction of the heating anvil and insulations are also being studied so as to improve the heater efficiency by reducing heat losses.

In addition to analyzing and modeling the foam decomposition products, another important aspect of this line of research is the gas diffusion modeling and experiments. In order to study the behavior of polystyrene foam under the extreme conditions of very high temperature and high heating rates, it is important to understand the gas diffusion phenomena through the polystyrene foam itself and also when a coating is applied. This would be helpful to suitably manufacture foam so that the gas diffusion could be better controlled. Once this is achieved, the foam decomposition could be controlled by carrying out the process in suitable environments. Although there are some diffusion models available in the literature, they generally do not take into account the heterogeneity present in the foam. A number of factors account for this heterogeneity, including broken cell walls, open channels, fusion level,etc. Hence a multi-scale approach was developed to measure the gas diffusion coefficients through the cell wall (mimicked with a polystyrene film) in order to develop the model for gas diffusion through the foam. By studying the morphology, a suitable entity would be included in the model to account for the heterogeneity in the foam.

Mold Filling and Metal/Foam Interactions

Experiments have been carried out at ORNL for observing mold filling and metal/foam interactions during both aluminum lost foam casting and magnesium lost foam casting at gravity casting conditions (one atmosphere). The purpose was to establish baseline data of lost foam casting at one atmosphere. The data will be used for comparing with data obtained in the Hitchiner process and the pressure assisted lost foam casting process.

Two types of patterns were used: one was a simple flat plate and the other was the GM window pattern. The plate pattern was used for observing mold filling and for evaluating porosity distribution. The window pattern was used for evaluating the castability of alloys. Five types of foam materials from Styrochem were tested: type A (T-17-170, ventless tool), type B1 (T-185, vented tool), type B2 (T-185, ventless tool), type C (T-170, vented tool), and type E (T-185 with Bromated additive, ventless tool). A high permeability coating was used for the testing. Castings of A356 alloy and AM60B alloy were made using the flat plate pattern and the GM window pattern.

Figure 3 shows the effect of casting temperature on the castability AM60B alloy. Castings were made using the GM window patterns made of B1 foam. The pouring temperature or the cast temperature has a major effect on the castability of the AM60B alloy window casting. Cold shot defect occurred at the corner where the metal filled last when the pouring temperatures were around 1400°F to 1450°F. Increasing the pouring temperature reduces the cold shot defect. When the pouring temperature was 1500°F, the cold shot defect was eliminated. However, 1500°F is about 355°F higher than the liquidus temperature of the alloy. Similar window castings were also made using A356 alloy, which has the identical liquidus temperature as the AM60B alloy. All the A356 alloy window castings had no cold shot defect when the pouring temperature was as low as 1400°F. Thus it is more difficult to cast magnesium alloy castings using the lost foam casting process.

An infra-red camera was then used to observe mold filling and metal/foam interactions of AM60B and A356 alloy during lost foam casting. The use of the infra-red camera made it possible to accurately measure the filling time. Figure 4 shows the measured filling times for the flat plate casting and the GM window casting. It took much longer time to fill the lost foam mold for magnesium alloy than that for aluminum alloy. Indeed, the density and the latent heat of magnesium alloy are smaller than that

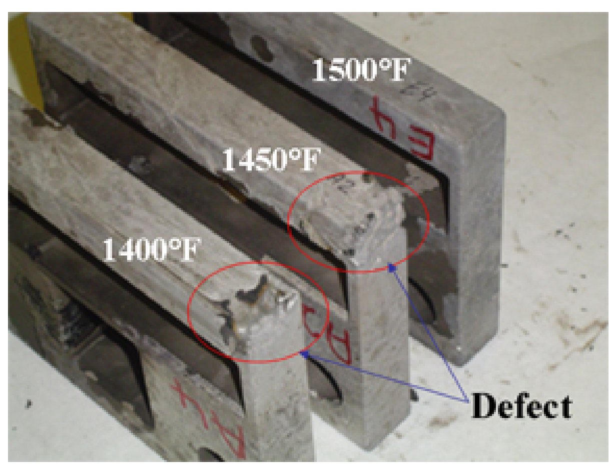

Figure 3. The cold shot defect at the corner of a GM window casting. The corner was the region last filled during mold filling. The defect can be reduced and finally eliminated by increasing the pouring temperature.

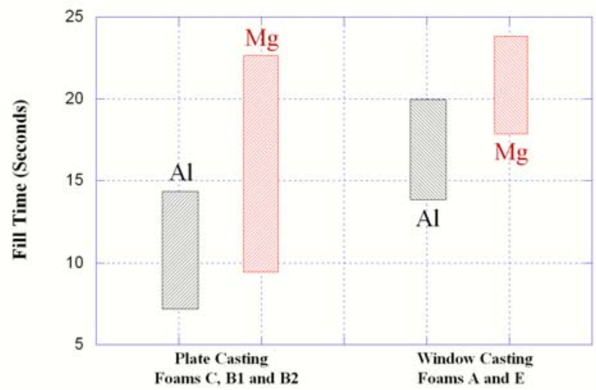

Figure 4. The measured fill time during lost foam casting of AM60B alloy and A356 alloy. The fill time is much longer for magnesium alloy than that for aluminum alloy.

of the aluminum alloy. As a result, less heat is available for the molten magnesium alloy to decompose the foam when compared with aluminum alloy. This accounts for the fact that cold shot defect occurs more easily during lost foam magnesium casting than during lost foam aluminum casting.

The microstructure of the castings were also characterized, especially porosity distributions. Flat plate castings were cut into small specimens. Each specimen was used for density measurement using the apparent density measurement method. Figure 5 shows the density distribution in a flat plate casting of aluminum alloy not degassed. The gate location is at the right side of the plate (x=35 and y=20). The local density is high near the gate and low away from the gate. A low density region occurs near the end of the plate. A significant amount of porosity exists in this region. Figure 6 shows the pattern of mold filling obtained using the infra-red camera. The metal advances faster near the edge of the plate casting because of the decompose product of the foam can easily escape from the edges. As a result, the flow front is V shaped. The low porosity region occurs at the center of the V shaped region partly because of entrapped foam residues and partly because of the fact that the metal front collects more hydrogen as it is in contact with decomposed atmosphere for a longer time than the metal away from the front.

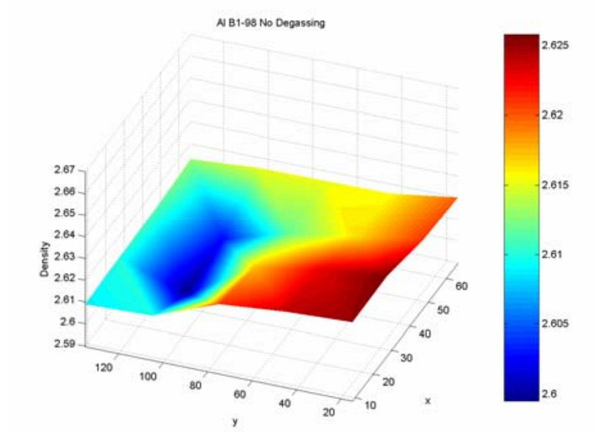

Figure 5. The measured density distribution in a lost foam aluminum A356 casting (flat plate casting not degassed). The casting was gated at the right side. A low density region is identified near the left side of the casting.

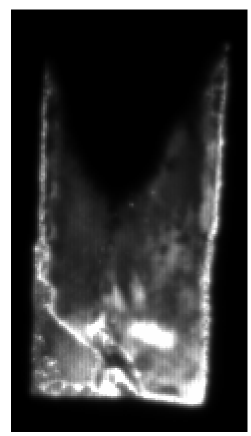

Figure 6. An Infra-red image of the flow front of the molten aluminum A356 alloy during mold filling. The flow advances faster near the edges of the casting, forming a V-shaped flow front. Foam residuals tend to be entrapped by this V-shaped front at the end of mold filling.

The flat plate casting made using degassed aluminum contained less porosity and hence had higher density than the undegassed aluminum. Figure 7 shows the density distribution of the degassed aluminum plate casting. The density of the casting is higher than 2.634. However, a low density region still exists near the end of the flat plate casting. The comparison of the degassed and undegassed lost foam casting suggests that the hydrogen content in the bulk melt contributes to the

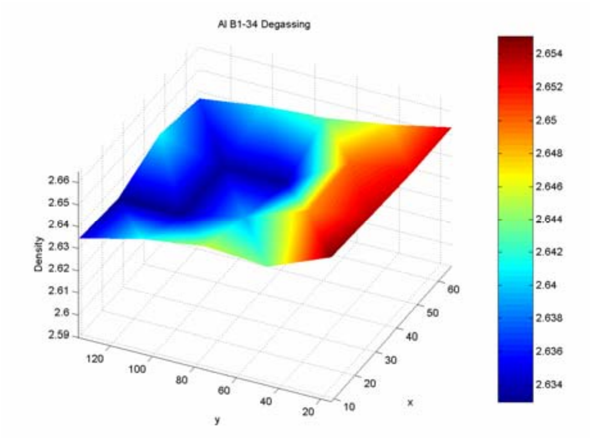

Figure 7. The measured density distribution in a lost foam aluminum casting when the molten metal was degassed before pouring. The density distribution is identical to that without degassing but density values are much higher in the degassed casting than in the undegassed casting.

porosity formation as well as the metal/foam reactions during lost foam casting of aluminum alloys.

The density distribution of the magnesium flat plate casting is shown in Figure 8. The density distribution is almost uniform throughout the casting. Unlike lost foam aluminum castings, the density distribution in lost foam magnesium casting is insensitive to the hydrogen content in the bulk melt. Degassing is not significantly affecting the porosity distribution in the magnesium lost foam casting.

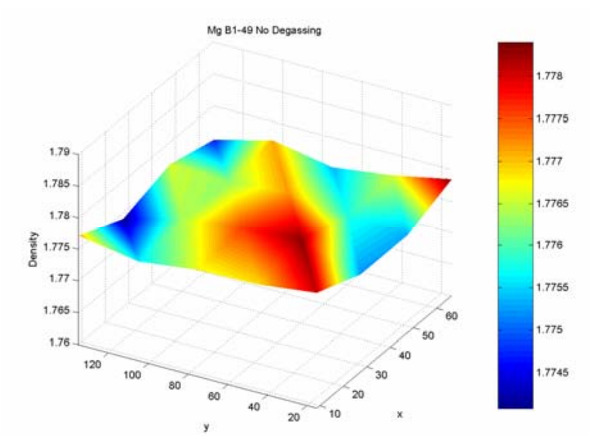

Figure 8. The measured distribution in a lost foam magnesium casting. The density values are fairly uniformly distributed throughout the casting.

Conclusions

The objectives of the first year research of this project have been completed. Melting and lost foam casting capabilities have been developed at the Tennessee Technological University and at Oak Ridge National Laboratory. These capabilities can be used for testing counter gravity (Hitchiner) and pressure assisted lost foam magnesium casting. A burn chamber has been developed/modified for studying polystyrene foam decomposition for a broad range of heating rates for oxidizing and non-oxidizing environments. This burn chamber will be used to quantify liquid pyrolysis behavior for its chemical and physical properties in normal and differing atmospheres. Lost foam castings of magnesium and aluminum alloys have been made.

Presentations/Publications/Patents

Q. Han and H. Xu, "Fluidity of Alloys under High Pressure Die Casting Conditions," Scripta Materialia., 2005, vol. 53, pp. 7-10.

4. ENABLING TECHNOLOGIES

A. Joining of Advanced Materials by Plastic Deformation

Principal Investigator: J.L. Routbort (co-workers: D. Singh, Cinta Lorenzo-Martin, and G. Chen)
Argonne National Laboratory
9700 S. Cass Avenue, Argonne, IL 60439-4838
630-252-506; fax: routbort@anl.gov

Chief Scientist: James J. Eberhardt
(202) 586-9837; fax: (202) 586-9837; e-mail: James.Eberhardt@ee.doe.gov
Field Technical Manager: Philip S. Sklad
(865) 574-5069; fax: (865) 576-4963; e-mail:skladps@ornl.gov

Contractor: Argonne National Laboratory
Contract No.: W-31-109-ENG-38

Objective

- Join advanced materials such as ceramics, cermets, intermetallics, composites, biomaterials, etc., by plastic deformation, collaborate with industry and universities to produce sensors.
- Characterize the interfaces using scanning electron microscopy and fracture tests.
- Investigate grain rotation that is assumed to occur during grain–boundary sliding resulting in deformation bonding.

Approach

- Apply a modest compressive load to two pieces of similar or dissimilar materials that have had little surface preparation in the temperature region where the materials are known to deform by grain-boundary sliding.
- Examine interfaces by scanning electron microscopy.
- Measure residual stresses after joining dissimilar materials and compare to finite-element analysis.
- Measure strength of the interface by 4-point bend tests.
- Characterize electrical properties of sensors.
- Use electron back-scattered diffraction to measure grain rotation as a function of strain.
- Prepare for in-situ Advanced Photon Source experiment to measure grain rotation during deformation.

Accomplishments

- Strong, pore-free joints have been made with various ceramics, cermets, intermetallics, composites, and more recently, biomaterials, with and without various interlayers, fracture occurs away from interface.
- Patent application applied for oxygen sensor with internal reference.
- R&D 100 Award for oxygen sensor.

Future Direction

- Joining intermetallics to ceramics, joining biomaterials.
- Use functionally graded materials to distribute and reduce interfacial stress concentrations.

- Measure in-situ grain rotation during deformation or joining using the Advanced Photon Source, pending completion of installation of Materials Testing System in beamline and available funding.

Introduction

Joining by plastic deformation has been successfully applied in this program to various advanced ceramics (yttria-stabilized zirconia (YSZ)/alumina composites, mullite, SiC and TiC whiskers in a zirconia-toughened alumina (ZTA) matrix, metal-matrix composites and even an electronic ceramic, $La_{0.85}Sr_{0.15}MnO_3$ [1-5] or a bioceramic, hydroyapatite [6]. Techniques have been developed to minimize sample preparation procedures and the temperature at which the joining takes place, amongst them a spray applications technique [2] or use of nanocrystalline powders or dense interlayers stand out [2, 3]. We have formed pore-free joints in Ni_3Al. We have been informed that a patent will shortly be issued; a new one has been applied for, and we are in the process of filing an application for another. We have been awarded an R&D 100 for one of the best technical inventions of 2005 for our work with Ohio State University in developing a very compact oxygen sensor with an internal reference. As the sensor requires no external gas reference and hence no external plumbing, it can be located directly in the combustion chamber allowing for rapid response.

Joining of optical materials is one area that we had not previously explored. Hence, this year we have investigated the deformation and joining of MgF2 as a model optical material. In this case, the quality of the bond can be determined by optical spectroscopy, namely Fourier Transform Infrared Spectroscopy (FTIR), because any porosity at the joint would scatter and cause an increase in the attenuation.

While there still remains considerable work in the area of joining by plasticity, including the joining of intermetallics to ceramics, a technologically important area, there remains one fundamental question. Namely, what is the mechanism of joining? Most, if not all, of the materials that we have been able to join deform by means of grain boundary sliding. As long as there is no cavitation, the strain, it is assumed, is accommodated by grain rotation in response to diffusion as a result of unequal atomic mobilities along grain boundaries. To our knowledge, grain rotation has never been measured in a ceramic. To answer this question, with the strong encouragement of Dr. Sidney Diamond, we have undertaken a program to determine if the assumption is valid, and if it is, how much do the grains rotate? Initial experiments were performed ex-situ using Kikuchi lines as observed in the electron back-scattered diffraction mode in a scanning electron microscope.

In what follows, progress in FY05 on joining of optical and biomaterials and production of the oxygen sensor with an internal sensor will be discussed in more detail.

Plastic Deformation of Hydroxyapatite and its Application to Joining

Hydroxyapatite (HA) is a very common biomaterial that is generally used as a coating over a non-biocompatible material for implants such as teeth. Of course, coatings can be inexpensively applied using a number of different techniques.

However, producing complex shapes by these techniques is difficult. Joining by plastic deformation presents a new possibility for production of complex pieces of HA. Therefore, the first phase of this work was to determine the conditions under which HA exhibits plasticity because the plasticity of HA has not been studied in detail.

HA was deformed in compression into steady state between 1175 and 1275°C in air. Details can be found in reference [6]. The principal results are shown in Figure 1 plotting the logarithm of the steady-state flow stress versus 10000/T for 4 strain rates. HA was capable of strains of ≈0.25 (25%) without cavitation or fracture. The stress exponent was very close to 1 indicating that HA deforms by a viscous flow mechanism. The activation energy of 354 kJ/mole is within a factor of 2 of what is observed for deformation of most oxides materials when normalized by the melting points. The above factors and the absence of grain shape changes as determined by transmission electron microscopy (see Figure 3) are consistent with a grain-boundary

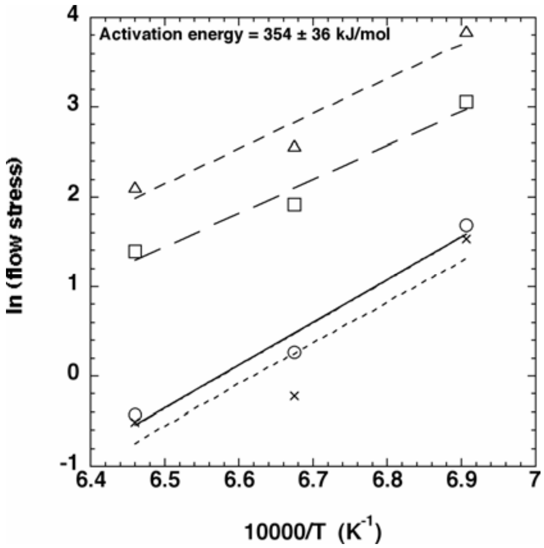

Figure 1. Flow stress as a function of test temperature at a constant strain rate (x: 5 x 10^{-6}/s; ○: 1x10^{-5}/s; □: 5x10^{-5}/s; Δ: 1x10^{-4}/s.

sliding deformation mechanism. Note that the grains are clean and have not cavitated.

Using this information, two pieces of HA were successfully joined within the stress/temperature range in which HA exhibited extensive plasticity. A scanning electron micrograph of a joint formed at 1275°C at a strain rate of 1 x $10^{-5}s^{-1}$ is shown in Figure 2. Note that the joint, as indicated by the arrows, contains no porosity.

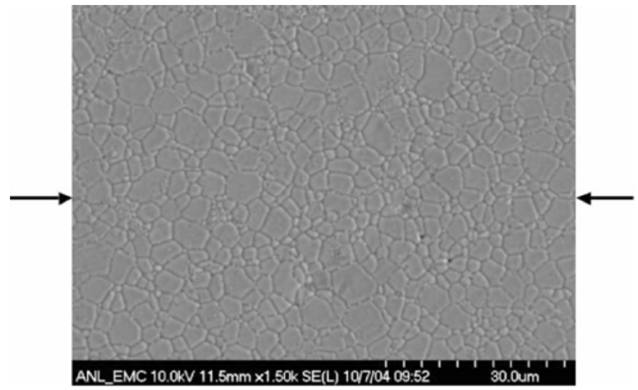

Figure 2. Scanning Electron Micrograph of HA samples joined at 1275°C at 10^{-5}/s strain rate; arrows indicate the joint interface.

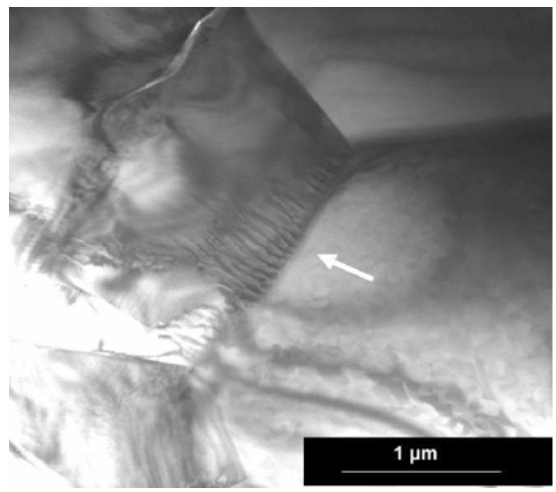

Figure 3. TEM micrographs of HA sample deformed at 1225°C.

Optical Ceramics Case Study: MgF_2 Collaborators: J. Johnson, and J. S. Schlueter

MgF_2 was chosen as a case study representing optical ceramics because it is protypical of ceramics used in optical windows. MgF_2 transmits in the infrared (2-10 μm). Not only is the joining of optical materials important, but characterization of the joints by optical measurements affords another, and different, test of the quality of the bond. In particular, if the joint contains porosity the optical absorption will increase as a result of light scattering from the pores.

Two pieces of MgF_2 each having dimensions of 3x3x5mm were compressed together in our atmosphere-controlled Instron at 800°C in argon at a strain rate of 5x$10^{-6}s^{-1}$. Surfaces were saw-cut from larger pieces with no further surface preparation. The MgF_2 had submicron grain sizes as shown in Figure 4.

SEM of the joined samples indicated that the porosity at the joint was equal to that in the bulk and hence the joint appears to be excellent. The more stringent test result is shown in Figure 5. In this figure the results are presented from the FTIR transmission measured from 3 areas of the unjoined and joined sample, compensated only at 2000 cm^{-1} using an absorption coefficient of 0.02 cm^{-1} for the different lengths of the optical path. The conclusion is that the joining does not affect the IR transmission.

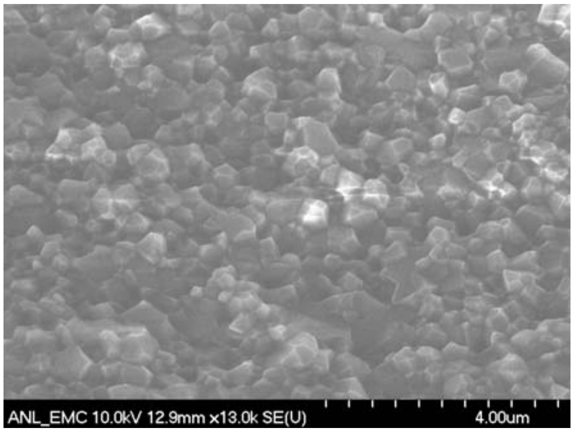

Figure 4. Scanning electron micrograph of the as-received MgF_2.

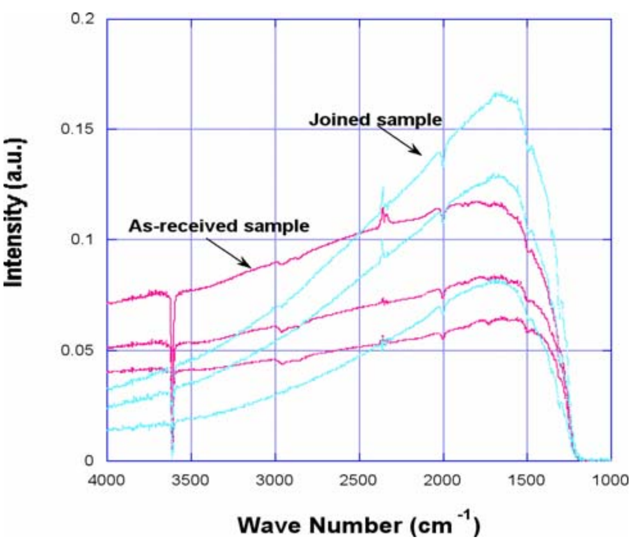

Figure 5. FTIR transmission compensated for optical path only at 2000 cm^{-1} obtained on unjoined and joined samples of MgF_2 (gray color, three locations on as-received sample, black, three locations on joined sample).

Air-Reference Free Potentiometric Planar Oxygen Sensor (Collaborators: R. Ramamoorthy, J. V. Spirig, S. A. Akbar, and P.K. Dutta, all of Ohio State University)

In the previous annual report the use of plastic deformation to form gas-tight seals that allowed the production of miniaturized oxygen sensors that contained metal/metal oxide powders was discussed. The use of an internal reference eliminates using an external reference gas and its costly plumbing equipment. Additionally, the sensor is more robust and can withstand the thermal cycling that causes cracks to form in the previous designs that required a ceramic-glass seal.

We have produced several sensors containing Pd/PdO powders. The output of these sensors is in agreement with the Nernst–Einstein relation. They have shown long-term stability, attesting to ability of the gas-tight seal to withstand thermal cycling. Several sensors have been sent to our industrial partners for long-term testing and possible licensing. The sensor is shown in Figure 6.

A patent application has been filed for the oxygen sensor. Another application extending the plastic deformation method of joining is in progress. OSU, Makel Engineering, and ANL have submitted a proposal to DOE's Office of Industrial Technologies, to use the plastic joining principal to produce a wide-variety of sensors. Most important, the oxygen sensor has won one of the 2005 R&D 100 awards.

Grain Rotation (collaborator, J. Johnson)

A critical experiment both from a basic and applied point-of-view is to determine if grains rotate while undergoing deformation by grain-boundary sliding. The literature is very limited for metals [7] and as far as we can determine, non-existent for ceramics. Recently simulations have shown that microstructual inhomogeneities can result in grain rotation during large-strain grain-boundary diffusion-assisted plastic

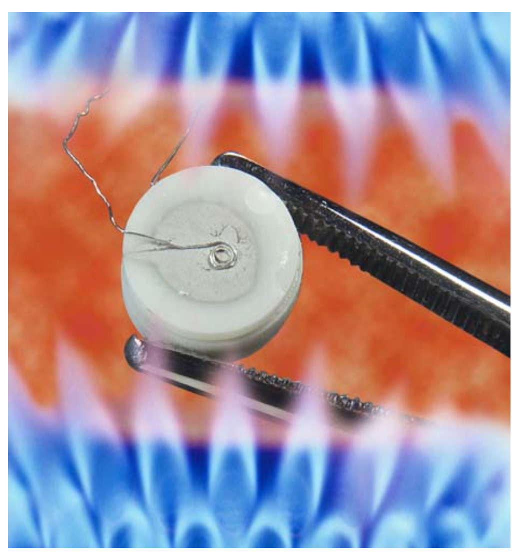

Figure 6. Oxygen sensor with an internal reference in simulated combustion atmosphere.

deformation [8]. Therefore, there is some theoretical justification to expect grains to rotate during deformation.

Our first attempt to measure the orientation of grains in a fine-grained polycrystalline ($BaTiO_3$) ceramic using the high-energy x-rays of the Advanced Photon Source was successful. The orientation of over 50 grains in the ≈6μm grain size sample was measured. However, rotation could not be measured because deformation was accomplished ex-situ and it was never established that the same grains were being illuminated after returning the deformed sample to the beam. This lead to the conclusion that experiments must be performed in-situ. Plans are underway to install a servo-hydraulic mechanical testing machine on one of the diffraction beam lines at APS. There are also plans to install an infrared heating source. Hence, it is anticipated that, depending on funding, in-situ grain rotation experiments will take place in the beginning of FY07.

However, in the meantime, we have measured grain rotation in 6 μm grain sized $SrTiO_3$ as a function of strain using electron backscattered diffraction. The $SrTiO_3$ sample was carefully polished and SEM was used to identify about 20 grains. Such an SEM image is shown in Figure 7. Microhardness indents were made to insure that we could locate and orient the same grains after deformation at 1300°C in steps of 0.02 strain. The movement points obtained from the Hough transformation of the Kikuchi lines (see insert in Figure 7) were used to determine grain rotation as a function of deformation.

The two grains shown in Figure 7 (#23 and #24) rotate as shown in Figure 8. There appears to be saturation after about 4% deformation. Interestingly, the amount of rotation observed is not that different from the amount predicted by the simulations of Coble creep that were performed for an ideal system [8]. We also measured the form factor for all 20 grains and it remains unchanged during deformation. Coble creep would predict that the grain shape must change in accord with the strain. That this is not observed is further evidence that creep in these fine-grained ceramics occurs via grain-boundary sliding.

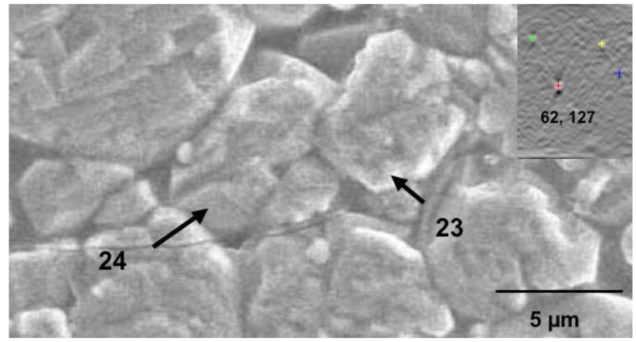

Figure 7A. SEM used to identify and orient two selected grains in undeformed $SrTiO_3$. Insert is the Hough transformation points of the Kikuchi lines from EBSD.

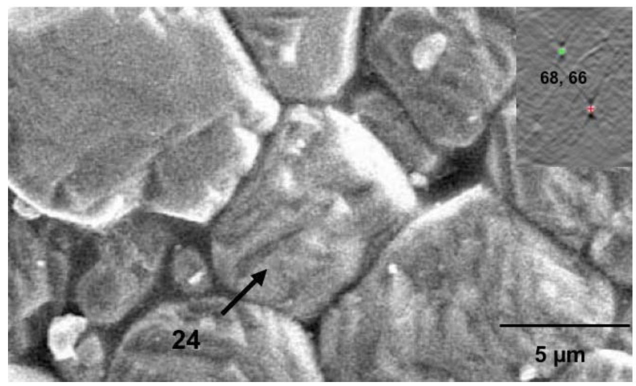

Figure 7B. SEM of same grains as shown in Figure 7A after strain of 0.08 at 1300°C. Insert is the Hough transformation points of the Kikuchi lines from EBSD.

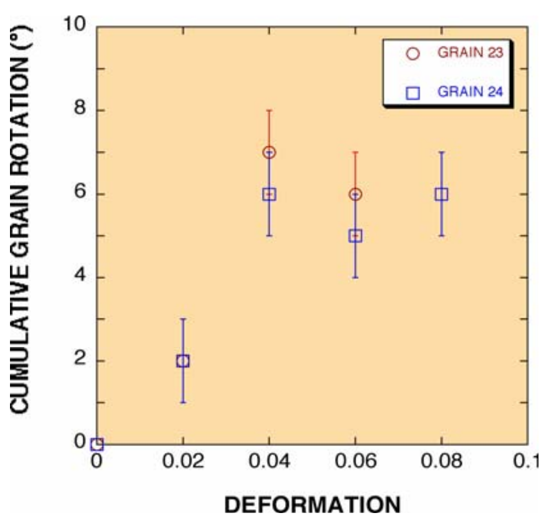

Figure 8. Cumulative rotation of grains 23 and 24 as a function of strain.

The nature of the rotation is a very statistical process as illustrated in Figure 9 in reasonable agreement with the simulation studies [8]. This figure shows the cumulative rotation for seven of the grains. Much theoretical and experimental work remains.

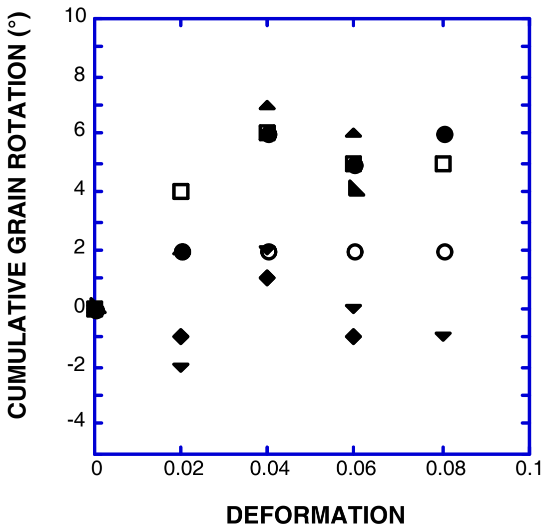

Figure 9. Cumulative grain rotation angle as a function of strain measured for seven grains, each shown by a separate symbol. This illustrates the statistical nature of the rotation.

Conclusions

We have shown that we can form pore-free, very strong joints in a wide-variety of important materials by plasticity. We have reported on joining structural and electronic ceramics, metal-matrix composites, Ni_3Al, whisker-reinforced ceramics, and cermets, bioceramics, and optical ceramics. Little surface preparation and modest temperatures are required for deformation joining. Those factors make the process attractive for commercialization. Using the alumina/ zirconia system as a model material, we have shown that the fracture of a joined bar of the same composition has the same strength as the matrix. The fracture of a joined 4-pt bend bar of dissimilar compositions does not fracture at the interface, but at a position near the maximum residual tensile stress. The optical transmission of joined MgF_2 is the same as that of an as-received sample of MgF_2, providing yet another assessment of the excellent bond quality achieved by deformation joining.

We have applied the technique to a practical problem, namely, producing a gas-tight oxygen sensor. The sensor won an R&D 100 Award and a patent application has been filed. Furthermore, several sensors are out for industrial testing with the view of licensing. A new patent application is in preparation.

We have demonstrated, for the first time to our knowledge, that during grain-boundary sliding, grains rotate in a statistical nature to accommodate the strain. Grain orientations were determined by ex-situ electron back-scattered diffraction patterns. These experiments will set the stage for in-situ grain rotation experiments to be performed in the beginning of FY07, pending available funding.

In the meanwhile, we will perform joining experiments on intermetallics and metals to ceramics using the plastic deformation technique. We hope to be funded to continue and expand the work on miniaturized gas sensors.

References

1. F. Gutiérrez-Mora, K. C. Goretta, S. Majumdar, J. L. Routbort, M. Grimdisch, and A. Domínguez-Rodríguez, "Influence of Internal Stresses in Superplastic Joining of Zirconia Toughened Alumina", Acta Materialia, 50 3475-3486 (2002).

2. K. C. Goretta, F. Gutiérrez-Mora, J. J. Picciolo, and J. L. Routbort, "Joining Alumina/Zirconia Ceramics", Mat. Sci. and Eng., A341 158-162 (2003).

3. F. Gutierrez-Mora, K. C. Goretta, J. L. Routbort, and A. Dominguez-Rodriguez, "Joining of Ceramics by Superplastic Flow", in Advances in Ceramic Matrix Composites VII, Ceramic Transaction # 128, edited by N. P. Bansal, J. P. Singh and H. T. Lin, p. 251. The American Ceramic Society, Westerville, Ohio (2002).

4. N. Chen, F. Gutierrez-Mora, R. E. Koritala, K. C. Goretta, J. L. Routbort, and J. Pan, "Joining Particulate and Whisker Ceramic Composites by Plastic Flow", Comp. Struct, 57 135-139 (2002).

5. F. Gutierrez-Mora and J. L. Routbort, "Electrical Characterization of a Joined Electroceramics $La_{0.85}Sr_{0.15}MnO_3$ ", J. Am. Ceram. Soc., 85 [9] 2370-2372 (2002).

6. D. Singh, M. De la Cinta Lorenzo-Martin, J. L. Routbort, F. Gutierrez-Mora, and E.D. Case "Plastic Deformation of Hydroxyapatites and Its Application to Joining" Applied Ceramic Technology, 2, 247-255 (2005)

7. 7] H. F. Poulson, L. Margulies, S. Schmidt, and G. Winther, "Lattice rotations of individual bulk grains Part I: 3D X-ray characterization", Acta Mater. 51 3821-3830 (2003).

8. D. Wolf, private communication (2005).

B. Rapid, Low-Cost Tooling Development

Principal Investigators:
Cliff Eberle
Oak Ridge National Laboratory, Oak Ridge, TN 37831-8048
(865) 574-0302; fax: (865) 574-8257; e-mail: eberlecc@ornl.gov

Curt Lavender
Pacific Northwest National Laboratory
902 Battelle Blvd, P.O. Box 999, Richland, WA 99352
(509) 372-6770; fax: (509) 375-4448; e-mail: curt.lavender@pnl.gov

Ed Ungar
Taratec Corporation
1251 Dublin Road, Columbus, OH 43215
(614) 291-2229; fax: (614) 291-2867; e-mail: eungar@tarateccorp.com

Chief Scientist: James J. Eberhardt
(202) 586-9837; fax: (202) 587-2476; e-mail: James.Eberhardt@ee.doe.gov
Field Technical Manager: Philip S. Sklad
(865) 574-5069; fax:(865) 576-4963; e-mail:skladps@ornl.gov

Contractor: Oak Ridge National Laboratory / Pacific Northwest National Laboratory
Contract No.: DE-AC05-00OR22725 / DE-AC06-76RL01830

Objectives

- Assess status and need for low-cost tooling technologies for lightweighting materials.
- Evaluate state-of-the-art capabilities for rapid, low-cost tooling approaches.
- Determine the socioeconomic factors that are likely to significantly impact the development and implementation of advanced tooling technology.
- Recommend Department of Energy (DOE) course of action with respect to investments in tooling technology development.

Approach

- Engage industrial tool die and mold manufacturers (TDMs) and tool users to evaluate socioeconomic drivers affecting implementation of new tooling technology.
- Identify and engage or develop other stakeholders that will address socioeconomics factors.
- Evaluate potential tooling technologies that are most likely to be fielded and impact fuel efficiency.

Accomplishments

- Met with a small group of leading North American TDMs and the Center for Automotive Research (CAR).
- Initiated tool sourcing analysis by CAR to determine effects of tool sourcing models on health of tool mfg industry, and its ability to incorporate new technology.

Future Direction

- Work with industry to foster communication and collaboration, and to develop an "industry-owned" roadmap.
- Engage other interested government parties to co-sponsor research and development (R&D).
- Commence performing selected R&D.

Introduction

The introduction of advanced polymer-based composites and lightweight material manufacturing processes to commercial vehicle manufacturers and their supplier base is thought to be severely impacted by the high cost of tooling and long tooling development time. Often the use of lower-cost materials and less efficient structural designs is dictated by the fact that tooling for the manufacture of advanced composites and other lightweight materials cannot be justified from a cost-per-part basis, and from the long development times or procurement lead times that are required. In addition, the unique production volumes associated with commercial vehicles—which are significantly lower than automotive production volumes, yet well above aerospace production numbers—make current tooling design and development methods unsuitable.

An example of the cost and schedule challenges faced by commercial vehicle manufacturers is that a fully tooled door system for a Class 8 tractor can cost upward of $20 million and require over 24 months to fabricate and qualify the tooling. When advanced materials such as carbon fiber composites or lightweight metals such as aluminum or magnesium are considered, tooling design, material forming characteristics and surface finish requirements make today's manufacturing approaches very high-risk. The result is often that manufacturers fall back on less efficient structures that use conventional steel and fabricated structural designs.

The purpose of this project is to assess current tooling technologies to identify key deficiencies in cost, prototype and fabrication methods, and design and modeling tools that prevent the increased use of lightweight metals and composites structures in low- and medium-volume commercial vehicles. Data have been gathered from government–industry workshops, published data sources, and numerous follow-up interviews with workshop participants and other key industry experts. The team is working with industry to develop a roadmap that will guide the development and implementation of advanced tooling technology that reduces the risk of using advanced lightweight materials in commercial vehicle applications.

Project Deliverables

The project team has delivered to DOE a report containing findings from an industry workshop conducted in FY2004, follow-up interviews, energy analysis, and socioeconomics review. The primary future deliverables are a joint government-industry roadmap for tooling technology development and implementation, and a list of co-sponsors that will share the R&D costs with DOE.

Technical Approach

The technical approach for this project is largely based on gathering and analyzing information to enable informed decision-making regarding future R&D investments. A key part of the project has been to plan and conduct a workshop that served as a forum for soliciting information from industry experts and for networking among industry peers. The workshop was followed by interviews with selected key industry contacts, most of whom were attendees at one or more workshop sessions, to validate the workshop findings. Additionally, potential energy and socioeconomic impacts were analyzed.

TDM Roundtables

In December 2004 and June 2005, the project leaders met with a select group of leading TDMs. The purpose of these meetings was to create a small leadership group of individuals who can help to create an industry strategy to establish the conditions under which new technology can be infused into the industry.

The attendees represented a cross-section of both large and small North American TDMs, all of whom focus on large tools. The attendees were either the presidents or vice presidents and owners or part-owners of their companies.

A key portion of the first TDM Roundtable was the presentation of the project team's findings from FY2004 workshops and analysis. The presentation provoked considerable discussion. The group generally concurred with the findings presented. The project team planned to commence roadmap development at this meeting, however it quickly became evident that the TDMs need the opportunity to address their business climate before they can objectively participate in developing a technical roadmap After much discussion, the group concluded that the TDMs need to make the case to the OEMs that through early collaboration the TDMs can bring value to the OEMs. This early collaboration will help the OEMs design product that can be manufactured at lower over-all cost. By so doing, they believe that the OEMs will derive value from the geographic proximity of a healthy TDM industry.

A second Roundtable was conducted in June 2005 at the CAR, with CAR participating. CAR was identified as a renowned and respected voice in the automotive industry that understands the business issues affecting TDMs. CAR was asked to conduct a "lifetime tool sourcing analysis" that would analyze how OEM tool sourcing practices affect OEM costs, TDM industry health, and the TDM industry's ability to incorporate new technology. This analysis has been initiated. After this analysis is completed and disseminated, we expect the tool manufacturing community to work with us to develop an "industry-owned" tooling technology roadmap. We have identified CAR as a renowned and respected organization that can address the critical business issues associated with tooling technology, freeing the DOE participants to focus on technology roadmapping and development.

Conclusions

Tooling is a major expense in manufacturing vehicles, especially at low production volumes, and therefore constitutes a major barrier to lightweight materials implementation on vehicles. There are opportunities to lower this barrier with properly planned and targeted tooling technology development and implementation. However, industry workshops and analysis conducted in FY2004 indicated that promising technology alone is not sufficient; rather economic barriers to new technology implementation need to be understood. In FY 2005, the project team engaged key TDMs and initiated analysis to investigate how tool sourcing practices affect OEM costs, TDM health, and new tooling technology incorporation. We plan to commence developing a roadmap in FY 2006.

Acknowledgements

The principal investigators gratefully acknowledge expert assistance by technical and administrative staff at ORNL, PNNL, and Taratec Corporation.

C. Improved Friction Tests for Engine Materials

Principal Investigator: P. J. Blau
Oak Ridge National Laboratory
P.O. Box 2008, Oak Ridge, TN 37831-6063
(865) 574-5377; fax: (865) 574-6918; e-mail:blaupj@ornl.gov

Chief Scientist: James J. Eberhardt
(202)586-9837; fax: (202)587-2476; e-mail: james.eberhardt@ee.doe.gov
Field Technical Manager: Philip S. Sklad
(865) 574-5069; fax: (865) 576-4963; e-mail: skladps@ornl.gov

---

Contractor: Oak Ridge National Laboratory
Contract No.: DE-AC05-00OR22725

Objectives

- Develop a realistic, engine-correlated laboratory-scale test method to be used in selecting diesel engine piston ring and liner materials, and work with ASTM Committee G-2 to establish it as a standard practice.
- Investigate the effects of new versus engine-conditioned (EC) lubricants on the ability of the new test method to detect small friction and wear behavioral differences in engine materials in a repeatable manner.

Approach

- Review and critique past attempts to develop laboratory tests for piston ring and liner materials.
- Develop a testing protocol for friction and wear in reciprocating, lubricated contacts that simulate key aspects of the diesel engine environment.
- Evaluate sources of engine-conditioned lubricants that can be used to conduct friction tests of piston ring/cylinder material evaluations.
- Work with ASTM, through Committee G-2 on Wear and Erosion, to develop a standard practice for conducting laboratory-scale piston ring and liner friction and wear tests in an EC oil environment.

Accomplishments

- Published a report describing and critiquing past efforts to develop engine-correlated laboratory-scale tests for materials and lubricants proposed for use in both spark-ignition and diesel engines.
- Established an ASTM task group on ring and liner wear and populated the task group with representatives from diesel engine companies, automotive companies, testing machine manufacturers, oil companies, government laboratories, and universities.
- Developed a technique to simulate the surface finish of production cylinder liners on simple test coupons.
- Developed a method to run-in piston rings to provide consistent friction data in bench-scale tests.
- Studied the effects of oil condition on friction using diesel oils generated in standardized engine tests.
- A new ASTM standard for friction testing of ring/liner materials was approved and published in FY 2005.

Future Direction

This project was completed in FY 2005. The companion wear standard is complete but has not yet been approved by ASTM. Both standards are currently in use in our laboratory to investigate advanced materials and surface treatments for piston ring and liner applications.

Introduction

Friction between moving parts robs engines of useful energy and lowers the vehicle's fuel economy. Depending on engine speed, the piston ring and liner system in an internal combustion engine can account for over 50% of the total engine frictional losses. New materials, lubricants, and coatings offer the potential to reduce frictional losses; but the development cost for such materials can be high, especially when full-scale engine tests are involved. Smaller-scale, simulative laboratory tests can be a cost-effective alternative for preliminary material and lubricant screening if their results correlate well with the performance of the materials in actual fired engines.

The design of laboratory-scale, simulations of the friction of diesel engine rings and liners is not trivial. Improperly designed simulations can produce misleading results. Tests must enable a proper ranking of alternative materials and lubricants in the same order of merit as they would perform in service. That goal required identifying the mechanical, thermal and chemical influences on friction and wear behavior, and controlling them within a laboratory environment.

By working through ASTM Committee G-2 on Wear and Erosion, this effort has benefited from the diversity of experience of ASTM members. In FY 2001, key elements required for effective ring/liner simulation were identified. In FY 2002, an industry advisory group was formed under the auspices of ASTM committee G-2 on Wear and Erosion. In FY 2003, friction and wear tests were conducted using new and used engine oils to refine the initial test methodology. In FY 2004, based on test results, a draft standard practice was prepared, reviewed by the industry advisory group, and formally submitted for balloting. In FY 2005, the standard practice was approved by ASTM and designated ASTM G-181-04, completing the goal of this project. Work continued on a companion standard for wear.

Description of the Standard

The many technical challenges that had to be overcome in developing the standard practice were described in previous reports; however, selection of suitable, engine-conditioned lubricants was a key element in the final standard. A series of well-characterized diesel test oils were obtained from Southwest Research Institute (SWRI) and used to generate data on which lubricants would provide the varying degrees of aggressiveness needed to screen materials for various types of engines. Results of this work were presented at several meetings and published in the engineering literature (see the Reference list).

The testing machine shown in Figure 1 was modified to hold diesel engine piston rings and liner specimens. The upper specimen holder that oscillates in a heated oil bath was prepared from a production piston from a Caterpillar C-15 diesel engine. At the rear of the photo is the variable-speed motor which is coupled to a Scotch yoke reciprocating drive. The load is applied through a series of linkages below the base platform.

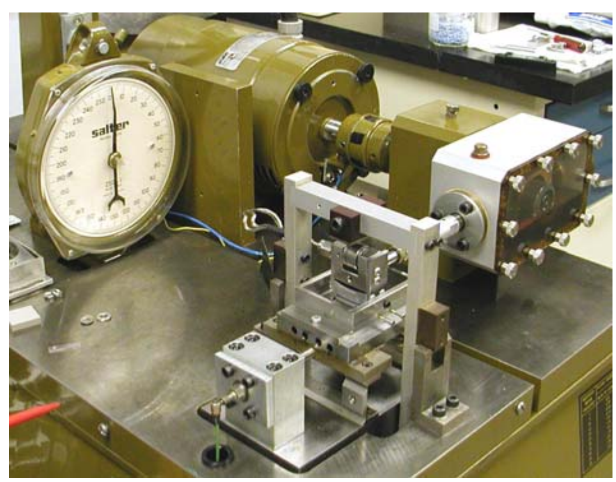

Figure 1. This reciprocating friction and wear testing apparatus was used to develop the new test standard.

The new standard, ASTM G-181-04, is called "Standard Practice for Conducting Friction Tests of Piston Ring and Cylinder Liner Materials Under Lubricated Conditions." It was first published in Volume 03.02 of the ASTM Annual Book of Standards in August 2005 (pp. 748-756) and consists of eleven procedural sections and two appendices of supplementary information.

The first appendix describes a special running-in procedure that was developed to ensure that the ring and liner specimen were accurately mated before the actual data were recorded. Proper running-in is essential to ensure that friction measurements are repeatable from one test to the next. The second appendix describes the process of selecting engine-conditioned lubricants so that results of the friction test can be meaningfully correlated to the performance of the materials and surface treatments in actual engines.

Development of a Companion Standard for Wear

Initially, it was believed that wear evaluations could be incorporated within the friction standard, but in the course of experimentation, it became apparent that there were sufficient differences in procedure for friction and for wear such that the two could not easily be combined in a single document. Therefore, a companion draft standard procedure for wear measurement of piston ring and liner materials was also prepared.

The wear test procedure contains a mathematical procedure to accurately calculate wear volume losses on surfaces with compound curvatures, like piston rings and liners. The derivation, by J. Qu of Oak Ridge National Laboratory (ORNL), enables more accurate wear determinations than are possible using the approximations used by other investigators.

After the new wear procedure had been developed, it was used to study the behavior of candidate light-weight materials and surface treatments. For example, Figure 2 compares the results of a bare titanium alloy and one on which a special oxidation

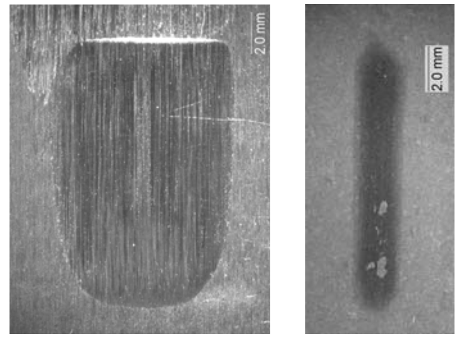

Figure 2. The new ASTM G181 standard was used to study the effects of surface treatments on the friction of light-weight titanium alloys. The specimen on the left is Ti-6Al-4V alloy. The thermally-oxidized Ti-6Al-4Valloy on the right had friction levels similar to those of lubricated cast iron liner material but over 40,000 times less wear than the non-treated titanium on the left.

treatment was applied. The bare specimen on the left ran only 11 minutes in hot oil (but at half the standard test load). The treated specimen of the same alloy, on the right, ran six hours at twice the load on the piston ring.

The draft wear standard was submitted for ASTM Committee G-2 balloting in the summer of 2005, and it is hoped that within the next year it will join its companion as a published standard.

Conclusions

A new ASTM standard for conducting lubricated diesel engine piston ring and liner materials tests was developed and approved. A series of presentations and publications were prepared to describe its development and use to the transportation industry (see below). The new test method can distinguish differences in friction characteristics of diesel oils run under fired engine conditions and will serve as a means to pre-screen new materials and surface treatments for use in energy-efficient engines. A companion standard for wear evaluation is undergoing ASTM balloting.

Within the past year, ORNL has received a number of requests for information on the new standard from automotive and truck engineers as well as from universities that conduct research on internal combustion engines.

Presentations and Publications

1. P.J. Blau (2001) "A Review of Sub-Scale Test Methods to Evaluate the Friction and Wear of Ring and Liner Materials for Spark- and Compression-Ignition Engines," Oak Ridge National Laboratory Tech. Report, ORNL/TM-2001/184, 19 pp.

2. P.J. Blau (2001) "Simulation of Cylinder Bore Surface Finish Parameters to Improve Laboratory-Scale Friction Tests in New and Used Oil," in Engine Systems: Lubricants, Components, Exhaust and Boosting System, Design and Simulation, Amer. Society of Mech. Engineers, ASME ICE Vol. 37-3, pp. 57-63.

3. J.J. Truhan, J. Qu, and P. Blau (2003) "A Rig Test to Measure Friction and Wear of Heavy Duty Diesel Engine Piston Rings and Liners Using realistic Lubricants," presented at 'Conference on Boundary Lubrication for Transportation,' Copper Mountain, Colorado, August 3-7.

4. J.J. Truman, J. Quiz, and P. Beau (2005) "The Effect of Lubricating Oil Condition on the Friction and Wear of Piston Ring and Cylinder Liner Materials in a Reciprocating Bench Test," presented at the 15th International Conference on Wear of Materials, San Diego, and April 2005.

5. J.J. Truman, J. Quiz, and P. Beau (2005) "The Effect of Lubricating Oil Condition on the Friction and Wear of Piston Ring and Cylinder Liner Materials in a Reciprocating Bench Test," *Wear*, Vol. 259, pp. 1048-1055.

6. J.J. Truman, J. Quiz, P.J. Beau (2005) "A Rig Test to Measure Friction and Wear of Heavy Duty Diesel Engine Piston Rings and Cylinder Liners using Realistic Lubricants," *Teratology International*, Volt 38 (3), pp 211-218.

7. ASTM G 181-04 (2005) "Standard Practice for Conducting Friction Tests of Piston Ring and Cylinder Liner Materials under Lubricated Conditions," ASTM Annual Book of Standards, Vol. 03.02, pp. 748-756.

D. Equal Channel Angular Extrusion Processing of Alloys for Improved Mechanical Properties

Principal Investigator: Thomas M. Lillo
Idaho National Laboratory
MS2218, P.O. Box 1625, Idaho Falls, ID 83415-2218
(208) 526-9746; fax: (208) 526-4822; e-mail: tml@inel.gov

Chief Scientist: James J. Eberhardt
(202) 586-9837; fax: (202) 587-2476; e-mail: James.Eberhardt@ee.doe.gov
Field Technical Manager: Philip S. Sklad
(865) 574-5069; fax:(865) 576-4963; e-mail:skladps@ornl.gov

Participants:
John Flinn, University of Idaho
Ricardo Schwarz, Los Alamos National Laboratory
Darrell Herling, Pacific Northwest National Laboratory

Contractor: Idaho National Laboratory
Contract No.: DE-AC07-05ID14517

Objective

- Investigate equal channel angular extrusion (ECAE) as a deformation processing technique to manipulate the microstructure and improve material properties such as strength, formability, fatigue, and corrosion.
- Apply ECAE processing to produce advanced, lightweight materials with enhanced formability, higher strength-to-weight ratio, and higher stiffness, ultimately leading to reductions in vehicle weight and thus more fuel-efficient vehicles.

Approach

- Assess the effects of ECAE processing parameters on the mechanical properties of a magnesium alloy (ZK60A) and aluminum metal matrix composites (MMC). These are lightweight alloys with potential for use in lightweight structural applications in vehicles.
- Determine the optimum ECAE processing schedule for the maximum increase in mechanical properties.
- Characterize the microstructure and mechanical properties of the ECAE-processed material.

Accomplishments

- Demonstrated extreme microstructural refinement in magnesium alloy by low temperature ECAE processing.
- Determined superplastic forming potential of ECAE-processed magnesium alloy through strain rate jump tests to determine strain rate sensitivity parameter.
- Performed superplastic tensile tests at $\leq 250^{o}$C on ECAE-processed magnesium alloy.
- Removed residual porosity from a metal matrix composite (MMC) through ECAE-processing.
- Demonstrated an increase in elastic modulus (>15%) of a powder metallurgy MMC with increasing number of ECAE passes.
  - ECAE improved second phase distribution.

- ECAE improved tensile properties (ductility >10% vs <1% as-received).
- ECAE processed similar commercial MMC's made by casting methods.

Future Direction

- Superplastic tensile testing of ECAE-processed magnesium alloy at >250°C.
- Microstructural characterization of ECAE-processed magnesium alloy before and after superplastic tensile testing.
- Publish results of superplastic testing of ECAE-processed magnesium alloy.
- Compare mechanical properties of ECAE-processed MMC made by powder metallurgy (Dynamet AL6061+10 % B_4C) with those of ECAE-processed commercial MMCs made by casting methods.
- Microstructural characterization of ECAE-processed MMCs.
- Publish results of the ECAE processing study of MMCs.

Introduction

The mechanical properties, especially the yield strength and the ultimate strength, of metallic alloys can be improved through a refinement of the microstructure. The Hall-Petch relationship predicts that the increased yield strength is inversely related to the grain size. Deformation processing, e.g., rolling, forging, swaging, etc., followed by heat treatment is traditionally used to reduce the grain size. These deformation processing methods result in a change in the dimensions of the work piece, typically reducing the work piece dimension in at least one direction while increasing one or more other dimensions. Therefore, these methods are geometrically limited in the amount of deformation that can be imparted to the material. However, equal channel angular extrusion (ECAE) is capable of repeatedly imparting a large amount of deformation into a material without significant dimensional changes. (In ECAE, a billet is forced around an internal angle inside a die. The change in direction, without a change in billet dimensions, imparts the deformation.) The goal of this project is to explore the limits of microstructural refinement and the effects on mechanical properties.

During the previous year the research focus for this program was narrowed to two areas. One area involved the use of ECAE processing of lightweight magnesium alloys to develop an extremely fine microstructure suitable for achieving high strain rate superplasticity. The other area is focused on ECAE processing metal matrix composites (MMCs) to homogenize the distribution of the hard reinforcing phase and, thereby, impart significant ductility to these materials, which are typically very brittle.

Significant progress has been made in both areas. Namely, a very fine grain size has been achieved in the magnesium alloy, ZK60A, through ECAE processing, Figure 1. Tensile samples were made and the superplastic potential of this material was evaluated through strain rate jump tests.

In the work with the MMC it was demonstrated last year that ECAE processing increased the density and ductility of a metal matrix composite, AL6061+10 wt% B_4C, by compacting, sintering and hot isostatic pressing AL6061 and boron carbide powders. The

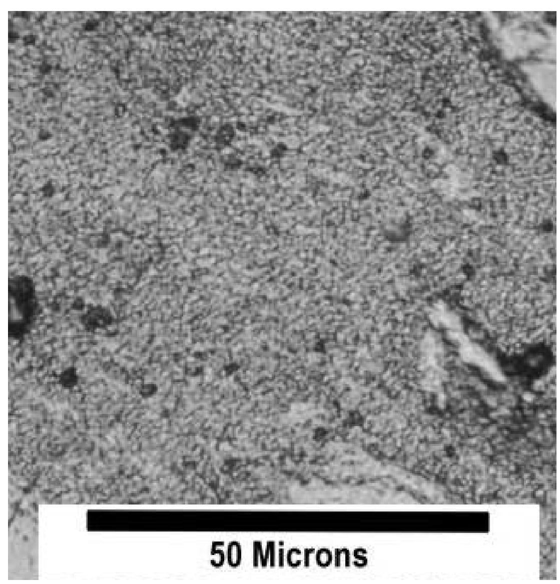

Figure 1. The etched microstructure of ECAE-processed ZK60A.

distribution of the boron carbide phase showed significant signs of homogenization during ECAE and the tensile ductility increased from <1% elongation in the as-received condition to greater than 10% after ECAE processing. ECAE also improved the relative density and the elastic modulus, although these values were still somewhat lower than theoretical. So, new ECAE processing parameters were used to process additional material in an effort to further improve the ductility as well as increase the elastic modulus. Also two commercially available aluminum alloy MMCs made by *casting techniques* were added to the test matrix and ECAE processed.

Both of the materials studied are lightweight and could significantly reduce vehicle weight, increasing fuel efficiency. The goal is to develop lightweight alloys with good formability and high stiffness with significant ductility for application in the transportation sector.

ECAE Processing of Magnesium Alloys

The magnesium alloy billets for superplastic evaluation were ECAE-processed according to Table 1. The ECAE processing schedules shown in Table 1 were meant to explore the effects of processing temperature, processing route and number of ECAE passes on the superplastic forming behavior. Additionally, sample ZK60-S4, -S6 and -S7 attempted to look at the effect of precipitation from solid solution *during* ECAE processing.

Strain rate jump tests were performed at 180, 225, 250 and 275°C on the ECAE-processed samples from the first four billets in Table 1 to assess the potential for superplastic behavior. The strain rate sensitivity factor, *m*, was calculated from:

$$m = \log(\sigma_2/\sigma_1)/\log(\dot{\varepsilon}_2/\dot{\varepsilon}_1) \quad , \qquad (1)$$

where $\dot{\varepsilon}$ was the strain rate, σ was the flow stress and the subscripts 1 and 2 referred to the values before and after the strain rate jump, respectively.

The strain rate sensitivity factor has been plotted as a function of test temperature in Fig. 2 for the first four samples in Table 1.

Table 1. ZK60A ECAE processing schedules

Billet ID	Initial billet condition	ECAE temperature (°C)	ECAE route	Back stress level, ksi
ZK-1	T5	150	8B	15.1
ZK-R1	T5	150 135 120	2B 1B 1B	15.1 15.1 19.7
ZK-R5	T5	150 130	2B 4B	15.1 15.1
ZK60-S4	Solution treated	200 150	2B 6B	10.6 21.2
ZK60-S6	Solution treated	200 150 140 120	2B 2B 2B 2B	11.2 14.0 18.3 22.5
ZK60-S7	Solution treated	200 150 150	2A 1B 1A	11.2 14.0 14.0
ZK-4N	T5	150 140 130 120	2B 2B 2B 2B	16.8 16.8 16.8 22.5

The plots for ZK-R1 and ZK-R5 (4 and 6 ECAE passes, respectively) are quite regular. The strain rate sensitivity passes through a maximum as the temperature increases. Also, as the strain rate increases, the maximum m value occurs at higher temperatures. In fact, for samples, ZK-R1 and ZK-R5, the maximum m value for strain rates $\geq 3 \times 10^{-4}$/second appears to occur at temperatures higher than those tested, probably around 300-325°C.

The other two samples, which have the most ECAE passes, are somewhat more ambiguous. ZK-1 (8 ECAE passes) exhibits a minimum between 225 and 250°C, while the ZK60-S4 sample (8 ECAE passes on a solutionized billet) seems to show the maximum m values occur below 180°C for strain rates *less than* 3×10^{-4}/second while the maximum m values for strain rates of 1.6×10^{-3}/second, 7.8×10^{-3}/second and 3.4×10^{-2}/second occur around 225°C.

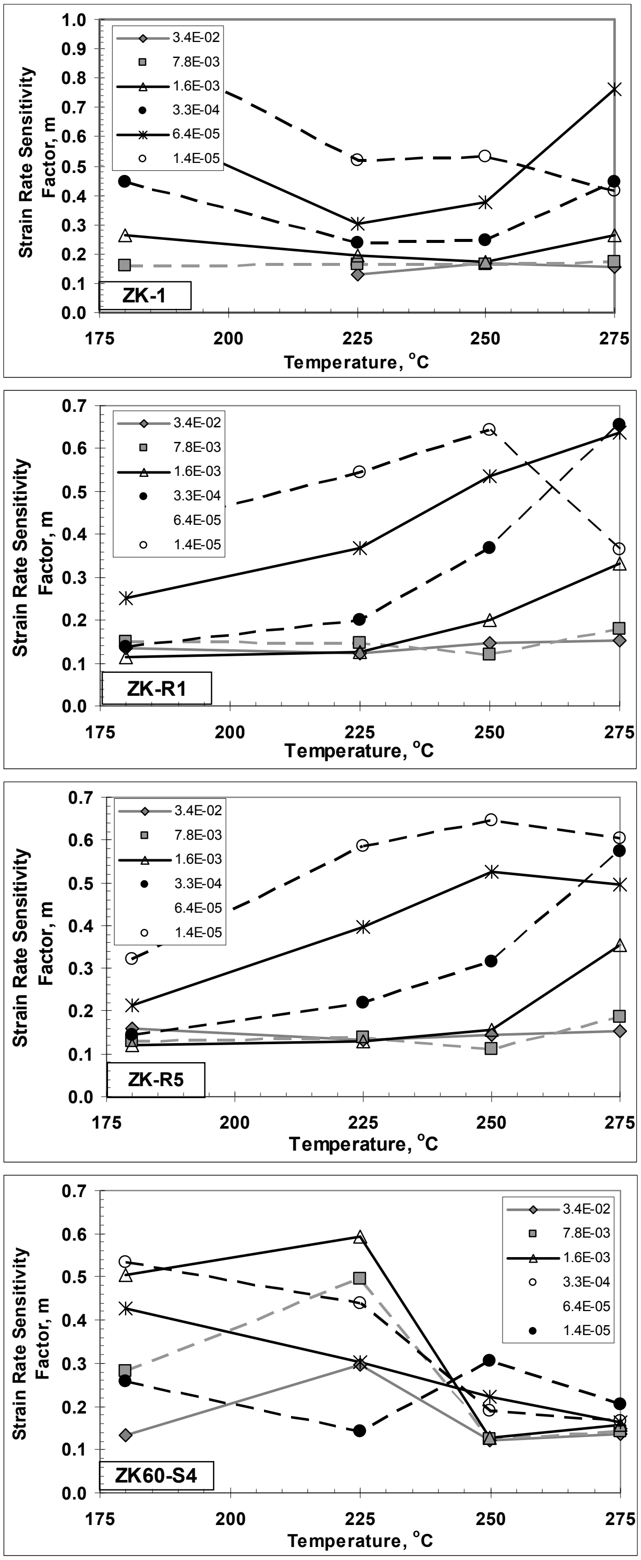

Figure 2. Strain rate sensitivity of ECAE-processed ZK60A at various temperatures.

Based on these strain rate jump tests, certain ECAE processing schedules should produce superplastic behavior. (Superplastic behavior is usually associated with m values greater than 0.5.) Elevated temperature tensile tests were begun to elevate the extent of superplastic deformation possible. From a commercial aspect, a material may be superplastically formed, economically, if a minimum elongation of 200-300% can be attained at a strain rate on the order of 10^{-2}/second or greater. Figure 3 shows an example of the elevated temperature tensile results for a strain rate of 10^{-2}/second. An elongation of greater than 150% has been obtained at 250°C. Table 2 summarizes the results for the samples tested so far. Based on the strain rate jump tests, greater elongations are expected for higher

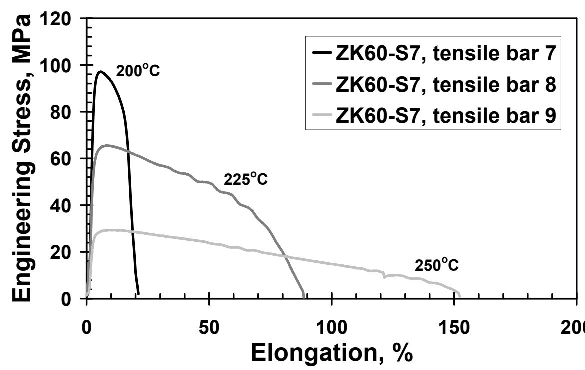

Figure 3. Example of elevated temperature tensile behavior of ECAE processed alloy ZK60. Strain rate = 10^{-2}/second

Table 2. Elevated Temperature Tensile Results

Billet ID	Elongation, %	Test Temperature, °C	Strain Rate, s^{-1}
ZK -1	176	200	0.006
	90	200	0.013
	83	200	0.025
ZK-R1	90	200	0.006
	45	200	0.025
ZK-R5	156	200	0.006
	98	200	0.013
	92	200	0.025
ZK60-S4	188	200	0.006
	181	200	0.013
	150	200	0.025
ZK60-S7	21	200	0.01
	89	225	0.01
	153	250	0.01

temperatures which are planned for early in FY06. Therefore, high-strain-rate superplasticity may still be found in this ECAE-processed magnesium alloy. This would facilitate the use of magnesium alloys in automotive applications. Superplastic forming would allow net-shape fabrication of components and minimize waste of this relatively expensive alloy, making it more economically competitive with traditional iron-based materials. High-strain-rate superplastic forming also offers the potential for rapid fabrication, resulting in higher productivity and making this alloy more competitive with conventional automotive structural materials. Ultimately, vehicles incorporating magnesium alloys would be lighter than those that rely on traditional alloys, and therefore more fuel-efficient.

ECAE Processing of Aluminum Alloy Composites

Two commercial metal matrix materials were added to this research area during the first half of FY05. The materials were made by Duralcan and were obtained from Dr. Darrell Herling at PNNL. The first material, designated F3S.20S-T6**,** consisted of an aluminum alloy 356 matrix with 20 wt% SiC particulate and was made by a casting process. In the as-received condition, this MMC exhibited an elastic modulus (106.8 GPa) that was approximately 55% greater than typical aluminum alloys. The other material, designated W6A.15A-T6, consisted of an AL6061 matrix with 15 wt% Al_2O_3 particles. This material was made by extrusion of powdered material and exhibited an elastic modulus approximately 28% greater than typical aluminum alloys. Both materials were fully dense and exhibited well-dispersed particulate reinforcement, Figure 4. The particles in the SiC composite are on the order of 10-15 microns while those in the Al_2O_3 composite are on the order of 20-30 microns. The boron carbide particle size in the AL6061/B_4C composite made by Dynamet is on the order of 50 microns. The commercial composites will be used to compare the effects of ECAE on the prototypical Dynamet material with MMCs made by other means. The goal is to determine the utility of ECAE processing of MMCs of all types.

The specific schedules used are shown in Table 3. The ECAE-processed billets remained intact and were free of cracks and other flaws commonly found in materials of low ductility that are ECAE-processed without back pressure. Tensile bars were made and tested for B3528-10 (Dynamet material). Tensile bars for the other two ECAE-processed MMCs are being made and will be tested in early FY06. This sample set will allow the benefits of ECAE processing on MMCs to be determined.

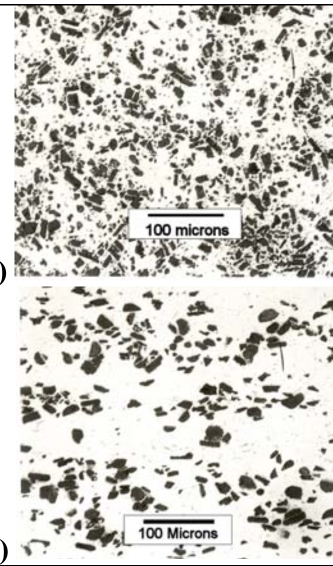

Figure 4. The as-received microstructure of a) F3S.20S-T6 and b) W6A.15A-T6

Table 3. Processing schedules for Commercial MMCs

Sample	Initial condition	ECAE temperature (°C)	ECAE route	Back stress (ksi)
F3S.20S-2	solutionized	300 150 100	2B 2A 1A	14.0 19.7 21.1
W6A.15A-1	solutionized	300 150 100	2B 2A 1A	5.6 19.7 21.1
B3528-10	T0	300 150 100	2B 2A 1A	9.8 21.1 21.1

However, the effect of ECAE processing parameters on the elastic modulus and the density for the different MMCs was determined after each ECAE pass of the processing schedule using ultrasonic methods and the water immersion technique, respectively. Figure 5 shows the variation of these quantities as the billets were ECAE processed. Unfortunately this behavior was not determined for

B3528-10 so sample B3528-7 has been included for reference. The obvious difference is that ECAE processing seems to have quite a large initial effect on the prototypical Dynamet material (B3528-7) where as ECAE processing has little effect on the commercial MMCs. ECAE processing of the Dynamet material removes residual porosity and increases the relative density which results in a significant increase in the elastic modulus over the as-received billet. After the first pass through the ECAE die, subsequent passes do not have as great an effect on either the density or elastic modulus for B3528-7, i.e., the ECAE effect becomes similar to those observed in the fully dense commercial MMCs. Tensile testing will determine whether ECAE processing has produced a beneficial refinement of the microstructure which yields improved mechanical properties such as strength and/or ductility.

Conclusions

ECAE processing has the potential to refine the microstructure and improve the mechanical and/or formability of commercial lightweight alloys. Work during this fiscal year has shown that ECAE processing may enable a magnesium alloy to be superplastically formed at relatively high strain rates ($\geq 10^{-2}$/second). Net shape superplastic forming, with little material waste, may enable the use of this, and other, ECAE-processed magnesium alloys in transportation applications to reduce vehicle weight and increase fuel efficiency.

ECAE processing may also be used to remove residual porosity of lightweight, high stiffness metal matrix composites produced by powder metallurgy techniques. Additional benefits of ECAE processing of MMCs appear to be improved distribution of the elastically hard, particulate phase as well as increase in the ductility of the MMC. It remains to be seen if ECAE processing has similar effects on MMCs made by casting or extrusion. Work in early FY06 should provide insight into this issue.

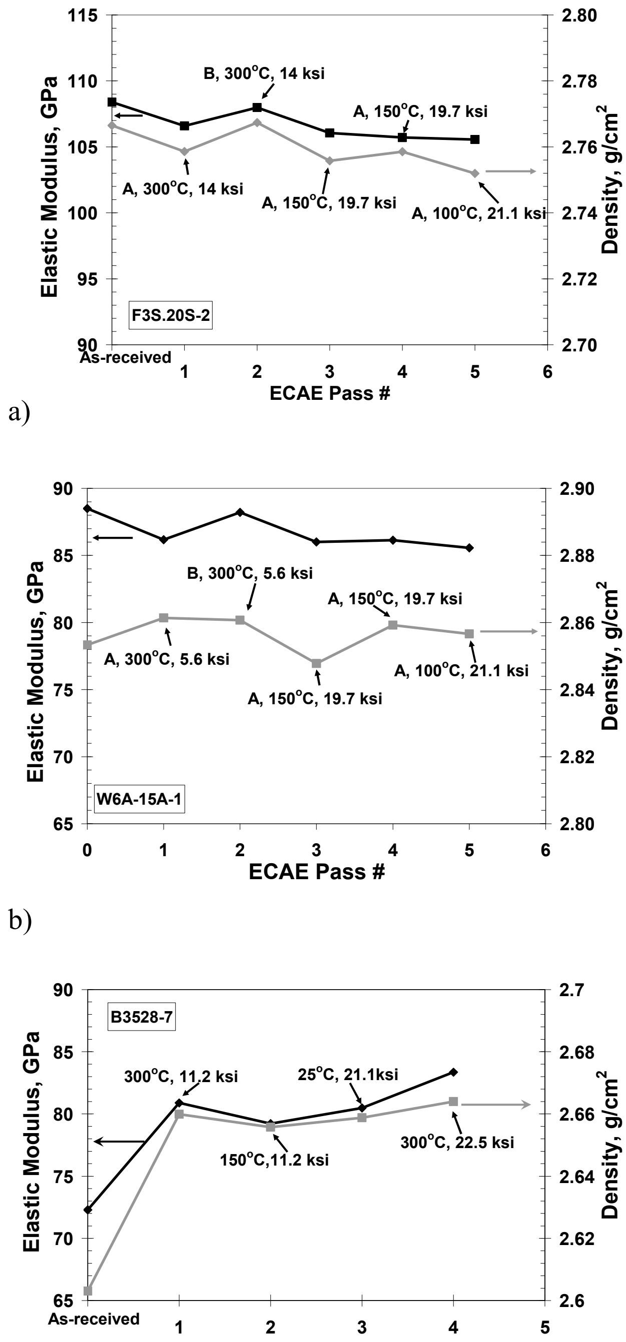

Figure 5. Effect of ECAE processing on elastic modulus and density. a) F3S.20S-2, b) W6A.15A-1, c) B3528-7

Publications and Presentations During FY05

T.M. Lillo, "Enhancing Ductility of AL6061+10wt% B_4C Through ECAE Processing", poster session in the Langdon Symposium at the 2005 TMS Annual Meeting & Exhibition in San Francisco, CA. A manuscript has been accepted for publication in Materials Science and Engg. A.

S.R. Agnew, P. Merhota, T.M. Lillo, G.M. Stoica, P.K. Liaw, "Texture Development During the Equal Channel Angular Pressing of Magnesium Alloys AZ31, AZ80, Mg-4wt% Li, WE43 and ZK60", presented at 2005 TMS Annual Meeting & Exhibition in San Francisco, CA. Manuscript has been prepared for proceedings.

D.P. Field, R.C. Eames, and T.M. Lillo, "The Role of Shear Stress in the Formation of Annealing Twin Boundaries in Copper" submitted to Scripta Materialia.

Schwarz, R.B. ; Shen, T.D. ; Harms, U. ; Lillo, T., "Soft ferromagnetism in amorphous and nanocrystalline alloys", *Journal of Magnetism and Magnetic Materials* Volume: 283, Issue: 2-3, December, 2004, pp. 223-230.

Agnew, S.R., Mehrotra, P., Lillo, T.M., Stoica, G.M., "Texture evolution of five wrought magnesium alloys during route A equal channel angular extrusion: Experiments and simulations", *Acta Materialia,* Volume: 53, Issue: 11, June, 2005, pp. 3135-3146.

E. Attachment Techniques for Heavy Truck Composite Chassis Members

Principal Investigator: Lynn B. Klett
Oak Ridge National Laboratory
P.O. Box 2008, Oak Ridge, TN 37831-6053
(865) 241-8112; fax: (865) 574-8257; e-mail: klettlb@ornl.gov

Principal Investigator: Darrell R. Herling
Pacific Northwest National Laboratory
P.O. Box 999, Richland, WA 99352-0999
(509) 375-6905; fax: (509) 375-4448; e-mail: darrell.herling@pnl.gov

Chief Scientist: James J. Eberhardt
(202) 586-9837; fax: (202) 587-2476; e-mail: James.Eberhardt@ee.doe.gov
Field Technical Manager: Philip S. Sklad
(865) 574-5069; fax: (865) 576-4963; e-mail: skladps@ornl.gov

---

Contractors: Oak Ridge National Laboratory, Pacific Northwest National Laboratory
Contract Nos.: DE-AC05-00OR22725, DE-AC06-76RL01830

Objectives

- Overcome the technical issues associated with joining composite materials in heavy vehicles by developing technically robust and economically attractive joining techniques.
- Develop and validate one or more joint designs for a composite structural member attached to a metal member that satisfies the truck chassis structural requirements both economically and reliably.
- Solicit input from truck original equipment manufacturers (OEMs) and suppliers on the technical hurdles and needs associated with joining structural composite members in heavy vehicles. Use this information to guide the joint design and development activities.
- Publish information on the design, modeling, and testing methodologies that are developed to support the incorporation of composite materials into other chassis components.

Approach

- Collaborate with the National Composites Center (NCC) and its OEM partners to identify and address technical needs related to the manufacturing, joining, and implementation of a composite chassis component.
- Design attachment components and configurations in close coordination with the composite structural component development.
- Use modeling techniques to predict the performance of various joint designs, taking into account damage mechanisms and fatigue/life requirements.
- Characterize various composite materials and mechanical joint configurations through mechanical testing, considering variables such as hole size, hole fabrication method, bolt pre-load, inserts, combined loading, vibration, fatigue, and durability.
- Validate joint design for the composite structural member through shaker and track testing.

Accomplishments

- Conducted tension-tension, compression-compression and variable stress level fatigue testing of candidate 3-D glass reinforced composites.
- Ran static and fatigue tests on 3-D glass and hybrid reinforced composite/steel joints in lap shear (Mode I) and cross tension (Mode II).
- Tested adhesively bonded joints for comparison with bolted joints with Mode I and Mode II static and fatigue loading.
- Conducted bolt bearing tests to investigate the effects of variations in torque level which may result from creep of a composite material in a bolted joint.
- Conducted double lap shear static and fatigue tests to investigate changes in bolt pre-load resulting from through thickness creep of the composite and damage progression.
- Conducted finite element analysis (FEA) modeling, taking advantage of the progressive failure analysis available in GENOA, to evaluate the damage at bolt holes in composite material.
- Conducted FEA to evaluate the current steel to steel component and joint and compared alternative lightweighting designs.

Future Direction

- Continue bolt bearing and fatigue tests to investigate design modifications, molded-in holes, 3D reinforcement levels and acceptable hole clearance levels to minimize damage in the composite and improve the fatigue life of a composite-to-steel joint.
- Evaluate the impact of using adhesive bonding in combination with bolting, as well as the effects of environmental exposure and testing rate for the composite/steel Mode I and Mode II fatigue specimens.
- Continue FEA modeling with input from the composite and joint tests to further optimize and predict the performance of the composite/steel joint.
- Continue to work closely with the industrial team to develop the composite component and composite-to-steel joint design solutions to meet the demanding requirements of the heavy vehicle chassis environment.

Introduction

In May 2003, researchers at Oak Ridge National Laboratory (ORNL) and Pacific Northwest National Laboratory (PNNL) began collaboration on a 4-year research effort focused on developing technically robust and economically attractive joining techniques to overcome technical issues associated with joining lightweight materials in heavy vehicles. This work is being performed concurrently with an industry program led by the NCC to develop and commercialize composite chassis components, which will require resolution of the joining challenges. The industry project serves as a "focal project" that provides real load and service data to this project and will potentially field-test and implement the technology developed in this project. The initial focus of research is development and validation of one or more joint designs for a composite structural member attached to a metal member that satisfy truck chassis structural requirements both economically and reliably. Broadening the effort to include other structural joints, including composite-to-composite joints, is anticipated. Durability shaker testing of the first prototype composite component and joint is planned for the first half of 2006.

Composite Material Testing

Tensile and Compressive Fatigue Comparison

Both the component independent baseline Extren® pultruded fiberglass material and a 3D reinforced vinyl ester material supplied by the NCC were tested in compressive and tensile fatigue. The fatigue tests were run with $R = 0.1$ at 70%, 50% and 30% of ultimate stress at a frequency of 5 Hz. Shorter length specimens were used for the compressive fatigue to prevent buckling. The results, shown in

Figure 1, indicate that the 3D reinforced composite performed better in compression-compression fatigue at lower stress levels compared to tension-tension fatigue. For the pultruded fiberglass, the performance is similar for both compressive and tensile fatigue with a few outliers. Note that the fatigue curves have been normalized to % of ultimate stress to account for the differences in the strengths of the two materials.

Variable Amplitude Fatigue

Components in a truck chassis undergo complex random variable amplitude fatigue loading during their service lifetime. Previous studies reported in the literature indicate that standard methods employed for variable amplitude fatigue life prediction can overestimate the actual experimentally measured life for fiber reinforced composite materials. The inaccuracy is due in part to the different failure mechanisms and property degradation when compared to metals.

One of the most commonly used damage laws is the Palmgren-Miner linear relationship which assumes that fatigue cycles at a specific load level always result in the same damage regardless of the loading history. The overall damage accumulation is determined as a ratio of the loading cycles to the failure cycles at each stress level.

In an attempt to characterize the variable amplitude fatigue behavior of the 3D reinforced glass/vinyl ester composite material, fatigue tests with block

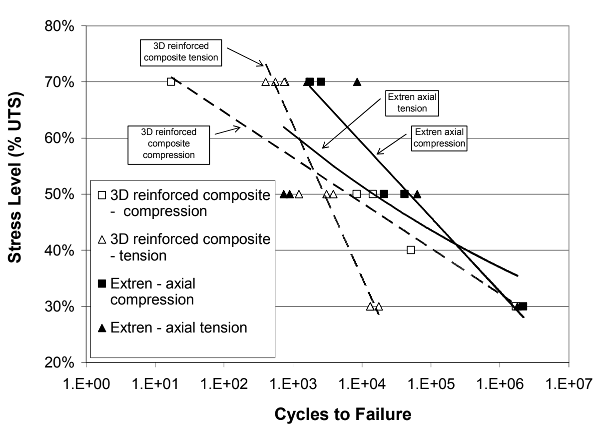

Figure 1. Comparison of tensile and compressive fatigue behavior for 3D reinforced vinyl ester composite and Extren® pultruded fiberglass.

loading cycles at 2 different stress levels were conducted. Although there was a significant amount of scatter in the fatigue data, the deviation from the Palmgren-Miner's prediction was pronounced. Additionally, it seems that a low stress level applied prior to the high stress level is more damaging than when the high stress level is applied first.

The research team has been working closely with AlphaSTAR Corporation to integrate a damage model into GENOA that will take into account the deviation from the Palmgren-Miner prediction. The progressive failure analysis in GENOA may assist in developing an understanding of the damage development and evolution which may result in the different behavior based on loading sequence. The ultimate goal would be to have a predictive tool that could be used for a more realistic random amplitude fatigue spectrum.

3D Glass Reinforced Epoxy Resin

In order to improve the temperature limit of the composite material, the NCC has provided 3D reinforced epoxy specimens that were tested in tension and fatigue. These specimens were fabricated with the same 3D glass reinforcement that was used for the prior 3D glass/vinyl ester composite discussed in the 2004 annual report. The glass/epoxy specimens had similar average tensile strength and modulus values (402 MPa and 23.7 GPa) as well as comparable fatigue performance. This indicated that the tensile and fatigue properties are dominated by the reinforcing fibers and are not dramatically affected by changing the matrix material.

Loss of Bolt Pre-Load for Bolted Composite/Steel Joints

An important component of a composite/steel bolted joint design is the bolt preload at assembly, which is selected to achieve the desired clamp load for proper function of the joint throughout the service life of the assembly. A minimum clamping force is required to overcome vibration-induced loosening, joint separation, slippage, fatigue, leakage and other similar failures. The maximum clamp force should be below a threshold value that would cause bolt yielding, joint crushing, stress cracking, premature fatigue failure, or other related service failures.

The low through-thickness properties typical of most composite architectures suggest that bolted composite assemblies will experience a loss of preload over time due to the relaxation or creep of the softer composite material.

As discussed in the last reporting period, a testing methodology has been developed to study the effects of bolt pre-load with composite to steel joints.

Washer Load Cell vs. Bolt Load Cell

Indirect measurements of bolt pre-load have been made with several types of washer load cells and a strain gaged bolt. To compare the different load cells, the bolt pre-load was monitored for a steel to steel bolted specimen with both a washer load cell and the bolt load cell. After torquing, the pre-load did not change significantly with time for the washer load cell, which would be expected for steel plates. However, the bolt load cell indicated the pre-load continued to drop to 86% of the initial bolt preload after 70 hours. Although the bolt load cell would be desirable for use in static and fatigue joint tests from a simplicity standpoint, it is unsuitable for monitoring bolt preload due to this drift or creep of the load cell itself. An Interface washer load cell, Model LW2550-30K, was chosen for use for the static and fatigue joint testing to monitor the loss of bolt preload.

Loss of Pre-Load in Huck Bolted Composite to Steel Joint

Several composite and steel plates were Huck bolted together to evaluate the loss of bolt pre-load at the high torque levels seen in this common joining technique for chassis components. A 9.53 mm thick hybrid glass/carbon reinforced composite as well as a 6.35 mm thick Extren® composite were used with 12.7 mm thick steel and 12.7 mm bolts. After 500 hours, the thicker hybrid composite/steel assembly retained slightly more of the initial preload compared to the 6.35 mm Extren®/steel assembly (Figure 2). As expected, the composite/steel assemblies have significantly more loss of preload than the corresponding steel/steel assembly. Note that the Huck bolt preload was simulated by a torqued bolt for the steel/steel assembly due to restrictions on the length of available Huck bolts.

Static and Fatigue Double Lap Shear Joint Testing

Initial testing to monitor the loss of bolt preload during static and fatigue loading has focused on the double lap shear tensile test geometry in which a composite specimen was bolted between two steel plates with a Grade 8 12.7 mm bolt (Figure 3).

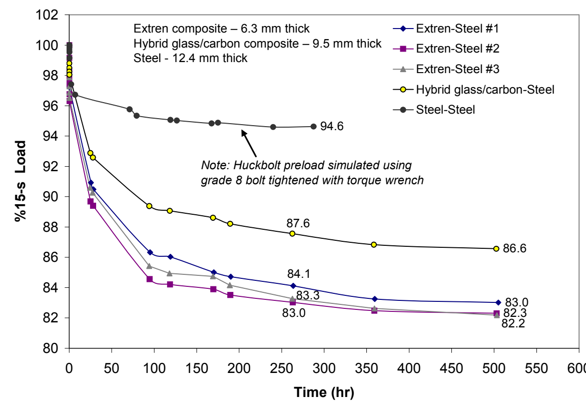

Figure 2. Normalized loss of preload for Huck bolted composite to steel assemblies.

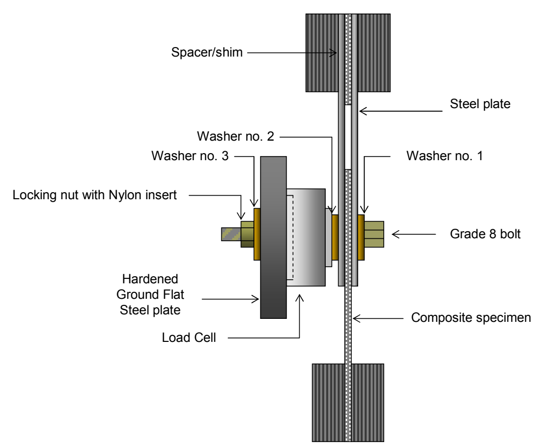

Figure 3. Test schematic for the double lap shear tests for composite/steel assemblies.

Joint testing has been conducted with specimens of both 3.17 mm thick Extren® pultruded fiberglass and 2.54 mm thick 3D glass reinforced vinyl ester composite material provided by the NCC. For these tests, the torque level and corresponding bolt preload were varied. The maximum fatigue stress was established as a percentage of the ultimate tensile strength of comparably prepared specimens. The fatigue tests were run with a stress cycle R factor of 0.1 and a frequency of 5 Hz.

In static tensile tests, the higher bolt preloads increase the ultimate strength of the assembly (Figure 4). Failure modes shift from a bearing type failure at the lowest preloads, typified by local composite crushing at the washer perimeter, to composite material tensile failure initiating from the perimeter of the hole. There was a steady reduction in bolt preload during the static tests, which was up to 15% at the initial load peak for the specimens with the highest bolt preload with a continuing decrease up to failure. At very low preloads (finger-tight) the load cell indicated a slight increase in bolt load during loading.

Double lap shear composite/steel assemblies withstand reasonably high fatigue stress levels without failure. For instance, an Extren®/steel double lap shear specimen achieved runout with over 3 million cycles at a fatigue level of 50% of the ultimate failure stress for a torque level of 41 Nm. The higher torque levels drive the fatigue failure location away from the hole and into the bulk composite.

For specimens assembled with higher bolt torques, there is a steady decrease in the bolt preload with additional fatigue cycles up to failure (Figure 5). This occurs both for specimens with and without failure at the hole and is partly attributed to composite relaxation. A number of specimens failed with 85-95% of the original bolt preload, regardless of the original torque level. There has been no indication thus far of a change in the monitored bolt preload which would indicate imminent failure.

For specimens prepared with low bolt preload (finger-tightened), the bolt preload increased with number of fatigue cycles until failure. This increase may be due to a localized material deformation at the hole perimeter resulting in increased compression of the load cell.

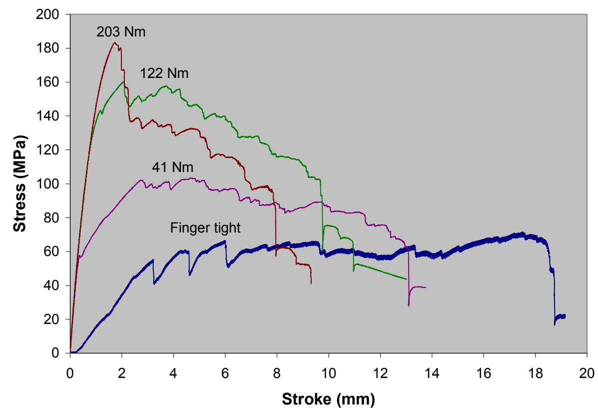

Figure 4. Tensile stress vs. stroke curves for composite/steel double lap shear assemblies with varying bolt torque levels.

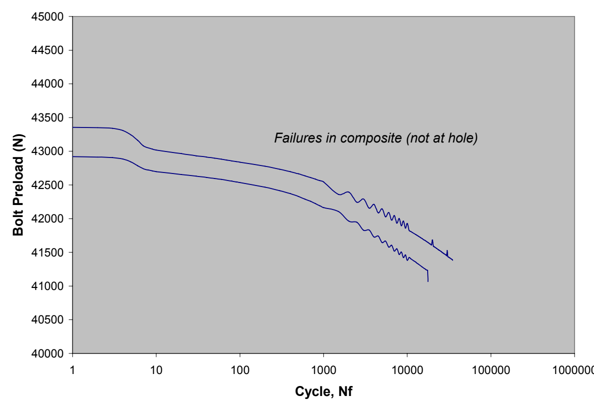

Figure 5. Bolt preload vs. fatigue cycle number for Extren®/steel double lap shear joint with initial bolt torque of 122 Nm.

Experiments have demonstrated that the fatigue life of double lap shear specimens assembled with a minimal bolt preload can be significantly enhanced by applying an epoxy adhesive between the composite and steel plates prior to bolting. Figure 6 shows that the fatigue life for the joint with a combination of bolt and adhesive increases from 10,000 to over 1 million cycles for both the Extren® and the 3D reinforced composite materials. Additionally, the joints which included the adhesive tolerated increased stress amplitudes. As expected, the adhesive facilitates the transfer of stresses away from the hole perimeter and lowers the stress concentration factor for the joints with low clamp forces.

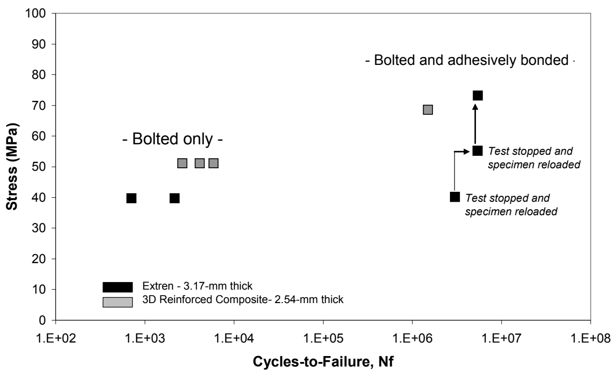

Figure 6. Fatigue data for finger tight double lap shear composite/steel bolted joints with and without adhesive.

3D Reinforced Composite-to-Steel Joint Evaluation

Joint Strength Characterization with Thick Composite Materials

In evaluating composite/steel joint assemblies, 3D woven carbon/glass hybrid composites and 3D glass-polymer composites were investigated. The hybrid composite consisted of two layers of carbon (each 1.02 mm thick) and three layers of glass (each 2.5 mm thick) for a total composite thickness of 9.53 mm. The glass composite consisted of four layers of glass for a total composite thickness of 9.53 mm also. Lap shear specimens of both composite types and 6.35 mm thick Grade 6 steel were assembled with a Grade 8 bolt.

For the hybrid composite/steel joints, the bolt was torqued to 393 N-m. For the glass composite/ steel joints, the bolt was torqued to 325 N-m to simulate joints assembled with a Huck bolt. For the hybrid composite/steel joints, the joints were assembled with the hybrid composite on top and the glass layer of the composite at the faying surface of the joint.

Due to limited material, only two static strength tests were conducted for each joint assembly configuration. The average static strength of the hybrid/steel jointed assemblies was 61.5 kN (about one-half of the strength of the baseline steel/steel Huck bolted design discussed during the last reporting period) and the average static strength of the glass/steel assemblies was 60.3 kN. These peak loads served as a guide for the fatigue strength tests.

Effect of Structural Adhesive

Experiments were performed to investigate the effect of structural adhesive on the joint performance of composite/steel assemblies. 3D-reinforced glass composite (2.54 mm thick) and 1008 steel (~1.4 mm thick) lap shear joints were assembled with Betamate 4601 and PL731 SIA adhesive to understand the fatigue behavior and failure mechanisms of joining composite to steel with adhesive only.

Again, due to limited material, two static tests were conducted for each configuration to serve as a guide for the fatigue tests. The average static strength of the assembled joints was 15.6 kN using the Betamate adhesive and 9.7 kN for assemblies using the SIA adhesive.

At 10^6 cycles, the fatigue strength of the joints assembled with Betamate adhesive is approximately 2 times greater than the joints assembled with PL731 SIA adhesive. An adhesive failure was observed in joints assembled with the SIA adhesive. Failure occurred at the adhesive-steel substrate interface where the adhesive separated from the steel. This is typically indicative of a bonding or adhesion problem. However, joints assembled with the Betamate adhesive, failed cohesively, illustrating the bond with the substrate was adequate, but the strength of the adhesive may need to be enhanced.

At 10^6 cycles, the fatigue strength of the joints assembled with the Betamate adhesive was approximately 30% higher than the same joint assembled with a bolt. These results illustrate the potential of utilizing adhesives to join composite and steel substrates.

Joint Strength Characterization with Steel Inserts

In order to mitigate the loss of bolt preload due to the through thickness properties of the composite material, cylindrical and tapered steel inserts have been evaluated experimentally.

Initially, a steel cylindrical insert with a 15.9 mm inner diameter and a 25.4 mm outer diameter and an equivalent 30^o angular (tapered) insert with a 15.9 mm inner diameter and a 35.3 mm (top) and

25.4 mm (bottom) outer diameter were placed in a 9.5 mm thick, 3D reinforced glass composite. Preliminary composite/steel lap shear specimens were assembled with the metal inserts adhesively bonded to the composite substrate.

The average joint strength for the composite/steel lap shear assemblies with an insert is approximately 20% less than the assemblies without inserts. Premature interfacial failure between the steel insert and the composite material always preceded the final composite failure.

The fatigue performance of the joints with inserts was also evaluated and compared to the same joint configuration without inserts. At 10^6 cycles, the fatigue strength of the joints assembled with inserts is also approximately 20% less than the comparable joint without an insert. As for the static tests, interfacial bond failure was the dominant failure mode under fatigue loading (Figure 7). The conclusion is that one can not assume that a perfect bond exists between the metal insert and composite panel. In this geometry, the metal insert does reduce the creep in the joint, but reduces the overall strength because of the increased size of the hole in the composite material. Therefore, unless the geometry of the composite or the bolt pattern can change for a given joint design, the steel inserts have a negative impact on the joint strength.

Joint Strength Characterization with Steel Plate Reinforcements

Next, the concept of a steel plate sleeve was developed to reduce the loss of pre-load due to creep and improve the fatigue performance of a composite/steel joint assembly. 76.2 mm x 61.0 mm x 1.52 mm steel plates were adhesively bonded to both sides of the composite substrate for the lap shear joint (Figure 8). Both static and fatigue strength tests were conducted on lap shear specimens. The static joint strength increased approximately 25% and the fatigue strength increased approximately 23% at 10^6 cycles compared to the equivalent joint without inserts. Figure 9 illustrates the fatigue test results for several of the joint designs investigated in this study in comparison to the baseline steel to steel joint assembly.

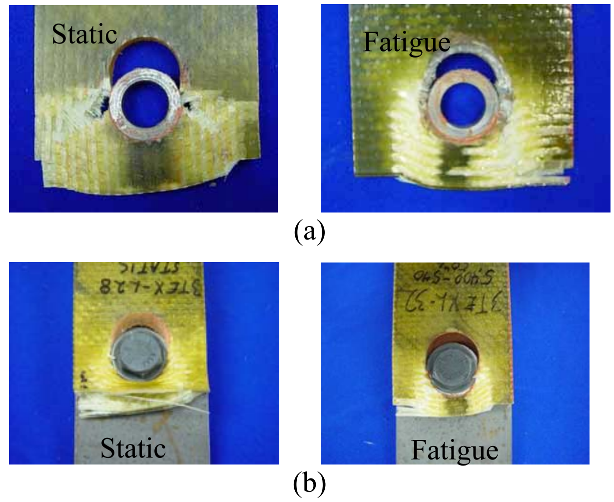

Figure 7. Typical joint static and fatigue failure mode observed for (a) the cylindrical steel insert and (b) the tapered steel insert composite/steel lap assemblies.

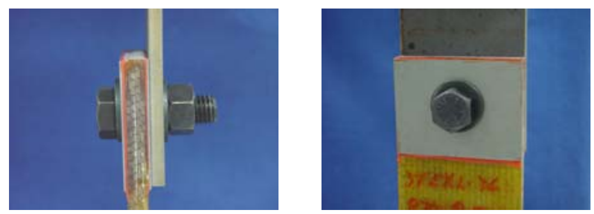

Figure 8. The 3D composite/steel lap shear joint assembly with adhesively bonded steel plates.

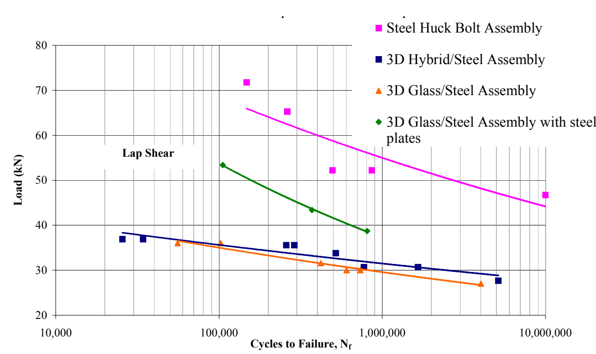

Figure 9. Fatigue strength test results of 3D-reinforced composite/steel lap shear assemblies with various design modifications compared to the baseline steel/steel assembly.

Modeling

Different modeling techniques are being evaluated and developed to assist in the performance prediction of various joint designs taking into account damage mechanisms and fatigue and life requirements. Having reliable models will allow for more efficient design optimization of structural composite joints to minimize and focus the expensive and time consuming mechanical testing.

Washer Size Effects

Creep in the composite due to the initial bolt torque was evaluated for two different washer sizes. Material creep was assumed in the following form:

$$\varepsilon^{cr} = \alpha\sigma t^{n},$$

where material coefficients $\alpha = 1.8x10^{-8}$ and $n = 0.19$ were estimated by curve fitting data from a through thickness compression test. Washers of two different sizes from previous experiments were modeled. The smaller washer caused larger stresses in the composite plate during testing, thus a larger magnitude of loss of pre-load was expected. This analysis assumes homogenized material properties with an isotropic creep model (linearly dependent on the stress level) for the composite and linear elastic behavior for the steel. The effect of contact was not considered. In order to accurately model the actual experiments, these assumptions need to be reexamined. Despite these simplifying assumptions, the analysis predicted that the loss of preload would be approximately 10% lower for the larger washer configuration after 24 hours.

Insert Evaluation

Building upon the insert analysis reported on during the last reporting period, further traditional finite element analysis was conducted to determine the effect of both the cylindrical and tapered inserts at the bolt hole in the composite during composite/steel lap shear testing. First, the bolt shank was pulled with controlled displacement to simulate the bolt pre-tensioning. As expected, the model predicts a higher bolt load for the assembly with the steel inserts. Next, the bolt load was held for 25 hours to determine the creep behavior. The model predicts that the inserts help to minimize the creep with little difference between the two insert geometries.

At the last step of the analysis, the steel plate was fixed and the top composite plate was pulled. Assuming no interfacial failure between the insert and composite, it was predicted that joints with inserts would have higher strengths compared to the joint without inserts. However, the experimental lap shear testing results show that the inserts actually cause a significant decrease in the joint strength due to the failure of the bond between the insert and the composite. In this model, perfect contact was assumed between the insert and the composite.

<u>GENOA Progressive Failure Analysis of the Joint with Steel Inserts</u>

AlphaSTAR engineers have assisted in enabling GENOA to run the analyses with ABAQUS as a solver. This new capability allows for the contact algorithm in ABAQUS to be used with GENOA's multiscale progressive failure analysis. The bolt assembly model has been imported into GENOA to predict the damage in the composite around the bolt hole.

Damage due to clamping loads was evaluated for both the cylindrical and tapered inserts. A calibrated material model for 8 mm thick 3-D glass reinforced material was used for the composite plate. The model predicted that damage would occur at the insert-composite interface at 10 times the normal assembly clamping load with five active damage criteria indicating that the existing assembly procedure should not damage the composite.

A two step model simulating the pre-clamp and subsequent loading was developed which included the adhesive layer between the composite and the insert. This model predicts that damage occurs simultaneously in all the layers of the composite and in the adhesive at approximately 26 KN for lap shear loading. At this point, the load carrying capability of the joint is significantly reduced. The threshold for damage for the tapered insert is 32 KN with failure in the composite layer in contact with the steel plate. As shown in the earlier insert analysis, the tapered inset performs better than the cylindrical insert.

Structural Component Sub-Assembly Model

Component level elasto-plastic finite element analyses have been performed to study the detailed loading path and possible failure location/modes of the actual steel to steel joint sub-assembly with displacement controlled loading conditions provided by the OEM.

From this model, the predicted contour of Von Mises stress for the loading conditions shows static and overloading failure near the bolt holes. This suggests that the specified loading conditions are too severe for this sub-assembly.

Next, the components of the steel to steel joint subassembly were replaced with lighter weight composite components with the same topology as the steel components and material properties obtained from the candidate 3D composite. Under the same displacement controlled loading conditions, the FEA model predicts highest stresses at the edges of the bolt holes. However, the magnitude of the stresses is low indicating that the component and joint has become more compliant with the incorporation of the composite. Cast magnesium is being evaluated to incorporate into the design to enhance the stiffness without adding significant weight.

To further assess the effects of light-weighting with composites at the sub assembly level on the system vibration response, modal analyses of the sub-assembly have been performed under free boundary conditions. The predicted natural frequency and vibrational mode for Mode 7 corresponds to the vibrational frequency mode that is of most relevance for the normal heavy truck operating conditions. The natural frequency of the existing design is higher than the lighter weight designs incorporating composites and/or magnesium. Further design modifications are needed to enhance the stiffness of the system to more closely match the performance of the all steel sub-assembly.

Acknowledgements

The principal investigators would like to acknowledge the valuable contributions of other members of the research team, including Barbara Frame, Vlastimil Kunc and Tom Battiste at ORNL and Xin Sun, Elizabeth Stephens and Siva Pilli at PNNL.

Summary

ORNL and PNNL are collaborating on a 4 year research effort focused on the development of technically robust and economically attractive joining techniques to overcome the technical issues associated with joining composite chassis components in heavy vehicles. This work is being performed concurrently with an industry program to develop and commercialize composite chassis components, which will require resolution of the joining challenges. This report discusses the FY 2005 research activities.

Fatigue testing, including tension, compression and variable amplitude, has been conducted on the baseline component independent pultruded material as well as several 3D glass reinforced composites. Loss of bolt pre-load due to through the thickness creep of the composite has been monitored for composite/steel joints under static and fatigue loading. Mode I and Mode II joint fatigue tests have been done to evaluate the design modifications in composite thickness, steel inserts, steel reinforcing plates and adhesives. Modeling activities have focused on developing techniques to evaluate through thickness creep for joints with different washer and steel insert designs. Damage at the bolt holes has been evaluated taking advantage of the progressive failure analysis available in GENOA coupled with the contact algorithm in ABAQUS as the solver.

F. Laser Texturing of Propulsion Materials

Principal Investigators: Ali Erdemir, Oyelayo Ajayi, Robert Erck, Osman Eryilmaz, George Fenske, and Izhak Etsion (Technion University)
Affiliation: Argonne National Laboratory
Address: Energy Technology Division, Argonne, IL 60439
(630) 252-5190; fax: (630) 252-4798; e-mail: gfenske@anl.gov

Chief Scientist: James J. Eberhardt
(202) 586-9837; fax: (202) 587-2476; e-mail: James.Eberhardt@ee.doe.gov
Field Technical Manager: Philip S. Sklad
(865) 574-5069; fax:(865) 576-4963; e-mail:skladps@ornl.gov

Contractor: Argonne National Laboratory
Contract No.: W-31-109-ENG-38

Objective

- Assess and optimize the tribological performance of laser-textured (or dimpled) surfaces under a wide range of sliding contact conditions.
- Determine durability and tribological operational limits of laser textured surfaces.
- Elucidate fundamental tribological mechanisms that control friction and wear of these surfaces.
- Design and produce novel hard coatings over dimpled surfaces and explore their synergistic effects on friction and wear.

Approach

- Control and optimize dimple size, depth, and density. Determine their effects on friction and wear.
- Develop a reliable test protocol, specify test conditions, and perform well-controlled tests using a number of friction and wear test machines.
- In collaboration with Prof. Izhak Etsion (who supplies the dimpled surfaces), analyze test results and make judgments on the performance of the dimpled surfaces.
- Specify and apply hard coatings over laser-dimpled surfaces. Perform friction and wear tests to assess performance improvements.
- Characterize worn surfaces; elucidate mechanisms that control friction and wear.
- Promote/present findings at appropriate forums and generate more industrial interest.

Accomplishments

- Demonstrated significantly lower friction and wear under mixed lubrication regimes in tests using a unidirectional pin-on-disk machine.
- Demonstrated up to 90% increase in resistance to scuffing on laser-dimpled surfaces using a reciprocating wear test machine.
- Designed and built a test rig that simulates sliding motion between the ring and liner of an internal combustion engine.

- Completed a series of screening tests and found that the bulges around the dimples caused severe wear damage on the ring side. Parallel studies performed by Prof. I. Etsion at the Technion University have confirmed that up to 30% reduction in friction is feasible with laser-textured surfaces.
- Applied copper and superhard coatings on dimpled steel substrates and demonstrated much higher resistance to wear and scuffing.
- Completed work on laser-textured SiC seals and demonstrated 40 to 50% reductions in frictional torque.
- Performed a series of new tests to measure the lubricant film thickness of laser-textured surfaces.

Future Direction

- Concentrate on laser-dimpled piston rings and cylinder liners; determine effects of partial laser surface technology (LST) on friction and wear; optimize size, shape, and density of dimples to achieve the greatest beneficial effect.
- Develop and implement a reliable test protocol that is more prototypical of actual ring-liner sliding conditions; characterize worn surfaces; assess benefits of standard and partial LST and LST+superhard coatings.
- Assess friction reduction and energy-saving benefits of laser-dimpled rings and liners.
- Determine effects of LST on scuffing performance of superhard coatings.
- Determine effects of oil viscosity and/or ambient temperature on friction and wear behavior of dimpled and/or superhard-coated surfaces.
- Finalize current work on laser-textured piston rings and cylinder liners after removing the bulges around dimples. We will also explore the effects of surface roughness on friction and wear and determine if texturing of ring, liner, or both sides gives the best overall performance.
- Determine microstructural, chemical, and mechanical characteristics of heat-affected zones at or near the dimpled areas and determine their impact on friction and wear.
- Improve imaging technique to achieve better measurement of lubricant film thickness.
- Apply electrohydrodynamics modeling to LST-treated surfaces and correlate film thickness prediction with experimental measurements.

Introduction

Argonne has been evaluating the potential usefulness of laser texturing for a wide range of engine applications, including rings and liners, piston pins, water pump seals, and other tribological components where a significant amount of energy is spent to overcome friction. Laser texturing was originally developed by Prof. I. Etsion of the Technion University and was optimized over the past several years to become more cost-effective and, hence, viable for large-scale applications in diesel engines.

Laser texturing has enormous potential for increasing efficiency and durability of these engines. Specific components that can benefit from laser texturing are piston rings and liners, tappets, cam and follower interface, gear systems, water pump seals, and other bearing systems. Many of these components operate under different lubrication regimes during actual engine uses; hence, combining laser texturing with advanced coating technologies may have beneficial synergistic effects on friction and wear. Specifically, such coatings on textured surfaces may further reduce friction and wear and prevent scuffing under severe loading conditions, where direct metal-to-metal contact occurs.

The dimples created by pulsating laser beams on a surface are typically 4-10 μm deep and 70 to 100 μm wide. During the dimpling process, material melts and/or evaporates to create the dimples. A portion of the molten material is accumulated around the edges of the dimples and requires post-process removal; otherwise, the dimples can cause severe wear and high frictional losses during sliding contacts.

The micro dimples created by this method can act as miniature hydrodynamic bearings that reduce friction and wear by increasing the load-bearing capacity and, hence, the hydrodynamic efficiency of such sliding surfaces. They can also trap wear debris particles that generate during sliding contacts and hence prevent them from causing third-body wear. Accordingly, the primary objective of this project is to produce and further optimize the size, shape, and density of shallow dimples on sliding and rotating contact surfaces and to explore their effectiveness in reducing friction and wear in critical engine components. Furthermore, synergistic effects of soft and hard coatings on friction and wear of laser-dimpled surfaces are explored.

Experimental Procedures

Friction and wear testing of laser-textured surfaces was performed in a pin-on-disk machine while scuffing tests were conducted in a reciprocating test machine. The pins used in friction and wear tests were made of 9.55-mm-diameter hardened 52100 steel balls with a nominal hardness value of 60 HRC. On these balls, we created a flat spot having a diameter of about 4.7 mm. The disc samples, 50 mm in diameter and 10 mm thick, were made from hardened H-13 steel with 60 HRC. Dimpled and un-dimpled samples were used for the generation of friction maps that can show regions for hydrodynamic, mixed, and boundary lubrications. For the generation of these maps, we used normal loads ranging from 2 to 20 N that corresponded to nominal contact pressures of 0.16 to 1.6 MPa. The rotational speed varied between 10 and 500 rpm, corresponding to linear sliding speeds of 0.015 and 0.75 m/s. Two fully formulated, commercially available engine oils with differing kinematic viscosities were used for this study. Each friction test was conducted at a constant load starting with the lowest speed of 0.015 m/s. The sliding speed was increased in a stepwise manner after 3 min at each speed, until the maximum speed of 0.75 m/s was reached. With this procedure, each test starts with a very thin fluid film, and as the speed increases, the lubricant film thickness increases, allowing the contact to move from a boundary to a mixed, and, finally, to a hydrodynamic lubrication regime. Indications of the operating lubrication regime were assessed from the friction coefficients.

Reciprocating tests were performed in two test machines. One was used to study the friction and wear performance of cut segments of piston rings and cylinder liners, while the other was used to determine the resistance of laser-textured surfaces to scuffing. Scuffing is defined as a sudden catastrophic failure of a lubricated surface. It is poorly understood and a major source of reliability problems in numerous engine and drivetrain components. In the literature, the scuffing has always been associated with lubrication breakdown, wear particle and deposit formation, and steep temperature rise due to severe contact conditions. Scuffing tests were performed in a reciprocating test rig, and the specific test conditions involved stepwise increasing of the sliding speed from 1 to 5 Hz in 1 Hz increments. The time interval for each step was 2 minutes. If scuffing did not occur under a given load and up to 5 Hz, then the normal load was increased, and the above procedure was repeated at a different location with a different ball. The stroke length was 21 mm, and the lubricant used during these tests was a fully formulated synthetic commercial motor oil (10W/30).

Results and Discussion

Using the pin-on-disk machine and the specific test conditions described earlier, we generated a series of lubrication maps showing the regions where full hydrodynamic as well as mixed lubrication can be achieved with the laser-textured surfaces. Figure 1 shows that with laser-textured surfaces, the hydrodynamic regime has been greatly expanded to cover almost all of the load and speed ranges evaluated in this study. For un-dimpled surfaces, however, the hydrodynamic regime could only be maintained under light loads and at high speeds. These results can clearly illustrate the beneficial affects of laser texturing on controlling friction even under severe sliding conditions. We believe that shallow dimples created on the sliding surfaces increased the load-bearing capacity of these surfaces by acting as miniature hydrodynamic bearings and thus reduced friction. Microscopic inspection of

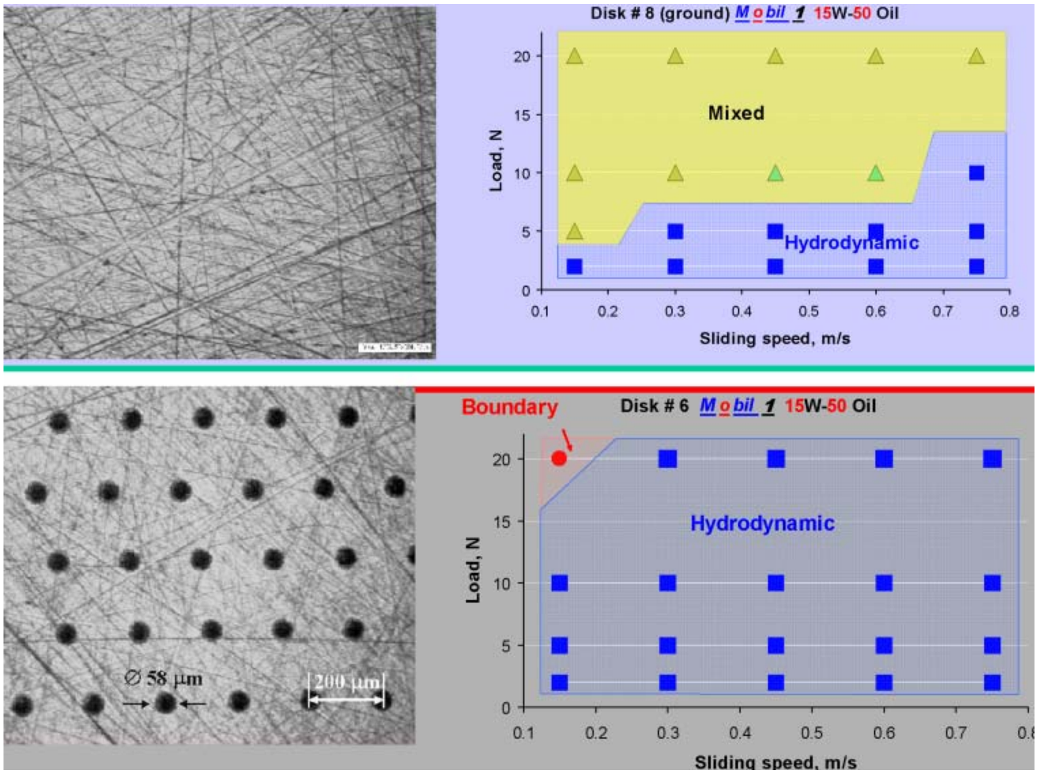

Figure 1. Comparison of lubrication performance of un-textured (top) and laser-textured (bottom) surfaces.

sliding surfaces after the sliding tests has revealed very little wear (mostly in the form of minor scratches) on these surfaces, while significant wear damage had occurred on the un-dimpled surfaces. We feel that the superior wear performance of dimpled surfaces may have been primarily due to the fact that very few metal-to-metal contacts had occurred on dimpled test pairs. Furthermore, any wear debris that may have been generated during sliding contact was trapped within the dimples, and hence third-body wear did not take place on dimpled surfaces.

The results of sliding friction and wear tests under reciprocating sliding contact conditions are shown in Figure 2. These tests were run with 9.55-mm diameter M50 steel balls. As is clear, the un-textured surface exhibits the highest friction, while the laser-textured surface has the lowest friction. The friction coefficient of a laser-textured surface with additional hard coating (included in this figure for comparison) was between that of the un-textured and textured surfaces.

Using the same reciprocating test machine, we also explored the scuffing resistance of laser-textured surfaces. As shown in Figure 3, compared to that of the un-textured surface, the scuffing resistance of the laser textured surface was much higher. In an attempt to determine the scuffing limit of laser-textured surfaces, we pursued further tests by increasing the test load stepwise until sliding surfaces scuffed. As shown in Figure 4, these surfaces could endure loads of up to 890 N without scuffing. However, upon further increasing the load to 1100 N, they scuffed. During post-test investigation of scuffed surfaces, we noticed that the dimples on the laser-textured surfaces were destroyed and filled with plastically flowed steel (see inset in Figure 4); hence, they were no longer able to store lubricant and perhaps act as miniature hydrodynamic bearings. We concluded that severe metal-to-metal contact had occurred on these laser-textured surfaces at high loads, and this greatly diminished their ability to resist scuffing.

In an effort to further increase the resistance of laser-textured surfaces to scuffing, we applied a soft

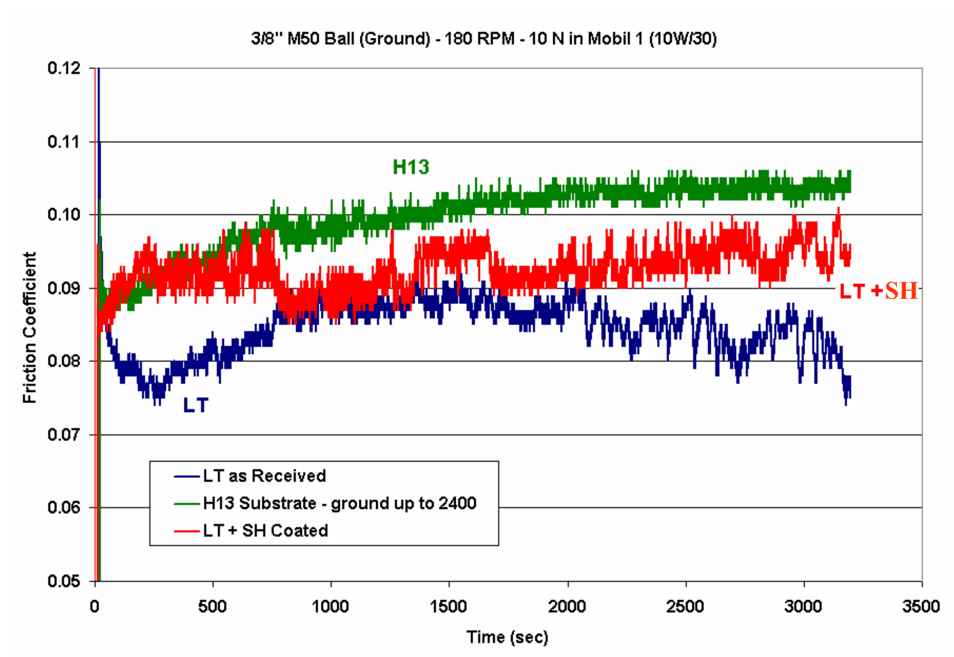

Figure 2. Friction performance of as-received H13, laser-textured (LT) H13, and laser-textured and superhard (SH) coated H13 under boundary-lubricated sliding conditions.

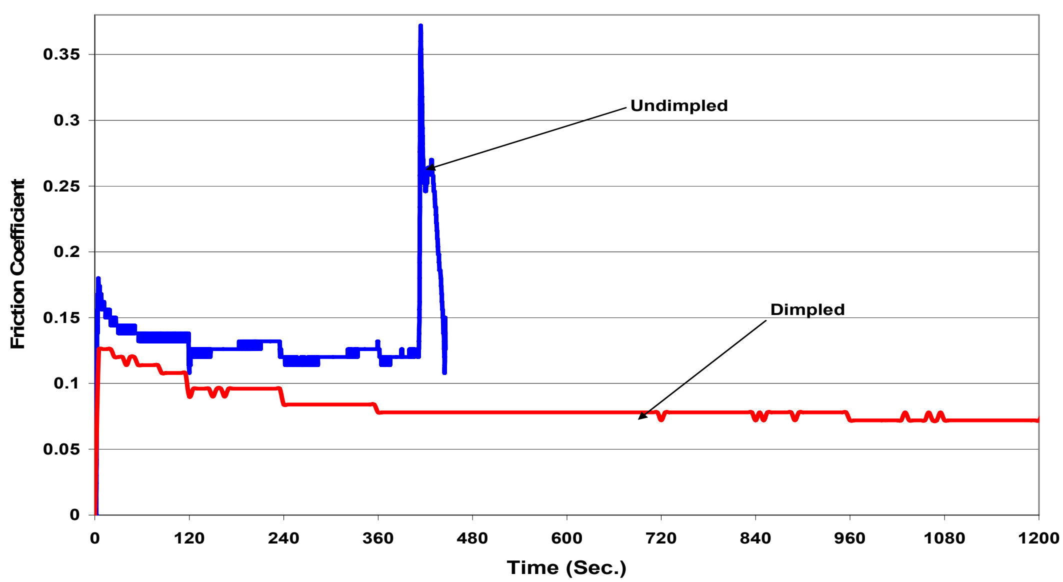

Figure 3. Comparison of scuffing resistance of an un-dimpled and laser dimpled steel sample. The undimpled sample scuffed rather quickly after sliding for about 6 min, while the dimpled sample kept sliding without any sign of scuffing for more than 20 min.

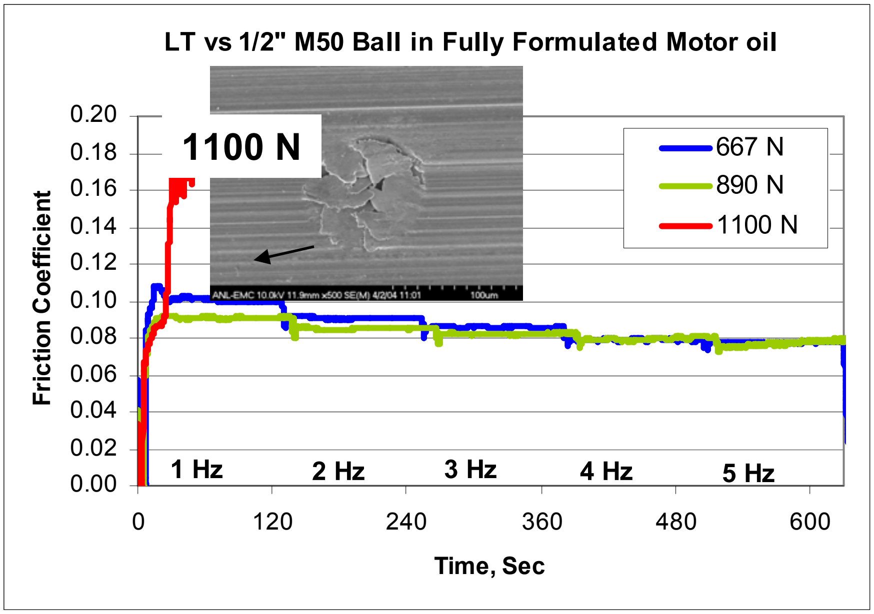

Figure 4. Scuffing performance of laser dimpled steel surfaces that passed the 667 and 890 N load tests, but failed at 1100 N.

(Cu) and a superhard coating over the laser-textured surfaces. We felt that such coatings may have beneficial synergistic effects on the scuff resistance of dimpled surfaces. The dimples were completely filled with Cu, and then the excess Cu was removed from the surfaces by progressively grinding them until the steel substrate was reached, as shown in Figure 5. In the case of a superhard coating, the thickness was kept uniform at around 2 µm inside and outside the dimpled areas. Figure 6 compares the scuffing performance of all samples tested in our study. As is clear, laser texturing combined with Cu and superhard coatings provides the best overall resistance to scuffing. In the case of Cu-filled dimples, microscopic inspection revealed that Cu was smeared on the sliding surfaces and was able to act as a solid or back-up lubricant. Cu is mechanically soft and chemically reactive toward certain ingredients (such as S) in the additive package of lubricant oil and hence can form a low-shear boundary film to prevent scuffing.

In the case of superhard coated surfaces, the resistance to scuffing was the highest of all samples tested, as shown in Figure 6. Superhardness in combination with the hydrodynamic lubrication effect of dimples seems to provide the best surface engineering strategy for preventing scuffing on laser-textured surfaces. In short, integration of surface coatings (both soft and hard) with laser texturing has a beneficial synergistic effect on the scuff resistance of textured surfaces.

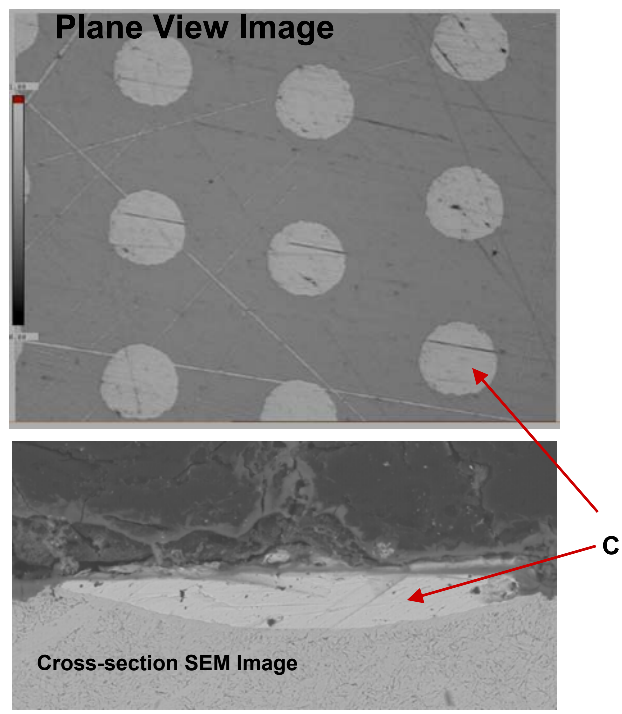

Figure 5. Plane view and cross-sectional SEM images of dimples filled with Cu.

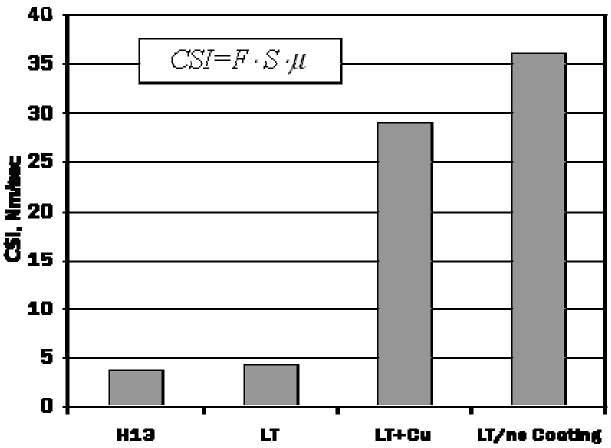

Figure 6. Scuffing performance of H13 base steel, laser-textured H13 steel (LT), laser textured and superhard coated H13 steel (LT/nc-coating), and laser-textured and copper coated (LT+Cu) surfaces. (CSI is the contact severity index, where F is the critical scuffing load in newtons, S is the critical scuffing sliding speed in m/sec, and μ is the friction coefficient shortly before scuffing.)

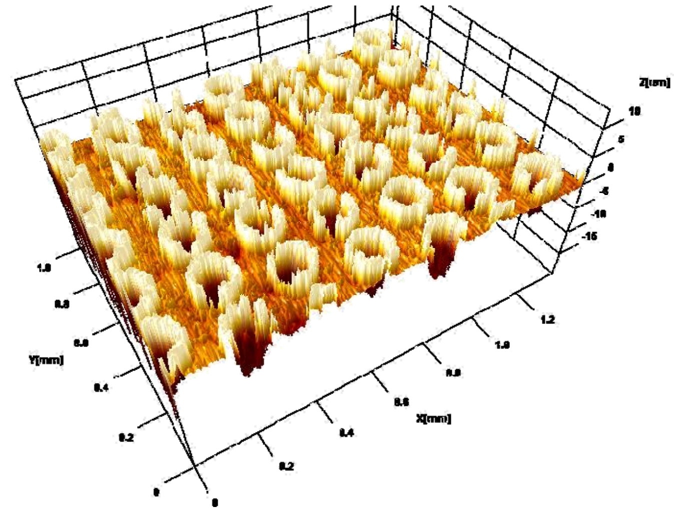

Figure 7. Physical shape of bulges that formed around the dimpled regions during laser texturing.

During this period, we also performed numerous tests on laser-textured rings and liners using a ring-on-liner test machine. The results of these tests have shown that extremely detrimental bulges formed around the dimples. Specifically, these bulges caused high friction and severe wear losses on the counterface rings. Figure 7 shows the shape and morphology of these bulges. We are removing these bulges from sliding surfaces and will soon run new tests to determine the beneficial effects of dimples on friction and wear of rings and liners. With the polishing of these bulges, we expect to significantly reduce the friction of such sliding pairs. To achieve even better tribological performance, we plan to create partial laser texturing on the ring side and to apply copper and superhard coatings on both rings and liners.

Conclusions

During this work period, we have concentrated on assessing the friction, wear, and scuffing performance of laser-textured surfaces. We have demonstrated that laser texturing can have a significant beneficial effect on friction and wear of lubricated sliding surfaces. Specifically, it increases the boundaries of hydrodynamic lubrication toward lower speed and higher load values. Applying a soft or hard coating over laser-textured surfaces has additional beneficial effects on friction and wear. Such coatings can also dramatically increase the resistance of laser-textured surfaces to scuffing. At present, we are focusing our attention on laser-textured piston rings and cylinder liners. Initial tests with as-dimpled liners revealed the detrimental effect of bulges found around the rims of dimpled areas. With effective removal of such bulges, we expect to significantly improve friction and wear of rings and liners as well.

Publications

During this period, we published and/or presented several new papers on laser texturing. The following is a list of these papers.

1. The Effect of Laser Surface Texturing on Transitions in Lubrication Regimes during Unidirectional Sliding Contact, A. Kovalchenko, O. Ajayi, A. Erdemir, Tribology International, 38 (2005) 219-225.

2. Review of Engineered Tribological Interfaces for Improved Boundary Lubrication, A. Erdemir, Tribology International, 38 (2005) 249-256.

3. Effect of Counterface Properties on Laser Textured Surfaces, A. Kovalchenko, O. O.

Ajayi, A. Erdemir, G. Fenske, I. Etsion, Presented at the 60th Annual Meeting of the Society of Tribologists and Lubrication Engineers, Las Vegas, NV, May 15-19, 2005.

4. Scuffing Resistance of Laser Textured Surfaces. M. K. Kazmanli, O. L. Eryilmaz, A. Erdemir, L. Ajayi, I. Etsion, and M. Urgen, Paper to be Presented at the World Tribology Congress, Washington, DC, September 12-16, 2005.

5. Tribological Behavior of Oil-lubricated Laser Textured Surfaces in Conformal and Point Contacts, A. Kovalchenko, O. O. Ajayi, A. Erdemir, G. Fenske, I. Etsion, Paper to be Presented at the World Tribology Congress, Washington, DC, September 12-16, 2005.

6. Integrated Surface Engineering Approaches to Improved Boundary Lubrication: Merging Multifunctional Surface Coatings with Laser Texturing, A. Erdemir, Presented at the International COST 532 Conference, Porto-Portugal, October 12-14, 2005.

7. Investigation of Scuffing Resistance and Tribological Performance of Laser Modified Surfaces, S. Aldajah and O. O. Ajayi, Presented at the World Tribology Congress, Washington DC, September 12-16, 2005.

G. Friction Stir Joined Aluminum Sheet Materials for Heavy Vehicle Cab Structures

Principal Investigator: Glenn J. Grant
Pacific Northwest National Laboratory
P.O. Box 999, Richland, WA 99352-0999
(509) 375-6890; fax: (509) 375-4448; e-mail: glenn.grant@pnl.gov

Chief Scientist: James J. Eberhardt
(202) 586-9837; fax: (202) 587-2476; e-mail: James.Eberhardt@ee.doe.gov
Field Technical Manager: Philip S. Sklad
(865) 574-5069; fax:(865) 576-4963; e-mail: skladps@ornl.gov

Participants:
Leon Kaunitz, Scott Wazny, and Brian Fulbright, Freightliner LLC
Douglas Waldron and Keith McTernan, Advanced Joining Technologies, Inc.
Tom Sanor, Drive Automotive
Gene Paik, Alcoa, Inc.

Contractor: Pacific Northwest National Laboratory
Contract No.: DE-AC06-76RL01830

Objective

- Develop and deploy friction stir joining (FSJ) as a weight and cost-saving manufacturing technology for heavy vehicle cab structures.

Approach

- Demonstrate the use of aluminum tailor-welded blanks (TWBs) for heavy vehicle applications.
- Develop weld process parameters to lower manufacturing cost, increase joint reliability, and explore dissimilar material blanks that can afford additional weight savings.
- Develop and prototype lightweight, cab-in-white structures including door inners, door opening panels, back-wall, and floor structures for Class 7-8 trucks using FSJ technologies.
- Address manufacturing issues to lower blank fabrication cost and other barriers to implementation of Al TWBs.

Accomplishments

- Developed process parameters and joining conditions to fabricate blanks in several similar and dissimilar aluminum alloys that were subjected to stamping trials.
- Characterized the local mechanical properties of the weld metal and surrounding region of AA5052-H32 and AA5182-O TWBs to understand the effect of the welding process on the ductility of the weld metal.
- Investigated new part configurations, using thin-gage heat-treatable alloys and dissimilar alloy combinations (5000 and 6000 series aluminum TWBs).
- Constructed three, full-scale Class 8 truck cabs using friction stir welded TWBs for the door inners, door opening panels, backwall, and floor.
- Passed full scale crash and durability testing for the constructed cabs (no weld related structural failures were observed).

- Investigated the interaction between the weld in the TWB and the joining method used to assemble the blank into the vehicle and determined how this interaction influenced long-term vehicle durability and crashworthiness.
- Developed welding process parameters to minimize cost and maximize performance of truck components.

Future Direction

- Continue with the weld process and tool development for dissimilar alloy combinations and hard alloys (6xxx, 5xxx H3x, etc.) that would employ greater cost and weight savings.
- Develop and optimize the welding process parameters of dissimilar aluminum alloys of different thicknesses (5182-O and 6022 aluminum alloys).
- Conduct a design of experiments on tool development and process design for high speed welding (+150 inches per minute) to decrease cost parity with monolithic sheet stampings.
- Focus on friction stir joining as a low-cost enabler of lightweight, low-cost vehicle assembly (non-TWB).

Introduction

This work is a collaborative effort between Pacific Northwest National Laboratory (PNNL), Freightliner, LLC, Advanced Joining Technologies, Inc., Drive Automotive, and Alcoa. This project aims to develop and deploy FSJ as a weight and cost-saving manufacturing technology for heavy vehicle cab structures. To date, the project has focused on 1) developing the appropriate FSJ process parameters to create high-reliability joints that survive stamping operations; 2) prototyping full cabs using FSJ technologies and testing for durability and crash performance; and 3) addressing manufacturing issues including lowering blank fabrication cost and other barriers to implement the technology. The challenge is to develop stamped panels that can meet the unique strength and durability requirements of heavy vehicle cab structures.

Aluminum TWBs consist of multiple-thickness and multiple-alloy sheet materials welded together into a single, variable-thickness blank. Figure 1 shows a typical fusion-welded TWB before and after a stamping application. A TWB is assembled as a series of flat sheets joined together, which are then submitted to a stamping process. The technology allows production of a weight-optimized, variable-thickness vehicle body component. TWB technology gives automotive and truck designers the ability to selectively vary body panel thickness to optimize the use of material. Successful use of the technology ultimately results in reducing vehicle weight without compromising final strength, stiffness, and durability. The manufacture of TWBs and their application in body panels requires that the weld material deform under biaxial loading during sheet metal stamping. The deformation of weld materials and their limits of formability are important aspects of TWB technology.

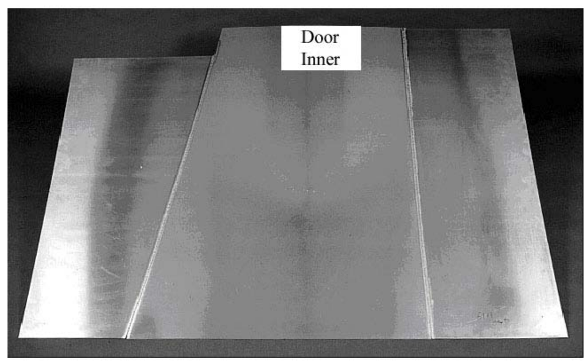

(a)

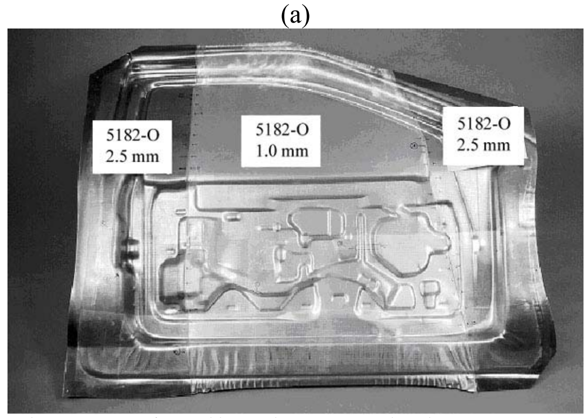

Photos courtesy of Reynolds Metals Company and Ogihara America Corp.

(b)

Figure 1. (a) A TWB viewed in the as-welded condition, ready for submission to the stamping process. The shape shown is typical for a door inner stamping operation. (b) Aluminum TWB after stamping to produce a door inner panel.

The primary challenge of using aluminum TWBs in the past has been the relatively low ductility of aluminum fusion welds, which often results in premature fracture or lack of reliability of weld materials during stamping. Improving aluminum weld quality, understanding and describing the formability of the weld region, and predicting its formability are the primary technical challenges in using aluminum TWBs.

FSJ is a revolutionary joining technology that employs severe plastic deformation to create solid state joints between wide varieties of different materials. Invented by TWI, Ltd., about 12 years ago, FSJ is capable of producing aluminum alloy welds as good as (or significantly better than) fusion welds in terms of joint efficiency, mechanical properties, and environmental robustness. The advantage of using this solid state joining technique is the ability to avoid liquid metal during joining, where aluminum has low molten viscosity, high reflectivity, and a relatively high propensity to form internal porosity because of the high solubility of hydrogen in liquid aluminum.

Friction stir welding (FSW) can also eliminate hot cracking and minimize heat-affected-zone (HAZ) issues in 6000-series heat-treatable aluminum alloys. Avoiding the liquid phase of the materials also avoids the formation of various large eutectic constituent particles or other undesirable intermetallic particles that develop in particular alloys or with certain types of weld or materials contamination.

The use of FSW also better facilitates welding of heat-treatable materials, since the HAZ is normally smaller or less pronounced compared with fusion welding. The use of solid state joining enables a variety of types of dissimilar aluminum alloy joining not normally possible using fusion welding methods. The goal of producing a highly formable weld joint may be achievable with friction stir welding because of the wide range of weld heat, plastic work, and weld metal grain size manipulation that is possible.

FSJ Process Parameter Development

In a previous feasibility study, some alloy combinations were successfully stamped from TWBs fabricated by FSJ. However, weld line failures occurred in many other alloy combinations. The main thrust of this program is to better understand the weld process, forming parameters, and performance characteristics of TWBs and to apply them to a wider range of cab components. The use of FSJ to produce TWBs may result in dramatically improved weld quality and formability of aluminum TWBs —thereby enabling this weight and cost-saving technology.

In order to develop and use FSJ to make high-quality aluminum TWBs for intermediate- and high-volume truck applications, the FSJ process must be competitive with laser welding and other fusion welding technologies from a production rate perspective. The target weld speeds are 2–5+ meters/minute. The friction stir welds must also be significantly higher in formability compared with conventional fusion welds.

This project will develop process parameters to make successful welds in the following weld combinations, as they are representative of typical truck alloys and material thicknesses:

- 5182-O 2 mm to 5182-O 2 mm
- 6022-T4 2 mm to 5182-O 1.6 mm
- 6022-T4 2 mm to 5182-O 2 mm
- 5182-O 2 mm to 6022-T4 1.6 mm
- 5182-O 2 mm to 5182-O 1.6 mm
- 6022-T4 2 mm to 6022-T4 1.6 mm
- 6022-T4 2 mm to 6022-T4 2 mm
- 5052-H111 1.27 mm to 5052-H111 1.27 mm
- 5052-H32 1.6 mm to 5052-H32 1.6 mm

This project will determine, within the "defect-free" process window, where a set of parameters exists that produces a TWB with the best formability (see Figure 2). Within that process window, an optimum set of parameters exists for forming and stamping, and those conditions may not necessarily be the best for other properties (ultimate strength, etc.). The process and forming parameters are being developed by FSW test coupons at a range of weld conditions, which are then subsequently tested for strength and formability to establish optimum weld conditions for each material and thickness combination of interest.

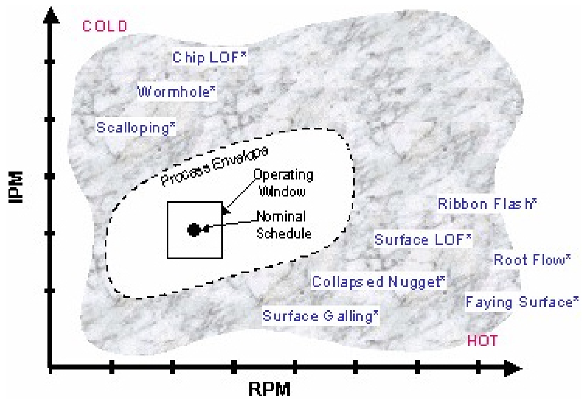

Photo courtesy of Bill Arbegast, SDSMT

Figure 2. An illustration of the process parameter window to determine the optimum set of parameters that produce a TWB with the best formability.

Limited Dome Height Testing

Limited dome height (LDH) testing and miniature tensile testing has shown that welded blanks with the highest dome heights can be correlated with those that have minimal property gradients across the weld zone. Minimal property gradients delay the onset of necking instability. Changes in process parameters will change the local mechanical properties and provide a way to "customize" the weld to the parent sheet. Picking process parameters that match flow stresses between the sheet and the weld zone may be a strategy to increase stamping performance.

A typical process parameter matrix is shown in Table 1. In this case, data is shown for a TWB with 5182-O, 2mm thick material on one side of the weld, and 6022-T4, 1.6mm thick on the other. Similar matrices were compiled for other material combinations but are not presented here. This data is sorted on decreasing LDH height at failure, and includes notes on the failure style. It can be seen that for this material combination at a weld travel speed of 75 inches per minute (ipm), the tested LDH height was 0.583 in. Higher dome heights were achievable with increasing traverse speeds up to 150 ipm, however, above 150 ipm, the dome heights dramatically decreased. At a travel speed of 275 ipm, the weld split easily at low load indicating a very poorly consolidated weld. From this data, based on LDH testing, 150 ipm at 2000 rpm are inferred to be the optimum welding parameters for this tool and welding conditions.

Table 1. Example test matrix – 5182-O 2mm joined to 6022-T4 1.6mm

	Travel Speed (IPM)	*Rotation Speed (RPM)*	*LDH Height (in.)*	*Failure Type*
Weld 4.2	150	2000	0.624	Failed in thin sheet (6022), parallel to weld, right on weld
Weld 4.4	100	2000	0.598	Failed in thin sheet (6022), parallel to weld, 0.1" from weld
Weld 4.1	125	2000	0.589	Failed in thin sheet (6022), parallel to weld, 0.1" from weld
Weld 4.3	75	2000	0.583	Failed in thin sheet (6022), parallel to weld, 0.15" to 0.2"
Weld 4.5b	175	2000	0.533	Failed in weld, parallel to weld, off centerline on retreating side
Weld 4.6b	200	2000	0.510	Failed in weld, parallel to weld, on centerline
Weld 4.7b	250	2000	0.428	Failed in weld, parallel to weld, on centerline
Weld 4.8b	275	2000	N/A	Failed early in test, "unzipped" on centerline at low load
Weld 4.9b	300	2000	N/A	Failed early in test, "unzipped" on centerline at low load

From the LDH data, process maps can be constructed like that shown in Figure 3. For welded blanks with 5052-H111 on both sides of the joint (and similar thicknesses), good LDH performance relative to an unwelded blank is achievable at generally higher tool rotation speeds. Also, welded blank dome heights 90% as high as monolithic (unwelded) sheets can still be achieved at traverse speeds up to 130 ipm.

In a manufacturing environment, high weld traverse speeds are important for good throughput. One objective of the process parameter development program was to see how LDH results varied with increasing weld speeds up to the limits of the experimental setup or process. Maximum weld traverse speed is very much a function of tool design, so the results obtained in this study only reflect the maximum weld speeds for the single tool used in this study. Figure 4 shows that for 5052-H111 a region exists where enhanced LDH results can be achieved if some tradeoff in ductility can be tolerated. The best dome heights are found at the slower traverse speed for welds made at both

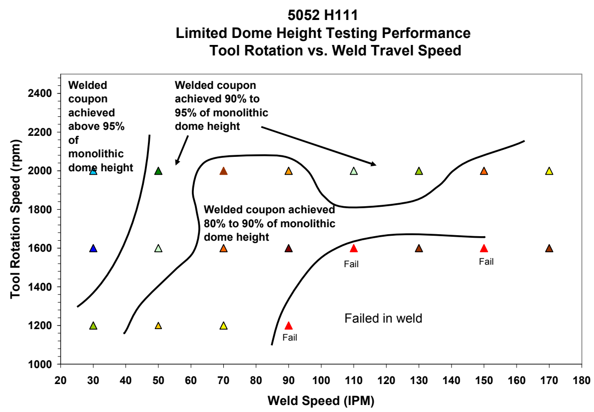

Figure 3. Process parameter map showing how a welded blank with 5052-H111 material on each side of the weld compares to a monolithic (unwelded) sample of the same material. The data is grouped by the percentage of monolithic dome height achieved by the welded assembly.

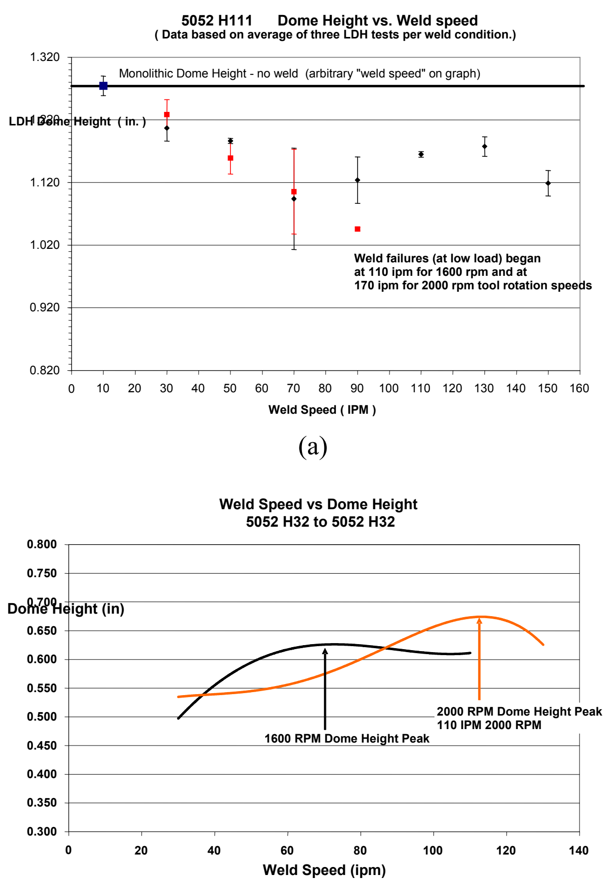

(a)

(b)

Figure 4. Dome height vs. weld speed for 5052 alloys. (a) Results of 5052 in an H111 temper, and (b) results for a H32 temper. Both tempers show enhanced ductility at high weld speed.

1600 rpm and 2000 rpm. However, for 2000 rpm a region exists around 120 to 130 ipm where ductility again increases. The reason for this is not clear, but it occurs in 5052-H111 as well as 5052 when it is in a work hardened, H32 temper. These formability "sweet" spots indicate some favorable balance of input heat, time at temperature, conduction, HAZ development, and nugget microstructure can combine to create favorable ductility, even at high process speeds. This study was limited to a maximum rotation speed of 2000 rpm, but the process maps suggest even higher rotation speeds may produce favorable results.

Once process parameters are established, maximum strains can be analyzed using optical techniques. In order to help predict the stamping performance of a FSW joined TWB, surface strains can be measured and midplane strains can be calculated for LDH specimens tested to failure. Post test strains developed in the specimen can be measured in the weld, the heat affected zone, and the parent sheet. The specimens tested during this study were full width LDH that undergo approximately equal biaxial stretching near the top of the specimen, and a complex and changing strain history in the region between the punch and the circular lockbead. A post-test strain analysis reveals only the final strain distribution from a sample that has had each material point follow a complex strain path. However, strain analysis of LDH specimens can provide data that correlates well with stamping trials and gives an indication of the maximum strains that will be achievable during biaxial stretching.

Figure 5 shows results from typical strain analysis. These results are from an LDH specimen taken to failure that has 5182-O 2mm on the left side of the FSW joint and 5182-O 1.6 mm on the other. The failure occurred by necking instability parallel to the weld about 0.2 inches from the weld edge in the thin side sheet. The region immediately adjacent to the necked zone showed a uniform major strain of about 18 to 21%. This is the maximum homogeneous strain to which this welded blank can be subjected at failure. This data and the Forming Limit Diagram in the lower part of Figure 5 can be used to estimate limit strains for finite element analysis of different die designs, and can help in part design and joint placement for stamping trials.

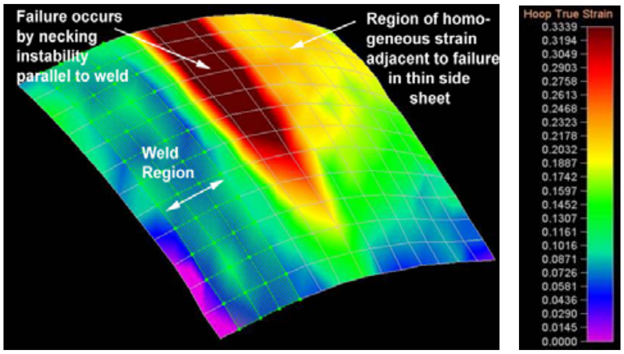

(a)

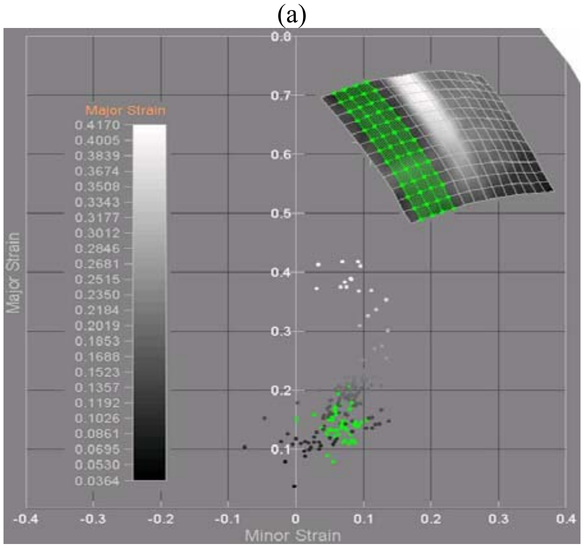

(b)

Figure 5. (a) Optical strain grid analysis of an LDH specimen of 5182-O 2mm joined to 5182-O 1.6 mm. FSW weld region is cross hatched on left side of specimen. (b) Forming limit diagram showing the distribution of strain near the failure.

Mechanical Property Gradients

Optical strain analysis on tested specimens can only provide data on the final strain distribution in the assembly. In order to effectively model the performance of a blank in a die design, data is needed on local property variation. Microhardness variation in cross section can be used to infer property gradients, but requires assumptions on the relationship between microhardness and yield stress. Miniature tensile testing is a useful, although time consuming, technique to determine the flow curves for each region of a heterogeneous assembly.

Tensile testing of miniature specimens produces the flow curves seen in Figure 6. Figure 7 illustrates the specimen design. For blanks with 5182-O on both sides of the FSW joint, the flow stress of the weld metal is very close to the flow stress of the parent sheet and displays a similar hardening profile. There is a slight increase in flow stress in the weld metal especially on the top side of the weld, but it is not large. The similarity of the flow curves is due to the fact the parent metal is already in a soft condition (O temper) and additional weld heat did not create additional softening.

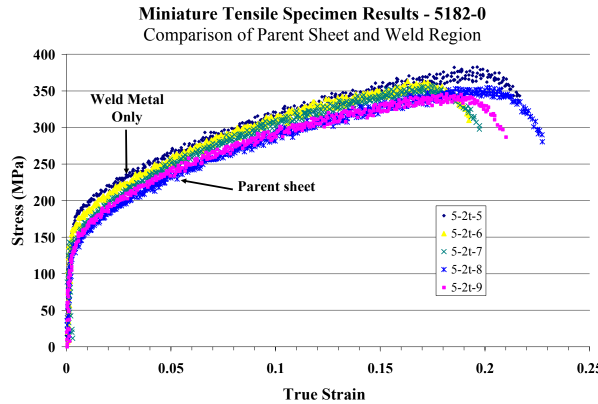

Figure 6. Flow curves for miniature specimens taken from weld metal and parent sheet at increasing distance away from the weld edge in 5182-O.

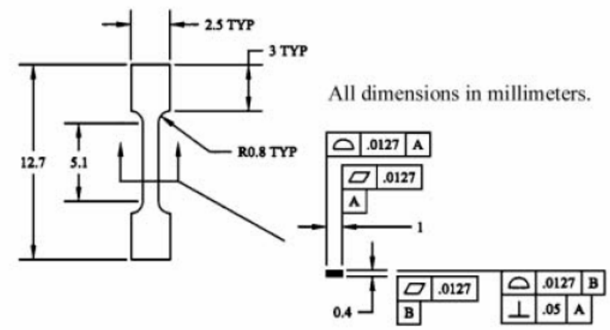

Figure 7. Miniature tensile specimen dimensions.

These results illustrate there is little effect on ductility due to the welding process. This feature is very important for producing a homogeneous distribution of strain in response to stress during stamping. Minimizing strain gradients is an important strategy to prevent early flow localization and failure during stamping.

In contrast, friction stir (or any joining process that introduces heat) can be challenging for later forming if the mechanical properties of the weld metal differ significantly from the parent material. Figure 8 shows the results of miniature tensile tests on specimens taken from a FSW joined blank of 5052 in a work hardened condition (H32). The weld metal has a significantly lower flow stress than the parent sheet due to the recrystallization in the nugget. The effects of partial annealing of the work hardened condition in the thermal mechanical affected zone can also be seen by the slight decrease in yield as the weld edge is approached from the parent sheet. Interestingly the ultimate strength of the weld nugget is higher than the parent sheet, and the ductility is, of course, significantly higher than the harder H32 material (Figure 9).

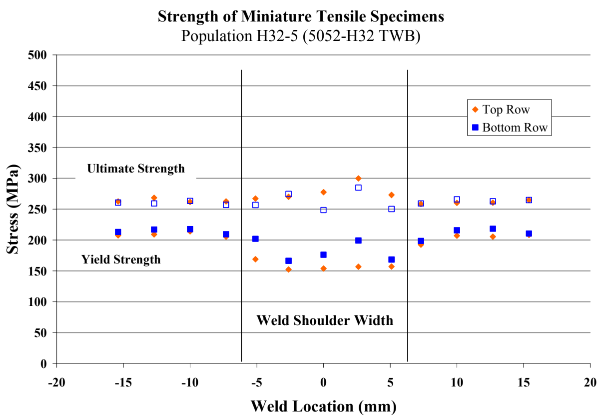

Figure 8. Yield and ultimate strength variation across a FSW in 5052-H32.

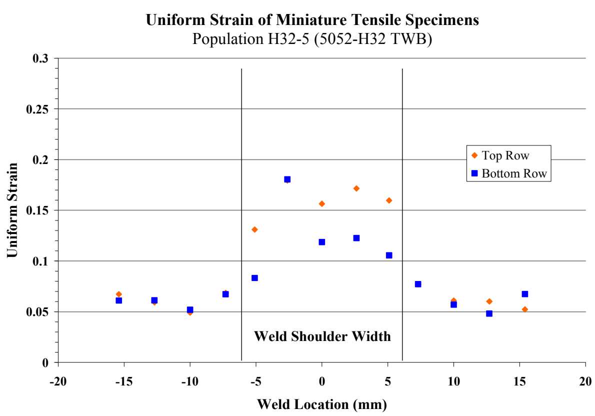

Figure 9. Local ductility of weld metal and adjacent parent material in a 5052-H32 welded assembly.

Stamping Trials and Assembled Cabs

When the weld process parameters were optimized for the material combinations investigated in this project, Advanced Joining Technologies, Inc. fabricated the blanks and the FSJ welded blanks were subsequently stamped by Magna utilizing conventional dies. Figure 10 illustrates several of the cab-in-white structures fabricated.

While many material combinations were successfully stamped, others, which would have had strong manufacturing arguments (cost and weight savings), were not successfully stamped. During stamping, some were less robust, especially hard alloys and some dissimilar material joints. For

(a)

(b)

Figure 10. Photos of stamped friction stir welded TWB cab structures. (a) Door inner panel. (b) Door opening panel.

example, joints in 5182-O had excellent formability performance, but joints in 5052-H32 sheet failed in the stamping trials. The weld metal in 5052-H32 has a significantly higher strain at failure (from the fine-grained, recrystallized nature of the nugget) than the parent sheet, leading to early localization in the weld metal. More process development is needed for 5052-H32 to enhance its stamping reliability.

For the successfully fabricated blanks in several similar and dissimilar aluminum alloy sheet combinations, the friction stir welded TWB stamped panels were shipped to Freightliner and assembled into three full-sized Class 7-8 cabs. Cabs were tested for durability (shaker table) and crash performance by Freightliner. The assembled cabs passed full scale crash and durability testing with no weld related structural failures observed.

Manufacturing Concerns

Ultimately, these TWBs need to be assembled into a vehicle, and the interaction between the weld in the TWB and the joining method used for assembling the blank into the vehicle needs to be understood. Automotive designers need to know whether these joints are within the target joint strengths for a particular application. In this project, the interaction of a friction stir welded 1.6 mm 6022-T4 and 2mm 5182-O TWB joined to 2mm 5182-O monolithic sheet material by a self-piercing rivet was investigated to determine how the interaction between the rivet and the friction stir weld in the TWB may influence long-term vehicle durability and vehicle crash worthiness.

First, a preliminary evaluation to determine the position of the rivet in the joint that yielded the weakest joint strength was conducted. Then, a more thorough investigation of the weakest joint configuration to determine the structural integrity and performance of the joint was conducted. Figure 11 illustrates the joint assembly and Figure 12 shows the cross section of one of the joint configurations investigated. Uniaxial tension tests were performed on lap shear and cross tension coupon assemblies to characterize the joint strength and the total energy absorption capability of the friction stir welded TWB/monolithic sheet self-pierce riveted joints.

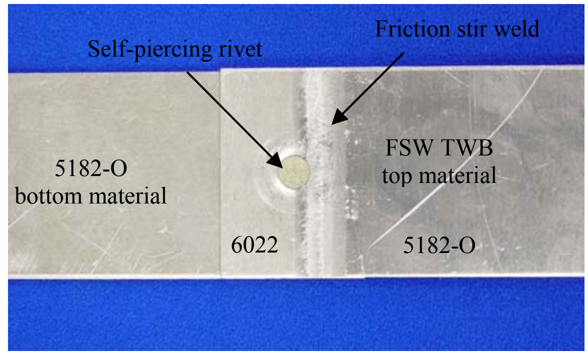

Figure 11. Photo of a friction stir welded AA6022-T4 and AA5182-O TWB (top material) joined to AA5182-O (bottom material) by a self-piercing rivet.

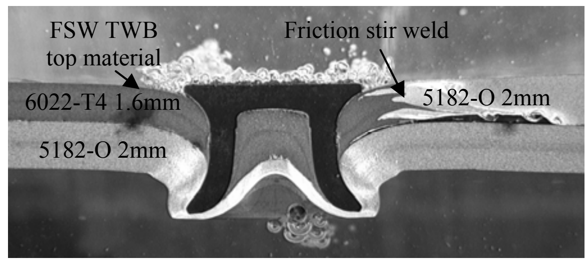

(b)

Figure 12. Photograph illustrating the cross section of the joint assembly where the SPR is piercing through the 6022-T4 sheet in the HAZ region of the TWB.

In this investigation, piercing through the heat-affected zone in the friction stir weld and through the thinner material (1.6mm 6022-T4) of the tailor welded blank exhibited the weakest static strength in comparison to piercing through the weld center and weld edge through the 2mm 5182-O sheet of the TWB. The heat-affected zone region in the 6022 sheet in the blank also had a dominant affect on the fatigue failure and failure location of the TWB/ monolithic sheet joints. In addition, the significant difference in sheet thickness of the blanks (20% thickness difference) is a contributing factor to the performance results observed. Essentially, this study suggests that it is best to avoid the weld region, particularly the HAZ in the thinner material of the TWB, if possible, during the assembly process. Details of this study are presented in *SAE Special Publication SP-1959*.

Conclusions

From this investigation, the following conclusions were derived:

- Friction Stir joining is suitable for fabricating aluminum TWBs.
- Weld speeds can be very high (up to 130 inches per minute using the tools in this study) and still produce good performance in LDH testing. Process maps suggest higher rotation speeds may allow even higher travel speeds (this study was limited to 2000 rpm rotation speed).
- Process parameters can be established through experimental programs that lead to joints that show up to 96% of the unwelded parent metal ductility.
- The FSJ process is "customizable" for mechanical properties and the weld process parameters can be optimized for formability.

Presentations and Publications

1. "Evaluation of the Mechanical Performance of Self-Piercing Rivets in Friction Stir Welded Structures" presented at Society of Automotive Engineers 2005 World Congress, Detroit, MI, April 13, 2005.

2. "The Formability of Friction Stir Welds in Automotive Stamping Environments" presented at Society of Automotive Engineers 2005 World Congress, Detroit, MI, April 13, 2005.

3. "Friction Stir Joined Aluminum for Heavy Vehicle Cab Structures" presented at 21st Century Truck Partnership Project Review Meeting, Oak Ridge, TN, September 14, 2005.

4. Grant, GJ, et al. 2005. "The Formability of Friction Stir Welds in Automotive Stamping Environments." SAE Special Publication SP-1959, SAE International, 141-151.

5. Stephens, E.V., et al. "Evaluation of the Mechanical Performance of Self-Piercing Rivets in Friction Stir Welded Structures." SAE Special Publication SP-1959, SAE International, 153-158.

H. Friction Stir Joining and Processing of Advanced Materials Including MMCs

Principal Investigator: Glenn J. Grant
Pacific Northwest National Laboratory
P.O. Box 999, 902 Battelle Blvd., Richland, WA 99352
(509) 375-6890; fax: (509)375-44; e-mail: glenn.grant@pnl.gov

Project Manager: Moe Khaleel
Pacific Northwest National Laboratory
P.O. Box 999, 902 Battelle Blvd., Richland, WA 99352
(509) 375-2438; fax: (509) 375-6631; e-mail: moe.khaleel@pnl.gov

Chief Scientist: James J. Eberhardt
(202) 586-9837; fax: (202) 587-2476; e-mail: James.Eberhardt@ee.doe.gov
Field Technical Manager: Philip S. Sklad
(865) 574-5069; fax:(865) 576-4963; e-mail: skladps@ornl.gov

Participants:
Bill Arbegast, Glen Stone, Stan Howard, Casey Allen
Advanced Materials Processing Center
South Dakota School of Mines and Technology
Rapid City, S.D.

Contractor: Pacific Northwest National Laboratory
Contract No.: DE-AC06-76RL01830

Objective

- Develop Friction Stir Joining and Processing (FSJ / FSP) to enable more widespread use of lightweight, advanced materials in heavy vehicle manufacturing.

Approach

- Develop new technologies within the broad topic area of friction stir joining and processing that facilitate lightweight manufacturing methods and new materials for use in heavy vehicle application.
- FY 2005 the project focused on three primary areas:
  - Use FSP to create engineered surfaces on lightweight materials that display enhanced surface properties
  - Use FSJ to join sheet materials for superplastic forming applications
  - Develop fundamental process models using a new approach: Smooth Particle Hydrodynamics (SPH)

Accomplishments

- Developed methods to incorporate ceramic powder into the surface of aluminum and cast iron to produce engineered surfaces for improved wear resistance.
- Developed the new area of Friction Stir Reaction Processing to create engineered surfaces that contain solid state, in-situ formed phases including nano-sized particles that impart unique properties to a material (increased strength, hardness, ductility, and fatigue life).
- Developed FSJ weld metal with superplastic properties to facilitate large multi-sheet SPF or integrally stiffened panel applications for heavy vehicle cab structures.

- Developed unique computational code based on SPH to predict material flow, mixing and defect formation in FSJ/P.

Future Direction

- Initiate wear testing of engineered surfaces created using FSP.
- Develop weld process parameters that enhance superplasticity in joined assemblies to allow for part consolidation in light-weight SPF cab structures.
- Test multi-sheet and integrally stiffened panel for strength, modulus and other mechanical performance metrics.
- Parallelize SPH computational code to run on supercomputers to improve the ability of the model to define fine features of flow, defect formation and tool designs in friction stir joined or processed material.

Introduction

One of the key strategies for making a vehicle energy-efficient is to manufacture it from lighter materials. Structural and functional requirements, however, lead to a situation where no single lightweight material is appropriate for all applications. A modern, weight-optimized vehicle structure is a hybrid of many materials. A critical problem that has emerged in the development of these hybrid structures is that for many material combinations, traditional joining technologies (e.g., fusion welding or mechanical fastening) are not appropriate. For some highly specialized materials, like aluminum MMCs, titanium, and advanced high-strength steels, a better joining technology can have significant impact on whether these materials have a role in future vehicle structures.

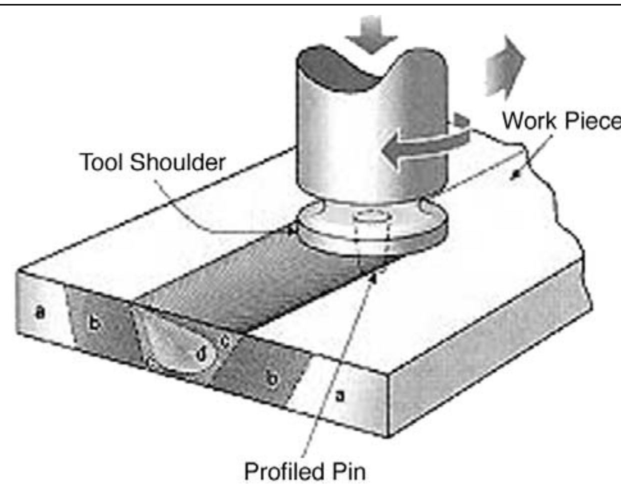

Figure 1. Friction stir joining and processing are accomplished by plunging a spinning tool into a material and translating the tool across the surface to form either a joint or a surface processed region (TWI, Ltd.).

In the last 15 years, a new joining technology, Friction Stir Joining (FSJ) has emerged and has the potential to join many lightweight materials. Invented by TWI, Ltd., FSJ is a solid state process that employs severe plastic deformation to create joints between a wide variety of different materials. A typical FSJ butt joint is depicted in Figure 1. The weld is created by clamping the materials to be joined and plunging a spinning tool into the surface. The spinning tool is then translated down the joint line, leaving behind a weld zone characterized by a fine-grained, dynamically re-crystallized microstructure. Typically, the tool is spun at 400 rpm to 2000 rpm and translated down the joint line at a rate of 4 to 300 in./min, depending on tool design, base material, and thickness. As the tool rotates and translates, complex flow patterns develop in the base material that creates an intimate mixing of materials from both sides of the weld. Heat input during plastic deformation generally creates a temperature in the weld between 0.6 and 0.8 of the absolute melting temperature so that no liquid phase is generated.

FSJ is capable of producing aluminum and magnesium alloy welds as good as or better than fusion welds in terms of joint efficiency, mechanical properties, and environmental robustness. A significant advantage of the process, for application to hybrid structures, is that since there is no melting during the process, a large variety of dissimilar material joints are possible, including dissimilar aluminum and magnesium joints that are not possible with conventional fusion welding.
In the last five years, FSJ has been shown to be a commercially important, energy-efficient, and

environmentally friendly process for joining aluminum. However, there are many opportunities for other higher-strength lightweight materials to be considered if good joining technologies for these materials existed as well. The objective of this project is to investigate how FSJ can be applied to advanced materials including AL-MMCs, titanium, steels, cast iron, and materials that display graded structures with unique surface properties. Moving the FSJ process from "soft" materials like aluminum and magnesium into advanced, higher-strength alloys has proved to be challenging because of the mechanical and thermal demands on the tool materials. In steels, for instance, the tools must survive high forge loads as well as tool temperatures of up to 1100°C.

Friction Stir Processing

Recently, a new research direction has emerged as an outgrowth of FSJ that recognizes that the same solid state deformation process can be used to modify the surface of a monolithic material for enhanced properties. This new research direction is called Friction Stir Processing (FSP).

During previous years, this project demonstrated that it is possible to create a particle-reinforced zone of 20-micron SiC or Al_2O_3 particles in a 6061 aluminum base alloy (Figure 2). Microscopy has shown that the stirred region is developed as deep as the pin probe (up to 0.25 inches in our tests), it is defect-free and it forms a graded metallurgical bond with the underlying surface. No interface is developed between the composite zone and the base material. The surface zone has the potential to be orders of magnitude thicker than conventional coating technologies; and it has the added benefit of producing a graded structure that does not have a sharp interface with the underlying substrate, thereby avoiding many of the problems seen in conventional coatings (coefficient of thermal expansion mismatch, etc.).

While lightweight wear-resistant materials could benefit from this compositing technique, perhaps the greater application could be in ferrous or hard alloy systems. Hard particle reinforcement of the surfaces of steels, titanium, brasses, or cast iron may have numerous industrial applications in reciprocating assemblies, engines, brake disks, or other situations where both bulk strength and surface wear resistance is needed. Lightweight high-strength steels with surface wear resistance may have numerous applications in both lightweight structures and lightweight vehicle power systems. FSP work during FY 2005 focused on developing methodologies to successfully surface-process high-temperature materials including steels and cast iron.

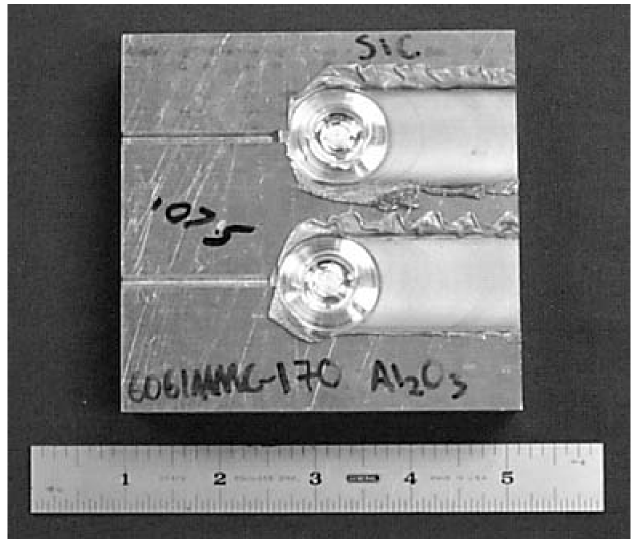

Figure 2. Friction stir processed 6061 plate with ceramic particulate incorporated into the surface.

Approach

The basic objective of this project is to investigate and develop FSJ and FSP as viable industrial techniques for advanced lightweight materials. The current approach is divided into three main task areas: (1) explore the potential to modify the surfaces of both conventional aluminum and advanced materials toward the goal of improving wear, corrosion, mechanical or thermal properties, (2) develop FSJ/ FSP as a process to join sheets that will be subjected to superplastic forming, and (3), to develop numerical, physics-based modeling strategies to help define the fundamental process and predict process conditions.

The first task focused on broadly investigating using FSP to create engineered surfaces. Surface modification was investigated in two areas:
(a) particle incorporation to create near-surface MMCs in cast iron, and (b) surface alloying by

reaction processing. In addition, to facilitate FSP in cast iron, we investigated the use of induction preheating to lower process forces in these hard-to-process materials.

The second major task area investigated in FY05 was the application of FSJ to superplastic forming environments. Numerous opportunities exist to use this manufacturing technology to reduce weight on heavy vehicles. One barrier to SPF manufacturing is that hang-on truck components are complex and often very large; larger than the standard coil widths. If sheets are joined together to make a large part by fusion welding, the weld region does not deform superplastically because of the microstructure of fusion weld metal. Friction Stir Joining produces a weld region that is formable by SPF and may be an enabler for complex or large structures that are joined, then later hot gas formed in single operations to form cab structures and panels.

The third major task area was the development of a numerical modeling process using an approach called Smooth Particle Hydrodynamics (SPH). This modeling approach has not been previously applied to FSJ/P but our preliminary work suggests that it may be able to provide significant insight into the fundamental nature of the heat generation and material flow that occurs during the FSJ/P process.

Results

Task 1 Surface Engineering – Cast Iron/TiB_2 FSP

The motivation for looking at surface engineering of the cast iron system comes from the need in many industrial environments to produce a more wear resistant cast iron. The bulk of the work in FY2005 on the FSP of cast iron has concentrated on developing methods to stir-in ceramic particulate into the surface of cast iron. This can produce a wear resistant surface on a material while retaining the original bulk properties. Cast iron is a difficult material to FSP and much of the FY05 effort was devoted to developing the process parameters and tool designs and materials needed to successfully process this material.

Two main tool designs and two tool materials were investigated during the program. The two tool designs used are the Stepped Spiral design and the Three Flat tool shown below in Figure 3. The two tool materials investigated were commercial W-25% Re and Polycrystalline Cubic Boron Nitride (PCBN).

Wear of the pin tool was found to be a significant problem initially requiring several strategies to be employed to mitigate the wear. Most important of these is the use of induction preheating of the substrate cast iron prior to tool traverse. Research at the South Dakota School of Mines and Technology has shown that induction preheating of the substrate prior to FSP can have an important effect on process forces and perhaps on the quality of the weld in difficult-to-weld materials. Figure 4 shows the

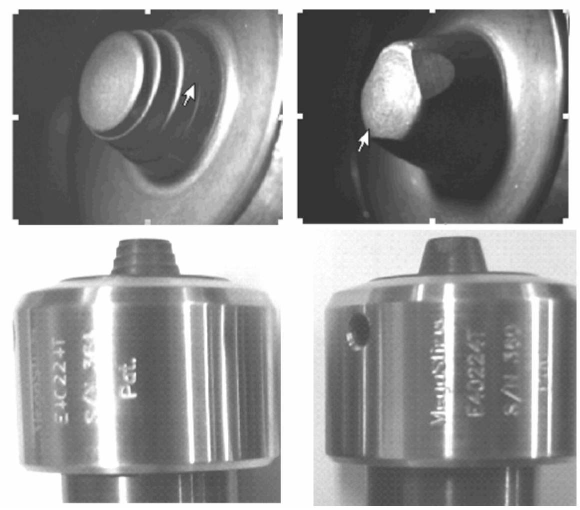

Figure 3. Stepped Spiral tools and Three Flat tools were fabricated in W-25%Re, and Stepped Spiral tools were fabricated in PCBN for use in the program.

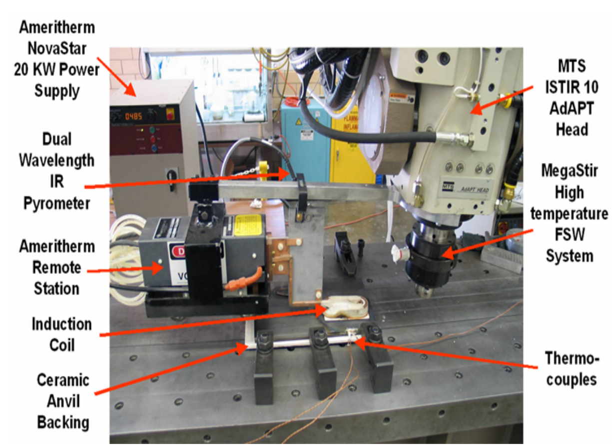

Figure 4. Induction Preheater installed on FSJ equipment at the South Dakota School of Mines and Technology

friction stir machine. Figure 5 shows that for 1018 steel, induction preheating can reduce process forces throughout the weld or processed region length [Ref 1]. Reduced process forces can be correlated with lower tool wear and better material flow in the weld. Induction preheating was found to be a necessary procedure in the FSP of cast irons to help reduce tool wear. It was found however that even with induction preheating, tool wear was still a significant problem with the W-25%Re tools. PCBN tools were found to be more wear resistant in this material system. In addition, the Stepped Spiral tools produced better nugget microstructures and larger plasticized zones in testing than the Three Flat tool designs. Figure 6 illustrates the current experimental setup found to promote the best tool survival and produce the best nugget microstructures. It was found that the initial plunge of a cool tool into a cool cast iron substrate also created significant wear. To mitigate this, a thin sheet (0.080" thick) of 1018 steel was placed on top of the cast iron. This plate of less abrasive material plasticizes first and allows heat to develop in the cast iron substrate, lowering the flow stress and producing a less aggressive wear environment for the pin during the plunge phase. The plate is also important for lowering x axis forces during processing, also decreasing pin tool wear.

Figure 7 shows nugget microstructure in cast iron and is typical of FSL/P in many material systems. Figure 8 shows a microhardness traverse across the nugget of the friction stir processed cast iron.

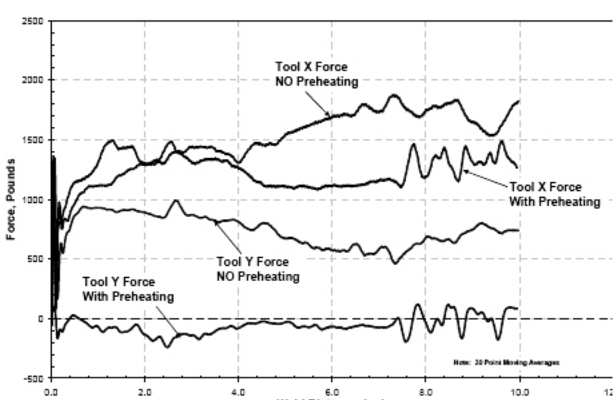

Figure 5. Work at South Dakota School of Mines and Technology has shown that induction preheating can lower process loads in difficult-to-weld materials like 1018 steel. (Figure courtesy of Tweedy, Arbegast, Allen, 2004).

Hardness is elevated well above the parent material in the HAZ, TMAZ and in the Nugget. Detailed microstructural investigation (Fig. 9) show the nugget is composed of fine grain ferrite and pearlite with all the coarse graphite dissolved in the matrix.

Experiments were also conducted in which 10 to 20 micron TiB_2 powders were introduced between

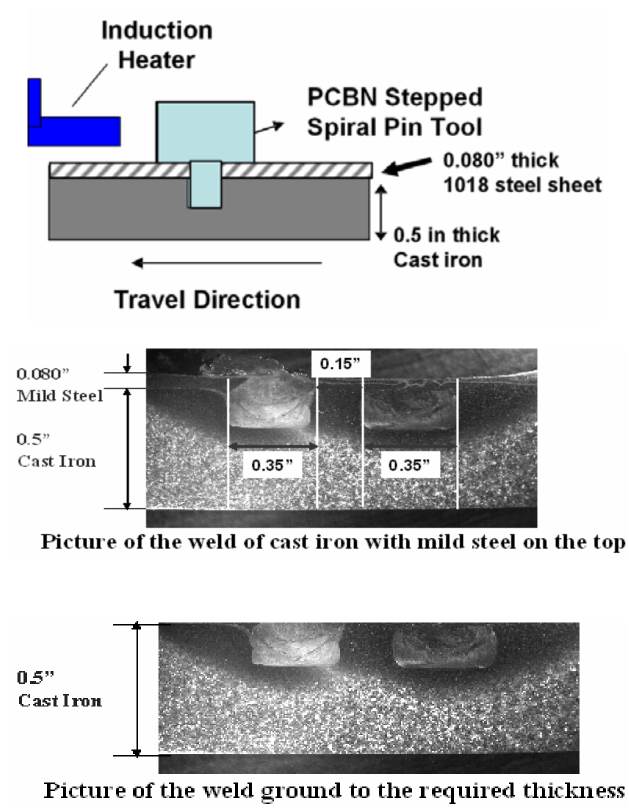

Figure 6. Top figure shows experimental set up. Middle figure shows as-processed cast iron with .080 plate on surface. Lower figure shows FSP cast iron with steel plate machined off, exposing nugget to wear surface. Final demo plates will be friction stir processed so that nuggets overlap.

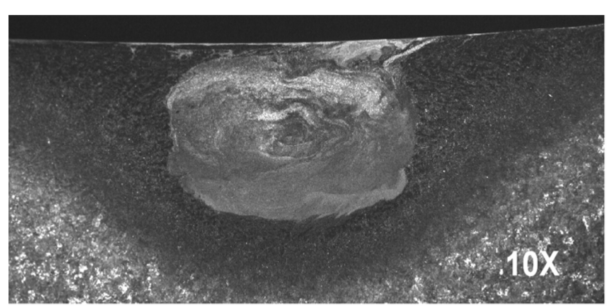

Figure 7. Cast Iron nugget microstructure showing consolidated nugget region.

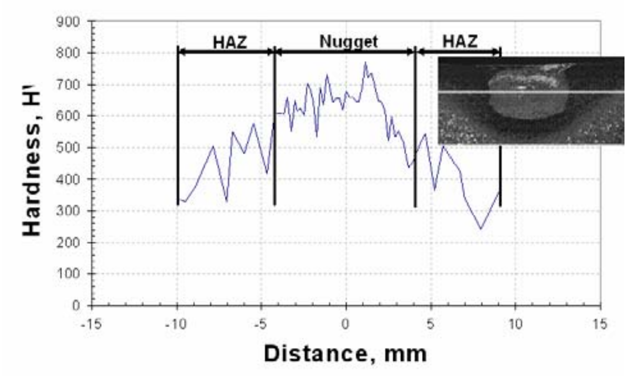

Figure 8. Hardness across FSP zone showing increased hardness in HAZ and Nugget over base material**.**

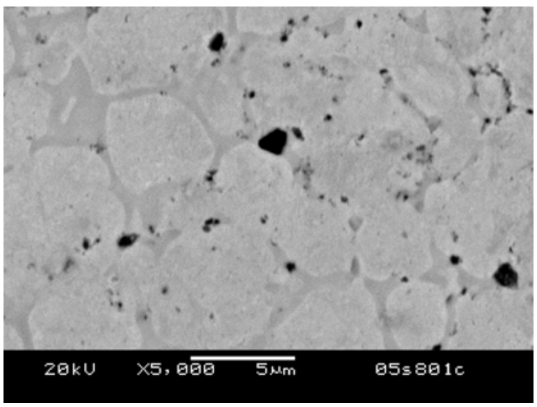

Figure 9. SEM backscatter image of stir zone showing 50 to 200 nm TiB2 in a fine grained ferrite / pearlite matrix (Uma Ramasubramanian, et. al. 2005)

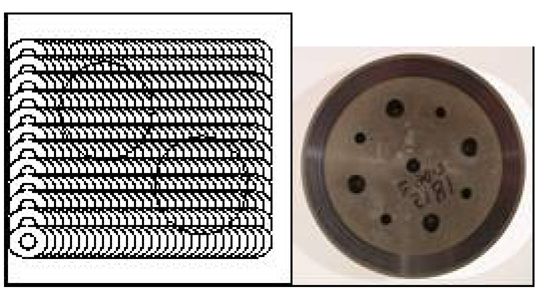

Figure 10. Overlapping pattern of FSP "beads" laid down on cast iron plate, then 4 inch diameter circular plates cut out and tested for wear performance

the 1018 steel plate and the cast iron substrate then the friction stir tool was passed through the assembly. These ceramic powders were successfully mixed into the nugget region to create a homogeneous distribution of ultrafine grained TiB_2 (50-200 nm). It is interesting to note that some of the fine TiB_2 powders reacted with the carbon in the cast iron to form TiC particles. This reaction occurs in the solid state and may enhance the wear properties of these surface engineered regions.

Friction Stir Reaction Processing (FSRP)

Much of the effort in FY 2005 was directed toward the new field of FSRP. Thermodynamic calculation of numerous potential solid state reactions indicates that energies available during FSJ/P may be high enough to initiate the formation of some compounds like TiB_2 from elemental constituents, especially considering all the new surface being generated by the severe plastic deformation under the pin tool. This process opens the possibility of making very finely divided reaction products in the near-surface region of a bulk material (see Table 1). These reactions can be tailored by the composition of the elemental powders introduced on the surface. In addition, highly exothermic (thermite style) reactions may be possible that can put large amounts of heat into the surface and potentially reduce the flow stress of hard-to-weld alloys, or allow the FSJ process to occur without significant tool wear. Claddings of materials rich in fine oxide dispersions, or other in situ–formed ceramic-rich materials, may be possible on low-cost ferritic base alloys (creep-resistant surfaces for engine applications). Work in FY 2005 concentrated on reactions in the Mode I category in Table I. These are metal oxides reacting with the aluminum substrate to form alumina and free metal.

Reactant powders were placed between plates of 1100 alloy aluminum as shown in Figure 11. The assembly was then friction-stir-processed to produce a microstructure, as shown in Figure 12. The nugget region contains very finely dispersed precursor reactants and SEM EDX reveals the presence of reduced metal phases, indicating that in-situ reaction did take place during the FSP.

Experiments were conducted with powders composed of SiO2, TiO2, CuO, NiO, in aluminum and NiO in steel. All experiments showed development of fine reduced metal or silicides and aluminides indicating chemical/mechanical assisted reactions are taking place. Interestingly the alumina phase that is the oxide reaction product was not identified in SEM suggesting that it may be an ultra fine grained, potentially nano-phase. More work in

Table 1. Reaction modes

Mode	Reaction	Examples
I	Base Metal (Al) + Reactant → Product	$3\ SiO_2 + 4Al \rightarrow 3Si + 2Al_2O_3$
		$3\ TiO_2 + 4Al \rightarrow 3Ti + 2Al_2O_3$
		$BN + Al \rightarrow AlN + B$
II	Pin Tool (Ti) + Reactant → Product	$3\ Ti + 2\ BN \rightarrow 2\ TiN + TiB_2$
		$Ti + AlN \rightarrow TiN + Al$
		$Ti + C \rightarrow TiC$
		$Ti + 2B \rightarrow TiB_2$
III	A + B → C + D	$4Al_{(powder)} + 3SiO_2 \rightarrow 3Si + 2Al_2O_3$
		$4Al_{(powder)} + 3TiO_2 \rightarrow 3Ti + Al_2O_3$

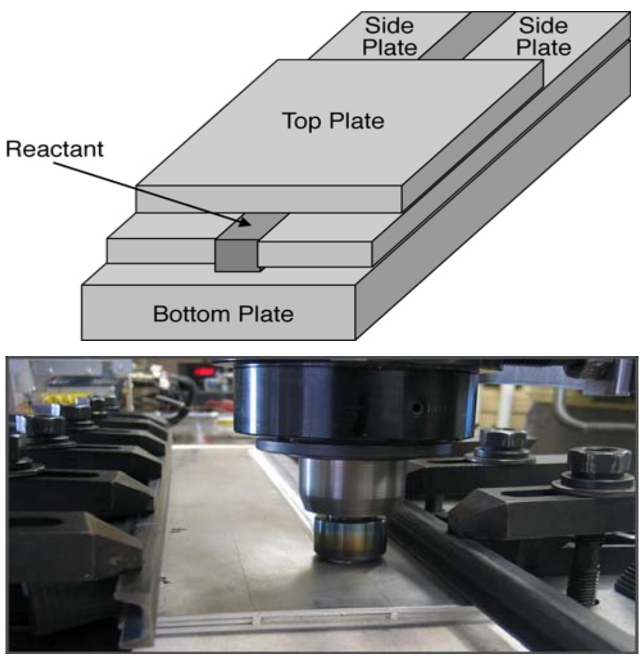

Figure 11. Reactant oxide powders are placed between plates, and the stir tool processes the entire thickness

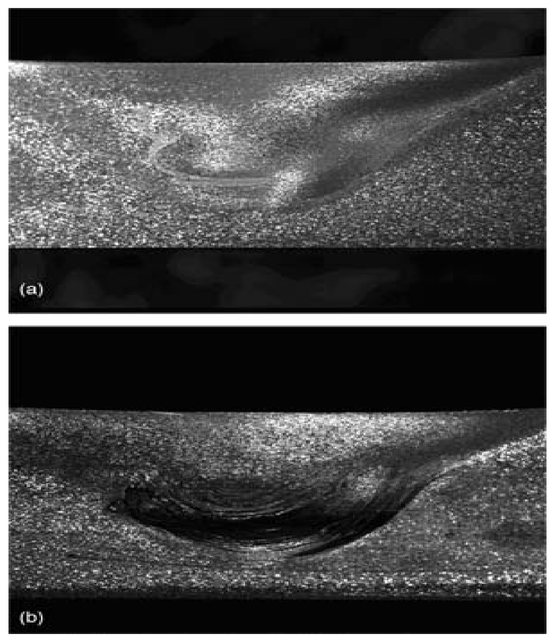

Figure 12. Cross sections showing fully consolidated weld zone. FSRP zone is 3/8-in (9.52 mm) thick: (a) SiO_2 and (b) TiO_2.

2006 is planned to see if this process might be able to create surface regions enriched in ultra fine grained alumina. If so, unique properties in the surface layer may be possible, such as ultra hardness or creep resistance as is seen in other nanophase alumina dispersions.

Task 2 - FSJ/P for SPF manufacturing

Superplastic forming (SPF) is a lightweight manufacturing technology that has shown to be cost effective and produce weight optimized structures through reduction in part count and through the use of lightweight materials.

One important factor that is relevant to the particular problems of heavy vehicle SPF is that truck parts are large. The parts are modulus (stiffness) driven, not strength driven, because of aero flutter and shear size. Big parts need stiffeners. This requires a complex assembly. One cost effective and lightweight option is to join multiple flat sheets together, then SPF the entire multi-sheet pack together in one operation. This incorporates the stiffener into the assembly. The problem with this strategy revolves around the method chosen to join the sheets together. If the sheets are fusion welded, the microstructure of the fusion weld region will not deform superplastically. Figure 13 shows the coarse microstructure of a fusion welded aluminum sheet. When these joints are subjected to superplastic forming the joint remains un-deformed. These un-deformed areas also have very poor post-forming mechanical properties. In contrast, Friction Stir Joining leaves behind a weld microstructure that is highly deformable at SPF conditions.

This project is investigating the particular weld process parameters and part geometries that could produce an integrally stiffened panel for a heavy vehicle cab application. The work to date involves fabricating multi-sheet assemblies as shown in Figure 14. These assemblies will be SPF formed into structural panels in three configurations, “egg crate”, “hat stiffened”, and “doughnut”. The purpose of the test forms is to discover the correct FSJ process parameters and the SPF deformation possible in these geometries. The panels are made using both linear FSJ and Friction Stir Spot Welding (FSSW) (Fig 15, 16). The FSSW joints are of particular

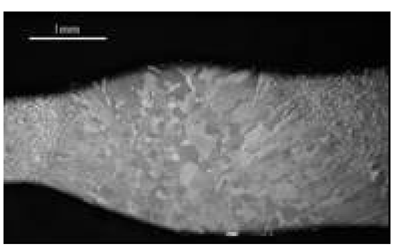

(a)

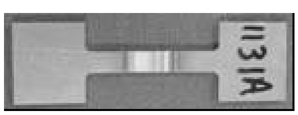

(b)

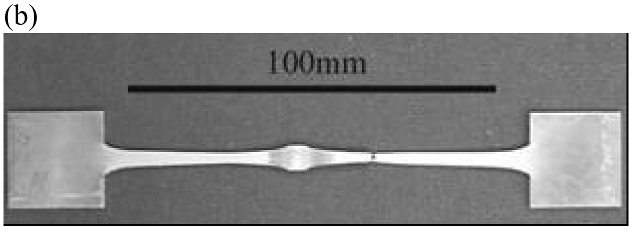

(c)

Figure 13. (a) Weld nugget region in a butt weld between aluminum sheet materials showing coarse, cast microstructure of a fusion weld. (b)Transverse tensile specimen (c) Transverse tensile test at SPF conditions shows the undeformed nature of the fusion weld metal.

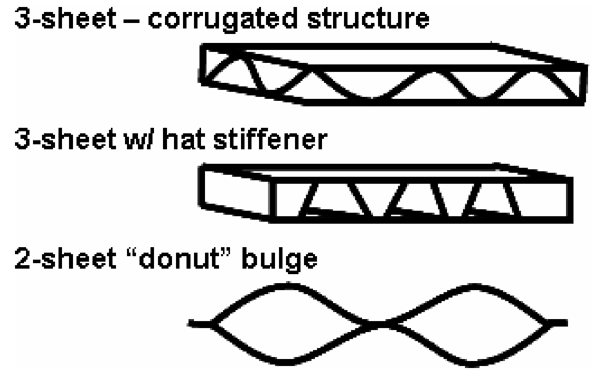

Figure 14. Geometries of test panels fabricated for this program

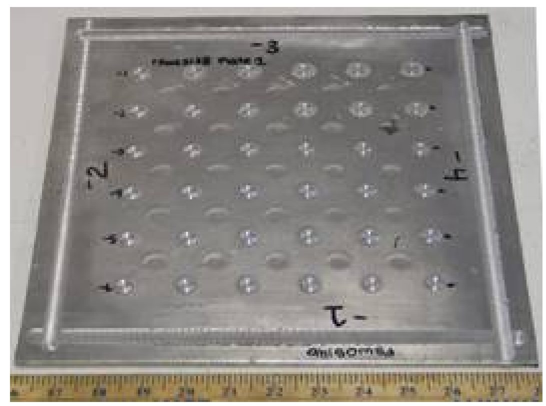

Figure 15. Friction Stir Spot Welded three sheet multisheet pack prior to SPF testing. This configuration is designed to produce the corrugated structure. Alternating spot welds are made from each side of the multisheet pack using the “Refill” (GKSS-Riftec) FSSW method at the SDSMT.

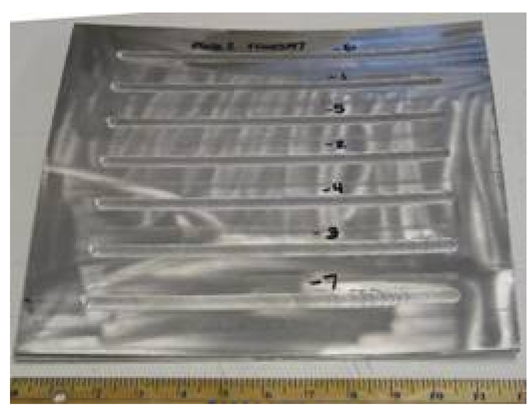

Figure 16. Linear Friction Stir Welded multisheet pack prior to SPF testing. This configuration is designed to produce the “3 sheet with hat stiffener” structure. Alternating linear welds are made from each side of the multisheet pack using a pin that penetrates only through the upper two sheets.

interest because they are made using a new process that does not leave an exit hole after the spot joint is made. This process, called the "refill" method was invented by GKSS (Riftec) and the panels were fabricated at the facilities of our project partner, South Dakota School of Mines and Technology.

It is envisioned that structural panels like those in Figure 17 can play a key role in a vehicle light weighting program. The panel shown in Figure 17 is fabricated in titanium. To fabricate the same structure in aluminum will present a significant challenge because of the aluminum oxide surface, and because of a particular feature of highly worked aluminum alloys that are subject to high temperature called Abnormal Grain Growth (AGG). Abnormal Grain Growth can limit the SPF forming performance and seriously restricts the post forming mechanical properties. AGG can be minimized with the correct choice of FSJ process parameters, but whether it will be a significant barrier to implementation has yet to be determined.

Task 3 - Numerical Modeling

Work also began in FY2005 on a new modeling approach to investigate the fundamental flow and heat generation properties of friction stir welds. The industry has struggled with modeling this process for 10 years because the high strains and high strain rates are simply not seen in very many other systems. Conventional modeling techniques such as Finite Element Modeling and Computational Fluid Dynamics suffer from many issues mostly surrounding the need for the model to track huge variations in strain, temperature-dependent flow stress, strain rate, and heat generation.

The modeling approach we have started to investigate in this program is a departure from other workers in the field and involves the use of Smoothed Particle Hydrodynamics. This is a fully Lagrangian particle method, so no grids are required. The code solves 2D and 3D equations for continuity, momentum, and energy balance. Currently the momentum equation is based on a fluid dynamic (Navier-Stokes) equation, but solid mechanics equations are being adapted so the materials databases are easier to incorporate as input parameters.

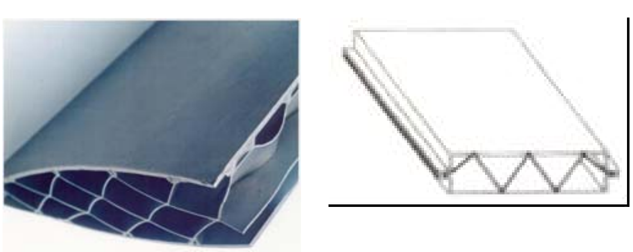

Figure 17. Possible structures formed from multisheet packs joined together as sheets then subsequently hot gas formed into a lightweight structural panel

The model currently can explicitly model mixing of materials, predict temperature generation at the surface of the tool as well as that due to viscous dissipation and can produce temperature and strain histories for any material point in the field. This may allow it to make micro-structural prediction at different parts of the weld since temperature and strain history can be tracked, although this has not as yet been implemented in the code. Figure 18 shows some example output from the model.

Conclusions

FSJ and FSP are technologies that will enable the application of many lightweight materials in the next generation of transportation systems. Many advanced materials are in need of effective joining technologies before their widespread use can be considered. Solid state FSJ/P avoids many of the problems with fusion joining and represents a revolutionary change in joining technology. FSP also has numerous opportunities in the growing field of surface engineering and thermal management.

The results of this work will allow designers to anticipate and implement structures that are a hybrid of many different materials, facilitate the application of lightweight superplastically formed structures, and suggest new materials and engineered surfaces that can help deliver lighter and more fuel-efficient vehicles.

Acknowledgements

The authors would like to acknowledge the substantial support over the course of this multi-year project given by Dr. Sidney Diamond. Dr. Diamond carried a high level of enthusiasm and a vision for how new technologies, such as friction stir processing, might be inserted into the heavy vehicle

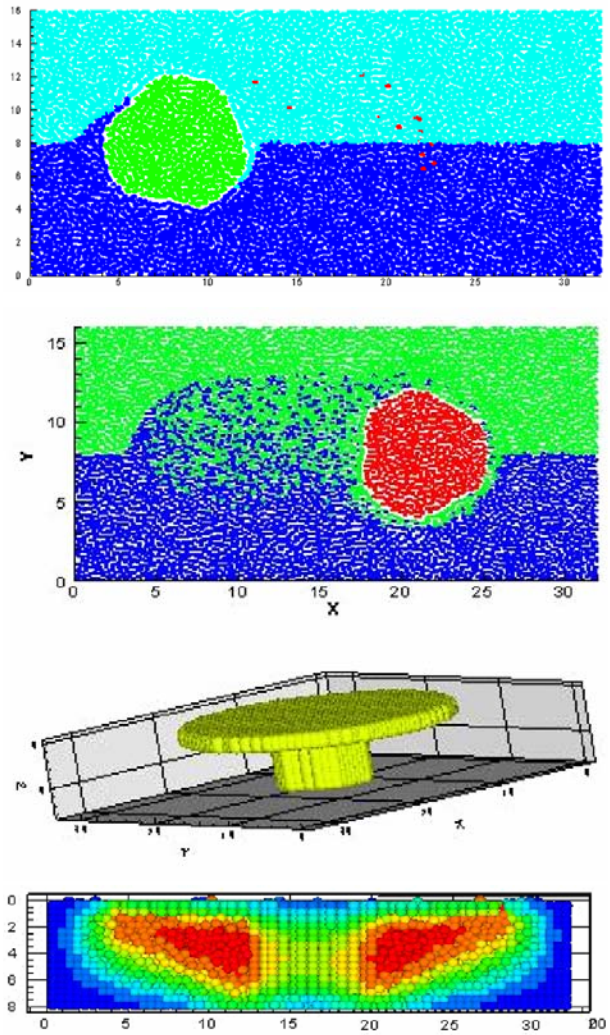

Figure 18. Model output. Upper two figures show mixing of dissimilar materials using a tool with three flats on the pin. (Only the tool pin is shown in this 2D simulation. The lower two figures show arrangement of 3D model and a temperature distribution. Highest temperatures are in a region near the pin root away from the pin surface, due to heat generated by plastic work and conduction into the pin.

manufacturing industry to help accomplish the goals of the Department of Energy's Freedom Car and 21st Century Truck programs. His guidance is appreciated.

References

1. B. M. Tweedy, W. Arbegast, and C. Allen, "Friction Stir Welding of Ferrous Alloys using Induction Preheating," in *Friction Stir Welding and Processing III*, ed. K. V. Jata, M. W. Mahoney, and T. J. Lienhert, TMS, 2005.

Presentations/Publications

G. J. Grant, *FY 2004 Annual Report:* Friction Stir Joining and Processing of Advanced Materials, Including Metal Matrix Composites, Nov 2004.

G. J. Grant, *PNNL Milestone Report* PNNL 21346 Evaluation of friction stir processing of steel for thermal barrier coating. Feb 2005

S. M. Howard, W. Arbegast, B. Jasthi, G. J. Grant, D. R. Herling, "Friction Surface Reaction Processing On Aluminum Substrates," ," in *Friction Stir Welding and Processing III*, ed. K. V. Jata, M. W. Mahoney, and T J. Lienhert, TMS, 2005

U. Ramasubramanian, W. Arbegast, G. Stone, G. J. Grant, "Friction Stir Processing of Class 40 Cast Iron," in *Friction Stir Welding and Processing III*, ed. K. V. Jata, M. W. Mahoney, and T J. Lienhert, TMS, 2005

I. Friction Stir Welding and Processing of Advanced Materials

Principal Investigator: Zhili Feng
Oak Ridge National Laboratory
1 Bethel Valley Road, Oak Ridge, TN 37831
(865) 576-3797; fax: (865) 574-4928; e-mail: fengz@ornl.gov

Chief Scientist: James J. Eberhardt
(202) 586-9837; fax: (202) 587-2476; e-mail: James.Eberhardt@ee.doe.gov
Field Technical Manager: Philip S. Sklad
(865) 574-5069; fax:(865) 576-4963; e-mail:skladps@ornl.gov

Participants:
Michael L. Santella, Oak Ridge National Laboratory
Tsung-Yu Pan, Ford Motor Company
Russell Steel and Scott Packer, MegaStir Technologies
Degen, Cassandra, South Dakota School of Mines and Technology
M. Kuo and R. S. Bhatnagar, Mittal Steel USA

Contractor: Oak Ridge National Laboratory
Contract No.: DE-AC05-00OR22725

Objective

- Develop the technological basis for friction stir welding and processing (FSW/P) of advanced high-strength and lightweight materials for the automotive industry.
- Gain fundamental understanding of the relationships between workpiece and tool material properties during FSW/P.
- Characterize the mechanical properties and microstructures of joints.
- Correlate the proprieties and microstructures produced by FSW/P to the process conditions.

Approach

- Conduct experimental welding and processing tests on advanced materials using the state-of-the-art FSW/P process development system.
- For particular workpiece materials, select the tool material based primarily on high-temperature strength, wear resistance, and chemical compatibility.
- Evaluate mechanical properties and their correlation with microstructures produced by FSW/P.
- Develop predictive modeling capability to study the properties as a function of process conditions.

Accomplishments

- Completed a study on friction stir processing to improve properties of cast magnesium alloy AM60B.
- Demonstrated the feasibility of friction stir spot welding of advanced high-strength steels.
- Conducted friction stir processing of steel 1080 for wear resistance improvement.
- Initiated friction stir processing of Ti.

Future Direction

- Investigate the effects of heat treatment on the fatigue life of FSP cast aluminum alloys.
- Develop new approaches for FSSW without the exit hole for improved structural properties of the joint.
- Carry out FSSW of other lightweight materials and dissimilar welds.
- Use transmission electron microscopy to characterize the microstructure improvements to the cast surfaces.
- Assess the ability of FSP to produce rapidly solidified surface microstructures.

Introduction

Friction stir welding (FSW) is a novel solid state joining method. The process characteristics and advantages for joining materials that are difficult to join by conventional fusion welding processes were discussed in the previous annual report.

Applications of FSW to aluminum alloys have been a great success. Currently, the technology forefronts are rapidly evolving: there is tremendous interest to extend the technology to welding high-performance and high-melting-temperature materials. Other novel applications of the process are emerging. For example, it can be used to thermomechanically process a material for microstructure refinement and property improvement.

This program aims at advancing FSW/P technology to promote the increased use and adoption of high-strength lightweight materials in automotive structures, particularly heavy vehicles. This supports the goals of the Office of FreedomCAR and Vehicle Technologies to increase fuel efficiency and reduce emissions of heavy trucks by weight reduction without sacrificing strength and functionality.

In FY05, we completed studies on friction stir processing of cast Mg alloy for properties improvement, and friction stir spot welding of advanced high-strength steels. In addition, we initiated studies on friction stir processing of Ti alloys and 1080 steel. This progress report will focus on the first two activities. The progress on Ti and 1080 steel will be reported in future reports when more comprehensive results are available.

Friction Stir Spot Welding of Advanced High-Strength Steels

Friction stir spot welding (FSSW), or spot friction welding, is a new process that recently has received considerable attention from the automotive and other industries [1]. A novel variant of the "linear" friction stir welding (FSW) process, FSSW creates a spot, lap-weld without bulk melting. The appearance of the resulting weld resembles that of a resistance spot weld commonly used for auto-body assembly. The solid-state bonding and other features of the process makes it inherently attractive for body assembly and other similar applications. Today's primary welding process for auto body structure assembly – the electric resistance spot welding (RSW) process – can be problematic for many new high-performance light weight structural materials such as Al alloys and advanced high-strength steels (AHSS) [2,3].

So far, the majority of the research and development efforts on FSSW have been on aluminum alloys. Because Al alloys are easy to deform at relatively low temperatures (below about 550°C) they are relatively easy to friction stir weld. Indeed, the development of FSSW for Al alloys has been quite successful. Mazda reported the first application of FSSW on its 2003 RX-8, a mass production car. The entire Al rear door was friction stir spot welded [4]. Other auto companies also announced introduction of FSSW to weld Al body parts. The FY04 annual report included our R&D activities on this subject.

Two distinctive variants of the FSSW process have been reported in the open literature [5-8]. The first approach, used by Mazda, employs a fixed pin tool geometry [5,7]. The protruded pin leaves a characteristic exit hole in the middle of the joint. The second approach [8] utilizes delicate relative motions of the pin and the shoulder to refill the pin hole. Based on the information available, the second approach would require relatively long processing time to accommodate the complex motions of the tool to fill the hole. In comparison, the fixed pin approach is very fast. For Al alloys, a weld can be made in less than one second [7]. Also, the welding machine and control system for the fixed pin approach is simple and easy to integrate on a high-volume mass production assembly line. Mazda reported over 90 percent operation energy savings and over 40 percent capital investment reductions when compared to the conventional resistance spot welding of Al alloys.

Today, steel is still the primary material for body structures of high-volume mass-produced cars by all major car makers. The great emphasis on safety and vehicle weight reduction to improve fuel efficiency has been driving the increased use of AHSS in automobile body construction. However, welding AHSS presents some unique technical challenges to both the steel suppliers and the auto end-users. Data available so far have indicated that resistance spot welding of AHSS with the welding practices developed for conventional mild steels may not be the preferred approach to achieve the full benefits of AHSS. The biggest technology barrier inhibiting the use of RSW for AHSS is the profound weld property degradation [2, 9-11]. Due to the extremely high cooling rate in RSW, the weld nugget region of AHSS would develop highly brittle microstructures and is prone to solidification related weld cracks/defects. Such problems tend to be more prominent in higher grade AHSS with relatively high carbon and alloying element contents such as DP1000, Martensitic, and TRIP steels. The shortened electrode life is another major issue for RSW of AHSS because of the chemical reaction between the Zn coating and the copper electrode and high welding force. Alternative welding processes that minimize the weld property degradation without adversely affecting the productivity of body assembling would be extremely important to fully realize the advantages of AHSS in structure safety and fuel efficiency.

The success of FSSW in Al alloy body structures has led to tremendous interests in applying the technology to weld advanced high strength steels. However, past research and development on linear friction stir welding have shown that steels are much more difficult to friction stir weld than Al alloys [12]. The technical difficulties stem from the very fundamental aspect of the FSW process – compared to aluminum alloys, FSW of AHSS must operate at much higher temperatures and it requires much higher mechanical loading for plunging and stirring. These technical difficulties are also expected for FSSW. The high-volume, high-speed, and cost-conscious requirements of auto-body assembly lines make the development of FSSW even more challenging.

In FY05, we conducted a feasibility study on FSSW of AHSS. While other forms of FSSW are being evaluated for welding steels and other high melting temperature materials [13], this study was based on the fixed pin approach, mainly because of its simplicity and relatively short welding time. The study was to explore the following: (1) the feasibility of producing FSSW in AHSS in a relatively short period of time acceptable to the industry, (2) the possibility of using existing tool materials for FSSW of AHSS, and (3) the microstructural responses of AHSS to the FSSW process.

Experimental

Two types of uncoated AHSS steels were selected for this feasibility study. The first one (DP600) was a dual-phase steel with nominal strength of 600MPa, and the second one (M190) was a martensitic steel with nominal strength of 1310MPa. The thickness of the material was 1.6 mm.

Table 1 provides the chemical composition of the steels.

Table 1. Steel Chemistry in Wt. percent.

	C	Mn	P	S	Si	Cu	Ni	Mo	Cr	Cb	V	Ti
DP600	0.084	0.94	0.011	0.006	0.313	0.02	<0.01	<0.01	0.02	<0.003	0.004	0.004
M-190	0.168	0.4	0.009	0.005	0.169	0.036	0.013	0.003	0.023	<0.003	<0.003	0.034

Welding trials were performed on a laboratory friction stir welding research and development system. Figure 1 illustrates the basic process of the fixed pin approach used in this study. The welding cycle begins with a rotating tool with a protruded pin plunging into the upper sheet of the lap joint. The plunge load is supported from the bottom side with a backing plate or anvil to sustain the plunging load. The heat generated by the rotating pin softens the material and facilitates the penetration of the pin. Much more heat is generated to further soften a large region of the material underneath the tool shoulder after the tool shoulder contacts the top surface of the upper sheet. The softened material is pushed and stirred to form the metallurgical bond around the rotating pin. The forge pressure from the tool shoulder also keeps the interface between the two workpieces in intimate contact to facilitate the bonding. The tool is retracted at the end, leaving the characteristic hole in the middle of the weld.

All welds were made under displacement control mode – the tool was plunged into the material to a pre-determined depth. For all the tests conducted in this feasibility study, the tool rotation speed was fixed at 1500 rpm. The total welding time varied from 1.6 sec to 3.2 sec through changes in the plunge rate.

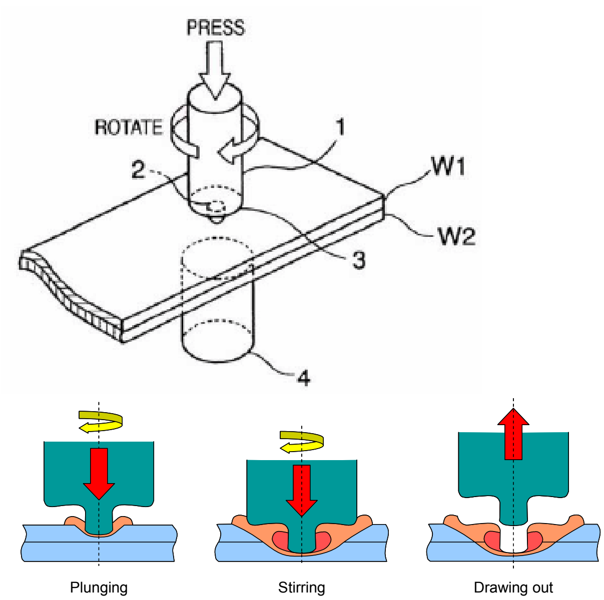

Figure 1. Principles of FSSW with fixed pin.

The tool had a tapered pin. It was 2.0-mm long. The shoulder of the tool was 10 mm in diameter.

As in the case of the linear friction stir welding, tool material is expected to be a critical technical issue for FSSW. In this work, the tool was made of polycrystalline cubic boron nitride (PCBN), a material that has been successfully used for linear friction stir welding of steel and other high melting temperature materials [14]. A single tool was used in this study. This single tool made over one hundred welds without any noticeable degradation or wear.

Tensile-shear and cross-tension mechanical testing were performed for selected welding conditions to evaluate the mechanical strength of the joints produced in this work. The tensile shear specimen was 38.1-mm wide and 127-mm long. The cross-tension specimen was 50.8-mm wide and 152.4-mm long, with the distance between the loading holes at 101.6 mm. The weld was made at the center of the overlapping (38 mm) region, as shown in Figure 2.

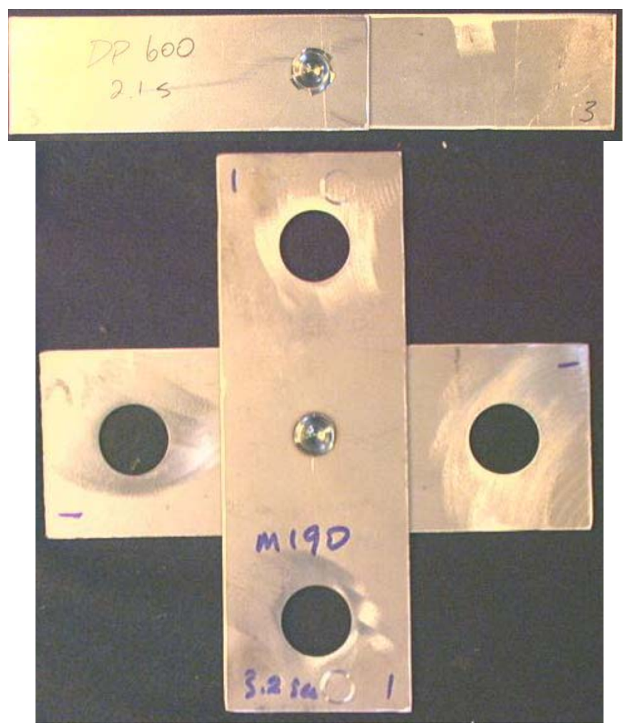

Figure 2. Appearances of the tensile shear and the cross-tension welded coupons. The welds were at the center of the overlapping region.

Results and Discussions

Figure 3 shows the overall cross-sectional views of both the M190 weld and DP600 weld made with 2.1 sec welding time. A close-up view in the bonding interface region of the M190 weld is given in Figure 4. Clearly, metallurgical bonding was formed between the top and bottom workpieces around the penetrating pin. As in the case of Al alloy welds, the material from the bottom piece was pushed up by the plunging action of the rotating pin, causing the workpiece interface to bend upward and form a “hook”. The solid-state phase transformations that occur in carbon steels during cooling make it difficult to directly observe details of the stirring/mixing of the material between the two sheets. The width of the bonding ligament, a critical factor determining the strength of the weld, was relatively small in this study. Additional efforts would be needed to further improve the size of bond ligament.

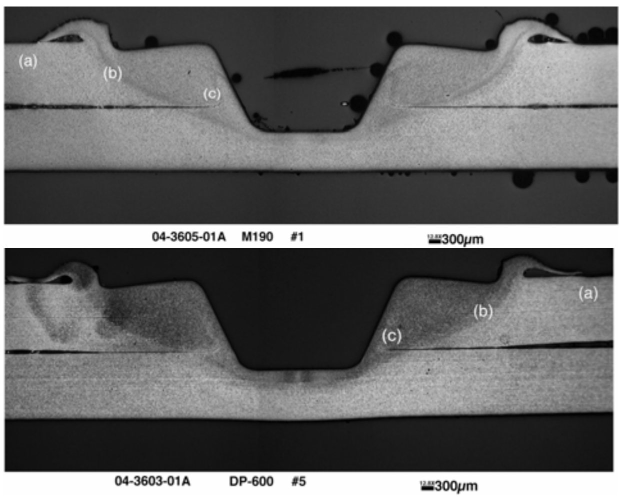

Figure 3. Cross-section of FSSW. Top: M-19; bottom: DP600. Welding time: 2.1 sec.

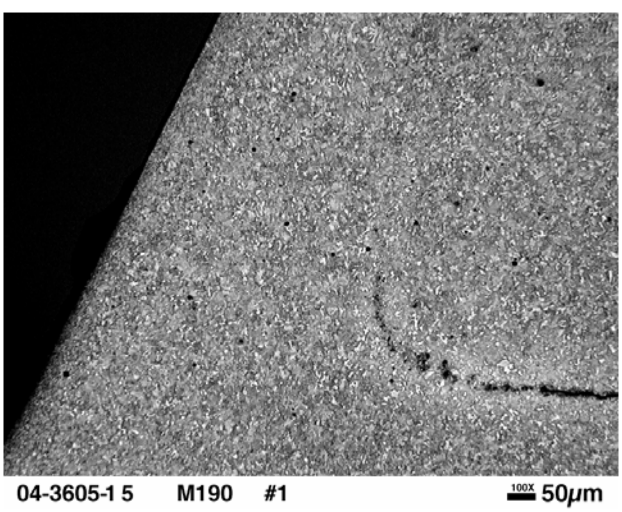

Figure 4. Close section view of the bonding interface region. M190 Steel, welding time: 2.1 sec.

To evaluate the effects of welding thermal cycle on the properties of the welds, variations in the microhardness were measured across them. Figure 5 shows the microhardness distributions in the top workpiece at three different depths, approximately ¼ (0.4mm), ½ (0.8mm), and ¾ (1.2 mm) of the plate thickness, as measured from the top surface. They are labeled as ¼t, ½t, and ¾t in the figure. The location of the exit hole and the periphery of the tool shoulder are also illustrated in the figure to provide the spatial reference for the discussion of the hardness variations.

The martensitic M190 weld shows considerable softening outside the stir zone. The minimum hardness, about 200 Hv, was located about 5-mm away from the weld center, corresponding to the shoulder radius of the tool. However, the hardness in the stir zone was fully recovered back to the 430 Hv base metal level. It is important to point out that the minimum hardness location is quite far away from the bonding region at the interface. The softened region was outside the thermomechanically affected zone (TMAZ) where substantial plastic deformation and material flow occur during the welding process.

Due to the differences in chemistry, DP600 steel showed very different microhardness profiles under the same welding condition. The softening, while still measurable, was relatively insignificant compared to the base metal microhardness level. The softening was mostly outside the shoulder diameter, particularly for the ¼ t and ½ t depth. On the other hand, the stir zone appeared to be hardened. The maximum hardness was about 250 Hv, compared to the base metal average of 210 Hv.

The above variations of the microhardness can be related to the microstructural changes in the different regions of the weld. While more detailed microstructural analyses are still on-going, the results obtained so far from the optical

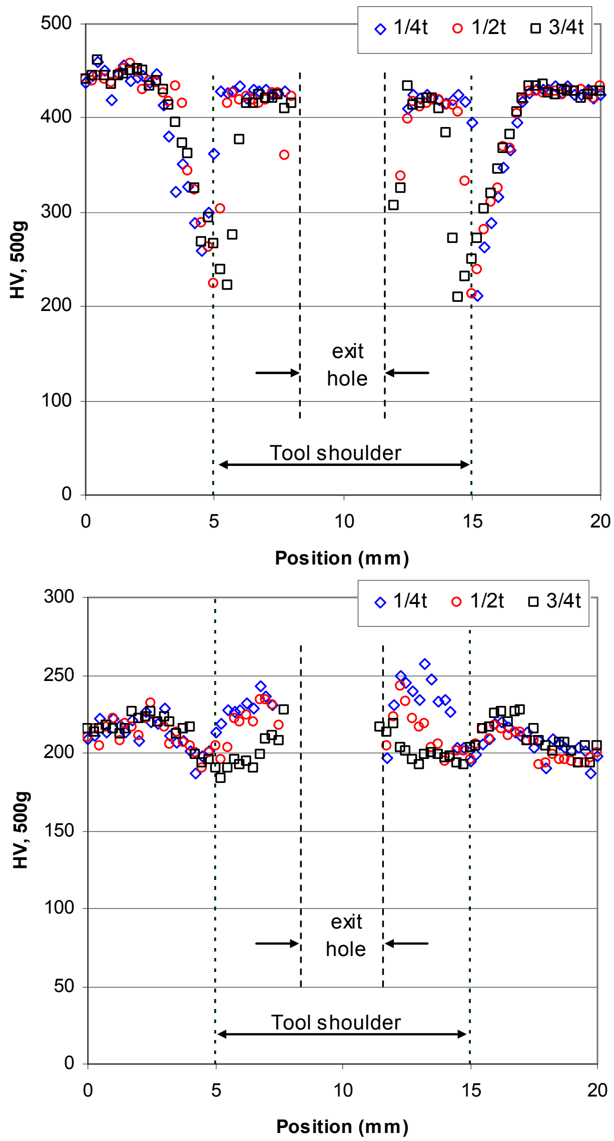

Figure 5. Micro-hardness distribution across the weld in top sheet. Top: M190; bottom: DP600. Welding time: 2.1 sec.

microstructure evaluation are presented below to help understand the hardness changes in the AHSS welds produced by FSSW.

Figures 6 and 7 show, respectively, the microstructures at three selected representative locations in the M190 and DP600 welds. The locations of these metallographic photos are schematically illustrated in Figure 3 by the corresponding labels. Label (a) indicates the base metal region, (b) the transition region exhibiting the reduction of hardness, and (c) the region near the bonding interface which is inside the TMAZ.

The base metal of the martensitic M190 steel has a martensitic microstructure (Figure 6 (a)). In the transition region located near the periphery of the tool shoulder, the material appeared to be heated to a peak temperature between the A1 and A3 temperature – the so-called intercritical region where the ferrite and austenite co-exist at the peak temperature. While the austenite will transform back to martensite on cooling, the ferrite remains. This results in a dual-phase (ferrite + martensite) microstructure in the intercritical region of the weld (Figure 6 (b)). The formation of the ferrite phase hence reduces the hardness from that of the complete martensite microstructure of the base metal. Outside this intercritical region, the material would experience a peak temperature below the A1 temperature. There the metastable martensite microstructure would decompose to a more stable ferrite+Fe_3C microstructure, which also would reduce the hardness. In the TMAZ (labeled as (c) in Figure 3), the material would be heated to above the A3 temperature. The material in the TMAZ would therefore be fully austenitized on heating and transformed back to martensite due to the high hardenability of the martensitic steel. Consequently, the hardness of the TMAZ is expected to reach that of the base metal. Because the bonding region is located in the TMAZ, it would exhibit the similar microstructure and hardness of the base metal.

As shown in Figure 7 (a), the base metal of the DP600 steel has a dual-phase microstructure consisting of a ferritic grain matrix and considerable amounts of the hard phase (bainite and/or martensite) islands mostly decorating the boundaries of the ferrite grains. In the transition region (Figure 7 (b)), the hardened phase region undergoes phase transformation to form fine grained structures. The resultant microstructure in this region is a network of fine grained microstructure surrounding the large ferritic grains. As in the case of M190 weld, it is expected that the peak temperature in this region falls within the intercritical temperature range to form a mixture of austenite and ferrite on heating. The austenite then transforms back to hard phases on cooling. The details of these fine grained

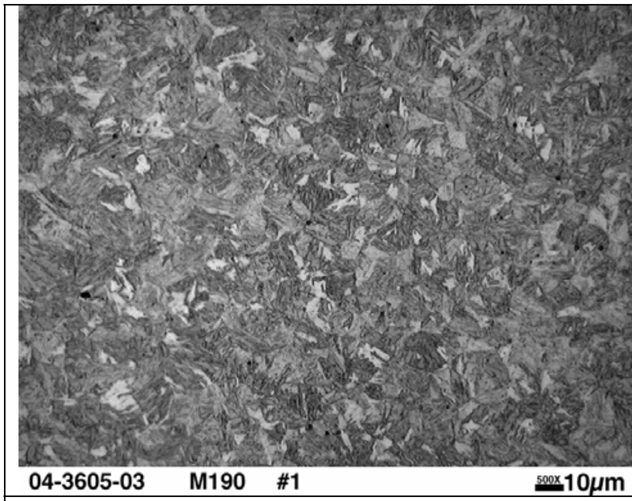

(a)

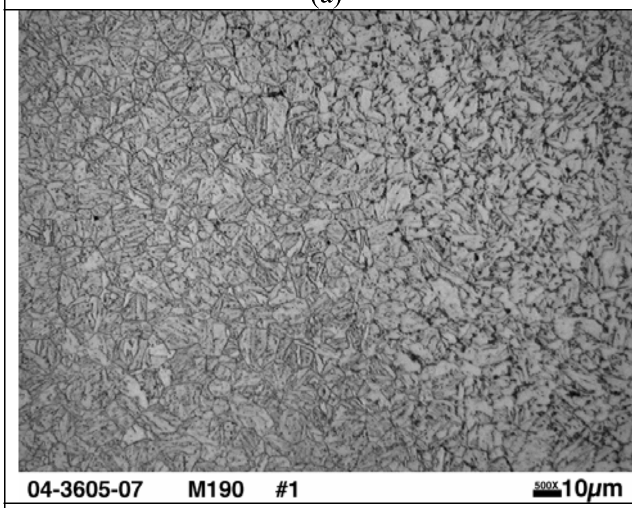

(b)

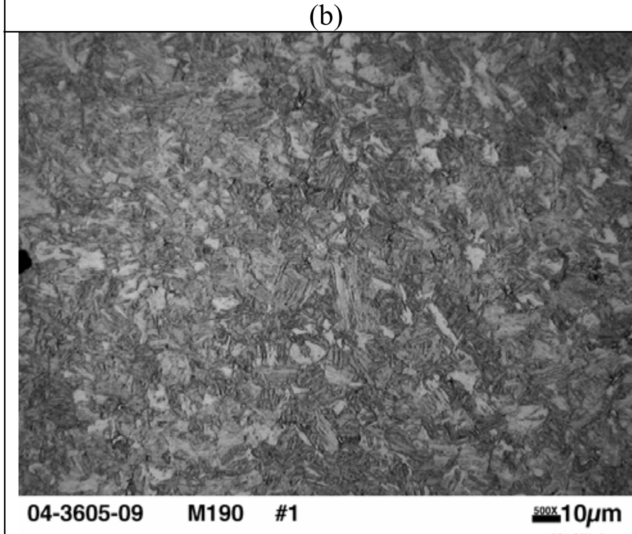

(c)

Figure 6. M190, 2.1 sec (a) Base metal, (b) transition BM to intercritical region (on the right side of the photo), (3) TMAZ. The locations are given in Figure 3.

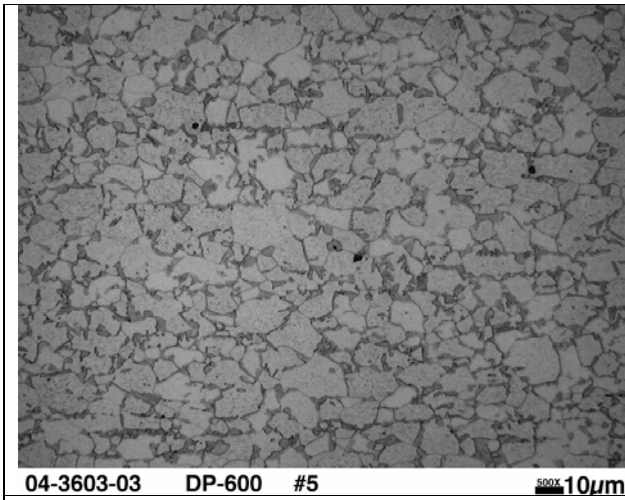

(a)

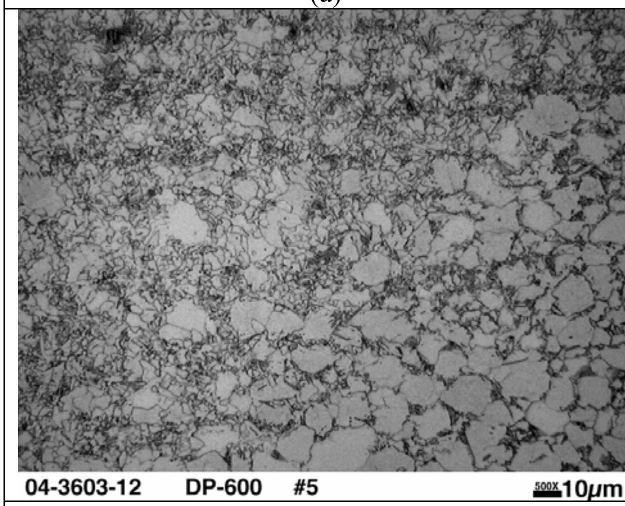

(b)

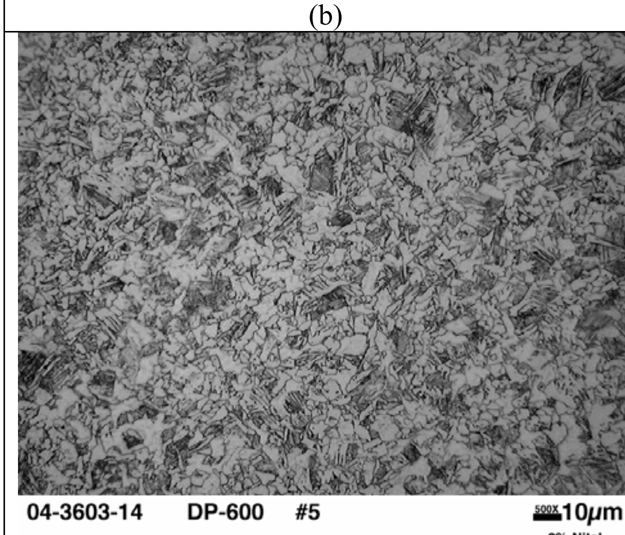

(c)

Figure 7. DP600. (a) base metal, (b) Transition from BM to the inter-critical region (on the left side of the photo), (3) TMAZ. The locations are given in Figure 3**.**

structures would not be resolved under the optical microscope. In the TMAZ, the material is expected to be fully austenitized on heating. Due to the relatively high hardenability of DP600 steel, an increased amount of bainite/acicular ferrite was formed on cooling, resulting in the increase in the hardness in TMAZ.

The above results suggest that, for the two advanced high-strength steels studied, the FSSW process was able to maintain, to a great extent, the hardness and the microstructure of the base metal *in the bonding interface region*. This could be attributed to the combination of moderate cooling rate [13] associated with the FSSW process (compared to RSW) and the relatively high hardendability of AHSS.

This provides the technical basis for further refinement and optimization of the FSSW process to control or maintain the microstructure and properties in the bonding region of the AHSS weld.

The resulting microstructure in the bonded region also suggests the material flow and bonding takes place when the material is fully austenitized. Such information would be important for the future process and tool material development for FSSW of AHSS.

Figure 8 shows the peak loads measured by the tensile shear test. Each data point represents the average of three samples made under the same welding and material conditions. For both DP600 and M190 steel, an increase in welding time from 2.1 to 3.2 seconds resulted in increases in the peak load strength. This correlated well with the increased bonding ligament width developed in the longer welding time conditions. The cross-tension testing results are presented in Figure 9, for the 3.2 welding time condition.

It should be pointed out that only small bonding ligament widths were obtained in this feasibility study. As the bonding ligament width is a controlling factor for the strength of the joint, it is expected that substantial improvement in joint strength can be achieved if the bonding ligament width can be increased through further process development and modifications to the tool geometry.

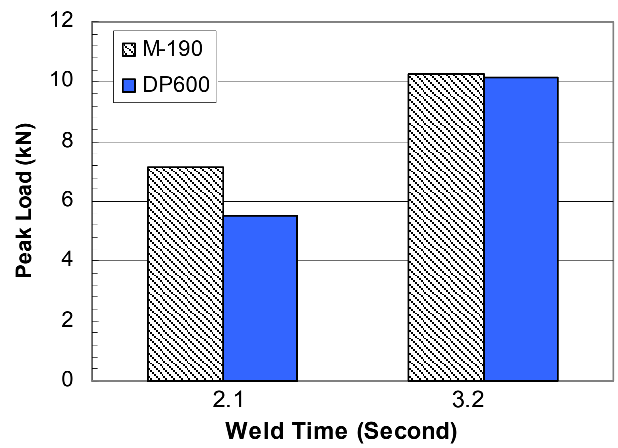

Figure 8. Peak loads from tensile shear test.

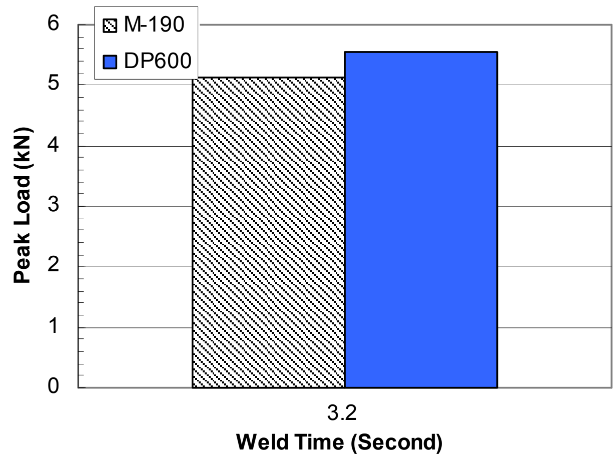

Figure 9. Peak loads from cross-tension test.

Conclusion

This study investigated the feasibility of friction stir spot welding advanced high-strength steel sheet metal for automotive applications. It was found that:

- It is possible to use the fixed pin approach to produce metallurgical bonding for both DP600 dual phase steel and M190 martensitic steel under 3 seconds of welding time.
- The PCBN tool material was capable of producing over a hundred welds without noticeable wear and degradation.
- The bonding region, located in the TMAZ, exhibited similar microstructure and hardness as in the base metal for both steels studied.
- The M190 steel showed considerable softening. However, this softened region is far away from

the bonding region where the failure occurred during the mechanical testing.

- The welding process conditions used in this study produced relatively small bonding ligament widths, thereby limiting the tensile strength levels of the joint. It is expected that substantial improvement in joint strength can be achieved if the bonding ligament width can be increased through further process development and modifications to the tool geometry.

Friction Stir Processing AM60B Magnesium Alloy Die Cast

Industry statistics show that worldwide shipments of magnesium totaled about 530,000 metric tons in 2003 with about 35% of the total being attributed to die casting. [15]. Due to the ease with which die castings are made, relatively little Mg is used in wrought products. One important industry segment where the interest in Mg die casting use is increasing is automotive. Currently, an average sized 1500 kg vehicle uses only about 5 kg of Mg, but this amount is growing at an annual rate of about 12% [15,16].

Magnesium alloys are being used in automotive applications primarily as substitutes for other lightweight materials including aluminum alloys and polymer-based materials. For manufacturing, Mg alloys have some important advantages over Al alloys. Their latent heat is only about 2/3 that of Al alloys. They have lower solubility for iron when molten and higher fluidity. For die casting processes this means that Mg alloys have shorter cycle times, they are less reactive with steels so casting dies last longer and they can be cast in thinner sections. Magnesium alloys can develop strength-to-weight ratios exceeding those of all other alloys found in automobiles including steels. They also have excellent damping properties which makes them attractive for improving noise-vibration-harshness (NVH) characteristics.

The increased use of Mg die castings for automotive applications is likely to be promoted by welding, joining, and surfacing technologies. Fusion welding of Mg die castings is likely to be problematic owing to their tendency to form excessive gas porosity in weld fusion zones [17,18]. In contrast, friction stir welding appears capable of producing sound joints with little or no porosity and good mechanical properties [19,20].

Experimental

Die cast plates with dimensions of 127 x 25 x 6 mm were made of the AM60B by a cold chamber casting process under protective atmosphere. The plates nominally contained (5.4-6.1) Al + 0.13 Mn wt% and about 5% porosity on average from gas entrapped during casting. For the friction stir trials the surfaces were left in the as-cast condition.

The friction stir processing was conducted on an MTS-ISTIR system in displacement-control mode. The stir tool was made of H13 steel with a shoulder diameter of 8 mm. The pin was cylindrical with a hemispherical tip; its dimensions were 3 mm diameter x 2 mm length. The working surfaces of the stir tool were smooth. Two tool rotation speeds were used: 1250 rpm and 2500 rpm. The translation speed was fixed at 1.7 mm/s throughout the experiments. These conditions were used to make stir passes with lengths of about 100 mm. Some testing and analysis was done using single stir passes. Other plates were processed with 5-6 passes overlapped on intervals of about 2 mm. Overlapping the passes created relatively consistent stir processed volumes on the plates with dimensions of about 1.5-2 mm x 10 mm x 100 mm.

The room temperature properties of the friction stir processed surfaces were measured by Vickers microhardness testing, and tensile testing. The microhardness measurements were made on metallographically prepared specimens taken to view the surfaces of single stir passes. The indentations were made under a 50 g load in 200 μm x 200 μm arrays extending from the stir zones into the base metal.

The bars with the overlapped passes were used to make tensile specimens. For the tensile specimens, blanks were electrical discharge machined (EDM) from the stir zones using the shape specified in ASTM E8 for rectangular subsized specimens. Slices 2-mm-thick were then EDM cut from both surfaces of the blanks to provide one specimen of base metal and one specimen where the gage section was entirely within the friction stir processed material. The gage dimensions were 1 mm thick x

6.2 mm wide x 25 mm long. The nominal strain rate for the tensile tests was 1 x 10^{-3}/s.

Results and Discussion

A cross-sectional view of a single pass surfacing layer made at 2500 rpm is shown in Figure 10. Large pores are visible in the base metal, but none were found in the stir zone. This behavior was typical of stir passes made for both conditions. Also, pores were not found in prior stir passes of specimens where stir passes were overlapped. The microstructure in the stir zone is shown in Figure 11. The stir zone consists primarily of very fine equiaxed grains with size in the range of 5-10 μm. There is no evidence of solidification structure and the material in the stir zone appears to contain only relatively small second phase particles. Examination of this stir zone in a scanning electron microscope (SEM) confirmed that it was largely single-phased. The $Mg_{17}Al_{12}$ compound which is a major phase in the as-cast material was apparently dissolved in the Mg matrix during the stir processing.

An optical micrograph showing a top surface view of single friction stir pass made at 1250 rpm is shown in Figure 12. The grid used for microhardness measurement is also visible. An image representation of the hardness distribution is shown below the micrograph. The average hardness over 1239 indents in the base AM60B metal was 59.3 ± 8.6 kg/mm^2. The average hardness in the stir zone over 861 indents was 71.7 ± 6.7 kg/mm^2 which represents an increase of ~ 21% over that in the base metal.

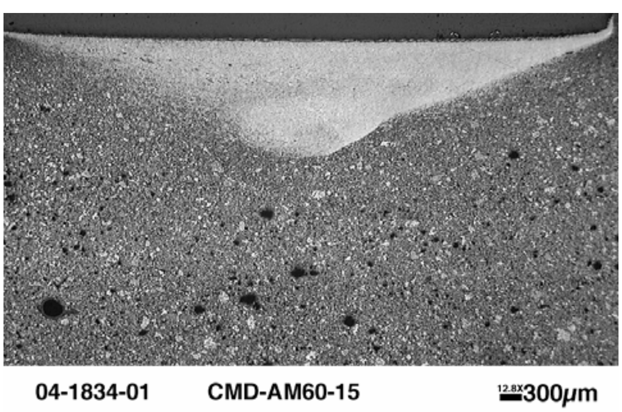

Figure 10. Optical micrograph showing cross section view of single stir pass in AM60B made at 2500 rpm.

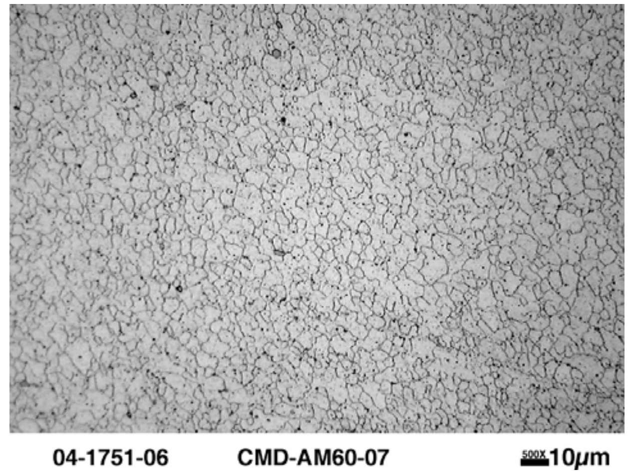

Figure 11. Optical micrograph showing microstructure of single stir pass in AM60B made at 2500 rpm.

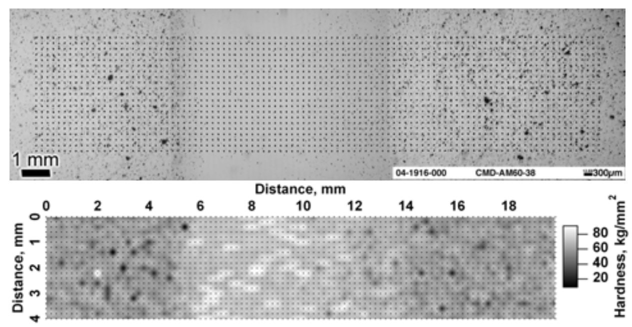

Figure 12. Optical micrograph showing top view of a friction stir pass on the surface of an AM60B plate. Microhardness distribution is shown on the bottom.

Data comparing the room temperature tensile properties of the AM60B base metal to friction stir processed metal are shown in Figure 13 and Table 2. Duplicate specimens were tested at both tool rotation speeds and the stress-strain plots are representative of the tensile behavior at each speed. Tabulated values are averages of two specimens at each condition. The friction stir processing increased each of the tensile properties over those of the die cast metal. Yield strengths were increased about 18%; tensile strengths were increased about 36%; and, ductility more than doubled. It should be noted that the die cast plates were heated by the friction stir processing. As a consequence, the die cast specimens were subjected to multiple undefined thermal excursions. These unintended heat treatments could influence property values of the cast metal. However, the stir processed material would have been subjected to similar heat treatments

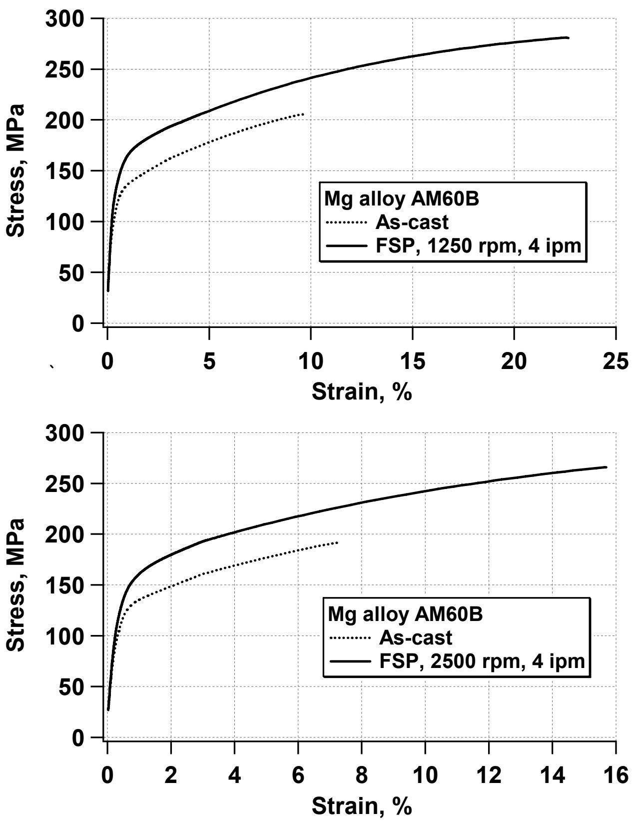

Figure 13. Stress-strain plots from room temperature tensile tests done on die cast and friction stir processed AM60B. Processing parameters are shown on the plots.

Table 2. Comparison of tensile properties for cast and friction stir processed (FSP) AM60B.

Condition	0.2% Yield Strength (MPa)	Tensile Strength (MPa)	Total Elongation (%)
1250 rpm			
Die cast	114	205	9.6
FSP	140	280	22.6
2500 rpm			
Die cast	119	192	7.2
FSP	141	266	15.7

so that the comparison of tensile properties is still considered valid.

Some insight into the effects of friction stir processing on the microstructure, increased hardness and improved tensile properties of the AM60B die cast metal can be gained by considering the phase equilibria for this alloy. The variations with temperature of calculated equilibrium phase amounts are shown in Figure 14. The predictions indicate that between the solidus temperature of 532°C and room temperature AM60B should contain a small amount, less than 1 wt%, of Al_xMn_y. The stochiometry of this compound should vary with the Al concentration increasing as temperature decreases. Presumably, the second-phase particles that are visible in optical micrographs such as Figure 11 are these compounds. Below about 286°C $Mg_{17}Al_{12}$ should also form in the microstructure, ultimately reaching a total amount near 11 wt%. The equilibrium with respect to the $Mg_{17}Al_{12}$ has the features of a classical precipitation hardening system. During friction stir processing it was observed that good visual appearance of the stir passes was usually obtained by allowing the temperature in the vicinity of the stir tool to reach near 250°C before translation was initiated. Various microscopic examinations of friction stir processed specimens confirmed that melting was avoided. Consequently it can be concluded that the friction stir passes were heated to the range of 250-532°C during processing. The time exposure in this temperature range was apparently long enough to permit the dissolution of most or all

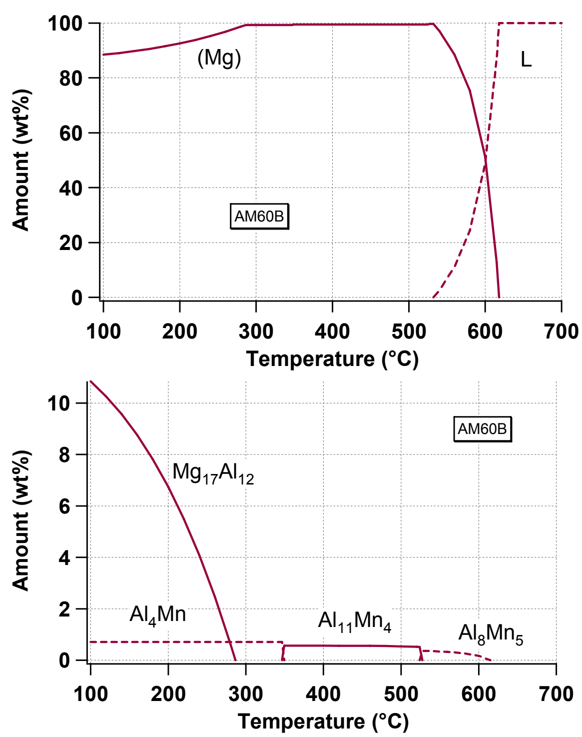

Figure 14. Variations of phase amounts with temperature for AM60B estimated from equilibrium thermodynamics calculations (ThermoCalc™ using Mg-DATA database [21]).

of the $Mg_{17}Al_{12}$ that may have formed in the original cast structure because it was not observed in the stir zones. This observation is in agreement with those from a similar study of thixomolded AM60B [22]. The increased hardness and yield strength in the stir zones can then be attributed to a combination of solid solution hardening by Al in the Mg matrix phase, reprecipitation of $Mg_{17}Al_{12}$ as fine particles, and refinements to the grain structure. The increases of tensile strength and ductility imply that areal fraction of porosity in the stir zones was lower than that of the as-die-cast metal [23].

Conclusion

The ability of friction stir processing to produce stir passes of high integrity on AM60B was demonstrated. Grain structure in the stir zones was largely equiaxed with grain sizes of 5-10 μm. The grains appeared to be all of a single phase and to contain a small amount of second-phase particles. Based on metallographic evidence and thermodynamic considerations the stir zone microstructures were assumed to consist of a Mg matrix, possibly supersaturated with Al, and Al_xMn_y particles. Tensile testing showed that the yield strength in the stir zones was 18% higher than that of die cast metal. Tensile strength in the stir zones was in the range of 36% higher than die cast metal. Friction stir processing doubled the tensile ductility of the AM60B.

Publications

Feng Z, Santella M L, David S A, Steel R J, Packer S M, Pan T-Y, Kuo M, and Bhatnagar R, S, (2005), “Friction Stir Spot Welding of Advanced High-Strength Steels - a Feasibility Study”, *SAE 2005 Congress*, SAE-International, Detroit, MI, Technical Paper No 2005-2001-1248.

Awang M, Mucino V, Feng Z, and David S A, (2005), “Thermo-Mechanical Modeling of Friction Stir Spot Welding (FSSW) Process: Use of an Explicit Adaptive Meshing Scheme”, *SAE 2005 Congress, SAE-International*, Detroit, MI, Technical Paper No 2005-2001-1251.

Arul S G, Pan T-Y, Pan J, Lin P C, Feng Z, and Santella M L, (2005), “Microstructures and Failure Mechanisms of Spot Friction Welds in Lap-Shear Specimens of Aluminum 5754 Sheets”, *SAE 2005 Congress*, Detroit, MI, Technical Paper No 2005-2001-1256.

Santella M L, Feng Z, Degen C, and Pan T-Y, (2005), “Modifying AM60B Magnesium Alloy Die Cast Surfaces by Friction Stir Processing”, *7th International Conference on Trends in Welding Research*, S. A. David (Ed.) TMS, Pine Mountain, GA.

Santella M L, Feng Z, Degen C, and Pan T-Y, (2005), “Friction Stir Processing to Improve the Surface Properties of Aluminum and Magnesium Castings”, *Materials Science & Technology 2005 Conference*, ASM International, Pittsburgh, PA. Santella, M. L., Engstrom, T., Storjohann, D., and

Pan T.-Y., (2005) “Effects of friction stir processing on mechanical properties of the cast aluminum alloys A319 and A356,”, Scripta Materialia, **53**(2), 201-206.

Feng Z, Pan T-Y, Santella M L, and David S A, (2005), “Friction Stir Spot Welding and Its Applications”, *AeroMat 2005*, ASM International, Orlando, FL.

Woo W, Liaw P K, Choo H, Brown D W, Feng Z, David S A, and Hubbard C R, (2004), “D-41 Two-Dimensional Mapping of Residual Stresses in 6061-T6 Aluminum Friction Stir Welds”, *Powder Diffraction*, 19:(2), 202.

References

1 Hancock, R., 2004, "Friction welding of Aluminum Cuts Energy Cost by 99%," *Welding Journal*, vol. 83, pp. 40.

2 Shi, S.G. and Westgate, S.A., 2003, “Resistance spot welding of high-strength steel sheet,” Corporate Research Program Report No 767/2003, The Welding Institute, Cambridge, UK.

3 Spinella, D. J., Brockenbrough, J. R., and Fridy, J. M., 2005, "Trends in Aluminum Resistance Spot Welding for the Automotive Industry," *Welding Journal*, 84(1), 34-40.

4 "*Mazda Develops World's First Aluminum Joining Technology Using Friction Heat*", Mazda News Release, February 27, 2003,

http://www.mazda.com/publicity/release/200302/0227e.html.

5 Iwashita, T. "Method and Apparatus for Joining." US Patent 6601751 B2, Aug. 5, 2003.

6 Sakano, R., Murakami, K., Yamashita, K., Hyoe, T., Fujimoto, M., Inuzuka, M., Nagao, Y. and Kashiki, H., 2001, "Development of Spot FSW Robot System for Automobile Body Members," Proc. 3rd International Symposium of Friction Stir Welding, Kobe, Japan.

7 Pan, T., Joaquin, A., Wilkosz, D. E., Reatherford, L., Nicholson, J. M., Feng, Z., and Santella, M. L., 2004, "Spot Friction Welding for Sheet Aluminum Joining," Proc. 5th International Symposium on Friction Stir Welding, Metz, France.

8 Allen, C. D., and Arbegast, W. J., 2005, "Evaluation of Friction Stir Spot Welds in 2024 Aluminum," SAE Technical Paper No 2005-01-1252, Society of Automotive Engineers.

9 Ferrasse, S. Verrier, P and Meesemeacker, F, 1998, "Resistance spot weldability of high-strength steels for use in car industry," Welding in the World, 41(2), p177-195.

10 Yamazki, K, Sato, K, and Tukunaga, 2000, "Static and fatigue strength of spot welded joint in ultra-high-strength, cold-rolled steel sheets," Welding International, 14(7), p533-541.

11 Peterson, W, 1997, "Dilution of weld metal to eliminate interfacial fractures of spot welds in high and ultra-high strength steels," Proc. Int. Conf Advances in Welding Technology, Columbus, 17-19, Sept, 1997, p331-346.

12 Gould, J.E., Lienert, T.J. and Feng, Z., 1998, "Recent developments in friction stir welding," SAE Technical Paper Series 981875

13 "Development of Friction Stir Spot Welding Process," ORNL Internal Research, 2004.

14 Packer, S. M., Nelson, T. W., Sorensen, C. D., Steel, R., and Matsunaga, M., 2003, "Tool and Equipment Requirements for Friction Stir Welding Ferrous and Other High Melting Temperature Alloys." *4th International Symposium on Friction Stir Welding*, Park City, Utah.

15 American Metal Market (http://www.amm.com).

16 K. Johnson, "Magnesium Automotive Applications", *Advance Materials & Processes*, 160(6), pp 62-65 (2002).

17 H. Zhao and T. DebRoy, "Pore Formation during Laser Beam Welding of Die-Cast Magnesium Alloy AM60B – Mechanism and Remedy", *Welding Journal*, 80, 204-s-210-s (2001).

18 A. K. Dasgupta and J. Mazumder, "Laser Welding of AM60 Magnesium Alloy", *Magnesium Technology 2004*, ed. A. A. Luo, TMS, pp 43-48.

19 N. Li, T.-Y. Pan, R. P. Cooper, D. Q. Houston, Z. Feng, and M. L. Santella, "Friction Stir Welding of Magnesium AM60 Alloy", *Magnesium Technology 2004*, ed. A. A. Luo, TMS, pp 19-23.

20 J. I. Skar, H. Gjestland, L. D. Oosterkamp, and D. L. Albright, "Friction Stir Welding of Magnesium Die Castings," *Magnesium Technology 2004*, ed. A. A. Luo, TMS, pp 25-30

21 N. Saunders, "Mg-DATA, a database for thermodynamic calculations for Mg alloys," Thermotech Ltd., Surrey Technology Centre, The Surrey Research Park, Guilford, Surrey GU2 7YG, U.K.

22 J. A. Esparza, W. C. Davis, and L. E. Murr, "Microstructure-property studies in friction-stir-welded, Thixomolded magnesium alloy AM60," *Journal of Materials Science*, 38, pp 941-952 (2003)

23 J. P. Weiler, J. T. Wood, R. J. Klassen, E. Maire, R. Berkmortel, and G. Wang, "Relationship between internal porosity and fracture strength of die-cast magnesium AM60B alloy", *Materials Science & Engineering A*, 395, pp 315-322 (2005)

J. Portfolio Analysis for Lightweight Materials

Principal Investigator: Edward Ungar
Taratec Corporation
1251 Dublin Road, Columbus, OH 43215
614-291-2229; fax 614-291-2867; e-mail: eungar@tarateccorp.com

Chief Scientist: James J. Eberhardt
(202) 586-9837; fax: (202) 587-2476; e-mail: James.Eberhardt@ee.doe.gov
Field Technical Manager: Philip S. Sklad
(865) 574-5069; fax: (865) 576-4963; e-mail: skladps@ornl.gov

Participants:
Paula Dunnigan, Taratec Corporation
Mike Carter, Taratec Corporation
Greg Palovchik, Taratec Corporation

Subcontractor: Taratec Corporation
Subcontract No.: 4000033939 under Contract No. DE-AC05-OR22725

Objectives

- To evaluate the impact of High Strength Weight Reduction (HSWR) projects on the fuel efficiency of the heavy vehicle fleet as well as commercial and technical risk factors associated with the HSWR project portfolio.
- To develop project clusters to assist in the evaluation of various groups of related HSWR projects.

Approach

- The project approach builds on Taratec's previous work for Oak Ridge National Laboratory (ORNL) for risk and impact analysis. Estimated weight reductions are translated to fuel savings through the NREL ADVISOR model and the Taratec-developed fleet drive cycle. Risk is determined through a combination of analysis and interviews with developers and commercializers.
- Penetration rates were determined using various market-driven factors for OEMs and end-users taking into account regulatory requirements.

Accomplishments

- In FY 05, Taratec analyzed the HSWR project portfolio to estimate project impact as measured by heavy vehicle fleet fuel savings and project technical and commercial risk factors. In addition, Taratec developed a cluster analysis which allows the user to examine the impact of project clusters on heavy vehicle fuel savings as well as the impact of individual projects on the cluster as a whole. The project cluster analysis results were used to display impact in the HSWR project peer review conducted at ORNL in September, 2005.

Introduction

The FY 2005 activities updated prior Taratec work on the risks and benefits of the heavy vehicles lightweight materials research portfolio. In addition, the technology penetration rates into the fleet were estimated and technology clusters were created.

Key Findings

There is a wide variance of impacts on fuel savings for the heavy vehicle fleet that depends on both the technology and the vehicle component to which it is applied. The maximum benefits are in the range of a million gallons of diesel fuel saved per year. More than half of the projects reviewed are enabling technology projects, which are focused on developing basic technology or knowledge, while the remainder are focused on developing specific vehicle components built from lightweight materials.

Ultimate deployment of the technologies is driven by a combination of cost, performance and regulations. The OEMs each have their own market data showing what they perceive to be the customer willingness to pay for weight reduction. This varies from no premium to a relatively small ($1-2/lb.) premium. Of course recent increases in fuel prices may change that perception. There is a significant concern that new materials must perform as well as older materials under the harsh conditions faced by Class 8 trucks. These factors impact the technology adoption rate. Even with these factors considered, Taratec's estimated penetration rates are faster than previous estimates made by DOE.

The penetration of the technology into the full heavy vehicle fleet must be weighted by miles driven. Approximately 80% of the new trucks enter the long-haul market and are driven 400-500,000 miles in about 3 years and then are traded in or re-sold. Thus, newer technology deployed in new trucks is driven a disproportionately higher fraction of the total vehicle miles driven than the rest of the heavy truck fleet.

Additionally, Taratec developed materials clusters both by class of material and by major materials applications (drive train, body panels, major structure, etc.) in both cases the impact of the cluster is driven by a few high-end applications. However, the role of enabling projects and low-criticality applications to help the OEMs to develop design comfort with new materials is illustrated by use of clusters.

Conclusions

Methodologies for evaluation of the impact of HSWR materials projects have been demonstrated.

K. Inventory of Heavy-duty Truck Lightweighting Candidates

Principal Investigator: Edwin H. Kraft
EHKTechnologies
10917 SE Burlington Drive
Vancouver, WA 98664-5383
(360) 896-0031; fax: (360) 896-0032; e-mail: ekraft@EHKTechnologies.com

Chief Scientist: James J. Eberhardt
(202) 586-9837; fax: (202) 587-2476; e-mail: James.Eberhardt@ee.doe.gov
Field Technical Manager: Philip S. Sklad
(865) 574-5069; fax:(865) 576-4963; e-mail:skladps@ornl.gov

Contractor: EHKTechnologies
Subcontract: No.: 4000031071 / 03/22/2004

Objective

- Identify components and systems of heavy-duty trucks that have the greatest total fleet weight savings potential for the purpose of increased fuel efficiency and productivity.
  - Inventory the systems and components of Class 8 tractor-trailers
  - Model the miles traveled and weight factor for the major component-system-vehicle combinations
  - Rank and estimate the fuel consumption contribution of the most significant components
  - Provide a model usable by potential component lightweighting developers to estimate the relative weight–miles contribution of candidate components

Approach

- Define the industry segments: types of vehicle bodies and vehicle configurations; define the numbers and annual miles of vehicles by type and configuration.
- Compile data on component and system configurations, weights, and materials of construction for the apparent major contributors to vehicle weight.
- Aggregate data on specific component weights and materials to prevent disclosure of individual manufacturers' proprietary information. Select representative values for component weights where a range of designs and weights are common.
- Determine the fuel economy distribution of weight ranges of heavy-duty trucks and calculate a representative fuel consumption of components per pound-mile.
- Design a model of the weight-miles traveled (pound-miles) and fuel consumption for any component or set of components to be considered for fleet weight savings and improved fuel economy.

Accomplishments

- Successfully used the various databases to calculate numbers and total annual miles of vehicles by body type, vehicle configuration (truck and truck-tractor, number of trailers pulled, number of axles and tires), weight sub-classification, and type of cargo hauled.
- Determined that buses and four types of trucks account for >90% of vehicle numbers and miles, and the four truck types account for the most trailer and haul unit miles.
- Determined that weight regulations normally impact the operation of platform, dump, and tank body vehicles, causing them to be weight-limited ("gross out").

- Obtained representative weights of major components common to all vehicle types and those specific to the four primary body types.
- Constructed an Excel-based model of component pound-miles and added a calculation of component fuel consumption.
- Identified the most significant contributors to pound-miles.
- Determined that data from 2002 Census did not require any significant change in the conclusions reached based on 1997 data.
- Determined that extensive use of aluminum, high-strength steel, and new designs has already contributed to weight reduction and that further use of these materials plus magnesium, titanium, and composites promises significant additional weight savings.
- Published Final Report and presented results.

Future Direction

At the direction of DOE and ORNL, discuss findings with vehicle and component manufacturers for consideration of focused developments, and with military agencies for applicability to military ground vehicles.

Introduction

The purpose of this project is to assist Oak Ridge National Laboratory (ORNL) and the Department of Energy (DOE) in prioritizing lightweighting technologies for heavy-duty trucks via an inventory of components that may aid in weight reduction. Identifying the components that contribute the most weight in the entire fleet of heavy trucks will enable ORNL/DOE to select projects with the greatest payoff in weight savings and reduced fuel consumption. The inventory considers not only the weight of typical components but also the number of vehicle miles traveled by heavy trucks using that component over a typical year (pound-miles) and the fuel consumed carrying those components. A model was provided that allows calculation of the pound-mile and fuel consumption figures for any component under consideration. It incorporates the effect of applying the component to various truck body types and the miles traveled by trucks that use it. The model may be used to provide a quantitative estimate for comparing the weight and fuel consumption reduction potential of any proposed component.

Project Deliverables

- A presentation was made to DOE and ORNL personnel.
- A final report was provided with details of the methodology and findings.
- A computer disk containing the model was provided for use by DOE, ORNL, and potential component developers for calculating and identifying the weight and fuel savings potential of any proposed component.

Heavy Vehicle Segments

Some components of heavy duty trucks and tractor trailers are used on every such vehicle; others may only be used on one vehicle type or configuration. In considering the development of a reduced-weight component, it is therefore necessary to understand its potential contribution to weight reduction over the entire vehicle fleet. To do so, it is necessary to have data on the number of vehicles of various types, and the miles traveled by each type, over a representative year. The weight or weight reduction potential of a component is multiplied by the number used on each vehicle type and the miles traveled by that type to obtain the pound-miles for the component. Adding the pound-miles for all vehicle types where a component would be used gives the total pound-miles for that component. If an average fuel economy figure is available for heavy trucks, it may be used to calculate the fuel consumed by each pound of weight of an average vehicle. The product of the pound-miles and the fuel consumed is an estimate of the fuel savings if that component were implemented across all applicable vehicles.

Several databases were used to construct a master database of numbers and miles traveled for all types of trucks in each weight range of Class 7 and 8 vehicles. It lists 29 body styles, including dry van truck and trailer containers, refrigerated van truck and trailer containers, tank trucks and trailers, flat bed trucks and trailers, dump bodies, and cement mixers. Another truck-trailer classification includes the type of truck (truck or truck tractor), number of trailers pulled, number of axles, and number of wheels. Thus, for example, all tank trucks with 4 axles and 14 wheels pulling a full tank trailer with 3 axles and 12 wheels will have one estimated number with that configuration and total miles traveled. Three-axle, 10-wheel truck tractors pulling one 4-axle, 16-wheel flatbed trailer will have a different estimated number and miles traveled. These differences have been found to be very significant. Analysis of these vehicle types was also expected to assist in focusing effort on the vehicle body types and components with the most contribution to pound-miles and fuel consumption.

This last benefit of the analysis is best accomplished by charting the number and miles traveled for the various truck types, and the number of trailers and "haul units" traveled by those types. A haul unit is defined as one container or support structure for cargo carried by a truck or trailer (e.g., a tank truck pulling a tank trailer constitutes two haul units.)

Figure 1 shows the number of vehicles by type with similar types combined. This result shows that relatively few body types account for the great majority of vehicles. This finding is even more pronounced when the results for body type by miles traveled are shown (Figure 2). We then find that just four body types account for 90% of the miles driven by heavy trucks/tractor trailers: the various forms of vans (dry, refer, insulated, and drop body), platforms (with and without added devices, and drop frame), dump bodies, and liquid haul tanks. Other body types travel far fewer miles and therefore contribute little to the overall miles driven by the total heavy-duty fleet.

Buses, including school, inter-urban, and city transit, have been included in this analysis thus far. It is apparent that they contribute significantly to the total miles driven by heavy vehicles. This analysis

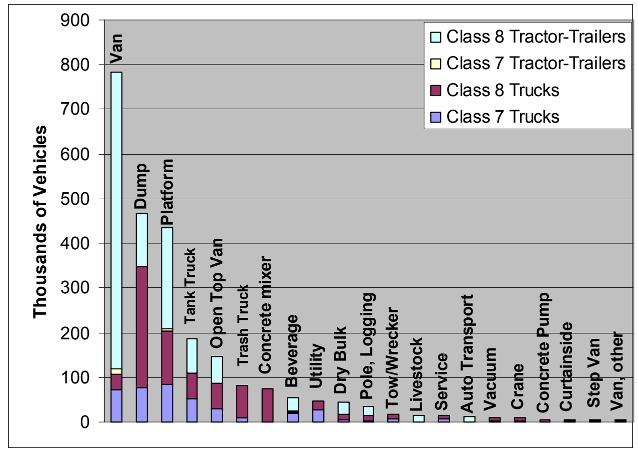

Figure 1. Number of vehicles by type in 2002.

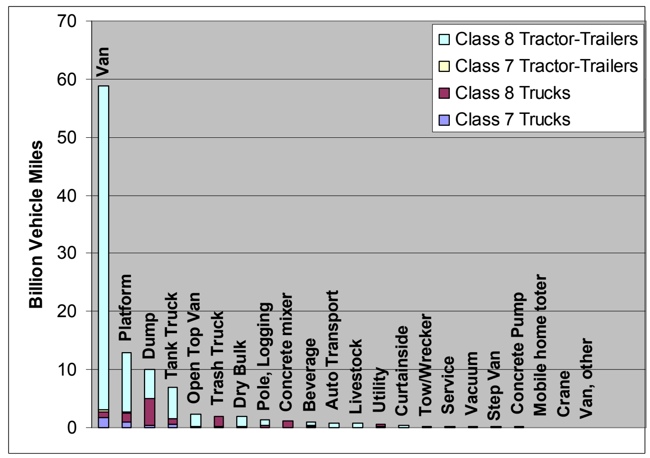

Figure 2. Miles traveled by vehicles of each type in 2002.

was conducted even though the original project scope included only trucks. During the investigation, it was found that, while bus weight and miles may be significant, the operation of buses is limited by passenger capacity and not by weight in most cases. Fuel savings by reduced weight is a secondary consideration for this industry. Therefore, owners and operators are not generally willing to pay any premium for weight savings. Methods to reduce bus weight may have significant fuel economy payoff but are likely to be adopted only if they carry no cost penalty. Since this topic was not in the original project scope, and buses are not generally weight limited, no further analysis was performed.

The number of trailer miles and of haul unit miles of the various types was analyzed to further confirm the overriding importance of the four types of vehicle bodies. Figure 3 shows the results for haul unit miles.

We can definitively conclude that vehicles with body types including types of vans, flat beds, dump bodies, and tanks make the most significant contribution to miles traveled by heavy duty vehicles. It is also apparent that Class 8 vehicles other than buses travel far more miles than Class 7 vehicles, which may then be ignored in analysis of potential weight and fuel savings. Analysis of components used either on multiple-body type trucks or on these four primary types will provide the greatest potential for weight and fuel savings.

Major Truck and Trailer Components

Some components of heavy vehicles are used on all body types and vehicle configurations, and others are specific to certain body types. Obviously, a relatively heavy component common to all types of vehicles will contribute much more to total pound-miles than a lighter component specific to only one body type.

Data were collected on the weights of components of all the major systems of trucks, tractors, and trailers. Much of this specific data, however, is proprietary and may not be disclosed. Attempts were therefore made to collect data from multiple manufacturers so that aggregate weights could be used in the analysis. In some cases, particularly where a wide variety of designs and weights are available for a type of component, representative weights were selected to facilitate the comparative.

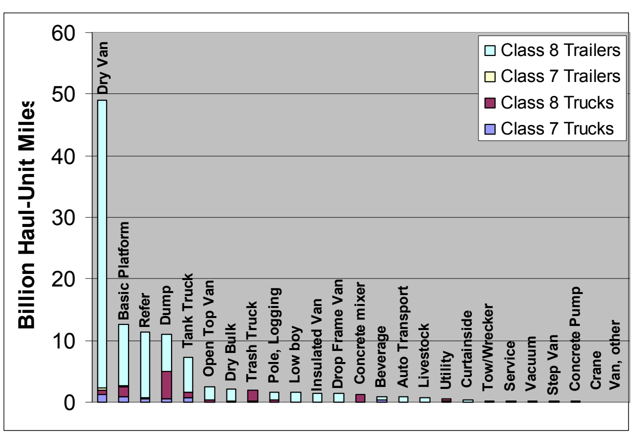

Figure 3. Miles traveled by haul units of each type in 2002.

analysis. Individual component weights discussed in this report therefore do not represent those of components from any one manufacturer

Common Components. All truck and truck-tractor components are used in all body types. Engines, transmissions, truck frames, exhaust systems, axles, suspensions, cab features, drivelines, wheels, and tires, among others, are common components. Since 70% of haul units are trailers, several other components, such as fifth wheels, couplers, landing gear, "bogie" sliders, bumpers, and underrides, are used by nearly all vehicles. Some components are used on several major body types, such as van and flatbed floors, lower and upper side rails, main and cross beams. It is also important to consider in our analysis that some components are used multiple times per vehicle, including tires, wheels, axles, brakes and suspensions; such multiple use may make a component of moderate weight significant.

The engine is one of the heaviest components and is used on all vehicles. While there are numerous engine designs and engine sizes, many components are common to all or most designs. Figure 4 shows the relative weights of many of the major components. It is apparent that the block and cylinder head are by far the heaviest components and most likely to be significant contributors to pound-miles and fuel consumption. Wheels and tires, used multiple times on all vehicles, have already been the subject of weight reduction efforts.

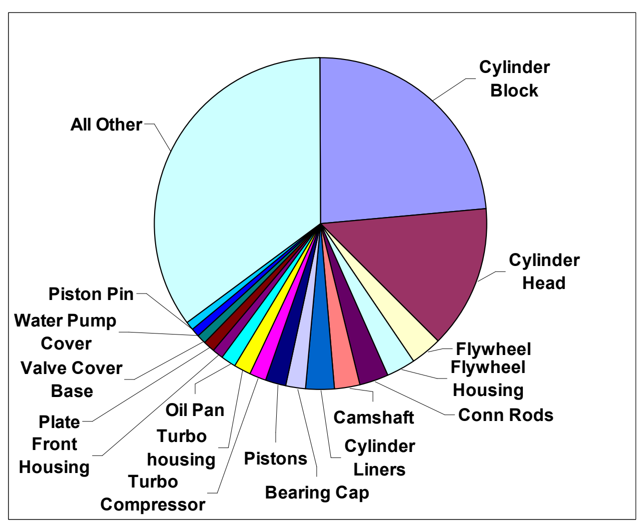

Figure 4. Approximate Major Engine Component Weight Distribution.

Traditional steel wheels have been partially replaced by light steel and aluminum wheels, with the latter being used on 40–50% of trucks but only about 10% of trailers. Super single aluminum wheel and tire combinations at ~240 lb per set are beginning to replace dual wheel/tires (~390 lb per set for conventional steel). Titanium provides weight and performance improvements for springs.

Body-Type-Specific Components. Since four types of bodies predominate in numbers and miles traveled, we expect that some of their components will be among the largest contributors to pound-miles and fuel consumption. Among those components are the sides of van body trucks and trailers, with typical trailer side weights of 2000–3000 lb per set; the floors of van body vehicles and flatbed vehicles, which also weigh about 2000 lb; and parts such as base/side rails, top rails, floor crossmembers, rear frames, main beams, dump bodies, and liquid haul tanks. Data were collected on more than 100 such component types.

Truck Fuel Economy

Various estimates of the fuel economy of heavy vehicles were encountered. To provide a supportable estimate for use in the comparison model, the VIUS database was exercised to provide the reported fuel economy of each 10,000 lb range in Classes 7 and 8. Class 8 fuel economy averages, weighted on miles reported, were calculated at 5.46 mpg, and the average vehicle weight at 64,400 lb. These points were used to calculate indicative fuel consumption by vehicle components of 2.84×10^{-6} gallons per pound-mile.

Pound-Mile Comparison Model

For the purposes of this study, a computational model is needed that includes the effect of component weight plus the number of times a component may be used in the entire fleet of trucks, and the fuel consumption per pound of vehicle. An MS Excel spreadsheet model was constructed including all of these factors. The full model includes consideration of the nine most common body types and all 49 vehicle configurations. To operate the model, the user enters a component name and weight and then decides the applicability of that component to each of the nine body types. Applicability may be due to fundamental suitability or to an estimate of the portion of the entire fleet that is likely to adopt the component. The user will next enter the quantity of that component that would be used for each of the 49 configurations of truck and tractor trailer. The spreadsheet model then calculates the pound-miles of that component in the entire fleet, plus an estimate of the fuel that would be consumed by weight-limited vehicles over the entire fleet.

Results

This procedure was followed for 74 of the heaviest components investigated. The results are shown in Figure 5 for the components with the greatest pound-mile and fuel consumption estimates. The values for the other 18 components are very small compared with these 56.

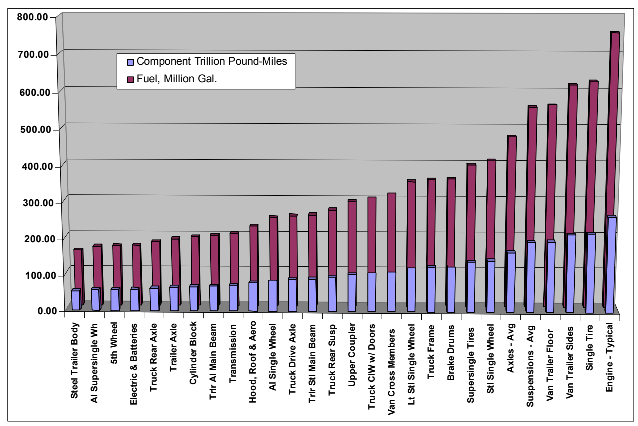

Figure 5. Most Significant Pound-Mile and Fuel Consumption Components.

Conclusions

Based on the results of the analysis of heavy vehicle fleet segments, component weights, and the Pound-Mile and Fuel Consumption model, we can provide the following conclusions:

1. Class 8 trucks and tractor-trailers with four body types predominate in number of vehicles, miles traveled, number of trailers, and number of haul units. Weight reduction efforts will have the greatest payoff for vehicles with components

common to all types, or to one or more of these four types. The four types are

- Van bodies (basic enclosed vans, refrigerated vans, insulated vans and drop-frame vans)
- Platform bodies (basic platforms, platforms with added devices, low boys)
- Tank bodies (liquid or gas haul tank trucks and trailers)
- Dump bodies (dump trucks, bottom and rear dump trailers)

2. Several factors act to make some components more likely to be major contributors to total fleet weight and fuel consumption. They include these:

   - All truck and truck-tractor components, and many trailer components, are used by all body types. These include engine, transmission, truck frame, exhaust, axles, suspensions, cabs, drivelines, wheels, and tires.
   - Since 70% of haul units are trailers, several other components are used by nearly all vehicles, including fifth wheels, couplers, landing gear, suspension sliders, and bumpers.
   - Some components, such as floors, side rails, and main and cross beams, are used by several of the predominant body types.
   - Some components, such as tires, wheels, axles, brakes, support cross members, and suspensions, are used multiple times per vehicle.

3. The pound-miles and fuel consumption contributions of a wide variety of components were determined so that they might be ranked in order of priority for lightweighting effort. The most significant contributors to pound-miles and fuel consumption include engines, tires and wheels, van sides, van and flatbed floors, suspensions, axles, brake drums, all frame members, cabs, couplers and fifth wheels, transmissions, and tanks. Some other component types are also significant contributors.

4. Efforts to reduce the weight of engine blocks and heads, for example, the use of aluminum or titanium, would likely produce the greatest payoff. Application of aluminum to additional components and titanium, magnesium, and composites to many components would result in many trillions of pound-miles of lightweighting and millions of gallons of fuel savings.

5. The conclusions drawn in this study do not appear to change with time as new industry census data are made available.

L. Basic Studies of Ultrasonic Welding for Advanced Transportation Systems

Principal Investigator: Zhili Feng
Oak Ridge National Laboratory
1 Bethel Valley Road, Oak Ridge, TN 37831
(865) 576-3797; fax: (865) 574-4928; e-mail: fengz@ornl.gov

Chief Scientist: James J. Eberhardt
(202) 586-9837; fax: (202) 587-2476; e-mail: James.Eberhardt@ee.doe.gov
Field Technical Manager: Philip S. Sklad
(865) 574-5069; fax:(865) 576-4963; e-mail:skladps@ornl.gov

Participants:
H. Wang, X. Zhang M. L. Santella, and E. A. Kenik, Oak Ridge National Laboratory
W. Zhang, Oakland University

Contractor: Oak Ridge National Laboratory
Contract No.: DE-AC05-00OR22725

Objective

- Develop a fundamental understanding of the ultrasonic welding (UW) process.
- Establish process conditions to optimize joint properties of aluminum alloys for auto body applications.
- Explore opportunities for joining dissimilar materials.
- Explore the feasibility of ultrasonic processing in other novel and unique situations in materials processing, such as metal powder consolidation, producing functionally graded components, and modifying surface properties.

Approach

- Perform UW experiments to develop correlations of process parameters with joint properties.
- Characterize details of joint microstructures.
- Model the fundamental interactions of ultrasonic waves with solids.

Accomplishments

- Determined the acoustic energy distribution by means of infrared thermography.
- Investigated the geometric effects on ultrasonic energy generation and dissipation during the welding process.
- Initiated experimental study on residual stress distribution in the bonding region.
- Developed an efficient computational model to study the acoustic energy distribution in the welded workpiece.

Future Direction

- Continue welding process development for dissimilar materials, including joining of amorphous metals.
- Study the structure-property relationship of joints.

- Model the acoustic energy distribution in the weld joint.
- Study the residual stress distribution in the bonding region.
- Assess the ability of ultrasonic processing for low-temperature metal powder compaction and consolidation.

Introduction

Ultrasonic welding (UW) uses high frequency mechanical vibrations to produce a solid-state metallurgical bond (weld) between metals. The basic process setup is illustrated in **Figure 1** for typical spot weld configuration. An electro-mechanical converter converts high-frequency electric current to mechanical vibration. The mechanical vibration is then modulated and amplified by the booster/horn before it is applied to the overlapping workpiece through the vibration of the sonotrode. A moderate clamping force is applied to ensure the mechanical vibration is transferred to the sheet-to-sheet interface (the faying surface) where the weld is created. Typically, the mechanical vibration is at 20–40 kHz with an amplitude range of 5–50 µm. The power delivered to the workpiece is in the range of several hundred to several thousand watts.

Figure 2 illustrates the essential underlying mechanisms involved in the formation of the metallurgical bond at the workpiece interface during ultrasonic welding. The combination of normal clamp pressure and literal mechanical vibration results in several important effects at the workpiece interface. The lateral mechanical vibration introduces relative motion at the interface. The frictional action at the interface due to the relative motion and the normal pressure breaks the surface oxides and other contaminants. As result, clean metal surfaces are brought into contact under pressure. Frictional heating also occurs at the bond interface. The heating promotes both localized deformation and diffusion in the region where the pressure is applied. When the process conditions are right, metallurgical bond is formed without melting at the bonding interface. The self-cleaning nature of UW and its ability to form metallurgical bonds without melting are two important advantages of the process.

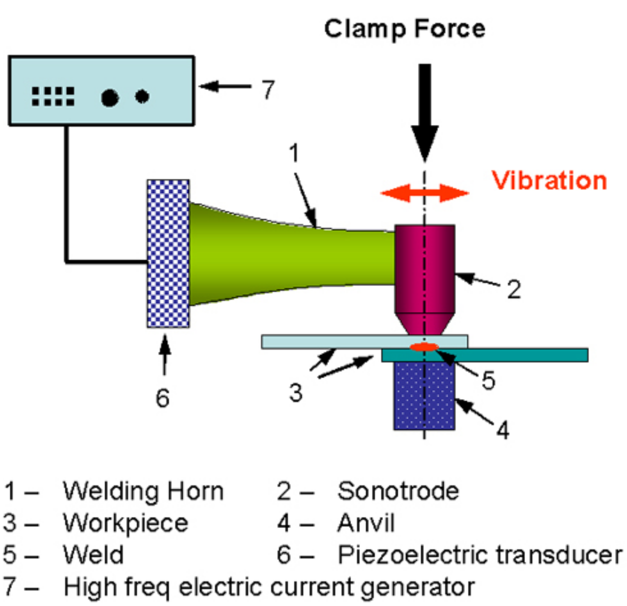

Figure 1. Schematic setup of ultrasonic welding process.

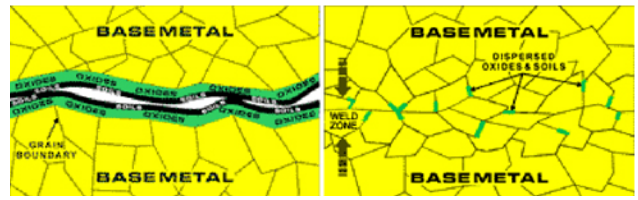

Figure 2. Schematic representation of bond interface before (left) and after (right) UW.

UW creates a joint without bulk melting. Thus, ultrasonic weld is inherently immune to welding defects associated with the solidification in various fusion welding processes (electric resistance spot welding, arc welding, laser welding etc). Solidification induced defects such as solidification cracking and porosity can be a major quality problem for a number of high-performance light-weight structural materials used in automotive body structures. In addition, UW is ideal for joining dissimilar metals such as Al to steel, Al to Mg, metal to metal composite that has been extremely difficult for the conventional fusion welding processes. Because melting is avoided, the ultrasonic welding process is much more energy efficient. UW has attracted considerable attention in the auto industry as an important enabling joining technology for assembling structural components made of aluminum alloys, magnesium and other high-performance lightweight materials.

In our research performed in FY04, it was observed that the ultrasonic weld quality depends strongly on a number of geometric factors such as the weld location, the shape and size of the workpiece, and the sonotrode vibration direction relative to the workpiece. Under certain circumstances, cracking occurs at unexpected locations. Destruction of prior welds by subsequent welding was also observed. These observations suggested that the acoustic wave propagation and reflection in the workpiece being welded are very complicated and would result in considerable weld-to-weld quality variations.

In FY05, the program focused on investigating the acoustic energy distribution during welding. By utilizing the real-time infrared (IR) thermography technique, localized temperature rise in the workpiece during UW was observed and recorded as a function of time. The influence of the geometry factors on the energy distribution was experimentally investigated to elucidate possible causes for the observed weld quality variations. In addition, an efficient elasticity based computational modeling approach was developed to further the understanding of the acoustic energy distribution in the workpiece.

This report is divided into two parts. The first part deals with the experimental study of the acoustic energy distribution in the workpiece and its correlation to the weld quality. The second part of the report describes the theoretical treatment and computational modeling results of the acoustic energy distribution.

Experimental Investigation of Acoustic Energy Distribution

Welding

All welding trials were conducted on a Sonobond® ultrasonic welder. The machine operated at 20kHz and had a maximum rated power output of 2500W. Al6111 and Al5754, two aluminum alloys widely used in the automotive industry, were used for this investigation. Welds were made on 25-mm-wide and 100-mm-long coupons. This is a standard coupon dimension commonly used by the auto industry for weldability testing of spot welds. The nominal thickness of the workpiece was 1 mm. The weld was made in the overlap configuration, as shown in **Figure 3**. The overlap distance and the location of the weld were varied to investigate the geometry effects.

The basic ultrasonic bonding process parameters were: 2400W, 70psi, and 0.5 second.

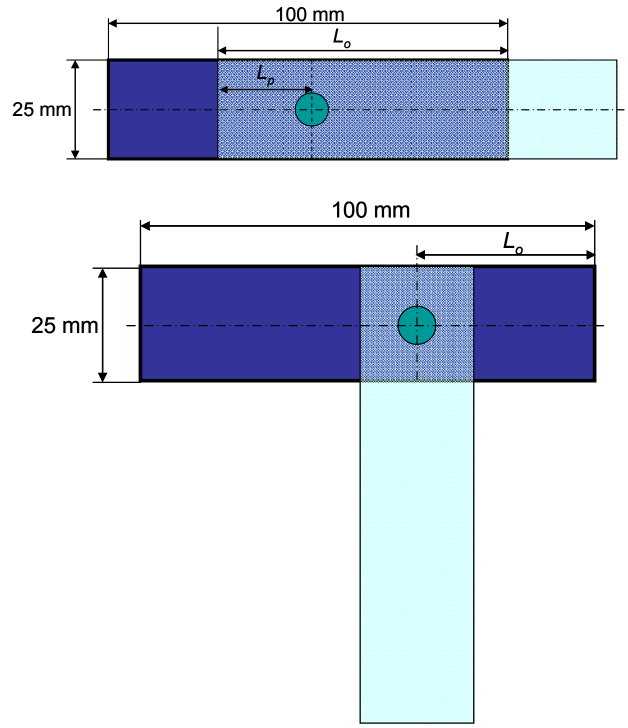

Figure 3. Weld coupon dimensions used in the study. Different overlap distance, *Lo*, and the weld position, *Lp*, were varied in the experiments.

IR Thermography Measurement

A Raytheon, Radiance HS®, mid-IR (3-5 μm) camera was used to monitor the heat generation and diffusion in the weld samples. The temperature history of the weld sample was recorded at 60 frames per second, with a field of view of 256 x 256 pixels. During welding, the IR camera was aimed at the top surface of the specimen. In some tests, a water-soluble black paint was coated on the observing surface to reduce surface reflection and other interferences from the environment. Both the spatial distribution and the temporal variation of the temperature field were used to infer how the heat (the dissipative part of the acoustic energy) is generated and distributed during UW.

Results and Discussions

In last year's study, unforeseen cracking phenomenon was observed during ultrasonic welding of Al5754 alloy. The occurrence of such unusual cracking was highly repeatable in the welding trials. The location of the cracks, while generally away from the weld, is highly dependent on the geometric factors such as the overlapping distance and the position of the weld relative to the edge of the specimen. For example, as shown in **Figure 4**(a), when the overlap distance was at 75 mm and the weld position was at 35 mm, the cracking occurs at a distance approximately 20 mm away from the weld. On the other hand, when the overlap distance was at 35 mm and the weld position was at 20 mm, the cracks were lined up with the weld – **Figure 4**(b). In both cases, cracks form near the edge of the specimen, and they are not connected to the weld. Such a cracking pattern implies that the acoustic energy density in the weld sample does not monotonically decrease as the distance to the applied acoustic energy source (i.e., weld center) increases. Rather, sporadic high acoustic energy concentration spots exist in the welded workpiece.

(a)

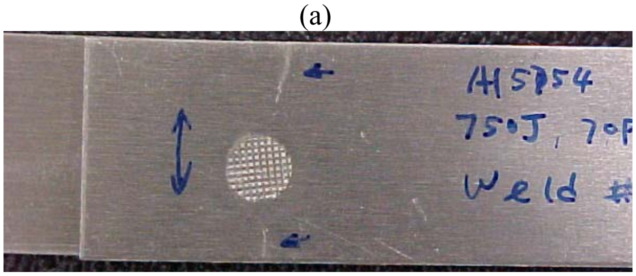

(b)

Figure 4. Unusual cracking during ultrasonic bonding of Al5754. The vibration direction of the sonotrode is along the width direction of the workpiece, as indicated by the vertical arrow marks.

Using the IR thermography, we were able to correlate the cracking phenomenon to localized temperature rise at the cracking location. **Figure 5** shows the temperature distribution in making the weld shown in **Figure 4**(a), as measured by IR thermography. There is clearly localized heating (the "hot spot") in the region where cracking occurred.

The same test was repeated with Al6111. While much less cracking was observed when welding Al6111, the localized heating behavior was consistent with Al5754 as shown in **Figure 6**.

Therefore, the localized heating is common to the Al alloys used in the experiment, although the cracking tendency is dependent upon the type of Al alloy.

It is well known that failure or cracking of materials results in heat generation as the stored elastic energy and plastic work is released and converted to thermal energy. The occurrence of the hot spot without cracking in Al6111 samples suggests that the localized heating away from the weld region is not caused by the cracking process. Rather, it indicates the existence of sporadic acoustic energy concentration points away from the weld region due to the complicated acoustic wave propagation and reflection behavior in the workpiece. The cracking (and the localized heating) is the result of the highly concentrated acoustic vibration.

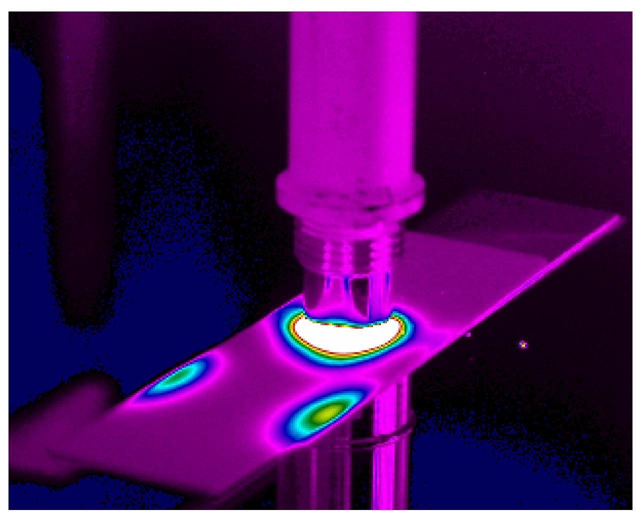

Figure 5. Pseudo color image of temperature distribution during ultrasonic welding of Al5754. Overlap distance: Lo=75 mm; weld position: Lp=35mm.

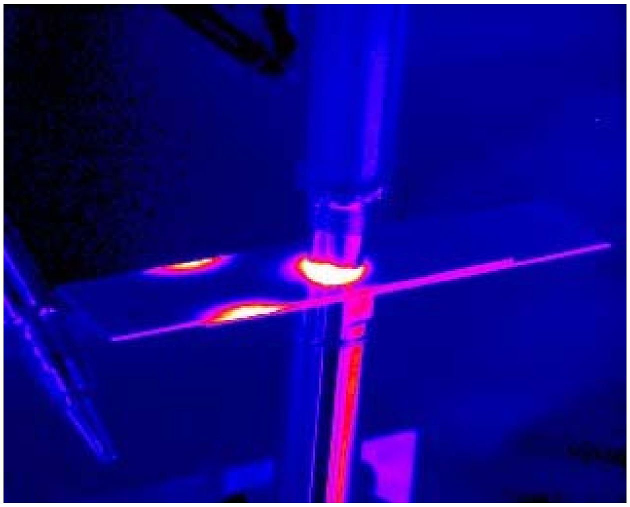

Figure 6. Pseudo color image of temperature distribution during ultrasonic welding of Al6111. Testing condition was identical to that in Figure 5.

To further elucidate the causes of the sporadic acoustic energy concentration spots, the following additional experiments were performed.

In the welding trials shown in **Figure 5**, the two Al sheets overlap each other and the hot spot is located within the overlapping region. Therefore, a potential cause for the localized heating would be the rubbing motion between the two Al workpieces in the hot spot area during ultrasonic welding. To test such hypothesis, welding trials were performed in which the bottom Al workpiece was rotated 90 degrees to form the T-stack up configuration. The result is shown in **Figure 7**. Clearly, the locations of hot spots are similar to the case in **Figure 5** and **Figure 6**. However, they are outside the overlapping region. This confirms that the localized heating and the subsequent cracking are not due to the mechanical interference between the two workpieces, but rather due to the acoustic vibration within the upper workpiece.

Figure 8 shows a very different heating pattern when the stack-up order of the T-configuration was changed. In this case, the vertical piece of the T was on top of the horizontal piece. In other words, the vertical piece was in contact with the vibrating sonotrode, and the horizontal piece was in contact

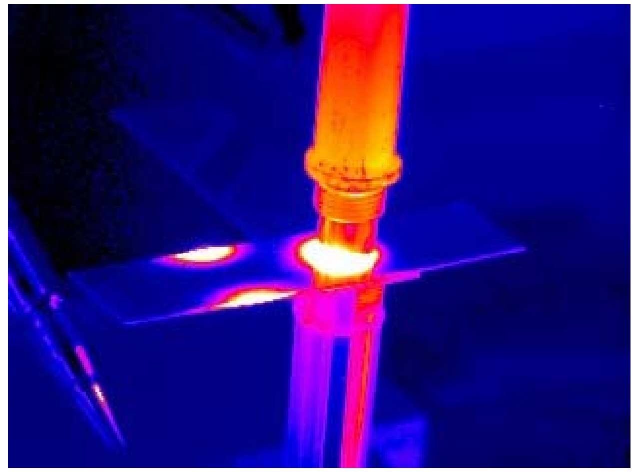

Figure 7. Pseudo color image of temperature distribution of T-stack up weld. Al 5754. The vertical piece sits on the bottom anvil. The horizontal piece is in contact with the upper sonotrode. The unusual localized heating occurs in the horizontal piece.

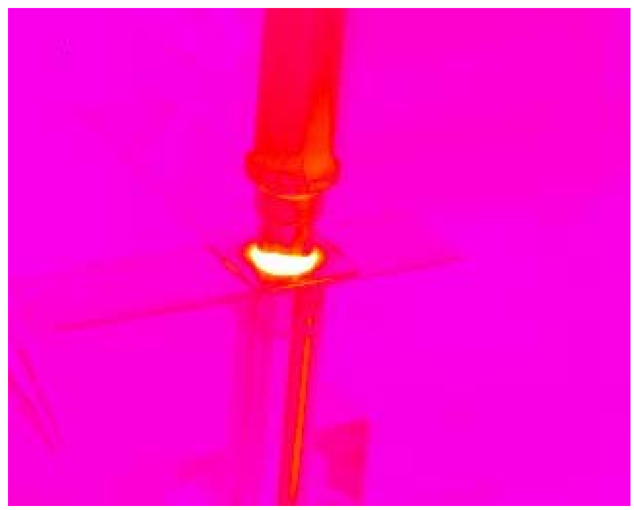

Figure 8. Pseudo color image of temperature distribution of T-stack up weld. Al 5754. The vertical piece is on the top. No unusual heating was observed.

with the stationary anvil on the bottom. The unusual heating pattern was not observed.

In another test, the orientation of both workpieces was rotated 90 degrees such that the vibration direction of the sonotrode was in parallel to the length direction of the workpiece. The unusual heating was not observed, as shown in **Figure 9**.

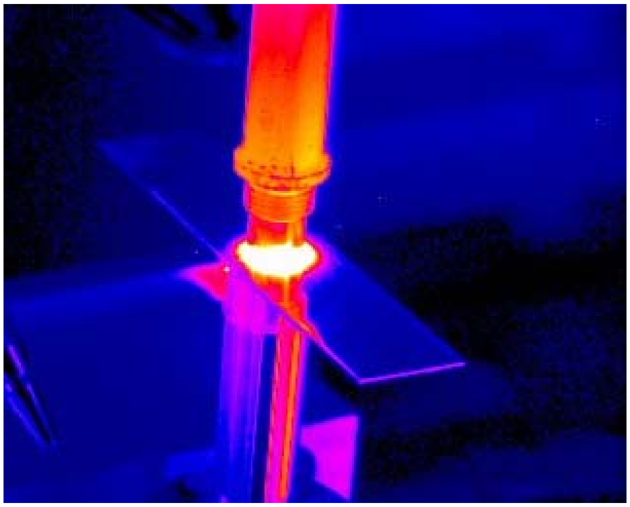

Figure 9. Pseudo color image of temperature distribution when both workpieces are lined to the vibration direction of the sonotrode. Al 5754.

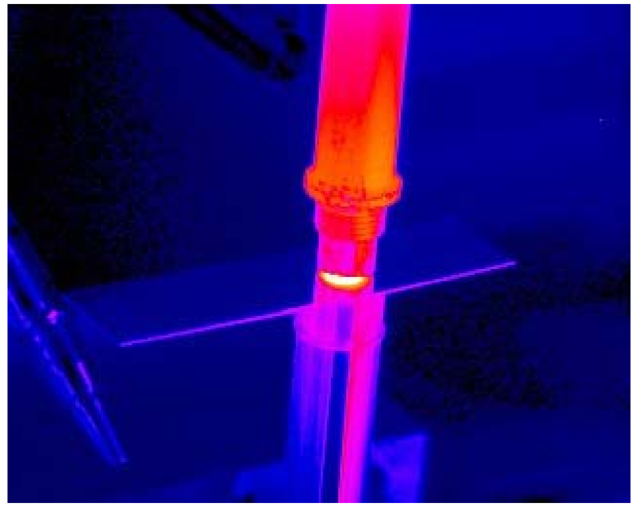

Figure 10. Pseudo color image of temperature distribution when only one Al sheet is used. Al 5754.

Figure 10 shows the case when only one Al piece is used in the test. There was no unusual heating. This suggests that the concentration of the acoustic energy and thereby the observed unforeseen heating/cracking are related to the existence of unbounded interface between the two Al workpieces underneath the sonotrode. This is further supported by the fact that the unusual heating/cracking occurred in the early stage of the bonding process as illustrated in **Figure 11**, when the metallurgical bonding is not formed or relatively weak.

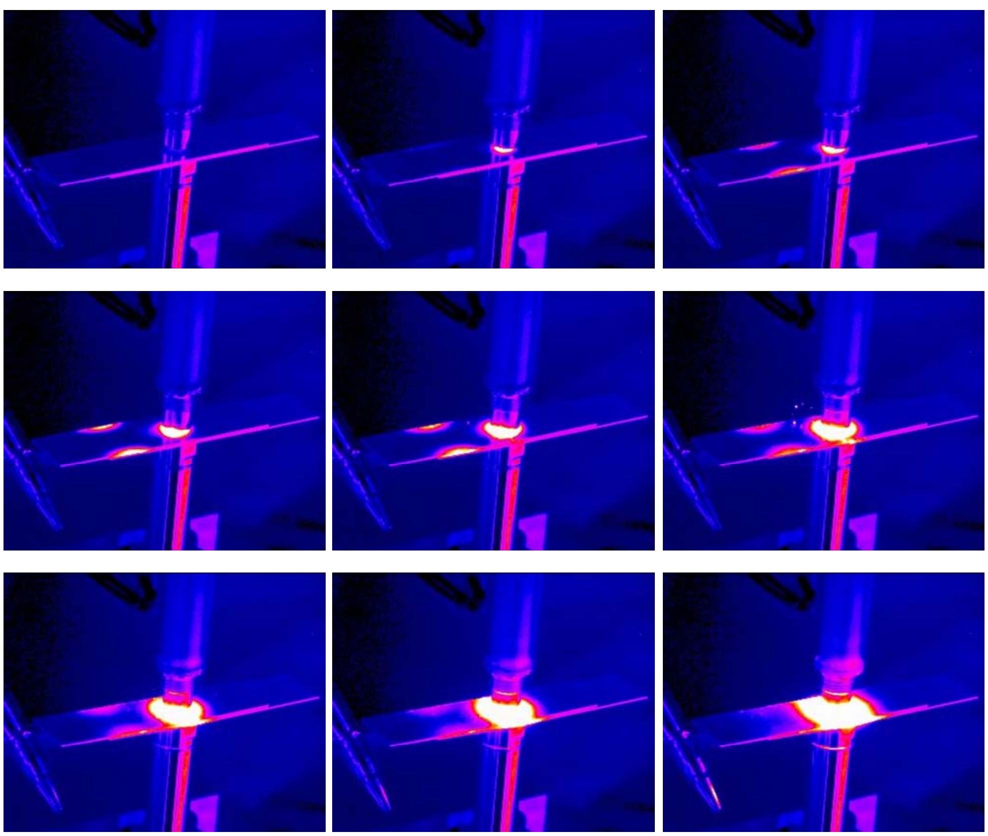

Figure 11. Sequential IR thermography image shots during ultrasonic welding.

Modeling of Acoustic Energy Distribution

Theoretical Treatment of Thin-Plate Vibration Pertaining to Ultrasonic Welding

Assume a thin plate situated in a three-dimensional rectangular coordinate system, (*x, y, z*), with thickness in the *z* direction. The plate is bounded by the planes $z = h$ and $z = -h$ and the thickness of the plate is $H = 2h$ at the start. Let *U, V, W* be the displacements of the plate in *x, y, z* directions respectively. We use the elastic model for high-frequency extensional vibrations of plate by Kane and Mindlin [J. Appl. Mech. 23 (1956) A-277-283]. In this model, it is proposed that the displacements in *x* and y directions are independent of the thickness of plate and the displacement in *z* direction varies linearly along *z* with no displacement at the middle plane of the plate. Hence, the three displacements can be written as

$$\begin{aligned} U(x,y,z,t) &= u(x,y,t) \\ V(x,y,z,t) &= v(x,y,t) \\ W(x,y,z,t) &= \frac{z}{h} w(x,y,t) \end{aligned} \quad (1)$$

where *u, v, w* is the so-called plate-displacements at the mid plane of the plate.

By introducing a constant multiplier to the thickness strain, Kane and Mindlin obtained the following plate-displacement system of equations of motion:

$$\begin{aligned} &(\lambda+2G)u_{xx} + Gu_{yy} + (\lambda+G)v_{xy} + \frac{\pi}{\sqrt{3}H}\lambda w_x + \frac{T_1}{H} = \rho u_{tt} \\ &Gv_{xx} + (\lambda+2G)v_{yy} + (\lambda+G)u_{xy} + \frac{\pi}{\sqrt{3}H}\lambda w_y + \frac{T_2}{H} = \rho v_{tt} \\ &G(w_{xx}+w_{yy}) - \frac{\sqrt{3}\pi}{H}\lambda(u_x+v_y) - \frac{\pi^2}{H^2}(\lambda+2G)w + \frac{3T_3}{H} = \rho w_{tt} \end{aligned} \quad (2)$$

where *λ, G* are Lame's constants, *ρ* is the mass density, $H = 2h$ is the thickness of the plate, T_1, T_2, T_3 are the components of surface traction in *x, y* and *z* directions.

Eq. (2) can be used to study the vibration of the workpiece under the acoustic excitation of a sonotrode during ultrasonic welding. Our model focuses on the distribution of the acoustic energy in the workpiece outside of the region underneath the sonotrode. Hence, the acoustic excitation from the sonotrode is assumed to be a temporal harmonic oscillation surface traction and its amplitude exhibiting exponential decay in the spatial domain from the center of the acoustic excitation. The temporal oscillation represents the vibration applied to a weldment throughout the process. The exponentially decaying spatial distribution of the amplitude represents that the vibration is concentrated in an area between the sonotrode and the anvil. The choice of a continuous surface traction is to avoid difficulties in solving Eq. (2) arising from spatial discontinuities.

In ultrasonic welding, strong friction exists at the interface of the two workpieces. This friction is simplified in the model by a damping term in each equation of motion in Eq. (2). Then the elastic model for ultrasonic welding is

$$\begin{aligned} &(\lambda+2G)u_{xx} + Gu_{yy} + (\lambda+G)v_{xy} + \frac{\pi}{\sqrt{3}H}\lambda w_x + C_1 e^{-\alpha\left[(x-x_s)^2+(y-y_s)^2\right]}\sin\omega t = \rho u_{tt} + \gamma u_t \\ &Gv_{xx} + (\lambda+2G)v_{yy} + (\lambda+G)u_{xy} + \frac{\pi}{\sqrt{3}H}\lambda w_y + C_2 e^{-\alpha\left[(x-x_s)^2+(y-y_s)^2\right]}\sin\omega t = \rho v_{tt} + \gamma v_t \\ &G(w_{xx}+w_{yy}) - \frac{\sqrt{3}\pi}{H}\lambda(u_x+v_y) - \frac{\pi^2}{H^2}(\lambda+2G)w + C_3 e^{-\alpha\left[(x-x_s)^2+(y-y_s)^2\right]}\sin\omega t = \rho w_{tt} + \gamma w_t \end{aligned} \quad (3)$$

where ω is the vibration angular frequency of the force applied to the weldment, (x_s, y_s) is the center of the welding spot on the weldment, C_1, C_2, C_3, α, γ are nonnegative constants. It can be shown that the kinetic energy density of the plate on the *xy*-plane becomes

$$T(x, y, t) = \rho h\left(u_t^2 + v_t^2 + \frac{1}{3}w_t^2\right) \qquad (4)$$

and the potential energy density of the plate on the *xy*-plane becomes

$$V(x, y, t) = h\left\{\lambda\left(u_x + v_y + \frac{\pi}{h\sqrt{12}}w\right)^2 + 2G\left(u_x^2 + v_y^2 + \frac{\pi^2}{12h^2}w^2\right) + G\left[\frac{1}{3}\left(w_x^2 + w_y^2\right) + \left(u_y + v_x\right)^2\right]\right\} \qquad (5)$$

Model Application to UW process

We now consider a rectangular plate. Let the spatial domain of the functions *u, v* and *w* be $[0, A]\times[0, B]$. In UW process, the sides of weldment are free. Hence, at the four sides of the rectangular plate we propose zero normal stresses and zero shear stresses along z-direction. The boundary conditions for Eq. (3) pertaining to the ultrasonic welding experiment of this study are:

$$\begin{aligned} &(\lambda + 2G)u_x + \lambda v_y + \frac{\pi\lambda}{h\sqrt{12}}w = 0 \\ &u_y - v_x = 0 \\ &w_x = 0 \end{aligned} \qquad (6)$$

at the boundaries x = 0 and x = A,

and

$$\begin{aligned} &\lambda u_x + (\lambda + 2G)v_y + \frac{\pi\lambda}{h\sqrt{12}}w = 0 \\ &u_y - v_x = 0 \\ &w_y = 0 \end{aligned} \qquad (7)$$

at the boundaries $y = 0$ and $y = B$. The initial conditions for Eq. (3) in our UW model are

$$u(x, y, 0) = v(x, y, 0) = w(x, y, 0) = u_t(x, y, 0) = v_t(x, y, 0) = w_t(x, y, 0) = 0 \qquad (8)$$

Eqs. (3), (6)-(8) forms a closed mathematical system of initial boundary problem of a system of linear partial differential equations.

For aluminum alloy, the following material constants are used in the model.

$$\lambda = \frac{\sigma E}{(1+\sigma)(1-2\sigma)}\frac{N}{m^2}, \quad G = \frac{E}{2(1+\sigma)}\frac{N}{m^2},$$
$$E = 7.0404172\frac{N}{m^2}, \sigma = 0.34, \rho = 2700\frac{kg}{m^3},$$
$$H = 0.001m, A = 0.1m, B = 0.025m,$$
$$x_s = 0.065m, y_s = 0.0125m$$
$$\omega = 169646.01Hz$$

The above system equations of elastic vibration and associated boundary conditions were solved numerically using the method of lines with central differences in the spatial discretization and variable-stepsize variable-order backward differentiation formulas in the time integration. Examples of the calculated vibration and energy distribution in the workpiece are presented below.

In the examples presented here, the dimensions of the rectangular plate and the location of the acoustic excitation are from the actual welding tests described in the experimental part of this report, to allow for comparison of the modeling results with the IR temperature measurement. Specifically, the plate dimensions were 25-mm wide, 100-mm long, and 1-mm thick. The position of the acoustic excitation, denoted Lp in **Figure 3**, was 35 mm. In the model and simulation coordinates the excitation is x = 65 mm. Also, the damping coefficient representing the friction action of the sonotrode was assumed to be 20 times of the mass density of the material (γ=20ρ).

Figure 12 shows the out-of-plane displacement of the plate (z-displacement) at six different moments during a cycle of elastic wave propagation, as calculated by the model. The direction of the driving excitation from the sonotrode is in the width direction of the plate (y-axis in the figure). This corresponds to the testing case shown in **Figure 5** and **Figure 6**. The calculated maximum vibration amplitude is concentrated at a particular location in the plate – near the edge of the plate and away from the excitation location. **Figure 13** shows the corresponding distribution of the sum of the kinetic and the potential energy density in the plate, averaged over the period of vibration. It is evident that the energy distribution in the plate is not uniform but rather sporadic. The predicted maximum energy locations are near the edge of the plate, which is consistent with the IR thermography experimental observations.

Figure 14 and **Figure 15** show a different case where the driving vibration direction is in the length direction of the plate (x-axis); all other conditions are identical to the previous modeling case. This corresponds to the testing case showing in **Figure 9**. The time-averaged energy density in the plate is completely different from the previous modeling case. Not only the location of the maximum energy density is changed, the overall energy density in the plate is also considerably lower. Again, this is consistent with the experimental observations.

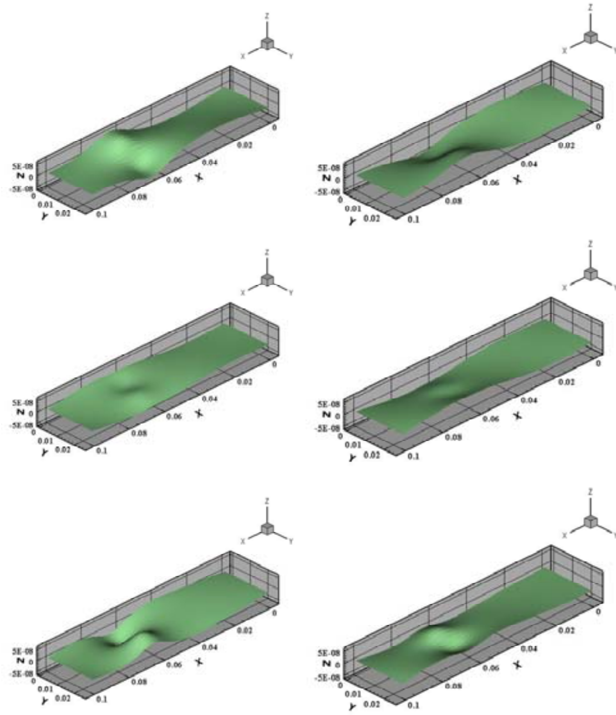

Figure 12. Vibration of the plate in the thickness direction (z-axis) during UW when the driving vibration is in the direction of y-axis. Acoustic excitation locates at x=0.065m and y=0.0125m.

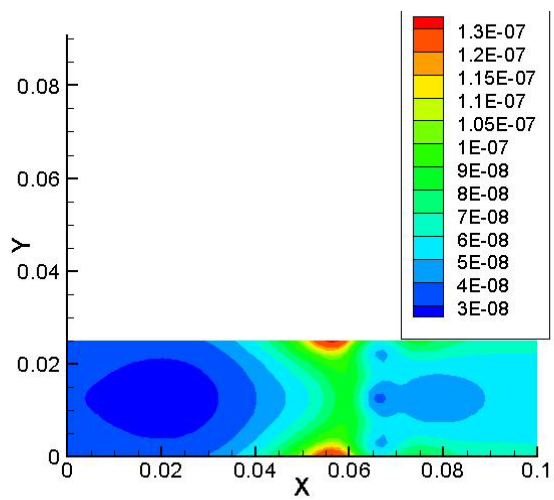

Figure 13. Distribution of the time-averaged sum of the kinetic and potential energy density in the plate during UW when the driving vibration is in the direction of y-axis.

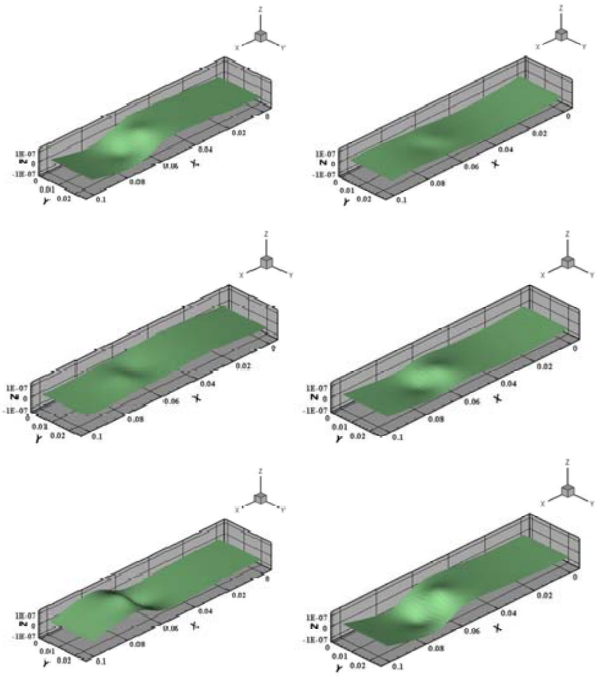

Figure 14. Vibration of the plate in the thickness direction (z-axis) during UW when the driving vibration is in the direction of x-axis. Acoustic excitation locates at x=0.065m and y=0.0125m.

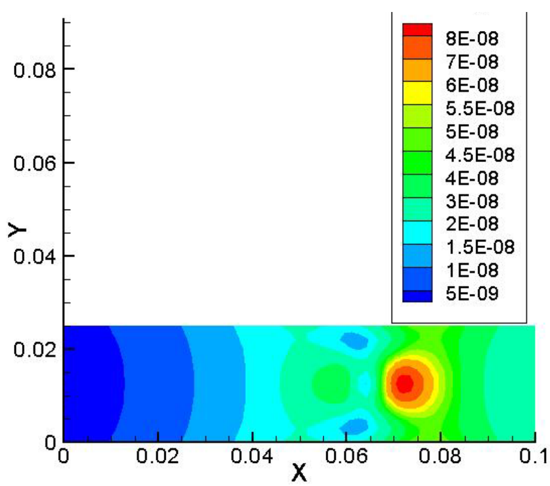

Figure 15. Distribution of the time-averaged sum of the kinetic and potential energy density in the plate during UW when the driving vibration is in the direction of x-axis.

Further studies are planned in FY06 to establish the validation of the model on a more rigorous base.

Summary

In FY05, high-speed IR thermography and computational analysis based on the elastic high-frequency extensional vibration model made it possible to investigate the localized acoustic energy distribution and heat generation during the ultrasonic welding process. The causes for the formation of unforeseen hot spot and cracking have been identified, and factors contributing to the acoustic energy generation and dissipation in the welded samples have been determined.

The research in FY06 will continue on understanding of the fundamentals of the process, as well as the factors controlling them, for the eventual optimization and intelligent control of the UW process for application in the automotive industry. We will continue on the IR thermography study of the ultrasonic joining process, including the multi-weld interactions, the effects of the thickness and coupon geometry. We will also continue on developing the computational models for the UW process to interrogate the fundamental factors contributing to the formation of the metallurgical bonding. Finally, we will explore the use of ultrasonic energy for low-temperature metal compaction and consolidation.

M. Effects of Highway Ice-Clearing Treatments on Corrosion of Heavy Vehicle Materials and Components

Principal Investigator: Elizabeth V. Stephens
Pacific Northwest National Laboratory
P.O. Box 999, Richland, WA 99352-0999
(509) 375-6836; fax: (509) 375-4448; e-mail: elizabeth.stephens@pnl.gov

Principal Investigator: Dane F. Wilson
Oak Ridge National Laboratory
P.O. Box 2009, Oak Ridge, TN 37831-8048
(865) 576-4810; fax: (509) 375-6605; e-mail: wilsondf@ornl.gov

Chief Scientist: James J. Eberhardt
(202) 586-9837; fax: (202) 587-2476; e-mail: James.Eberhardt@ee.doe.gov
Field Technical Manager: Philip S. Sklad
(865) 574-5069; fax:(865) 576-4963; e-mail:skladps@ornl.gov

Participants:
Stan Pitman, Karl Mattlin, Mike Dahl, and Clyde Chamberlin, Pacific Northwest National Laboratory
Claire Luttrell, Peter Blau, and Ed Kenik, Oak Ridge National Laboratory

---

Contractors: Pacific Northwest National Laboratory, Oak Ridge National Laboratory
Contract No.: DE-AC06-76RL01830, DE-AC05-00OR22725

Objective

- Evaluate the corrosion that may be associated with the various ice-clearing chemical systems that are in use by the various states and regions for snow and ice control.
- Develop a more fundamental understanding of the interaction of these chemicals with representative heavy vehicle materials and structures.
- Develop a unified modeling procedure to represent "rust jacking" (displacement of brake friction materials) caused by stresses induced by corrosion products at the interface of the brake shoe and the friction liner.

Approach

- Evaluate heavy truck corrosion damage to identify materials, components, and safety-related systems affected by anti-icing/deicing treatments.
- Identify and characterize $MgCl_2$ solutions and corrosion-inhibiting additives.
- Perform accelerated corrosion testing and corrosion characterization of heavy vehicle materials.
- Evaluate brake shoe failures to identify aggressive corrosion species and extent of corrosion.
- Determine the thermo-elastic and mechanical properties of the lining material, brake shoe table, and corrosion products.
- Incorporate the mechanical properties of the lining material, brake shoe, and corrosion products into computer-aided engineering (CAE) codes to predict the stresses associated with swelling of oxides on the shoe/lining interface.
- Identify more desirable ice-clearing chemical formulations and application methods.

- Generate "best practice" recommendations for reduced vehicle corrosion and improved safety.

Accomplishments

- Conducted in-service winter field evaluations in collaboration with Montana Department of Transportation (Phase 2 – Winter Season 2004/05).
- Characterized the effects of $MgCl_2$ anti-icing/deicing solutions and other ice-clearing chemical products on heavy vehicle materials (Phase 1).
- Prepared specimens with "lip" for demonstrating moisture retention time effects and added specimens to the field evaluation.
- Began accelerated corrosion testing of heavy vehicle materials.
- Conducted forensic analysis of failed brake shoes.
- Determined the remainder of the thermal and mechanical properties of the brakes.
- Evaluated the stresses that arise from the growth of corrosion products between the pads and the brake table
- Completed model of brake "rust jacking".

Future Direction

- Complete analysis of corrosion field evaluations (Phase 2).
- Complete assessment of Boeing's anti-icing technologies for heavy vehicles and trailers for the elimination of ice and ice-clearing chemical accumulation.

Introduction

In recent years, many states have introduced anti-ice liquid treatments, particularly $MgCl_2$ road treatments, to prevent the bonding of ice and snow before the onset of a winter storm. Spraying the treatment on roads before the onset of a storm potentially exposes vehicles to concentrated solutions for longer periods of time because the solution is not immediately diluted by snow or water. Increased corrosion damage to heavy truck components has been reported by truck fleets and owner/operators. Vehicle safety concerns have arisen, including accelerated corrosion damage in heavy truck brake systems, also known as "rust jacking" (Figure 1).

Although there is a strongly voiced opinion within the trucking community that accelerated damage is being caused by $MgCl_2$ road treatments, there is a lack of significant data to quantify the role of various $MgCl_2$ treatments on heavy truck component corrosion.

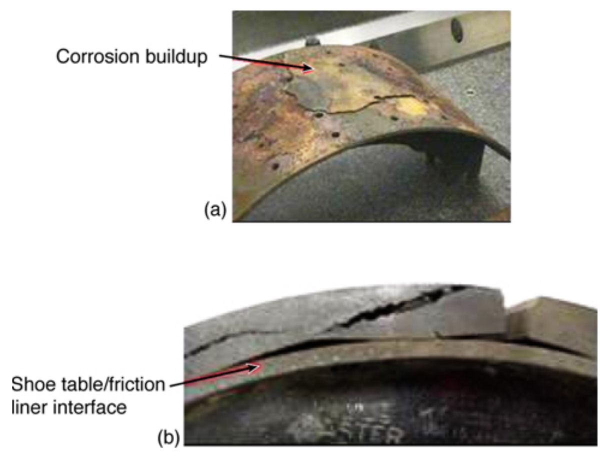

Figure 1. An illustration of rust jacking: (a) corrosion product buildup on the brake shoe table displaces the brake lining; (b) shoe table/friction liner interface.

In May 2003, Pacific Northwest National Laboratory and Oak Ridge National Laboratory began collaboration on a 2-year research effort focused on developing a more fundamental understanding of the interaction of these chemicals with representative heavy vehicle materials and structures.

Corrosion Field Evaluation

The corrosion field evaluation, in collaboration with the Montana Department of Transportation (MDT), continued for the 2004/05 winter season. The remaining corrosion coupon panels were removed in May 2005. Chrome-plated steel, 1008 steel with a lip, and stainless steel coupons have been added to the evaluation. These coupons will also be evaluated and compared with those removed at the end of the 2003/2004 winter season. In addition, a new exposure region was added to the evaluation to include corrosion-inhibited sodium chloride as the sole chemical used. Again, corrosion coupon racks were placed on select MDT liquid-dispensing and abrasive trucks that were exposed to different ice-clearing chemicals and winter conditions in various regions throughout western Montana (Figure 2).

Figure 2. An illustration of the seven urban regions in Montana.

The field evaluation continued in Utah for the 2004/2005 winter season. To include NaCl exposure as part of the test matrix, the Utah Department of Transportation allowed MDT to place four corrosion coupon racks on its liquid dispensing and abrasive trucks (also designating a region as the sole chemical used). Coupon racks also remained on one commercial hauler traveling the United States to include a national, mixed exposure to ice-clearing chemicals.

Winter Season 2003/2004 Phase 1

Last season, aluminum alloy 5182-O, cast aluminum A356, and 1008 steel corrosion coupons were exposed to approximately 4-5 months of ice-clearing chemicals. The coupons were exposed to the following ice-clearing chemical combinations:

- Corrosion- inhibited $MgCl_2$ only
- Corrosion- inhibited $MgCl_2$ and NaCl solid
- Corrosion- inhibited CaCl and NaCl solid
- NaCl solid or brine only
- Mixed exposure

The coupons were evaluated to determine the corrosion observed and a general corrosion rate. To date, no localized corrosion or pitting was observed on the 1008 steel and A356 cast aluminum specimens. Only general uniform corrosion was observed.

However, inter-granular corrosion was observed on all 5182-O specimens, regardless of exposure type. Mg_2Al_3 precipitates form a continuous path along the grain boundaries. Since, Mg_2Al_3 is a highly anodic second phase that is present, it corrodes preferentially and a selective attack of the grain boundary is observed. Figure 3 is representative of the corrosion observed on the aluminum specimens.

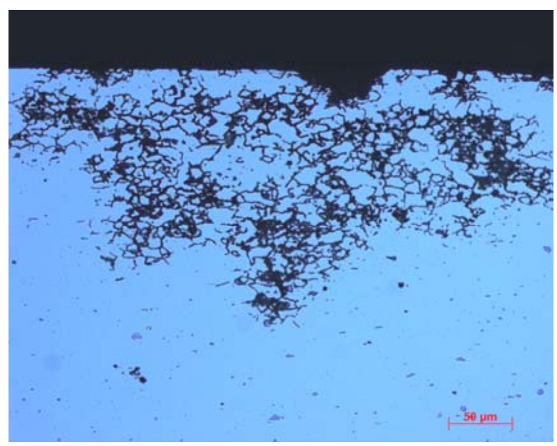

Figure 3. Photo representative of the inter-granular corrosion attack observed on 5182-O aluminum specimens from the field.

Corrosion rates were determined for each coupon specimen to evaluate the differences in corrosion behavior when exposed to different ice-clearing chemicals. The corrosion rate in mils penetration per year was determined by the following equation:

$$MPY = \frac{534W}{DAT}$$

where *W* is the weight loss in milligrams, *D* is the density in grams per cubic centimeter, *A* is the exposed area in square inches, and *T* is the exposed time in hours.

Figure 4a-c illustrates the corrosion rate results for each coupon material. Slightly varying trends were observed for each material alloy in regards to the region and chemicals it was exposed to. For instance, lower corrosion rates were observed for both 1008 steel and A356 cast Al specimens when exposed to a $MgCl_2$ in comparison to NaCl. However, lower corrosion rates were observed in 5182-O specimens that were exposed to NaCl in comparison to $MgCl_2$.

One trend that is dominant across all the alloys evaluated is larger corrosion rates typically observed in regions where both $MgCl_2$ and NaCl are being utilized. Further investigation of the quantities of materials used in each region and differences in exposure time and exposure truck mileage is needed to better understand the trends observed. In addition, further investigation of the effect of chloride content and/or cations present is needed. Correlation between the trends observed and previous electrochemical tests conducted that studied the anion and cation effect are needed.

Quasi-static tensile tests were conducted on several of the corrosion coupons received from Phase 1 to quantify the effect of the corrosion behavior observed on the structural integrity of the material. One inch by four inch strips were prepared from the corrosion coupons. Moderately corroded specimens were compared to severely corroded specimens (determined by corrosion rate). A non-exposed specimen was used as a baseline. In general, a decrease in strength was observed in corroded specimens ranging from approximately 3%-12% depending on corrosion severity and alloy type. Figure 5 illustrates the static results observed for 5182-O aluminum specimens. Further tensile tests are currently being conducted on all coupons from each varying exposure type, and region, to further assess the preliminary results.

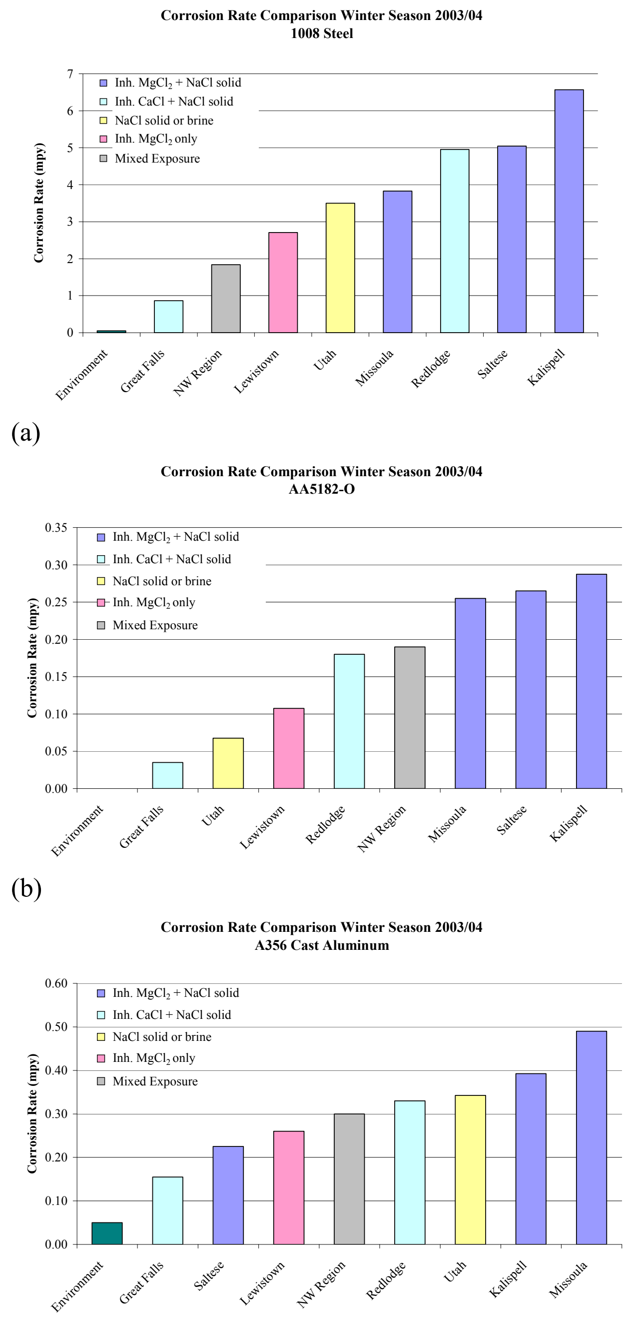

Figure 4. The corrosion rate results to date for the corrosion coupons removed from each region and varying exposure type. (a) 1008 steel specimen results. (b) 5182-O specimen results. (c) A356 cast Al specimen results.

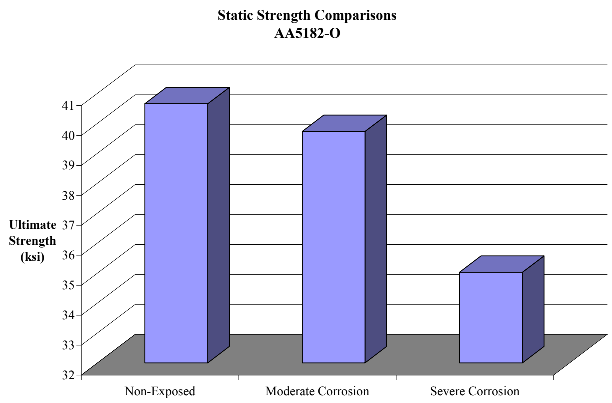

Figure 5. Illustration of the static test results for corroded 5182-O specimens from the field.

Accelerated Corrosion Laboratory Tests

Alternate immersion tests and SAE J2334 cyclic tests are currently being conducted. Figure 6 illustrates the alternate immersion set up and specimen design. Crevice washers were also utilized to study the effects of crevice corrosion.

The corrosion behavior of the specimens from each test will be correlated with the corrosion coupons from the field.

The alternate immersion tests are being conducted at 50ºC and 90% relative humidity, and at 0ºC, no humidity. The cyclic tests involve a humid stage at 50ºC and 100% humidity, a 15 minute salt application, and a dry stage at 50ºC. Four different deicer exposures are being conducted and seven alloys are being investigated. They include the following:

- 1008 steel,
- 304 stainless steel
- Chrome plated steel (cyclic tests only)
- 5182-O aluminum
- 5052-H32 aluminum
- 6061-T6 aluminum
- A356 cast aluminum

The alternate immersion tests at 50ºC and 90% humidity have been completed. Evaluation of the specimens is ongoing. General uniform corrosion has been observed in the 1008 specimens. Localized pitting and possible intergranular corrosion has been

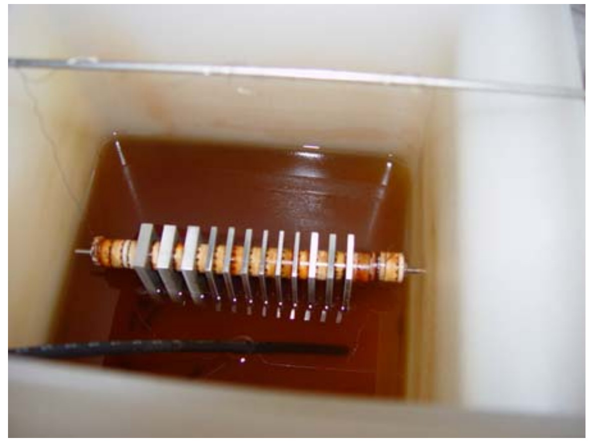

(a)

(b)

Figure 6. (a) The alternate immersion test set up and (b) specimen design.

observed in the A356 aluminum castings, and possible pitting has been observed in the 5182-O specimens. Further evaluation of all specimens is needed.

Modeling of Brake Lining Failure

A model of the brake lining material fracture phenomenon, caused by the forces produced by the growth of corrosion products at the shoe table/lining interface, has been developed. The mechanical properties of the lining material and oxides determined experimentally have been incorporated into analysis codes to predict the stresses associated with swelling of oxides on the shoe/lining interface.

Flexure Tests

Flexure tests have been completed on the brake pad material at room temperature, 100, 200, and 400°C. The results of these tests have been used to determine the modulus of elasticity for the finite element analyses of the brake lining model.

Modeling Efforts

Finite-element techniques have been used to predict stresses on the back side of the lining associated with swelling of oxides in the shoe/lining interface. Lining and oxide property data determined experimentally have been used as inputs for the model. Initially, two-dimensional (2D) analyses were used to determine the effects of oxide particles of different sizes inserted between the brake shoe and lining. The particle was assumed to be in the shape of half an ellipse. The major diameter of the oxide particles was assumed to be 3.2 mm. The minor radius, or height, of the half-ellipse was varied.

The first analysis assumed the assembly was at room temperature. The stresses due to a particle with a height of 0.4 mm, inserted in the center of the pad, were calculated. The results of this analysis are shown in Figure 7.

These stresses exceeded the strength of the pad material. The location of this particle was changed to compare the stresses with the oxide particle at another location. Since the lining is stiffer where the rivets are closer together, the particle was moved to a location where the rivets are closer together. The stresses due to the same size particle are higher for the second case. Figure 8 shows the results of this analysis.

Other analyses were performed assuming particle heights of 0.2 mm and 0.1 mm, located between the closely spaced rivets. The analyses were done at room temperature and assumed that the entire assembly was at 100ºC. The results were compared with the strength of the lining at the given temperature. It was determined that a particle with a height as small as 0.1 mm could cause the lining to crack. An additional calculation was conducted to more accurately determine the temperature distribution in the brake assembly. The results of this analysis show that although the temperature on the surface of the lining may be high, the low thermal conductivity of the lining material keeps the shoe/lining interface temperature low. With this temperature profile, an additional stress calculation was done with the 0.1-mm-high particle. The results of all these analyses are shown in Table 1.

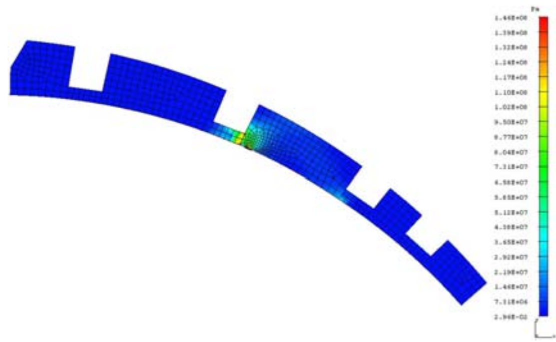

Figure 7. Stresses in the brake lining with the oxide particle located in the middle of the lining.

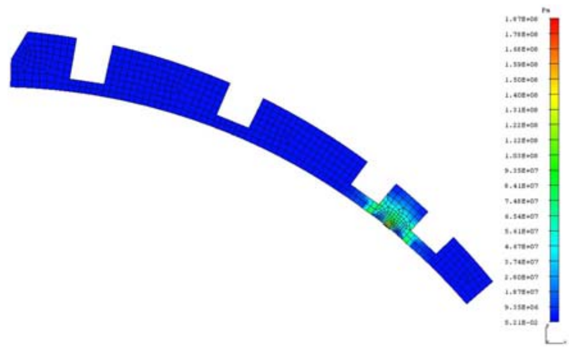

Figure 8. Stresses in the brake lining with the oxide particle located where rivets are close together.

Table 1. Results of 2D stress analyses.

Height (mm)	Temp (ºC)	Pad peak stress (MPa)	Strength (MPa)
0.4	RT	187	40.39
0.4	100	105	17.82
0.2	RT	93	40.39
0.2	100	52	17.82
0.1	RT	47	40.39
0.1	100	26	17.82
0.1	Temp profile	46	40.39

After examining the effect of oxide particle size and location with a 2D model, a 3D model was developed to include the actual assembly configuration. A 2D model assumes that the rivets fix the lining to the shoe in a line, rather than just at the rivet location. This makes the structure stiffer than it actually is. An analysis was done with an oxide particle with a height of 0.1 mm inserted between the rivets, as in the 2D analysis. The results of this case show that the stresses are actually less than were calculated in the 2D analysis. The results of this case are shown in Figure 9.

The finite element analyses of the brake lining/shoe assembly show that a particle with a height of 0.1 mm will exert stresses on the lining that are close to the strength of the material. A larger particle would cause stresses that exceed the material strength. The analyses show that the worst location for the oxide particles is in the stiff regions of the lining around the rivets. Other areas of the shoe can have larger oxide layers. Although the analyses show that the stiffer regions are more likely to fail, this does not take into account all the factors. The other areas, with fewer rivets, may allow more corrosive chemicals between the lining and shoe and therefore may have more corrosion. This could cause failure in those areas first.

Additional analyses were performed as a function of the major diameter or width of the oxide particle, the shape of the particle (elliptical to flat), the location of the particle, and the distance the particle covers into the brake shoe.

The width of the elliptical shaped oxide particle was varied from 3.2 mm to 14 mm. The 14 mm particle covered most of the area between the rivets as shown in Figure 10.

The results of these analyses showed that for any shape of the particle between the closely spaced rivets, the height of the oxide particle is the primary contributor to the stresses in the brake pad. These results are presented in the first four rows of Table 2. In row five, the results for the flat oxide particle (located as shown in Figure 10) with the height reduced to 0.08 mm is presented. The oxide particle for this case has a width of 14 mm and the length of 25.4 mm. Around the rivet holes, 0.08 mm is the limiting height before the strength of the pad is exceeded.

Analyses were performed for particles located away from the rivet holes. An oxide particle with a height of 0.1 mm, a width of 14 mm and a length of 25.4 mm was placed in the middle of the brake pad, as shown in Figure 11.

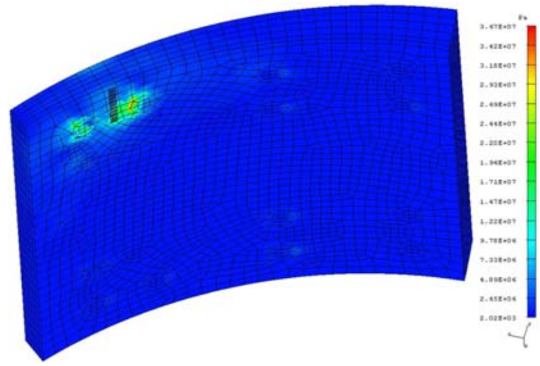

Figure 9. Brake lining stresses at interface for 3D analysis.

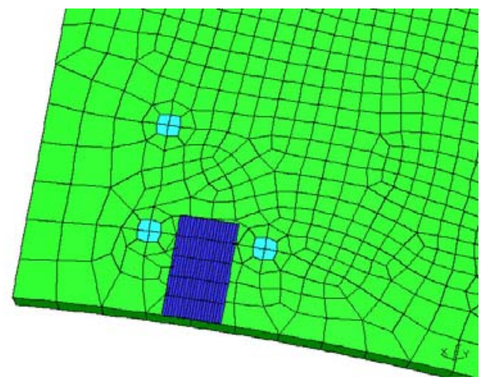

Figure 10. Model illustrating three rivets and a long wide particle.

Table 2. Predicted peak stresses for various particles.

Height (mm)	Width (mm)	Length (mm)	Shape	Peak Pad Stress (MPa)
0.10	3.2	25.4	Elliptical	45.1
0.10	8	25.4	Elliptical	45.3
0.10	14	25.4	Elliptical	47.6
0.10	14	25.4	Flat	47.7
0.08	14	25.4	Flat	39.2
0.10	14	25.4	Flat	5.46
0.20	14	25.4	Flat	34.9
0.10	14	62	Flat	43.7

The results for this case showed that the flexibility of the pad away from the holes allows an oxide particle located away from the hole to have a larger height than around the rivets. The results, presented in rows 6 and 7 of Table 2, show that the peak stresses due to a particle 0.2 mm high, away from the rivets, are below the strength of the pads. As the

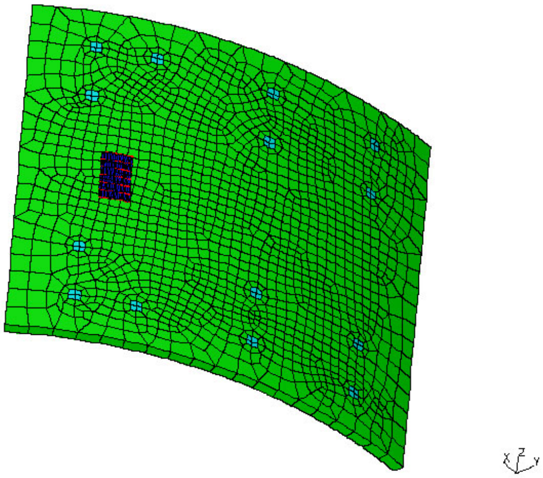

Figure 11. Model illustrating small oxide particle located between two rivets.

length of the oxide particle is extended toward the rivets, as shown in Figure 12, the stresses in the pads exceed the strength of the material. The peak stress in this case is presented in the last row of Table 2.

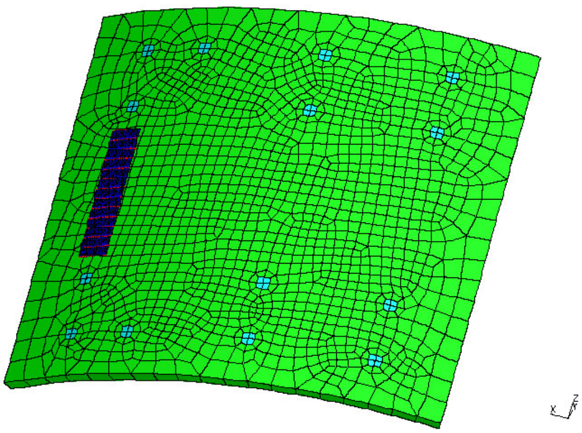

Figure 12. Model illustrating longer oxide particle located between two rivets.

Conclusions

- Intergranular corrosion occurred in all 5182-O Al coupons from the field regardless of exposure type.
- A significant corrosion effect being observed from field coupons exposed to both $MgCl_2$ and NaCl.
- For coupons that were severely corroded from the field, a ~10-12% reduction in strength was observed for 5182-O Al and 1008 steel specimens, ~6% reduction for A356 cast Al specimens.
- Different corrosion behaviors are observed from field coupons in comparison to lab tested coupons for 5182-O Al and A356 cast Al specimens to date.
- Determined that 0.10 mm oxide creates force larger than brake pad strength.
- Determined no difference in the layered corrosion products of brake tables exposed during operations to de-icing compounds with/or without $MgCl_2$.
- Demonstrated that a small amount of corrosion leads to large stresses in the brake lining.

Presentations

During this reporting period, three presentations were made to the following organizations:

- Montana Dept. of Transportation – December 6, 2004.
- Corrosion Forum, Western Transportation Institute, Montana State University- December 7, 2004.
- 21st Century Truck Partnership Project Review Meeting, Oak Ridge, TN - September 14, 2005.

5. LIGHTWEIGHT VEHICLE STRUCTURES

A. Lightweight Trailer—Liburndas Project

Team Leader: Ben Ubamadu
Heil Trailer International
1125 Congress Parkway, Athens, TN 37303-0160
(423) 745-5830; fax:(423) 745-1943; e-mail:bubamadu@heiltrailer.com

Principal Investigator: Kevin Tumlin
Heil Trailer International
1125 Congress Parkway, Athens, TN 37303-0160
(423) 745-5830; fax:(423) 745-1943; e-mail:ktumlin@heiltrailer.com

Co-Team Leader/Marketing Liaison: Bill Harris
Heil Trailer International
5741 Cornelison Rd, 6400 Bldg A, Chattanooga, TN 37411
(423) 855-3492; fax: (423) 855-3459; e-mail: bharris@heiltrailer.com

Chief Scientist: James J. Eberhardt
(202) 586-9837; fax: (202) 587-2476; e-mail: James.Eberhardt@ee.doe.gov
Field Technical Manager: Philip S. Sklad
(865) 574-5069; fax:(865) 576-4963; e-mail:skladps@ornl.gov

Senior Researcher: Michael Starbuck, Ph.D.
(865) 576-3633, fax (865) 574-8257; e-mail: starbuckjm@ornl.gov

---

Contractor: Heil Trailer International
Contract No.: WA-2003-054-ORO-786

Objective

- Reduce the net weight of an aluminum tank semi-trailer by 20% using a cylindrical design, assimilating available composite technology for functional components and remain within current (DOT constraints).

Approach

- Develop a new frameless vessel design incorporating a new cross-section, flangeless heads, and internal rings.
- Optimize design through finite element analysis (FEA) and field testing.
- Explore existing composite accessories.
- Conduct a focus group and a marketing study, including a campaign for the new design.
- Complete a manufacturing study, including a labor rate analysis.
- Manufacture and test prototype.
- Commercialization of the product.

Accomplishments

- Cylindrical vessel design complete.
- FEA and analysis of vessel design complete.
- Samples sent to ORNL for Friction Stir Welding evaluation.
- Flangeless, dishless head design and test complete.
- Marketing has defined acceptable loading head envelope parameters
- based on real world operational requirements.
- Vessel Details complete.

Future Direction

- Complete Prototype #1.
- Prototype #1 in-house testing results.
- Composite material study findings.
- Test track results (outside contract).
- Partner identification. Manufacturing cost study (includes tooling study).
- Complete Prototype #2.
- Prototype #2 field test results with partner.
- Complete Marketing campaign.
- Market Introduction.

Introduction

The Liburndas Project is Heil Trailer International's effort to design and build an aluminum semi-trailer for petroleum products that is lighter, stronger, and safer than any before it. By using a cylindrical cross section and assimilating composites into select trailer components, Heil's Program Engineering Group proposes to reduce the aluminum tank semi-trailer's net weight by 20 %. (See Figure 1).

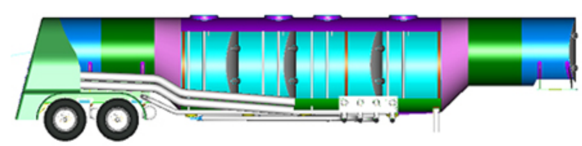

Figure 1. Liburndas trailer.

Relevance to 21 CT Goals

Investigating a new aluminum alloy for the cylindrical vessel will ultimately help reduce the mass of the main structure. In areas of the barrel where components are added for functional purposes alone, Heil will utilize a new composite material to reduce parasitic energy loss. The successful results of this project will allow transportation resources to safely deliver 2000 – 2500 lbs. more payload per trip, ultimately reducing the daily average amount of miles required to deliver product by about 1%. On a national level (current population of petroleum tank trailers is approximately 50,000 units), this could equate to over 200,000 miles per year in fuel savings or 30,000 gallons of fuel per year.

Investigating a new aluminum alloy for weight reduction in areas not regulated by the U.S. Department of Transportation (DOT) is an objective of the project as well. Areas such as the frame rails for the suspension and fifth-wheel plate are valid candidates. Although some weight savings is possible, this is secondary to the contributions the new cylindrical design and composite accessories will make to Heil's overall weight reduction goals.

Accessories made from composites are critical to meeting weight reduction goals and will ultimately reduce the mass of the trailer, reduce the aero-dynamic signature and improve corrosion resistance. This project's purpose is not to create or test a new composite for these areas. Existing composites will be explored that have been proven successful in the market. Areas that are likely candidates for composites are fenders, cabinets, hose holders, ladders, and suspension support structures.

Although a successful vessel design and notable composite integration will result in reaching weight reduction goals, it is paramount to the project's success that the market accepts the new design. Because of the competitive nature of the market, data will be collected covertly, without divulging the new trailer's design or benefit. Therefore, the marketing study initially will determine acceptable envelopes for piping and discharge outlets, as well as conduct a preliminary commercial viability study based on the design's limits and/or restraints. A marketing campaign to bolster product acceptance will take place near the end of the project. The initial marketing study began during Phase 1 of the project and should be completed before the first prototype is built. The marketing campaign will take place during Phase 3 (after the successful field testing of the second prototype) and should result in orders for production models.

Vessel Design

Cross Section

An important part of Heil's new design concept for its petroleum trailer is the cross section of the vessel. In today's petroleum trailers, the most common cross section used is an elliptical shape, used to lower the overall height and center of gravity of the trailer. Since petroleum trailers are not unloaded or loaded with pressure, the elliptical shape works well.

When the structure of a petroleum trailer's vessel is studied, it is simply analyzed as a supported beam with reactions at the suspension and kingpin plate. This condition places the bottom of the trailer vessel in tension and the top in compression. The advantage of a round cross section under these loads is that the radius of the top is tighter or smaller and therefore more resistant to buckling under the compression loads. This allows the shell thickness of the vessel to be thinned, compared with an elliptical cross section, and thus saves weight and material.

Even though petroleum trailers are not pressurized, they do occasionally see some low vacuum or pressure differentials during loading and unloading. Today's trailers are equipped with vents to prevent damage to the vessel if this condition becomes excessive. In the event of a vent failure, a round vessel is more likely to survive a pressure or vacuum overload, whereas an elliptical vessel will tend to fail.

A round vessel is therefore stronger, lighter, safer, and more stable than an elliptical vessel for an equivalent cross sectional area. The only advantage of an elliptical trailer is its overall lower height and center of gravity. Designing a round vessel with a drop center can offset this advantage (see Figure 2).

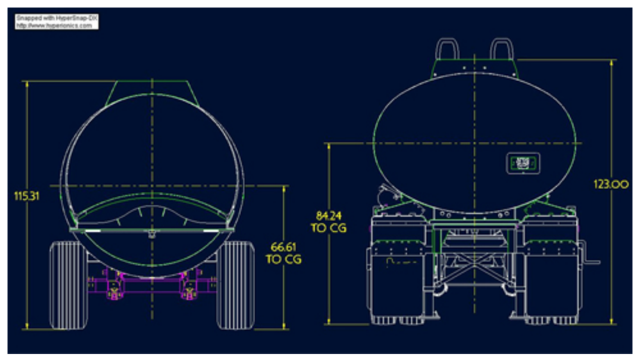

Figure 2. Height and center of gravity comparison.

Drop Center Design

Dropping the center of the vessel in relation to the front and rear not only lowers the center of gravity but also causes the lateral center of mass to stay near the longitudinal center of the trailer.

Federal weight laws call for manufacturers to design trailers with equal loads on the tractor's drive axles and the trailer's suspension. By designing a lower front *and* rear end section of the vessel, we can engineer the trailer so that the mass is equally distributed over the rear of the trailer and the tractor's rear axles.

Elimination of Surge Heads

Petroleum tank trailers are designed to DOT 406 specifications as found in the Code of Federal

Regulations Title 49. Section 178.345-7 of this code discusses circumferential reinforcements in trailers and mandates that the maximum unreinforced portion of the vessel's shell not exceed 60 in. Traditionally, this has been accomplished in petroleum trailers through the use of surge heads or baffles. These surge baffles are the same heads that separate the trailer's compartments, but they have holes formed in them to allow product to flow through them. These surge baffles help with the surge of the product during acceleration and deceleration and serve as the circumferential reinforcements.

Replacing these surge baffles with an adequately designed internal ring can achieve a considerable weight savings. However, rings will not help with product surge, and drivers will have to be trained to handle the "feel" of the tank in certain road conditions. The market's opinion (business owners and drivers) on internal rings and their advantages and disadvantages was one of the topics for the focus group and marketing study.

Liquid trailers without surge baffles are not uncommon in the chemical and food industry, where the cleanability of the inside of the trailer is important. Drivers in these industries have learned to drive safely without baffles; therefore, it is anticipated that the weight benefits will outweigh the surge issue. It should also be noted that there is no product surge when a trailer is completely full or empty.

Flangeless, Dishless Heads

A new concept with regard to the vessel design is being applied to the Liburndas Project. This is a redesign of the compartment heads that separate different commodities in a petroleum trailer. These heads are typically dished and flanged bulkheads that are connected to the shell via a single fillet weld. The Liburndas vessel will use a flangeless, dishless head, which will be connected to the shell via two fillet welds. A Pro-E model of the head is depicted in Figure 3.

Figure 3. Flangeless head concept.

The Liburndas vessel is a perfect application for the flangeless head—it is lighter, the welds are stronger, the strength is comparable, and the manufacturability is more precise than for the current style head. The flangeless head is much easier to manufacture and should offset part of the cost of the composites. One of the goals of marketing is to ensure that the Program Engineering group's new design—lighter, stronger, and more stable—does not cost more than the market will bear for those benefits. This offset strategy should keep the price of the new design within acceptable limits for the market.

Heil has developed new forming techniques for this new head with the Alcoa Technical Center and has already conducted preliminary testing of a "simulated" prototype head at its Athens, Tennessee, R&D facility. Initial testing was promising, and advanced prototypes are planned for continued testing.

Framing

The final design and FEA of the new frame has been successfully completed. It eliminated some framing requirements (and weight) for both the new and vessel mounting structure compared with current framing designs. The Liburndas new frame design can be seen in Figure 4 below.

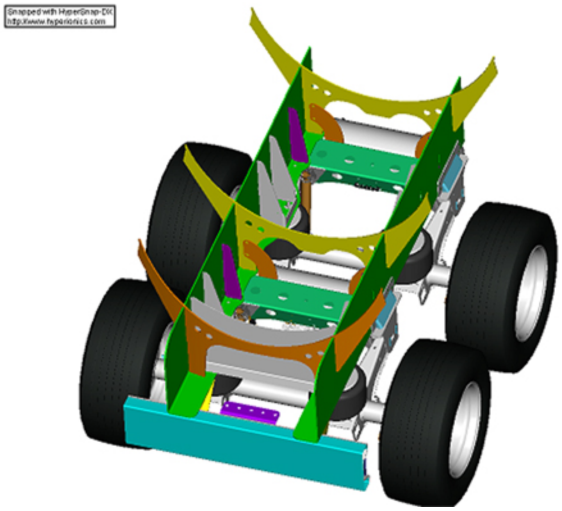

Figure 4. Liburndas Rungear frame.

The new Rungear frame is one of the most critical design areas for a petroleum trailer. The vessel experiences not only loads from the force of gravity acting on the payload but also loads due to articulation or twisting as it maneuvers over the road around corners. Consequently, a leak due to weld fatigue would most likely occur in this area. To simulate road conditions, FEA on the frame was completed for four load cases: (1) 2-G downward, vertical inertial; (2) 2-G forward, horizontal inertial; (3) 1-G lateral, horizontal inertial (10-ton axle load traveling around curves); and (4) 1-G lateral horizontal inertial load (turning on the spot).

The initial analysis indicated that the mild steel crossmember structure gave cause for concern with unacceptable stress levels under the load cases specified. However, the initial FEA model did not take into account the link of the top crossmember to the frame or the correct welding techniques. After further review and FEA remodeling, the new frame design actually experienced acceptable stress levels. To confirm our results, the new frame design was also tested by Hendrickson, the air ride suspension manufacturer. Hendrickson conducted similar FEA modeling and confirmed our final test results.

Vessel Weight Reduction

To date, the total weight reduction goals are as follows: from the shell, 15%; from the heads, 20%; by eliminating the overturn/flashing rails, 20%. The remaining 45% will come from the framing and accessories design.

Friction Stir Welding

During the project, Heil is also working closely with Oak Ridge National Laboratory to determine the feasibility of applying friction stir welding (FSW) to the manufacturing process for the Liburndas vessel. The most likely area will be the large, flat aluminum sheets that make up the barrel proper (currently done on a plasma table). FSW samples have been collected, along with both gas tungsten arc and gas metal arc samples, and bend and tensile testing will begin this phase.

Conclusions

Progress has been made on the vessel and new Rungear design and FEA during this phase of the project. Design and FEA of the fifth-wheel plate are now on schedule and should be completed by the end of the year. All Phase 1 deliverables should be completed by the end of the year, according to the new project schedule.

Continued study and testing will take place on the flangless head design. Once a die is acquired and actual test heads are constructed, mock-up prototype testing will be completed. It is anticipated that the flangeless head design will be very successful, which will accelerate the project into Phase 3—field testing of a prototype.

The marketing research completed to date reflects initial acceptance of the new design, with the exception of the existing accessory locations. Redesign of the accessories will take place quickly over the next year. Market acceptance of the cylindrical design, flangeless heads, and internal rings will make the Liburndas trailer a viable alternative to and inevitable replacement for the elliptical trailer. Once it is in the market, the popularity of the trailer is expected to increase exponentially because of its improved fuel delivery capabilities and roll stability.

B. Application of Superplastically Formed (SPF) Aluminum for Truck Body Panels

Principal Investigator: Nirmal M. Tolani
International Truck and Engine Company
2911 Meyer Road, Fort Wayne, IN 46803
(260) 461-1238; Fax:(260) 428-3661; e-mail: nirmal.tolani@nav-international.com

Chief Scientist: James J. Eberhardt
(202) 586-9837; fax: (202) 587-2476; e-mail: James.Eberhardt@ee.doe.gov
Field Technical Manager: Philip S. Sklad
(865) 574-5069; fax:(865) 576-4963; e-mail:skladps@ornl.gov

Contractor: International Truck and Engine Company
Contract No.: 400002669

Objective

- Investigate applications of superplastic aluminum for low to moderate volume (up to 30000/year) body panels to provide a light weight and low tooling cost alternative to steel and Sheet Molding Compound (SMC).

Approach

- Select a large exterior truck body panel having a complex shape and moderate production volumes.
- Develop part design, conduct forming simulation and Finite Element Analysis.
- Build prototype parts to demonstrate process capability and develop realistic part cost data.
- Evaluate the performance of the parts in the real vehicle environment.

Accomplishments

The program was initiated in March 2005. To date following tasks have been completed.

- Appropriate exterior truck body part has been selected.
- Part design has been completed. The part support structure design concepts developed.
- Forming simulations have been completed to verify the manufacturability.
- Finite Element Analysis of part design and support structure is completed.
- Second iteration Finite Element Analysis of part support structure is underway to optimize the design.
- Superplastic Forming tooling is nearly complete.

Future Direction

- Complete second iteration Finite Element Analysis of the support structure.
- Complete SPF and support structure tooling and produce prototype parts.
- Evaluate surface quality and material thickness variations of the formed parts.
- Develop realistic production tooling and part costs for comparison with alternate materials.
- Perform structural evaluation of the prototype parts under real vehicle environment.

Introduction

Traditionally, commercial truck (Class 5-8) cabs have been made from two materials – steel and aluminum. To stay profitable, the truck industry has been going through product rationalization. To reduce the tooling cost associated with two different cabs, there appears to be a trend to standardize to a single higher volume steel cab. This trend will make the class 7-8 vehicle cabs heavier and reduce the fuel efficiency.

This trend towards conversion from aluminum to steel in the heavy duty trucks can be reversed if formability of aluminum to produce future aerodynamic shapes is improved and tooling cost to produce aluminum cab panels can be significantly reduced. Deployment of superplastic forming (SPF) technology offers an opportunity to do so.

Superplastic forming of certain aluminum alloys offers the ability to produce complex aerodynamic shapes for truck body applications using lower cost tooling. This technology allows production of light weight highly integrated, net-shape components that often consolidate many parts into one. This reduces the number of parts, fasteners, and assembly operations required for complex truck body parts and enables the use of aluminum in place of steel at competitive costs.

A typical superplastic forming process is illustrated in Figure 1. The process uses a single-sided die rather than a matched two sided die. The sheet blank is clamped in the die and blow formed. Complex shaped parts can be formed that are not otherwise possible.

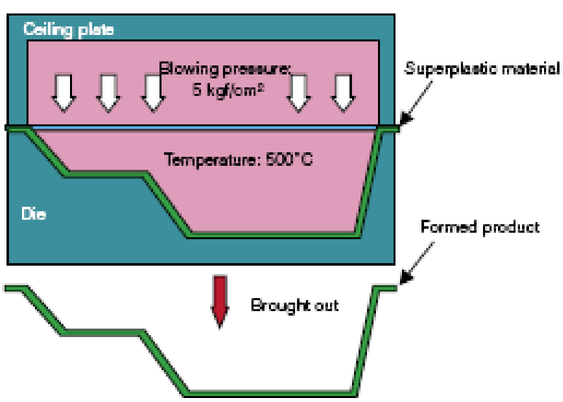

Figure 1. Illustration of typical superplastic forming process.

International Truck and Engine Company had studied the feasibility of using the SPF process for large truck panels in 1985. At that time the SPF aluminum process cycle times and superplastic aluminum material costs were high; also, "Class A" surface finish required for exterior body panels could not be achieved. Although the tooling costs were low, the part costs were very high. It was determined that SPF was economically viable only for very low Volumes (< 1000 pcs).

In recent years, significant new developments in the SPF materials and processes have been reported. It is reported that these developments have made higher production volumes, matching those of class 7-8 truck volumes, feasible through a combination of increased forming rates and lower material cost. It is also reported that for moderate levels of forming, the "Class A" surface condition required for exterior body panels is achievable.

These recent developments make SPF technology increasingly attractive for heavy vehicle applications. However, there is a strong need to validate the claims made about the forming cycle times, part costs, tooling costs, "class A" surface capability and fatigue properties as it applies to large cab panels and structural parts. The only way to convince the Heavy Truck Industry to deploy this relatively new technology is to demonstrate its feasibility for a large exterior body part.

Project Goal

The project goal is to initially demonstrate the feasibility of SPF technology for a large exterior body panel as phase 1 of the project. If results look promising, in the second phase, application of SPF will be expanded to make more complex body sub-assemblies and/or the entire truck cab depending on the funding level provided.

Project Plan

The phase 1 of the project involves design, analysis, prototyping and testing of the large exterior truck body part. The following task descriptions were proposed to address the key issues related to the application of SPF in heavy duty vehicle applications.

Part Design and Analysis: This task has helped to understand design and tooling considerations and limitations. It helped develop guidelines for future designs with SPF aluminum.

Build prototype parts: The production of prototype parts will help evaluate tooling issues, forming process cycle times, part wall thickness variations and capability of SPF aluminum to provide "class A" surface.

Perform Durability Tests: This will help evaluate assembly, stiffness and durability of SPF aluminum in the class 8 truck applications.

Conclusions

The application of SPF for truck body panels is well underway. Significant SPF prototype parts will be produced before the end of the 2005 calendar year. Durability tests have been planned for these parts.

Presentations/Publications/Patents

Nirmal Tolani, Heavy Vehicle Materials Program Review, Oak Ridge Tennessee, September 14, 2005.

C. Advanced Composite Support Structures

Principal Investigator: Brian Knouff
National Composite Center
2000 Composite Drive
Kettering, OH 45420
(937 -297-9458; fax (937) 297-9440; e-mail: bknouff@compositecenter.org

Project Manager: Jay Batten
Delphi Corp.
3900 Holland Rd
Saginaw, MI 48601-9494
(989-757-3895; fax (989) 757-42950; e-mail: jay.batten@delphi.com

ORNL Project Manager: Cliff Eberle
(865) 574-0302; fax: (865) 574-8257; e-mail: eberlecc@ornl.gov

Chief Scientist: James J. Eberhardt
(202) 586-9837; fax: (202) 587-2476; e-mail: James.Eberhardt@ee.doe.gov
Field Technical Manager: Philip S. Sklad
(865) 574-5069; fax: (865) 576-4963; e-mail: skladps@ornl.gov

---

Contractor: Oak Ridge National Laboratory
NCC/ORNL Contract No.: 4000039214

Objective

- Lead the rapid implementation of lightweight composite materials in Class 7/Class 8 vehicles via the development of advanced composite support structures, specifically chassis lateral braces, which can number up to six per vehicle. Mass reductions are targeted for 50%.

Approach

- Model composite support structures using finite element analysis (FEA).
  - Include part, subsystem, and system analyses and optimizations
- Determine guidance cost on production design.
- Fabricate sample plaques to determine affect of fatigue at different sequences of loads.
- Model failure mechanisms with progressive failure analysis (PFA).

Accomplishments

Modeling

- Obtained detailed loadcases from customer on system model.
- Analyzed current design system model and determined loadcases for subsystem model.
- Analyzed subsystem model and began composite model optimization.
- Further crack propagation VCCT (Virtual Crack Closure Technique) model.

Future Direction

- Determine design and ROM (Rough Order of Magnitude) production costs for design scenarios.
- Insert final design into system model to ensure no change in load path.
- Deliver prototypes to customer MAY06 for track and field testing.
- Initiate second application of Value Analysis Value Engineering (VAVE).

Introduction

The purpose of this effort is to lead the rapid implementation of lightweight composite materials in Class 7/Class 8 vehicles via the development of advanced composite support structures. This task specifically addresses lateral braces; primary beams are being targeted for future work. The mass reduction target is 50% with a minimum requirement of 30%. The benefits of mass reduction in commercial vehicle applications are well known. They include increased fuel economy and a larger payload, which translate into fewer total trips and thus fewer vehicles on the road. This leads to less traffic, which aids highway safety, and decreased emissions. Support structures offer an opportunity for significant weight savings. However, this area of the vehicle also represents a large hurdle in terms of composite applications and market acceptance.

The application of focus is a Class 8 tractor lateral brace. The estimated total annual usage of Class 8 lateral braces could exceed 1 million by 2007. Many are simple stamped parts which do not qualify for composite replacement on a per component basis. However, some are heavy duty and can benefit greatly from a composite redesign as is the present case. The application currently being studied has a production volume of about 50,000 per year. The total weight of the current design is 24 kg. A minimum weight savings of 30% is 7.2 kg per part. There are normally 2 of theses braces per vehicle totaling a minimum weight savings of 14.4 kg (31.7 lbs) per vehicle.

To facilitate this work and future endeavors advanced FEA and PFA software is being employed and developed. The FEA software contains a unique optimization algorithm that allows for the rapid optimization of such design variables as part thickness, fiber angle, fiber type, and even part shape while minimizing mass, strain, or even cost. PFA, although in development for composites, will provide the ability to model composite behavior in durability and fatigue situations.

Modeling

In order to model the part effectively, the loadcases were reexamined with the customer. It was determined that there are 2 main loadcases that need to be applied in the design: racking and twisting. Racking occurs when one primary beam shifts ahead of the other one. This occurs during cornering, for example. Twisting occurs when one side of the chassis is lifted or lowered compared to the other side. Driving over debris or speed bumps or hitting potholes results in this loadcase.

The modeling is now being done on 2 hierarchical levels. The system and subsystem models are shown in Figures 1 and 2 respectively. The subsystem model was extracted from the system model as follows.

The system model of the current design was analyzed with the steel lateral brace for both loadcases. The customer provided the Rigid Bar Element (RBE) design to represent the bolts as shown in Figure 3. The customer also represented the chassis springs and tires with elastic elements at the bottom of each hanger, Figure 4. (Note that the hanger is a new addition to the model).

Figure 1. System FEA model.

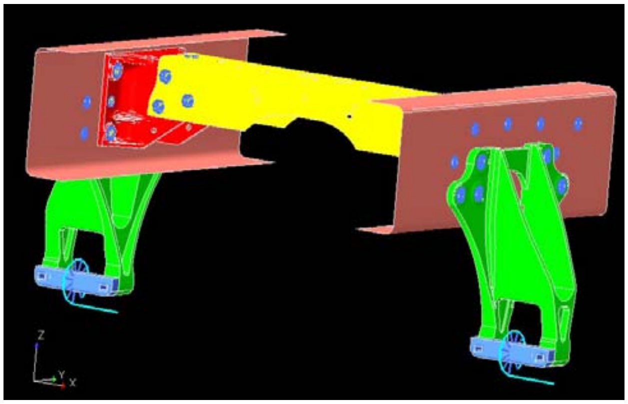

Figure 2. Subsystem FEA model.

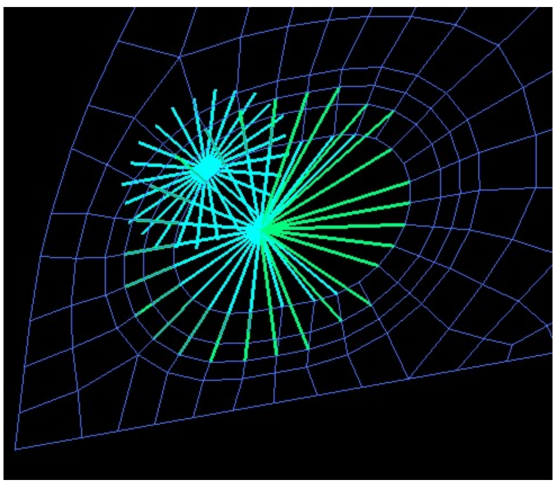

Figure 3. RBE assembly to represent bolts.

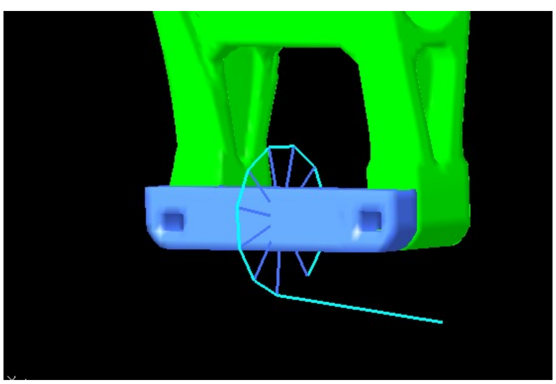

Figure 4. Representation of springs and tires via springs and bar elements.

To make the subsystem model, the primary beams were sliced on each side of the lateral brace. On the system model, the deflections at the edges of the primary beams and the deflections of the bottom of the hanger were determined from the analysis and used as the loads for the subsystem model. In other words, the loads for each loadcase are enforced displacements, and not applied loads.

The subsystem model was analyzed to determine the stresses throughout the parts. Figures 5 and 6 show the resulting von Mises stress contour for the steel center section for each loadcase. The stresses are maximum around the lower bolt holes. The racking loadcase tops out at 150 MPa (22 ksi) while the twisting loadcase is more severe at 250 MPa (36 ksi). Most of the part, however, only sees a stress of around 60 MPa (9 ksi).

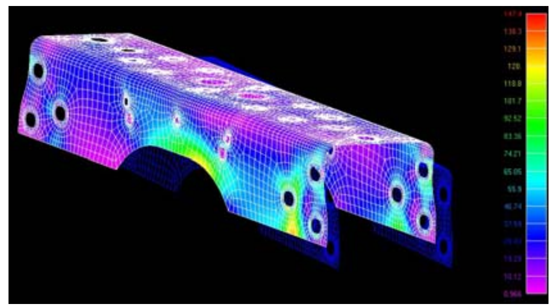

Figure 5. Racking stress contour for steel center brace

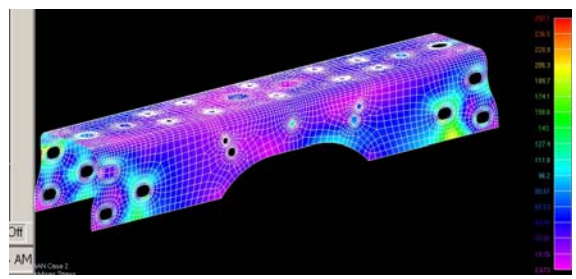

Figure 6. Twisting stress contour for steel center brace.

Similarly, the endbrackets, primary beam sections, and hangers were examined for maximum stress contours in Figures 7 – 12. In each case the twisting loadcase is more severe and the maximum stresses occur at the lower bolt holes. The results are finalized in Table 1. This information will be used for comparative purposes when optimizing the composite structures.

Composite Design

A new postprocessor, Design Studio® from Vanderplaats Research and Development, Inc., has been developed which has the ability to examine the stresses and displacements at each layer in a PCOMP element. A PCOMP element is a shell

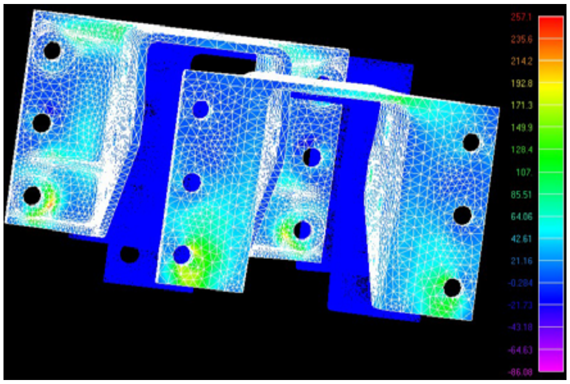

Figure 7. Racking stress contour for end brackets.

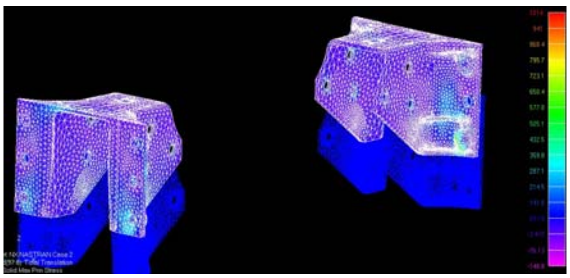

Figure 8. Twisting stress contour for end brackets.

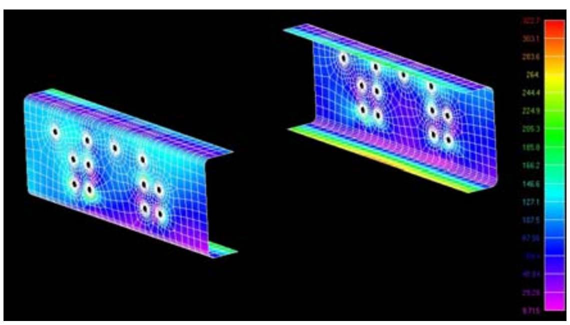

Figure 9. Racking stress contour for primary beam sections.

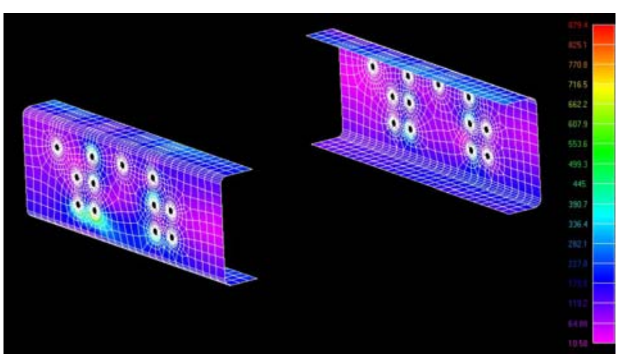

Figure 10. Twisting stress contour for primary beam sections.

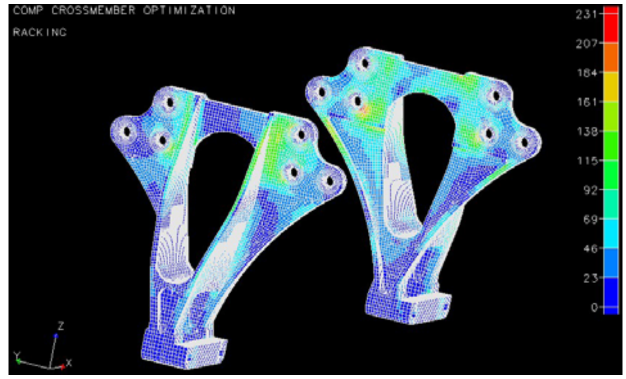

Figure 11. Racking stress contour for hangers.

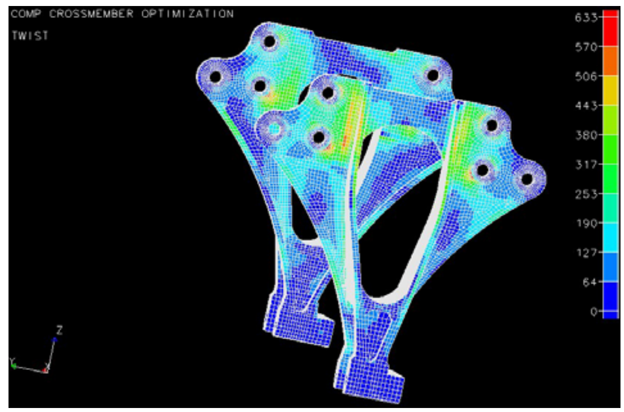

Figure 12. Twisting stress contour for hangers.

Table 1. Maximum stresses in MPa in current design.

	Racking	Twisting	Farfield
center	150	250	60
end brackets	260	1000	100
primary beams	325	875	200
hangers	230	630	50-150

Likewise the resulting forces were compared due to the simulated twisting loadcase

element which consists of many layers. This is used to simulate the various composite plies which occur at different angles in this model. Design Studio® was used to model the composite lateral brace in the subsystem model.

Scenarios

Recall that we were able to form a VAVE (Value Analysis Value Engineering) flowchart shown in chart 1 to determine the different scenarios for design and process development of this application.

Chart 1. VAVE flowchart for lateral brace.

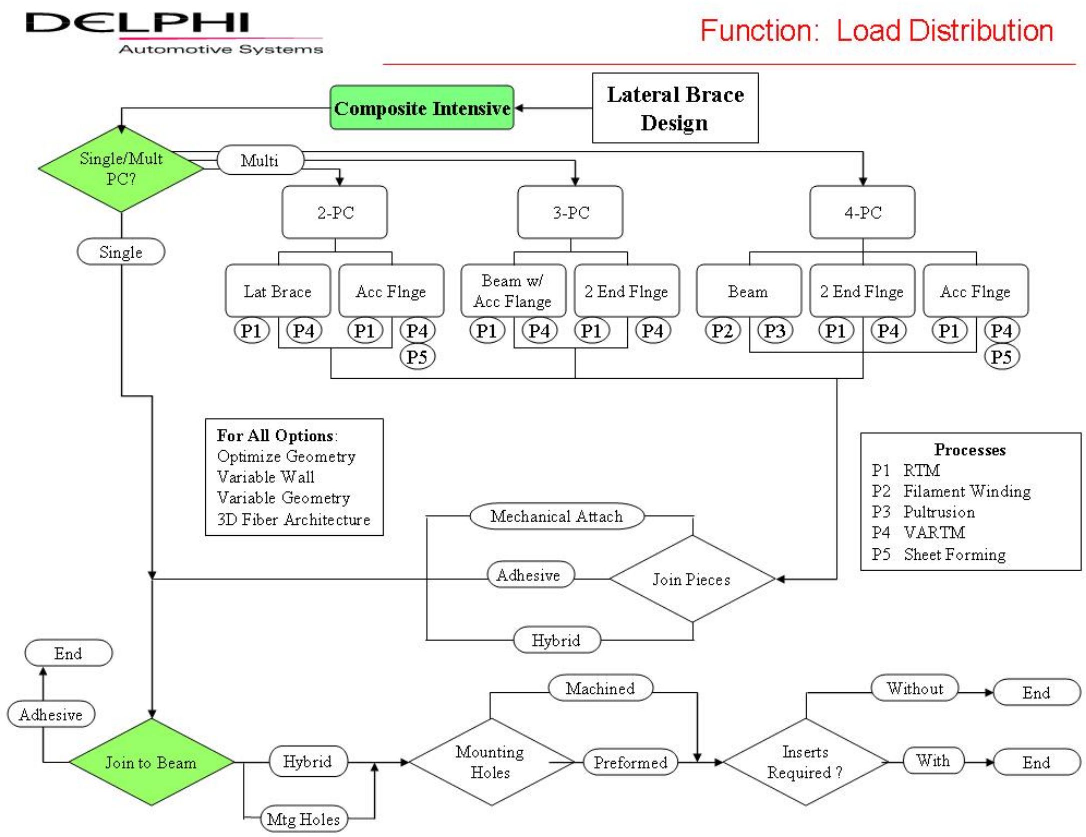

The design was previously narrowed down to 3 scenarios:

1. Composite center piece only
2. Composite/Metal hybrid
3. One-piece composite with inserts

From the bolt modeling done by our partner (contract nos. DE-AC05-00OR22725 and DE-AC06-76RL01830) performed with ABAQUS, it was discovered that there is not enough material to pursue option number 3. Using inserts requires the removal of material resulting in very little composite left to handle the stresses.

Design scenario 1 has begun. First, the holes from the steel lateral brace had to be copied to the box beam composite mode as shown in Figure 13. Then, the entire composite was optimized as shown in Figure 14. There were 10 layers in the first optimization $[0/\pm 12.5/\pm 45]_s$. The design variables were the thickness of each layer and the angle of the 45 degree layers. The 12.5 degree layer angles were held constant because previous analysis showed that to be the optimum angle and it is the lowest processable angle from our suppliers. The results are in Table 2.

The resulting thickness is 26.9 mm. Additionally, this part weighs 15.2 kg which is *heavier* than the steel brace. The reason is seen by looking at the

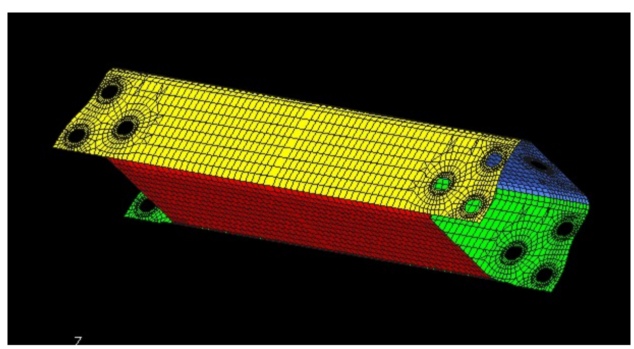

Figure 13. Incorporation of steel brace boltholes into composite box beam.

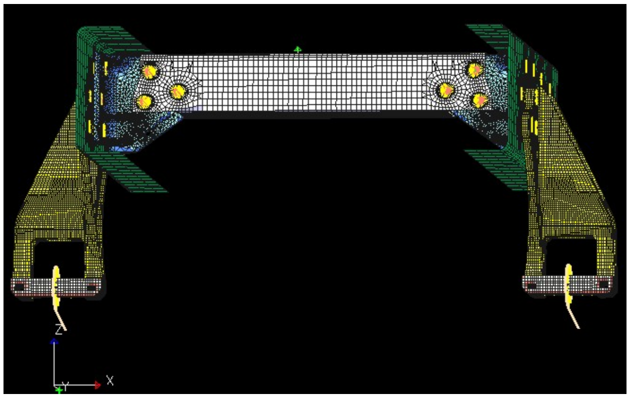

Figure 14. 1st optimization of composite center brace modeled composite as same lay-up everywhere.

Table 2. Results from 1st composite optimization.

Design Cycle	0 ply th, mm	12.5 ply th, mm	45 ply th, mm	45 ply angle
1	1.5	1.5	1.5	67.5
2	2.25	2.25	2.25	87.2
3	3.75	3.75	3.75	90.0
4	2.25	0.42	4.40	88.7
5	2.47	0.23	5.44	87.1
6	2.65	0.10	5.40	86.7

stress contour plot for layer 1 of the composite in Figure 15. The stresses around the holes reach above 230 MPa, but the rest of the part has near zero stress, which means it is much thicker than it has to be. This optimization was successful in designing the thickness around the joints, but not the rest of the part.

The second design scenario considered splitting the center piece into 2 sections: an end and a middle as shown in Figure 16. The end section utilizes the results from the first optimization since it is in the joining area. The lay-up here is [0/90/0] with thicknesses of 2.65, 21.6, and 2.65 mm. Optimization was performed on the middle section. There were 11 layers to start with $[0/\pm22.5/\pm67.5/90]_a$ with the design variables being the thickness of each layer and the angles of the 22.5 and 67.5 degree layers.

Table 3 displays the results. As expected, the thicknesses decreased greatly reducing the weight of this design to 6.6 kg.

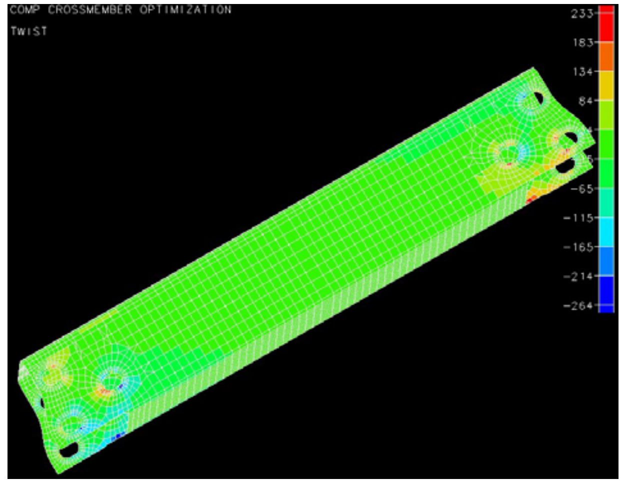

Figure 15. Stress contour of first design optimization.

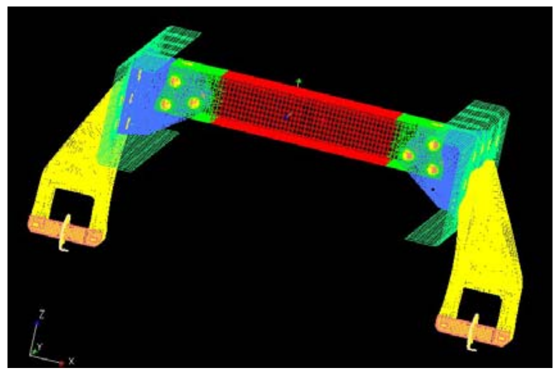

Figure 16. Separation of composite center brace into and end and middle for 2nd design optimization.

Table 3. Results from 2nd composite optimization (hard convergence on 6th cycle)

Design Variable	Final Value
0 ply th, mm	0.18
22.5 ply th, mm	0.13
67.5 ply th, mm	0.80
90 ply th, mm	0.57
22.5 ply angle	11.8
67.5 ply angle	90.0

Analysis of the resulting stress contours are shown in Figures 17 through 20. Figure 17 displays the composite section with both the middle and end parts. The contour here is for the first layer of the composite, which is the first 0 degree layer in both parts.

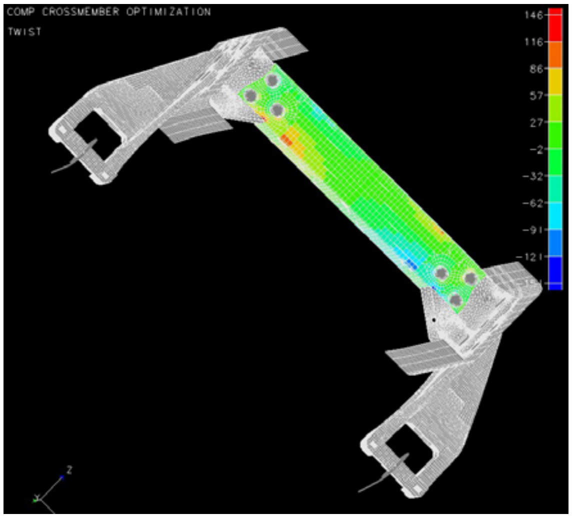

Figure 17. Twisting stress contour for 2 zoned composite center section after 2nd design optimization.

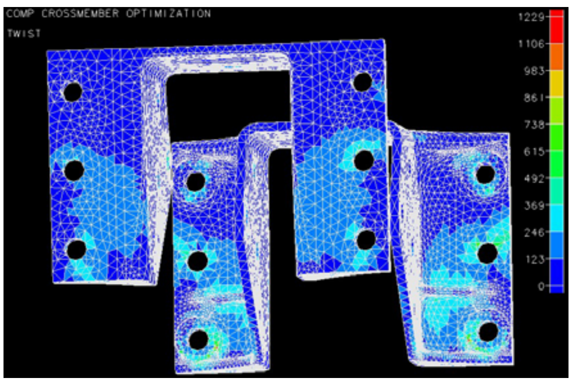

Figure 18. Twisting stress contour result for end brackets after 2nd composite optimization.

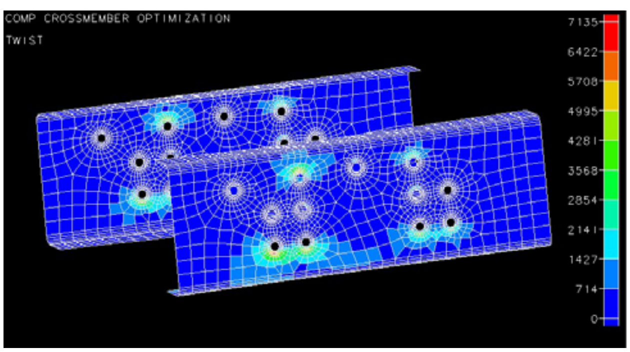

Figure 19. Twisting stress contour for primary beam sections after 2nd composite design optimization.

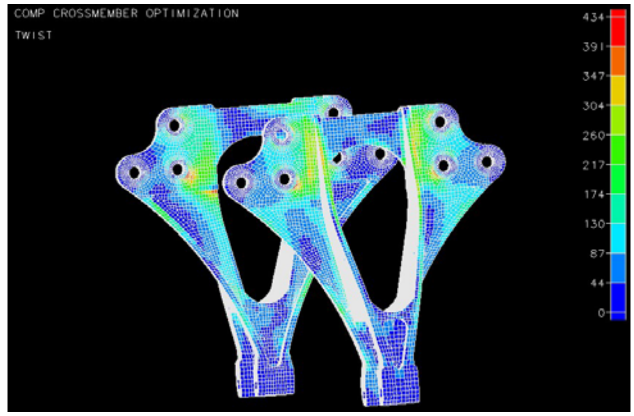

Figure 20. Twisting stress contour for hangers after 2nd composite design optimization.

Notice the stresses at the bolt holes are incredibly large especially in the primary beam sections. The truth is these are contact stresses, and for the value of these stresses to be known quantitatively a nonlinear and contact processor must be run. The processor for this optimization is linear and static and does not take into account contact stresses. Therefore, although we know these areas are stress risers, we don't know the actual values and the values shown are not real. However, the farfield stress contour is legitimate. Table 4 lists these stresses and compares them to the results in Table 1. They are actually pretty comparable since we expect the longitudinal failure stress for composites to be around 1000 + MPa to have a durable design. Our concern now really is to decrease the stresses in the end brackets and primary beam sections while reducing even more weight. It is possible this can be done by *decreasing* the stiffness of the composite center section.

Table 4. Maximum stresses in MPa in steel vs. 2nd design iteration for Twisting loadcase

	Composite	Steel	% Diff
center	+150	250	149
end brackets	1230	1000	23
primary beams	7000	875	700
hangers	450	630	29

Table 5. Farfield stresses in MPa in steel vs. 2nd design iteration for Twisting loadcase

	Composite	Steel	% Diff
center	-20	60	67
end brackets	300	100	200
primary beams	~300	200	50
hangers	130	150	13

After the composite is optimized, the nonlinear contact processor will be used to design the joints, which will enable us to minimize the mass in these areas while ensuring durability.

PFA

Progressive failure analysis has progressed to include a VCCT (Virtual Crack Closure Technique) as shown in Figure 21. This model will help to assist in the designs of the joints. It relies on a predefined crack path and fracture toughness data to work effectively. The advantages are that it can detect the failure mechanisms at both the macro and micro levels.

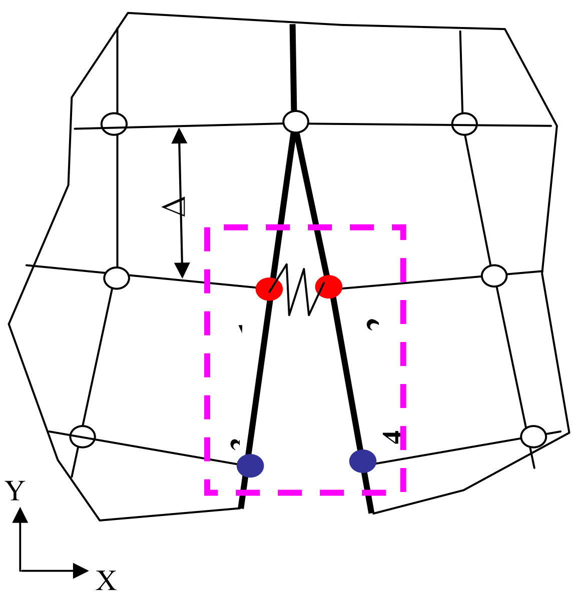

Figure 21. VCCT model.

Conclusions

Accomplishments in second half of FY 2005 include the following:

- Successfully obtained working loadcases from the customer
- Extracted a subsystem model with the new loadcases from the system model
- Analyzed the current design in the system and subsystem model
- Transferred the loadcase environment to a composite subsystem model
- Initiated composite design and optimization.
- Narrowed design scenarios down to 2.
- Added VCCT modeling for PFA

Future Direction

Modeling

The composite optimization will be completed by the end of Nov. 05. We will then work with our joining team to model the joints. This should be completed by Jan. 06.

Process Development

We are working with our customer to assemble a supplier list. We currently have 4 suppliers whom we are going to visit beginning Nov. 05. In Jan. 06 and Feb. 06 we will obtain ROM (Rough Order of Magnitude) guidance costs for our 2 design scenarios. In Mar. 06 we will select the design and supplier and obtain quotes for production. We will then initiate the cutting of the tools. We expect to have first prototypes by May 06.

D. New-Generation Frame for Pickup/Sport Utility Vehicle Application

Principal Investigator: Curt A. Lavender
Pacific Northwest National Laboratory
P.O. Box 999, M/S K2-03, Richland, WA 99352
Tel: (509) 372-6770; Fax: (509) 375-4448; e-mail: curt.lavender@pnl.gov

Kurt M. Knop
DaimlerChrysler Corporation
14250 Plymouth Road
Detroit, MI 48227
Tel: (313) 659-6076; Fax: (313) 635-5221; e-mail: kmk4@daimlerchrysler.com

Chief Scientist: James J. Eberhardt
(202) 586-9837; fax: (202) 587-2476; e-mail: James.Eberhardt@ee.doe.gov
Field Technical Manager: Philip S. Sklad
(865) 574-5069; fax: (865) 576-4963; e-mail:skladps@ornl.gov

Contractor: Pacific Northwest National Laboratory
Contract No. DE-AC06-76RLO 1830

Objective

- Evaluate the design of an optimized hybrid materials frame that represents a new generation of pickup/sport utility vehicle (PU/SUV) frame applications and vehicle architecture.

Approach

- Apply high-risk manufacturing and design methods to the PU/SUV frame to reduce mass while meeting cost goals consistent with a high-production vehicle.

Accomplishments

- Established performance, packaging, and weight targets for the second iteration of the new-generation frame “the next-generation frame” (NGF).
- Created a design for the NGF that projects a greater weight reduction and a decrease in the number of parts compared with the current steel baseline frame.
- Created a computer-aided engineering (CAE) model of the NGF and evaluated impact; noise, vibration, and harshness (NVH); and durability of the NGF.
- Completed CAE and design iterations to meet DCX 5-Star crash worthiness rating.
- Created complete bill of materials for the prototype and initiated procurement.
- The prototype frame has been constructed and delivered to DCX for torsion and stiffness testing after which the frame will be assembled into a full size vehicle and road tested at the DCX Proving Grounds.

Future Direction

- The frame will be evaluated by DCX for torsion and stiffness testing after which the frame will be assembled into a full size vehicle and road tested at the DCX Proving Grounds.

Introduction

Increased consumer demand for PUs/SUVs has resulted in increased fleet fuel consumption. The fuel demand for this class of vehicle has exceeded that of passenger automobiles and now consumes approximately 27% of the United States oil.[1] The objective of this project is to explore manufacturing methods and materials to reduce the mass of the SUV/PU frame, thereby reducing fuel consumption for this class of vehicle.

During the second quarter of FY 2003, DaimlerChrysler completed vehicle testing at the DCX Proving Grounds using an SUV/PU platform equipped with a hybrid frame. Results of the accelerated testing have proved that (1) the hybrid frame design had sufficient strength and durability to meet the vehicle performance requirements, and (2) the frame was probably somewhat overbuilt and heavier than required even with a substantial weight savings from the current baseline steel frame.

The next phase of the project will evaluate the use of a lighter frame, called the Next Generation Frame (NGF). The NGF uses a CAE approach and higher-risk manufacturing technologies. The projected weight for the NGF is lighter than the previously tested new-generation frame and requires 35% fewer components.

Approach

A CAE model of the NGF will be created and design iterations performed to meet the NVH, impact and durability requirements for a DCX 5-Star rating. A prototype of the frame will be fabricated and evaluated by frame flexure and road tests.

Progress

CAE analyses of the frame are complete and satisfy all of DCX requirements for 5-Star crash worthiness, NVH and durability. The frame has been completed and delivered to DCX and Magna for full scale automotive testing. Figure 1 shows the frame being fabricated in the assembly fixture.

Figure 1. Next Generation frame components and assembly fixture prior to final assembly.

Future Direction

The frame components have been assembled into the NGF and submitted to DCX for full frame testing. Tests will include full frame torsion and stiffness tests. After static stiffness tests, the frame will be attached to a full vehicle and road tested on the DCX Proving Grounds test track.

References

Light Duty Vehicle Trends: 1975 through 2004, United States Environmental Protection Agency, *EPA 420-R-04-00, April 2005.*

E. Advanced Superplastic Forming Development for Heavy Vehicle Structures

Principal Investigator: Curt A. Lavender
Pacific Northwest National Laboratory
P.O. Box 999, M/S K2-03, Richland, WA 99352
Tel: (509) 372-6770;fax: (509) 375-4448; e-mail: curt.lavender@pnl.gov

Don Trettin
PACCAR Technical Center
12479 Farm to Market Road
Mt. Vernon, WA 98273-9690
Tel: (360) 757-5241; fax: (360) 757-5370; e-mail:don.trettin@paccar.com

Nirmal Tolani
2911 Meyer Road
PO Box 1109
Fort Wayne, IN 46801-1109
Tel: (260) 461-1238; fax: (260) 428-366; e-mail:nirmal.tolani@nav-international.com

Chief Scientist: James J. Eberhardt
(202) 586-9837; fax: (202) 587-2476; e-mail: James.Eberhardt@ee.doe.gov
Field Technical Manager: Philip S. Sklad
(865) 574-5069; fax: (865) 576-4963; e-mail: skladps@ornl.gov

---

Contractor: Pacific Northwest National Laboratory
Contract No. DE-AC06-76RLO 1830

Objective

- Evaluate the use of superplastic forming for heavy vehicles.

Approach

- The project will focus on demonstrating the technology using mutually agreed on truck components, with the goal of developing the superplastic forming (SPF) design and material property knowledge base to the point where the individual companies have the ability to design and implement it for their new vehicle designs.

Accomplishments

- Room temperature tensile properties of 5083 sheet superplastically formed to a biaxial strain of 0.45 were performed.
- Superplastic tensile tests were performed on the baseline 5083 aluminum alloy.
- A die was designed to evaluate the elimination of secondary operations.
- Performed initial tests on the 6013 alloy to determine if a heat treatable alloy may be used in a low cost superplastic forming process. Results indicate that a post SPF aging treatment will be required.

Future Direction

- Additional trays will be formed and an S-N fatigue curve will be developed.
- Tests will be performed with the new die.
- A process for a low cost high strength SPF alloy will be developed.

Introduction

Replacement of low strength glass fiber-reinforced plastics with aluminum in heavy vehicle hoods and other cab components can significantly reduce the weight of Class 6-8 truck components. Although the use of aluminum has been viewed as a desirable weight savings approach for some time, the complex shape of aerodynamic hoods, bumpers and fairings, the limited room temperature formability of aluminum, and the high cost of forming tools have restricted its use. SPF, in the context of this proposal, is an elevated temperature gas pressure forming technology that has been widely used in aerospace applications, and more recently introduced by General Motors (in a modified form) for selected aluminum automotive components. Advantages of SPF include inexpensive tooling, the ability to form complex aerodynamic shapes, simplified die design compared to traditional stamping and the opportunity for significant part count consolidation. Although SPF is traditionally viewed as a slow forming process, recent advances in aluminum alloys and forming process procedures have reduced typical forming times to the point where SPF appears well-suited for typical heavy truck production volumes. However, a number of technical barriers remain; including the ability to form Class A surfaces, the availability of suitable SPF sheet materials for large components, and the performance of SPF components and structures in heavy-duty truck applications.

Approach

The objectives of this project are to evaluate current production SPF capabilities and limitations through parallel Truck OEM demonstration components, develop cost and design allowable tools that allow the OEMs to select proper applications for SPF, and to advance SPF materials and processing capabilities for heavy vehicle applications. The project team involves collaboration between two major truck manufacturers, International Truck and PACCAR Technical Center (PTC) (parent company of Kenworth and Peterbilt). Because of the competitive nature of the truck manufacturers, the project will focus on demonstrating the technology using mutually agreed on truck components, but will have the goal of developing the SPF design and material property knowledge base to the point where the individual companies have the ability to design and implement it for their new vehicle designs.

Progress

International and PTC have identified candidate components for prototype SPF components. International has initiated manufacturing of the components and PTC is completing a stress analysis of the selected component.

To facilitate design of the components, the Pacific Northwest National Laboratory(PNNL) superplastically formed samples of the 5083 aluminum alloy sheet to be used and measured tensile properties normal and parallel to the rolling direction after a biaxial strain of 0.45 at 850^{o}F and $1.3x10^{-3}$ s^{-1} strain rate. Room temperature tensile samples were removed from the long dimension of the formed tray, shown by Figure 1, and tested per ATSM E8. Additional samples were subjected to the

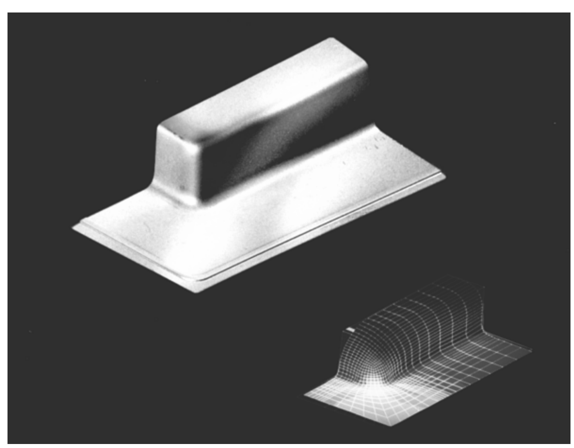

Figure 1. Sample SPF part used to characterize tensile properties from 0.047 inch 5083 aluminum sheet.

850°F thermal cycle only and compared to the tensile tests from formed trays.

The results of the tensile tests, when tested in the rolling direction, indicate that after forming to 0.45, at $1x10^{-3}$ s^{-1}, at 850°F the sheet properties were very similar to the as-annealed properties where yield strength, ultimate strength and elongation were 23,000 psi, 44,000 psi and 32% and 22,000 psi, 43,000 psi and 31% for the annealed and formed materials, respectively.

The results of the tensile tests, when tested transverse to the rolling direction, indicate that after forming to 0.45, at $1x10^{-3}$ s^{-1}, at 850°F the sheet properties were very similar to the as-annealed properties where yield strength, ultimate strength and elongation were 23,000 psi, 42,000 psi and 30% and 21,000 psi, 41,000 psi and 29% for the annealed and formed materials, respectively. The results of the tensile tests are summarized on Table 1.

Table 1. Summary of room temperature tensile tests performed on samples machined from superplastically formed trays made from 0.047 inch 5083 aluminum sheet; all trays were formed at an average strain rate of $1.3x10^{-3}$ s^{-1} and 850°F with a total cycle time (heat up to cool down) of 12 minutes.

		Yield strength (0.2% offset)	Ultimate strength	Elongation
Sheet Condition	**Orientation**	**1000 psi**	**1000 psi**	**%**
As-Received sheet	Rolling Direction	57	65	10
	Transverse	57	67	9
Annealed 850°F for 12 minutes	Rolling Direction	23	44	32
	Transverse	23	42	30
Formed tray	Rolling Direction	23	42	30
	Transverse	21	41	29

The 5083 alloy used for superplastic forming generally has a very fine grain structure developed by high levels of cold work that results in a low flow stress under the controlled temperature and strain rate conditions. The material supplied to PNNL was tested in tension at room temperature and was found to have a 57,000 psi yield and 66,000 psi ultimate strengths and an elongation of 10%. The high strength sheet material can be beneficial prior to SPF because of high scratch and dent resistance forming. However, it can result in higher material costs if the sheet cannot be coiled, particularly in thick gage.

The sheet material was tested for superplasticity at 850 and 950°F and exhibited tensile ductility and strain-rate sensitivity, m-value, expected from fine grain superplasticity in the 5083 alloy[1]. The samples were tested using constant strain rate as approximated by an exponentially increasing crosshead velocity[2] at $5x10^{-4}$, $1x10^{-3}$ and $5x10^{-3}$ s^{-1}. At a strain of 0.15, the crosshead velocity was increased by 20% and the stress increase was used to determine the strain-rate sensitivity, m-value, using the relationship:

$$m = \log(\sigma_2 / \sigma_1) / \log(\dot{\varepsilon}_2 / \dot{\varepsilon}_1)$$

A typical stress strain curve derived for an SPF tensile test has been included here for illustrative purposes as Figure 2. The superplastic tensile test results are summarized on Table 2.

Figure 2. Typical superplastic tensile test curve performed at constant strain rate with a 20% velocity bump at 0.15 strain to determine strain rate sensitivity, m. The results shown by Figure 2 were from tensile tests performed at 850°F from 0.047 inch 5083 aluminum sheet.

Table 2. Superplastic tensile properties measured for the 0.047 inch 5083 aluminum sheet.

Temperature	Strain rate			Initial Flow stress	Elongation
°F	**s^{-1}**	**Orientation**	**m-value**	**psi**	**%**
850	$5x10^{-4}$	Rolling	0.54	1200	300
		Transverse	0.50	1200	300
	$1x10^{-3}$	Rolling	0.49	1800	240
		Transverse	0.45	1800	240
	$5x10^{-3}$	Rolling	0.34	3300	190
		Transverse	0.33	3500	180
950	$5x10^{-4}$	Rolling	0.55	500	260
		Transverse	0.51	540	250
	$1x10^{-3}$	Rolling	0.50	1000	250
		Transverse	0.43	1000	230
	$5x10^{-3}$	Rolling	0.35	2000	260
		Transverse	0.37	2100	230

The m-values ranged from a low of 0.33 at 850°F at $5x10^{-3}$ s^{-1} to high of 0.55 at 950°F $5x10^{-4}$ s^{-1}. The elongation was relatively insensitive to testing conditions and was 230 to 300% except for the 850°F $5x10^{-3}$ s^{-1} test condition where elongation values dropped to below 200%. Consistent with high strain rate sensitivity of superplastic materials the initial flow stress of the sheets was dependent upon test conditions and ranged from a low of 500 psi at $5x10^{-4}$ s^{-1} and 950°F to a high of 3500 psi at $5x10^{-3}$ s^{-1} 850°F.

Recent developments in the automation of superplastic forming have significantly reduced the cycle time to load, form and unload an SPF part. The newly reduced cycle time and transfer presses may enable the use of a higher strength alloy that has a heat treat response analogous to "paint baking" in steels. Therefore, a brief study was initiated to determine if a higher strength and less stress corrosion cracking susceptible alloy 6103 could be used. The study used hardness data to determine if a solution heat treated sheet subjected to a rapid heat up to 850 and 950°F could exhibit an aging response and if a sheet formed at 850 to 950°F removed rapidly from a die could have a post SPF age response without a water quench.

Initial results showed that the hardness of a sheet heated and held at 850°F and 950°F even for only 1 minute were less than 10 HRB indicative of a fully annealed sheet. Thereby, suggesting that it is unlikely that the rapid heat up and short cycle time associated with an automated SPF process could result in a "paint bake" for a solution heat treated 6013 sheet. However, 6013 sheets heated to 850 and 950°F, removed quickly from a furnace and air cooled, exhibited an age response when held at 350°F. The hardness achieved in the air cooled sample was less than that of a sample that was water quenched. However, it did indicate that a post SPF aging treatment could result in a higher hardness without a water quench. Figure 3 is given here to show the aging curves.

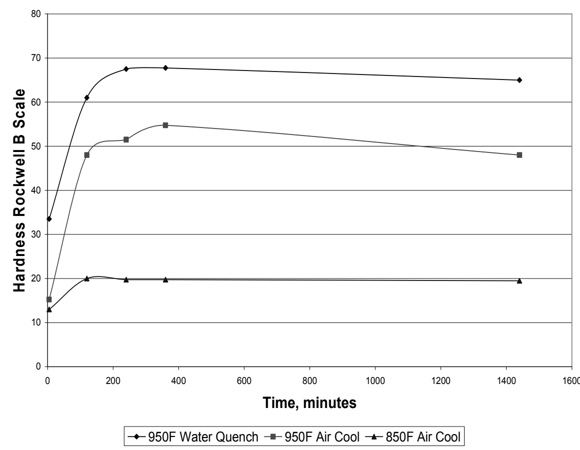

Figure 3. The age hardening response, measured in Rockwell B scale, of the aluminum alloy 6013 at 350°F after being subjected to air cooling and water quenching at temperatures typical of SPF.

A survey of the existing literature regarding 6XXX was performed. The data [3,4] indicate that by controlled thermomechanical processing, the 6013/6111 alloy could be made superplastic. The processes used required extended aging times that would be prohibitively costly for heavy vehicle sheet products. A variant will be developed at PNNL.

Future Direction

The development of data for the use in SPF component design will continue. Fatigue data from superplastically formed 5083 aluminum sheets will be determined.

The evaluation of a low-cost high strength alloy process for high rate SPF will continue with the development of a low-cost thermomechanical process.

References

1. J.S. Vetrano et al., "Superplastic Behavior in a Commercial 5083 Aluminum Alloy." *Scripta Metallurgica,* Vol. 30, pp. 565-570, 1994.
2. K.I Johnson, et al., "The Effect of Specimen Geometry on the Accuracy of Constitutive Relations in Superplastic 5083 Aluminum Alloy." *In the proceedings of the 1994 International Conference on Superplasticity in Advanced Materials,* (ICSAM-94), May 24-26, 1994. Moscow Russia.
3. L. P. Troeger and E. A. Starke, "Particle Stimulated nucleation of recrystallization for grain size control and superplasticity in an Al-Mg-Si-Cu alloy." *Mat. Sci. and Engr.* A293 (2000) 19-29.

4. Kaibyshev, R., et. al. “Effect of liquid phase on superplastic behavior of a modified 6061 aluminum alloy.” *Scritpa Met. 47* (2002) 569-575.

F. Development of Magnesium for Heavy Vehicle Powertrain Components

Principal Investigator: Darrell R. Herling
(509) 376-3892; fax: (509) 376-6034; e-mail: darrell.herling@pnl.gov

Chief Scientist: James J. Eberhardt
(202) 586-9837; fax: (202) 587-2476; e-mail: James.Eberhardt@ee.doe.gov
Field Technical Manager: Philip S. Sklad
(865) 574-5069; fax:(865) 576-4963; e-mail:skladps@ornl.gov

Contractor: Pacific Northwest National Laboratory
Contract No.: DE-AC06-76RL01830

Objective

Develop magnesium (Mg) composite casting technology and associated low-cost tooling for manufacturing of ultra-lightweight low-cost heavy-vehicle powertrain components. The project is focused on three development tasks, which include 1) development of compositing technologies to produce low cost MMC materials; 2) advanced shape casting manufacturing processes; and 3) innovative designs for new powertrain components.

Approach

Development of advanced Mg alloys and processing technologies is a major technical hurdle to widespread application of Mg in the heavy vehicle manufacturing industry. As such, the approach taken for this project includes active participation by a truck OEM, as well as suppliers where appropriate. The philosophy of this teaming approach is to insure meaningful technology transfer of enabling and new technical developments. Below is a project outline and general approach. The underlying focus is on process development and economical manufacturing methods for Mg and its composites. The approach and cost analysis will consider product design, material-specific characteristics and component performance.

- Address technical challenges for use of Mg
  - Development of high strength low-cost Mg MMC – Pacific Northwest National Laboratory PNNL/Supplier
    - Current Mg alloys will have limited application for heavy vehicles
    - High strength Mg-MMC that can improve strength while minimizing cost
    - Increase durability: fatigue life more demanding than automobiles and operating temperatures/creep resistance needed
  - Develop economical manufacturing/casting/compositing method
    - Stir-cast Mg process development
    - Hybrid lost-foam/pressure infiltration casting to be demonstrated
- Application of Mg to heavy vehicles
  - How and where best to use Mg – PNNL/OEM
    - Design guidelines and property database needed
  - Manufactured part cost – OEM/Supplier/PNNL
    - Issues with integration of Mg into vehicle manufacturing process

Accomplishments

- Down selection of Mg powertrain component for project application focus: transmission case w/ potential for 50% weight reduction over Al case.
- Experimental trials for stir-cast Mg-MMC production performed.

Future Direction

- Develop compositing ability to in-situ cast and mix a Mg composite casting.
- Evaluation of a modified lost-foam casting process that combines casting and compositing into one process step.

Introduction

Ultra-lightweight high-performance Mg MMCs can improve fuel utilization, while increasing component durability for heavy-vehicles. As a rule of thumb, light-weighting can contribute to roughly 6-7% mpg increase for every 10% reduction in mass an estimated 3000 lbs of mass can be targeted for reduction in heavy vehicle suspension, driveline, and transmission applications. There is roughly 200-500 lbs. of potential weight savings by redesign and replacing cast iron components with Mg-MMC. Down-sizing of ancillary fixtures can result in additional mass and fuel savings. Increased component durability in applications where wear is a factor can also lead to improved vehicle operating costs, which is an incentive for fleet owners and independent truckers to embrace the new technology.

Although Mg alloys can be easily machined into various parts, Mg really stands out when die cast. Mg can be formed into complex shapes and as a single piece, often reducing cost by eliminating several steel stampings and the associated assembly cost. One great advantage of Mg is its ability to be cast with very thin walls, optimizing design and decreasing the component's weight. The microstructure also gives the alloys good sound and vibration dampening qualities. In fact, many higher performance engines use Mg alloys for valve covers and other under-the-hood covers, to keep engine bay noise to a minimum.

Like aluminum, die cast Mg is attractive because it can design to specific yield strength, fatigue, and to a fair extent creep criteria. Even though there is little creep in Mg alloys at room temperature, at elevated temperatures (as low as 150ºC) component design needs to accommodate for significant creep factors.

Creep-resistant alloys are being developed; however, they may contain expensive alloying elements such as strontium, calcium or rare earths for stable performance at elevated temperatures. These additions have a tendency to sacrifice castability for the increased creep performance.

The objective of this project is to enhance the properties of Mg alloys by creating a Mg-ceramic composite. This class of material is usually referred to as a metal matrix composite (MMC), in which fine ceramic particles or very short fibers are added to the metal matrix to form a composite structure. The resulting composite has very high specific strength and stiffness, and significantly improved wear resistance. Thin cast sections are still possible, and in the case of Mg, NVH and load carrying capacity are increased beyond the basic alloy. This is especially beneficial for vocational trucks, where load capacity and noise are two of the more common design problems facing engineers.

Approach

This project was initiated in February of 2005, and is a collaborative effort with Mack Trucks. The project goal is to develop Mg composite casting technology and associated low-cost tooling for manufacturing of ultra-lightweight heavy-vehicle powertrain components. The project scope is broken down into three tasks: 1) Assess the potential to use Mg for vocational and long-haul trucks through technology development, evaluation of full-scale prototype components, and economic analysis; 2) Develop advance Mg materials and processing capabilities for heavy vehicle applications; and 3) Develop a low-cost shape-forming process that combines casting and in-situ compositing for metal matrix composite (MMC) components.

The specific technical approach and developments to pursue are outlined as follows:

- Address technical challenges for use of Mg
  - Development of high strength low-cost Mg MMC – PNNL/Supplier
    - High strength Mg-MMC that can improve strength while minimizing cost
    - Increase durability: fatigue life more demanding than automobiles and cost-effective alternates to elevated temperature creep resistance needed
  - Develop economical manufacturing, casting, compositing methods
    - Stir-cast Mg process development
    - Hybrid lost-foam/pressure infiltration casting to be demonstrated
- Application of Mg to heavy vehicles
  - How and where best to use Mg – PNNL/OEM
    - Design guidelines and property database needed
  - Manufactured part cost – EM/Supplier/PNNL
    - Issues with integration of Mg into vehicle manufacturing process

Metal Compositing Method

Stir-casting techniques are currently the most common commercial method to produce aluminum MMC materials. This approach utilizes mechanical mixing of the reinforcement particulate into a molten metal bath. A simplified compositing apparatus is shown in Figure 1, and typically is comprised of a heated crucible containing molten aluminum metal, with a motor located above the crucible that drives a paddle, or mixing impeller that is submerged into the melt. The reinforcement is poured into the crucible above or below the melt surface and at a controlled rate, in order to insure a smooth and continuous feed. As the impeller rotates at moderate speeds, a vortex is generated in the aluminum melt that draws the reinforcement particles into the melt from the surface. The impeller is designed to create a high level of shear in the aluminum melt, which helps strip adsorbed gases from the surface of the particles and engulfs the particles in molten aluminum, which promotes proper aluminum-reinforcement wetting. In addition, proper mixing techniques and impeller design must be employed, in order to produce adequate melt circulation and homogeneous distribution of the reinforcement throughout the matrix material.

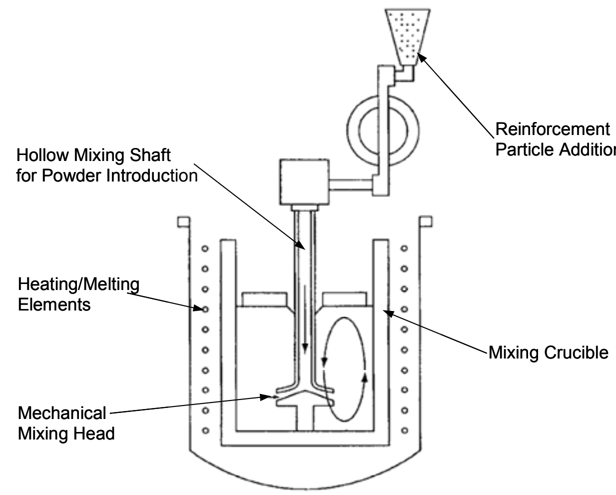

Figure 1. Schematic of MC-21 rapid mixing concept and compositing chamber setup.

Experimental investigation of stir-cast Mg-MMC production method was initiated in FY2005. This process will be developed, along with a hybrid compositing/casting method for the production of Mg-MMC components. The hybrid system will consist of combining evaporative pattern (lost-foam) casting techniques and low-pressure infiltration to create the metal-ceramic composite during the shape forming (casting) operation. This second process, though a higher technical risk for success, would significantly reduce component manufacturing cost. It is also expected to allow for easy selective reinforcement of cast components, where the reinforcement particles are placed only where there will have the greatest benefit to part performance.

Mg MMC Development

In order to develop proper Mg-MMC materials for powertrain components, it is necessary to investigate alloy-reinforcement combinations that will work best to achieve the mechanical performance and the environmental performance goals as well. To accomplish this task, a stir-cast metal composite mixer has been designed by MC-21 Inc., Carson

City, Nevada, that will be constructed and installed at PNNL in the first quarter of FY2006. With this capability, multiple combinations of alloy-reinforcement chemistry can be produced and evaluated.

The micromixer is to be designed based on MC-21's experience in aluminum MMC mixing units and proprietary mixing technology. This technology is unique in the fact that it is a highly efficient means of mixing together (compositing) ceramic and molten metal, resulting in a metal composite material.

The mixing unit will be constructed such that it can melt and mix Mg alloy, with the following capabilities:

- Utilize MC-21's rapid mixing technology and stir-head design for incorporation of ceramic particulate of various chemistries and sizes in the 5-50 micron range.
- A special mixing head will be employed for use with Mg composite mixing.
- Mixing container capable of tilt pouring all of the liquid in the crucible.
- Able to melt and stir 10 kg of Mg or aluminum metal in a single batch.
- Use of an electric resistance melter and temperature control capable of 1500°F maximum.
- Specially designed crucible for casting and mixing reactive metals such as Mg.
- Crucible and heating system will be designed for an inert-gas atmosphere or addition of a vacuum chamber for mixing in an atmosphere or down to 0.1 torr pressure.
- Perform mixing action in either liquid (fully molten) or semi-solid (partially molten) state.
- Stirring mechanism will be hydraulically driven, with variable speed control up to 2000 rpm.

Future Work

For FY2006, the project scope will focus on completing the economic analysis of commercial Mg MMC micromixer design, install the new stir-casting unit being constructed, and initiate compositing trials of new Mg alloy and ceramic particulate combinations. These composites will then be evaluated for mechanical and physical properties, and down-selected to the combination(s) that will meet design and component performance needs.

In-situ casting/compositing experiments will be pursued to demonstrate the ability to in-situ cast and mix a Mg composite casting. The project team will also generate a performance and design allowable matrix for selected prototype truck components.

Publications and Presentations

None to report.

Summary

Mg Metal Matrix Composites (MMC) have outstanding specific strength and stiffness properties, as well as NVH dampening characteristics greater than Mg alloys alone. They also have enhanced wear and creep resistance over unreinforced alloys. One drawback to Mg and its MMC is that the supply base has all but disappeared in North America, requiring OEMs and specialty/prototype casters to assume production roles. The focus of this project is to develop manufacturing technologies that allow for the production of low-cost Mg MMC components. It is intended that the low cost process can be applied by either an OEM, or the technology easily transferred to a supplier. The development of Mg composite casting technology will include low-cost tooling approaches for manufacturing of ultra-lightweight heavy-vehicle powertrain components, as well as the development of low-cost shape-forming process that combines casting and in-situ compositing for MMC components.

G. Lightweight Stainless Steel Bus Frame—Phase III

Principal Investigator: J. Bruce Emmons
Autokinetics Inc.
1711 West Hamlin Road, Rochester Hills, MI 48309
(248) 852-4450; fax: (248) 852-7182; e-mail: jbemmons@autokinetics.com

Chief Scientist: James J. Eberhardt
(202) 586-9837; fax: (202) 587-2476; e-mail: James.Eberhardt@ee.doe.gov
Field Technical Manager: Philip S. Sklad
(865) 574-5069; fax:(865) 576-4963; e-mail:skladps@ornl.gov

Contractor: Autokinetics Inc.
Contract No.: 4000010114

Objectives

- Investigate and demonstrate the mass saving potential of ultra-high-strength stainless steel as applied to the structure and chassis of a full-size urban transit bus.
- Finalize design and analysis and build a full-scale prototype of the body structure and chassis.
- Investigate all of the fundamental feasibility issues related to the structure and chassis:
  1. Fabricate and test large lightweight stainless steel sandwich panels
  2. Fabricate roll-formed, high-strength stainless steel sections
  3. Test feasibility of lightweight stainless steel cantilever seats
  4. Design and fabricate lightweight stainless steel independent suspension
  5. Integrate the traction motors into the suspension design

Approach

- Execute the basic body structure, including the floor/roof sandwich panels, pillar assemblies, longitudinal rails, and suspension subframes.
- Choose prototyping techniques that emulate the intended production process as closely as possible to aid in developing robust but cost-effective manufacturing techniques essential to meeting the objectives of the project.
- As computer-based design and analysis details of the bus develop, conduct hands-on physical experimentation in parallel to support the concepts and methods.

Accomplishments

- Received delivery of gear reduction units.
- Finalized detail drawings and preparations to cast rear suspension components.
- Progress on braking system.
- Progress on glass.
- Refinement of side impact analysis.
- Provided support for independent cost analysis.
- Received delivery of cooling system for motors and inverters.

- Fabricated driver controls.

Future Direction

- Complete the fabrication and installation of suspension, steering, and spring components.
- Assemble propulsion components.
- Assemble close-out panels.
- Complete fabrication and install glass.
- Prototype two seats.
- Testing of structure.

Introduction

Advanced technology transit bus concepts have made significant advancements in terms of light weight and fuel economy. However, these gains have come at the expense of higher manufacturing costs. In spite of attempts to use life-cycle costs to justify their purchase, initial cost remains a major obstacle to the introduction of fuel-efficient buses.

Autokinetics was approached by the Office of FreedomCAR and Vehicle Technologies (OFCVT) of the U.S. Department of Energy to attempt to solve this problem. Specifically, the OFCVT asked Autokinetics to develop concepts for a lightweight urban transit bus based on the use of high-strength stainless steel. In the passenger car field, Autokinetics had developed structural and manufacturing techniques for the cost-effective use of stainless steel in spaceframes and suspensions. The OFCVT wanted to determine whether this approach could be applied to transit buses as well.

The program was structured in three phases:

- Phase I – Initial Concept Development
- Phase II – Concept Verification and Initial Design
- Phase III – Final Design and Prototyping of Body and Chassis

Phase I and Phase II have been successfully completed. Phase III will result in a full-size body structure and suspension that will be tested statically and dynamically. The development of an optimized hybrid powertrain and other vehicle systems will be addressed in a separate project.

This project was unusual in that no formal mass or cost targets were given. The object was to save as much mass and cost as possible.

Current State of Progress

As stated in the previous progress report, the overall body structure is nearing completion. Much of the focus during this reporting period has been shifted to the final design of suspension components, and initiating their fabrication. Considerable effort was also spent on specification and acquisition of propulsion hardware such as traction motors, controllers, and reduction gears.

Rear Suspension Components

As reported previously, a change in the traction motor selection required adjustments in the rear suspension design to accommodate the different physical characteristics of the new motor. During this reporting period, much of this refinement work was completed and detailed designs for the rear suspension componentry were prepared.

Other open issues were resolved such as procuring physical hardware for the gear reduction unit and brake drums. At this point, we are now ready to begin releasing suspension components for fabrication.

Braking System

An extensive search was conducted to identify any readily available brake systems that would be compatible with this unusual suspension/drive system combination (i.e., hub-mounted motors in an independent suspension). Both drum and disc type brakes were explored. It was found that the selection of designs for 19.5 inch wheels is quite limited. Unfortunately, no brake systems were found that could meet the capacity requirements and be packaged in the available space.

Some common issues found among drum brake systems were; shoe position too far inboard interferes with the hub-mounted motors, "S" cam and hydraulic actuators further complicate this interference, shallower drums are too large in diameter to allow adequate cooling air space between drum and wheel, and shoe design interferes with wheel bearings.

Even among disc brake systems, significant issues were found which include; caliper position interferes with the wheel-motor at the rear axle and the steering arms at the front axle, and the low profile wheels necessitate a disc mounting configuration which would complicate maintenance and add mass.

As a result, a hydraulic drum brake system, unique to this application, was designed. It is based on the dual shoe principal (common practice) but omits the self-energizing, leading shoe geometry. This approach results in reduced sensitivity to fade, water, and oil. The design is proportioned to fit the wheel-motor and independent suspension arrangement. With this design, all major components are common among all four corners with the exception of wheel cylinders. The front cylinders are larger than the rear cylinders in order to achieve hydraulic proportioning of the brakes from front to rear. The wheel cylinders will consist of specially fabricated housings. However, commercially available pistons, seals and boots will be used. The brake shoe anchorage points and wheel cylinder mountings have been integrated into the knuckle casting design, eliminating the traditional large, heavy anchor plate. Webb Wheel Products (Cullman, Alabama) has supplied prototype brake drums by modifying an existing design. Autokinetics will fabricate the brake shoes and assemble the system.

It is expected this effort will yield a simple and effective brake system for this vehicle, and possibly find future applications in similarly configured suspensions.

Body Glass

Laminated glass was chosen for all glazing positions because it provides a number of benefits over tempered glass. Since it is stronger than tempered glass, thinner and therefore lighter panes may be used. Laminated glass offers much better damping characteristics, resulting in improved NVH performance. This is especially important with the relatively large, nearly flat windows. Laminated glass also provides greater safety in the event of breakage or vehicular crash. Furthermore, it was found the laminating layer could contain special materials for solar rejection and thermal absorption as well as tint. The lighter weight and thermal properties will contribute directly to energy efficiency of the overall vehicle.

Fox Fire Glass (Pontiac, Michigan) was selected to fabricate the prototype glass for all side windows and the two-part windshield. All tooling for the prototype glass was completed during this reporting period.

For the side glass, which requires only a simple, cylindrical curvature, stainless steel draping forms were designed and fabricated by Autokinetics using techniques similar to the floor and roof sandwich panels. All side window pieces can be formed on these common tools and trimmed to the required length per individual piece requirements.

The windshield, however, requires compound curvature and must be made on more complex ceramic tooling. To simplify fabrication and installation, one, two, and three piece windshield configurations were studied. It was determined the two-piece configuration would provide a good combination of piece size and economical tooling. Final surface data for the windshield halves was generated and sent to Fox Fire to create the tooling. A number of laminated glass samples with various color and solar rejection material combinations were created to evaluate through-visibility and general appearance. The combination of light blue-gray tint with Solutia's Vanceva^{tm} "honeycomb" solar rejection product, in the side and rear glass only, was chosen.

As of the end of this reporting period, all side glass has been fabricated. Glass for the windshield has also been formed and is in the final steps of processing. It is expected that all glass will be delivered and installed onto the body structure very soon.

Side Impact Analysis

As reported previously, initial side impact analysis indicated the necessity to reinforce the lower portion of the side pillars (in the impact zone). A variety of concepts were generated and evaluated to solve this problem. The most promising approach appears to be reconfiguring the pillar section profile as a "hat" section roll formed with the flanges and the open portion of the "hat" oriented toward the outside of the vehicle. This open portion would be bridged, by attaching (spot-welding) a strip from flange to flange, along the length of the pillar, to create a closed box section.

This arrangement is much more accessible for spot-welding, allowing more welds and locating the welds such that stresses on the individual welds are within allowable limits.

This configuration also potentially offers additional benefits such as; a simple one-piece joint for attachment of the pillars to the sandwich panels, more streamlined assembly, the ability to tailor material thickness along the length of the pillar, and to provide a continuous attachment flange around the entire periphery of the window openings.

This enhancement is proposed as a design change for future versions of the body structure only, and will not be incorporated into the current prototype build.

A nonlinear finite element analysis of this design modification was performed by Srdjan Siminovic and Gustavo Aramayo of the Oak Ridge National Laboratory (ORNL). The results of this analysis indicate a high likelihood of meeting side impact requirements in the production version of the bus.

Independent Cost Analysis

The Department of Energy commissioned IBIS Associates (Waltham, MA) to conduct an independent cost analysis of the stainless steel bus structure concept in comparison to current practices. (A separate description of the study can be found in Report 5.I in this same publication. A production forty-foot, low floor metropolitan transit bus was used as a basis for comparison. Separate *Technical Cost Models* were developed for a conventional bus body structure and the stainless steel concept with their respective processing techniques. Data collected from major North American transit bus and coach manufacturers were compiled for the conventional model, and Autokinetics provided data for the stainless steel concept.

Initial results were presented during this reporting period. The conclusions drawn indicate a compelling economic case for the stainless steel concept. The study found the weight saving design and associated processing techniques produced savings that more than compensated for the greater cost per pound of the stainless steel. IBIS also points out that further gains result as additional items are accounted for such as roof, flooring, and skins which are not considered part of a conventional structure but are integral to the stainless steel concept.

The actual manufacturing cost savings are projected to be on the order of 30%. This is a rather unusual result in that a new concept which improves performance and reduces weight can be manufactured at a lower cost.

Cooling System

A cooling system is needed to remove waste heat generated by the traction motors and controllers, and keep the temperature of critical electronics within acceptable limits. The two traction motors and controllers are liquid cooled, so a conventional automotive type radiator could be used. Brushless DC motors were specified for the pump and fans to increase efficiency and reduce maintenance. A complete cooling system was designed, and components of appropriate capacity were acquired and assembled.

Dissemination and Commercialization

10/18/04 – Emmons presented a project review at ORNL. Attended by Dr. Sidney Diamond, Dr. Joseph Carpenter (DOE), Dr. Phil Sklad, Srdan Simunovic, et.al. (ORNL), and Tony Mascarin (IBIS Assoc.).

11/02/04 – Meeting with Michigan State University (MSU). Attended by Al Bierut (MSU).

11/17/04 – Meeting with Electric Power Research Institute (EPRI). Attended by Kurt Yeager (EPRI) and entrepreneur John Friedl (TerraDyne).

11/23/04 – Meeting with NextEnergy. Attended by Rachel Kuntzsch (NextEnergy) and Vince Nystrom (Michigan Economic Development Corp - MEDC).

12/06/04 – Meeting with MSU. Attended by Gerry Skellenger (MSU).

12/17/04 – Emmons presented a project overview at MSU ARES lab. Attended by Dr. Harold Schock, Al Bierut, et al., (MSU) and Mr. James Croce (NextEnergy).

1/12/05 – Commercialization discussion with John Friedl (TerraDyne).

1/27/05 – Emmons attended Global Insight seminar "Future Heavy-Duty Powertrain Technologies".

2/22/05 – Meeting with MSU-HEV team. Attended by Dr. Harold Schock, Al Bierut, Gerry Skellenger, Dr. Elias Strangas, Dr. Peng (MSU), Rachel Kuntzsch (NextEnergy), and Vince Nystrom (MEDC).

7/ 18-7/20/05 – Emmons attended a Transportation Familiarization Tour in Chattanooga, TN. Sponsored by ATTI and the Chattanooga Chamber of Commerce.

9/14/05 – Emmons presented a summary of the lightweight bus project at a special project peer review at ORNL.

Conclusions

Autokinetics remains confident that high-strength stainless steel has the potential to achieve substantial mass reductions of bus structures. The bus body structure is now nearly complete; most of the identified technical risk issues have been resolved; and structural and chassis mass estimates remain nearly unchanged compared with early predictions. Ongoing fabrication of the physical prototype has provided concrete mass numbers and it is now expected the actual mass reduction of the complete battery electric vehicle will be close to 50%.

It is also hoped that practical commercialization can be achieved in the not too distant future. Low capital investment and ample knowledge base are key enablers for this. Much has been learned thus far about processing and assembling of the body structure and many useful techniques have been developed. Given the relative ease of constructing this prototype within our own facility, it is quite apparent that capital requirements for commercializing this technology will be relatively small.

The independent cost analysis commissioned by the Department of Energy supports this as well as the predicted mass and unit cost savings.

H. Side Impact Analysis of a Lightweight Stainless Steel Bus Structure

Principal Investigator: Srdjan Simunovic and Gustavo A. Aramayo
Affiliation: Oak Ridge National Laboratory
Address: P.O. Box 2008, MS-6164
(865) 241-3863; fax: (865) 574-7463; e-mail: simunovics@ornl.gov

Chief Scientist: James J. Eberhardt
(202) 586-9837; fax: (202) 587-2476; e-mail: James.Eberhardt@ee.doe.gov
Field Technical Manager: Philip S. Sklad
(865) 574-5069; fax:(865) 576-4963; e-mail:skladps@ornl.gov

Contractor: Oak Ridge National Laboratory
Contract No.: DE-AC05-00OR2272

Objective

- The objective of the research was to model and evaluate the structural performance of a Lightweight Stainless Steel Bus Structure (LSSBS) to a side impact by a Sport Utility Vehicle (SUV). The evaluation of the initial design led to design modifications that were shown to significantly improve the side impact performance.

Approach

- The impact analysis simulation is conducted using the Finite Element Method (FEM) computer program LS-DYNA. A detailed model of central five-column long section of the LSSBS has been developed to model the deformable area of collision. The front and end sections of the bus were modeled with less detail. Their role was to better simulate overall vehicle kinematics as compared to initial simulations reported in 2004. The FEM model of the SUV was developed at the Oak Ridge National Laboratory (ORNL) under a project sponsored by the Department of Transportation. The two models are combined into a side impact collision scenario. The simulations were performed on the ORNL Center for Computational Sciences supercomputers.

Accomplishments

- A detailed side-impact model of the LSSBS and has been developed. The simulations lead to several design modifications that resulted in a safer design without compromising on vehicle weight, production cost and energy efficiency.

Future Direction

- This report concludes the research on side impact structural safety of the LSSBS. The developed model can also be extended for other structural performance investigations that are outside the scope of current research, such as structural vibrations, dynamic response, and static loading problems.

Introduction

The ultra light stainless steel urban bus concept (LSSBS) was developed by Autokinetics, Inc. [1] with an objective to demonstrate feasibility of stainless steel [2] structural design for weight reduction in mass-transit vehicles. The resulting bus employs high strength stainless steels and monocoque design in order to simultaneously achieve the weight reduction and to maintain or surpass the performance of the conventional bus designs. Bus body structure is shown in Figure 1.

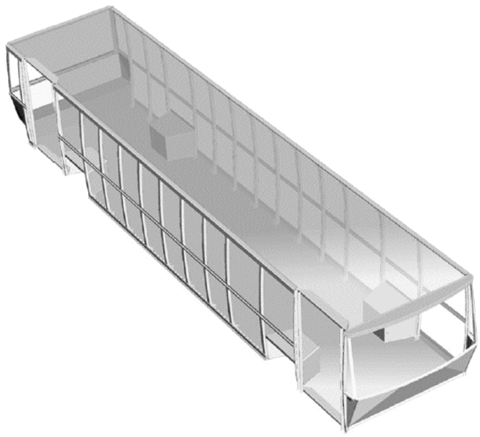

Figure 1. Ultralight Stainless Steel Bus Structure.

Bus performances with respect to torsional and flexural rigidities and axial impact have been investigated using computational models. The side impact response was the subject of this research. A collision model scenario that is considered to be a good measure of the side impact performance of the bus is a simulation of an impact of a mid-size SUV-class vehicle [3] into the half span of the bus. One of the distinctive performance advantages of the LSSBS is its low floor, but because such design makes the point of impact of the SUV above the bus floor, the impact load and energy management must be efficiently transferred to the floor and roof structures while maintaining a safe zone for the passengers. The other essential structural LSSBS component that comes directly into contact with the impacting vehicle is the lower reinforcement rail. This rail is supposed to distribute the impact force between the neighboring pillars. The bus floor and the roof are the final destinations of the SUV impact load. In order to achieve a controlled load transfer into the floor and roof it is necessary to maintain a reasonable stability of the pillars and the reinforcement rail. Joints connecting pillars into the floor/roof must distribute the load very quickly without creating local instabilities or joint failure. Figure 2 shows the initial design of the pillar and roof joint.

Impact simulations with the initial design showed that the open geometry of the pillar cross-section does not provide desired structural strength. The cross-section of the pillar has been changed to a closed top-hat section. The new pillar cross-section, together with the connection to the roof is shown in Figure 3.

Design changes in one component may affect the overall management of the impact load, so that this change lead to review and modifications of pillar connections with other components, primarily of the floor and roof brackets in order to optimize the structural response. Location, geometry and bonding of the joint brackets are important for local load transfer and therefore, it is necessary to model them in sufficient detail to determine the local stability of the connection. Detailed computational FEM models have been developed to adequately address the above issues, and to provide a framework for evaluation of the LSSBS in the side impact.

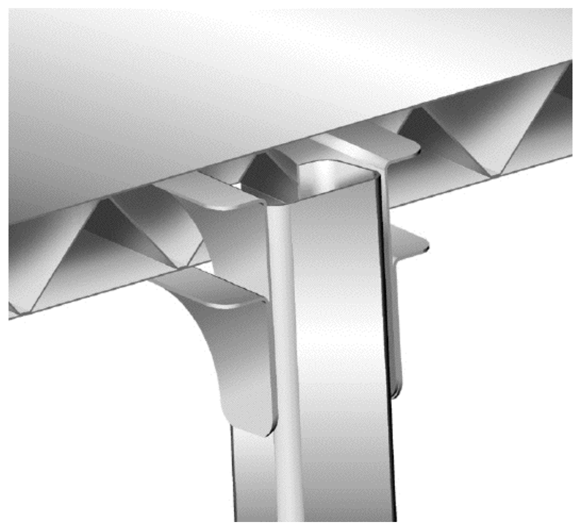

Figure 2. Pillar joint detail.

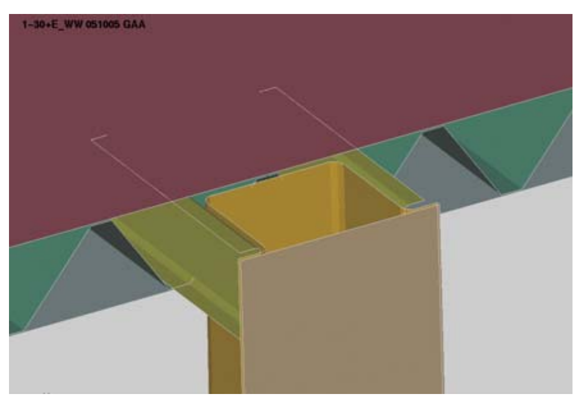

Figure 3. Modified pillar joint detail.

Development of the FEM Model

The development of the FEM model of the bus structure involved several steps. The basic geometry data was used to generate surfaces for the FEM mesh generation. The data was provided for a single typical section ('segment') of the structure, Figure 4. Repeated reflections and translations are used for the generation of the model used in the analysis.

The integrity of the body structure is provided almost exclusively by spot welds. Therefore, in order to create a realistic model for side impact it was essential to include them in the model. A graphical representation of the spot weld locations is shown in Figure 5.

The FEM model was developed using the spot weld locations as key locations for the mesh generation so that the location of the spot welds exactly matches the location specified in the solid model geometry. The developed FEM model for the ten base segments is shown in Figure 6.

FEM Simulations of Side Impact

The FE model has been developed as a combination of two components: a plastically deformable central section that includes the detailed model of the structural components and non—deformable

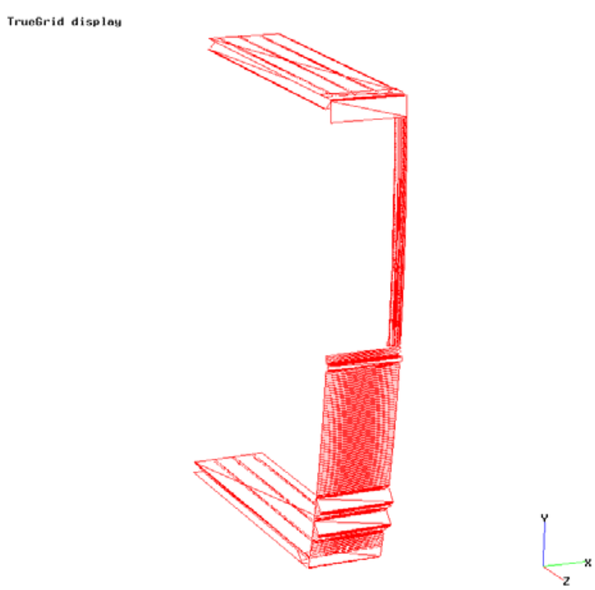

Figure 4. ViewPoint surfaces of bus 'segment' model.

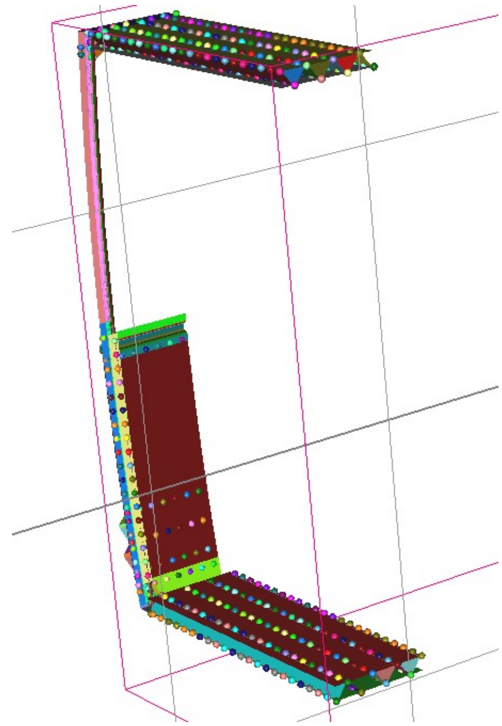

Figure 5. Spot Welds in Bus 'segment'.

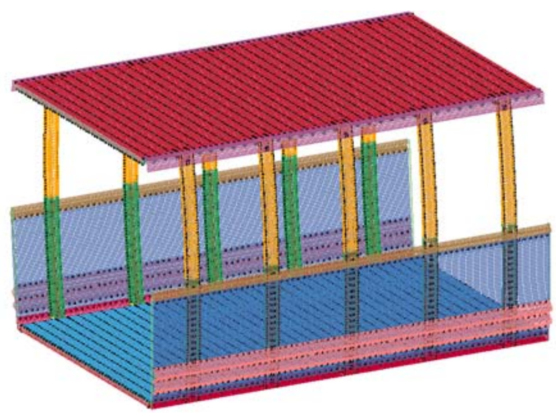

Figure 6. FEM Model of the central bus section.

idealization of the front and rear sections of the bus. The objective of the non-deformable components is to provide a good estimate for the overall kinematics and weight distribution. The non-deformable component and the final bus model are shown in Figures 7 and 8, respectively.

The final step in the development of a side impact simulation was the addition of the SUV model [3]. SUV's velocity is 25 mph. Figure 9 shows the assembled impact scenario.

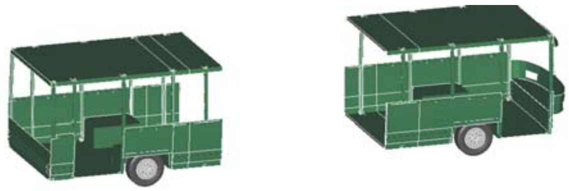

Figure 7. Non-deformable components of the FEM model.

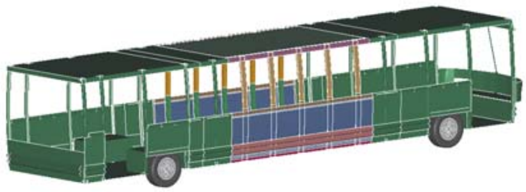

Figure 8. Final FEM model of the LSSBS bus.

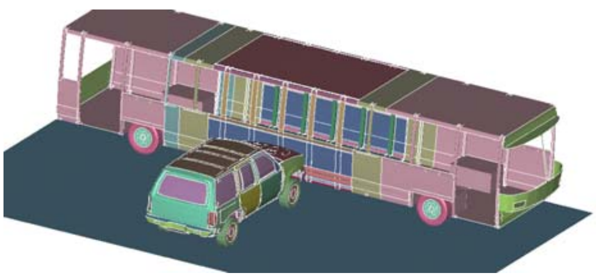

Figure 9. FE Model of Ford Explorer-BUS used in analysis

The combined Ford Explorer-BUS FE model has a total of 709723 nodes, 691258 shell elements, 3178 solid elements, 449 beam elements, 10396 spot-welds, 11 contact entities.

FEM analyses were performed for numerous bus designs under considerations. Figure 10 shows the cross section of the final model at the time of maximum intrusion in a plane that includes the pillar at the point of contact and normal to the axis of the bus. The intrusions were measured at a point in the pillars of side panels that is 528.32 mm (20.80 inches) above the top plate of the floor panels which corresponds to the seat locations.

Figure 11 shows the cross section of the model when deformation is completed and vehicles move as rigid bodies.

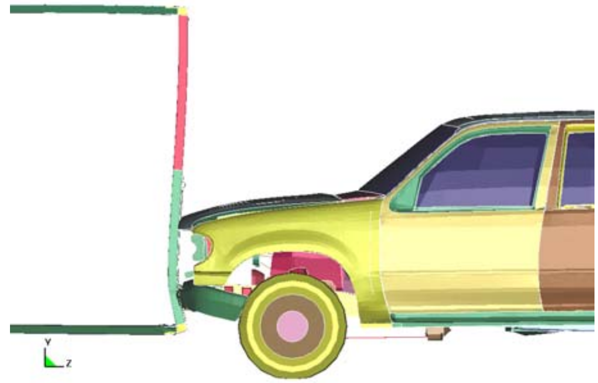

Figure 10. Cross-section of the bus at time of maximum intrusion.

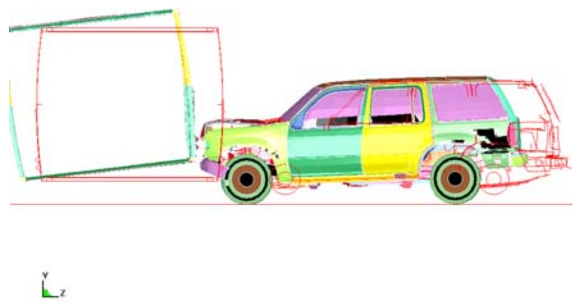

Figure 11. Cross-section of SUV-BUS at time 0.3 sec. The permanent intrusion at the pillar location at the 20.80 inch elevation is equal to 2.4 inches.

Conclusions

The results of the analysis, for the impact scenarios considered, show that the permanent intrusion at the pillar section and at the mid span between the pillars is under the recommended 3 inches. The models used in the determination of intrusion have several changes that include change of thickness in the pillar hat section, pillar outer plate, top and bottom floor plates. The analysis also indicated a need for increased spot weld capacity between the pillar hat and pillar plate, and between the pillar hat and web of the supporting channel brackets. Additional possible modifications in the welding topology may further reduce the calculated intrusions.

The analyses show that the requirement for low intrusion values is based on the ability to maintain integrity at the web-channel/pillar-hat interfaces in the roof and floor of the frame cross-section. The capability of the spot welds at these interfaces is a function of the shear capacity of these spot welds at the bracket-pillar interface that balances the moment associated with the impact force and the distance from the point of application of this force and the resultant shear force on the spot welds. It is likely that by re-arrangement of the spot weld pattern the stiffness of the bracket-pillar interface can be further optimized.

References

1. Emmons, J.B, Blessing, L.J., Ultralight stainless steel urban bus concept, SAE Technical Paper 2001-01-2073, Government/Industry Meeting, Washington, DC, 2001
2. Knueppel, B., "True Stress/True Strain plots for Nitronic 30 Material", ARMCO Inc, October 1996.
3. Aramayo, G., Parametric finite element model of a sport utility vehicle; development and validation, 7th International LS-DYNA users Conference, Dearborn, MI, 2002
4. Hallquist, J.O. LS_DYNA-Keyword User's Manual, Version 970, LSTC, April 2003

I. Stainless Steel Bus Structure—Manufacturing Cost Analysis

Principal Investigator: Anthony E. Mascarin
IBIS Associates, Inc.
1601 Trapelo Road, Suite 164
Waltham, MA 02451
(781) 290-040; fax: (781) 290-0454; e-mail: tony@ibisassociates.com

Chief Scientist: James J. Eberhardt
(202) 586-9837; fax: (202) 587-2476; e-mail: James.Eberhardt@ee.doe.gov
Field Technical Manager: Philip S. Sklad
(865) 574-5069; fax:(865) 576-4963; e-mail:skladps@ornl.gov

Contractor: IBIS Associates, Inc.
Contract No.: 4000030946

Objectives

- Provide the bus development program with manufacturing cost analysis and economic understanding to plan a technology and application development strategy.
- Assess the cost of conventional and proposed stainless steel bus structure fabrication.
- Explore the impact of key design and process assumptions.
- Characterize the potential commercial value of the concept.
- Extend previous baseline structure comparison to include floor, skins, and roof for conventional bus, and pillar reinforcements for stainless steel design.

Approach

- Collect design and assembly data from manufacturers, materials and pricing from suppliers.
- Characterize SS pillar reinforcements and assembly requirements.
- Update baseline analyses and comparisons.

Accomplishments

- Collected data on conventional floor, skin and side assembly from production facilities.
- Update cost model and scenario designs.
- Presented side-by-side cost comparison of stainless steel concept to incumbent practice.
- Analyzed sensitivities to annual production volume, throughput, assembly time, etc.

Future Direction

- Assess the impact of powertrain and interior systems.
- Analyze life-cycle and usage costs in terms of fuel, operation, and maintenance costs.

Introduction

DOE, in conjunction with Autokinetics, is pursuing a design and process technology development program for alternative metropolitan bus structure manufacturing. Central to the effort is the stainless steel roll-formed design concepts developed by Autokinetics. Key to the success of this program is a demonstration of commercial viability: reduced piece cost, lower capital investment, or improved lifecycle economics relative to incumbent practices. Based on process and design scenario information provided to IBIS from the DOE/ Autokinetics team, IBIS has evaluated the alternative design concepts for these structures and provided an analysis of manufacturing economics. This analysis seeks to quantify the commercial production economics of the design and production techniques developed by Autokinetics relative to incumbent practices for conventional bus manufacturing.

Bus Structure Scenarios

The basis for comparison of the conventional bus structure to the stainless steel concept is a 40-foot, low-floor metropolitan transit bus.

Conventional bus structure manufacturing involves labor-intensive arc welding of tube stock. Sides, floors, roofs, and front and rear end units are made separately in subassembly cells on semi-dedicated fixtures (which can be modified for bus length). After final structure assembly, the frame is subjected to grit blasting and a zinc phosphate coating. The resulting structure is a 6215-lb. weldement.

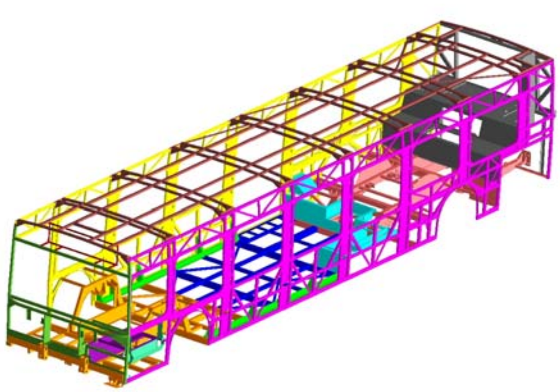

Figure 1. Conventional Bus Structure.

In summary, the stainless steel concept involves a floor and roof composed of three-layer panels made from welded outer skins and a corrugated, roll-formed core. Roll-formed pillars, rails, and sills complete the skeletal structure. Wheel wells and front and rear cap assemblies are welded from brake or press formings. The structure is assembled using spot welding.

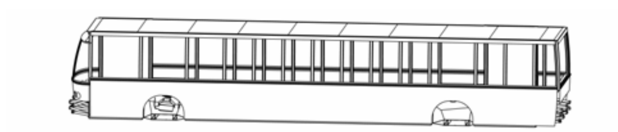

Figure 2. Roll-Formed SS Bus Structure.

The initial analysis as previously reported was strictly a structure-to-structure comparison. However, given that the stainless steel design incorporates functional floor, roof, and skins integral to the structure, the analysis was extended to include the secondary assembly of these elements in conventional scenario in order to present a more functionally equivalent comparison. Furthermore the side impact analysis suggested a need for additional reinforcement of the pillar structures for the SS design. These elements were added to the analysis and the resulting cost comparisons are presented.

Model Development

The model structures developed during the previous reporting period were used for the current analysis, using newly collected process data and updated structure designs. The conventional bus assembly cost model required the addition of an operation module to address the floor, roof, and skin assembly. The stainless steel bus model only required the addition of the additional reinforcement components and labor time for the welds required.

Data Collection

Data used in the technical cost models were collected through interviews and site visits with many sources, principally existing transit bus and motor coach manufacturers, as well as metropolitan transit authorities. Autokinetics provided design information for the stainless steel concept.
Conventional bus floors are 0.75-inch marine grad plywood. Assembly requires three laborers for ten hours to cut, place, and fasten the floor. Skins are

2.0-2.5mm Aluminum sheets that require a three-person crew fifteen hours to assemble. The roof is a two piece fiberglass (35% glass) molding. Modification to the SS design included the additional of 24 reinforcing plates requiring 110 spot welds each and improved pillar bracket designs.

Analyses

For comparison and simulation manageability, operations for each scenario were grouped as shown in Figures 3 and 4. The resulting cost breakdown by operation and sensitivities to annual production volume are shown in Figures 5 through 8. Figures 9 and 10 show the comparison of the direct manufacturing cost between the conventional and stainless steel scenarios.

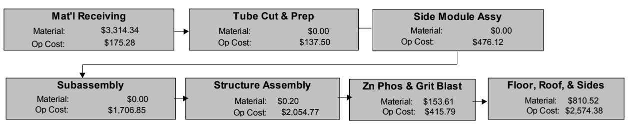

Figure 3. Conventional Process Flow.

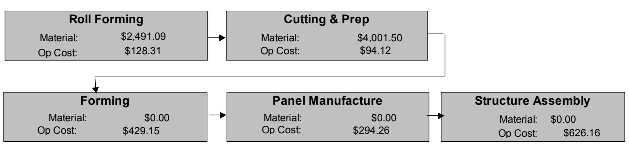

Figure 4. SS Structure Process Flow.

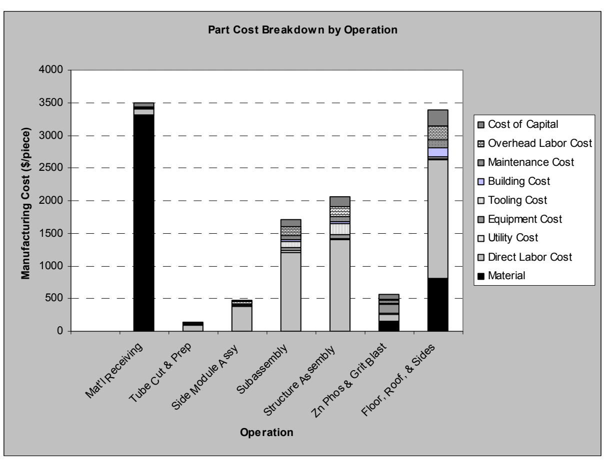

Figure 5. Conventional Manufacturing.

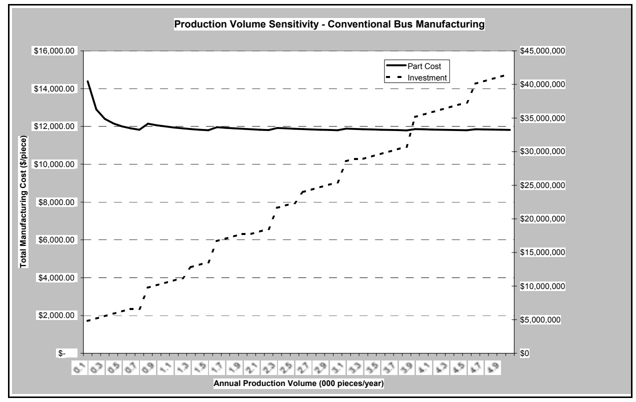

Figure 6. Production Volume Sensitivity.

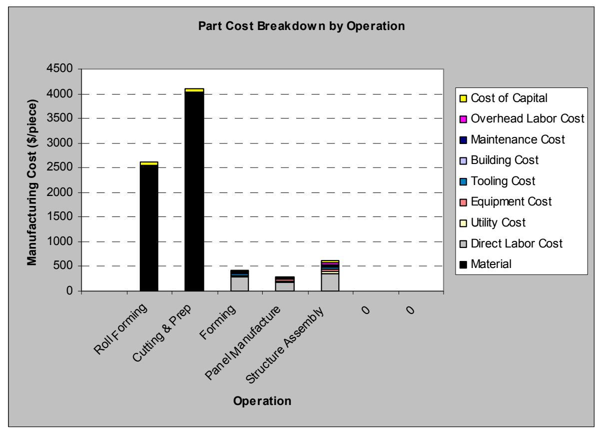

Figure 7. SS Structure Manufacturing.

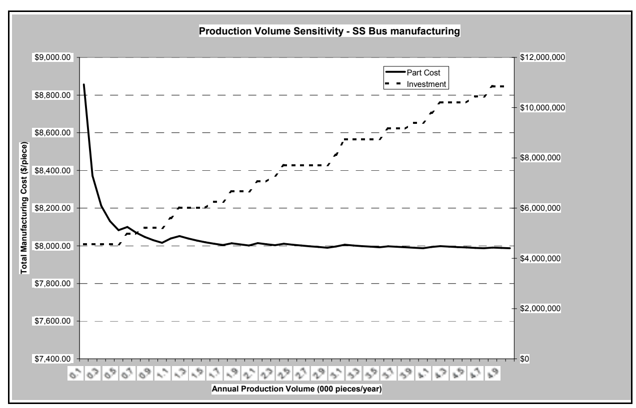

Figure 8. Production Volume Sensitivity.

COST SUMMARY BY OPERATION	$/part Conventional	$/part Stainless	
Total Material	$3,468.15	$6,492.59	Total Material
Roof, Floor, & Side Material	$810.52		
Mat'l Receiving	$175.28	$128.31	Roll Forming
Tube Cut & Prep	$137.50	$94.12	Cutting & Prep
Side Module Assy	$476.12	$429.15	Forming
Subassembly	$1,706.85	$294.26	Panel Manufacture
Structure Assembly	$2,054.77	$626.16	Structure Assembly
Zn Phos & Grit Blast	$415.79		
Floor, Roof, & Sides	$2,574.38		
TOTAL MFG COST	$11,819.37	$8,064.59	

Figure 9. Cost Comparison Table.

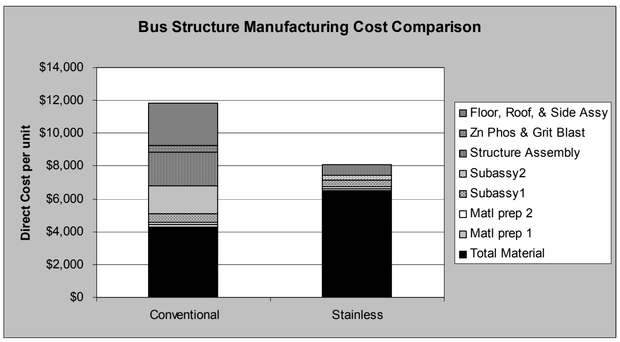

Figure 10. Cost Comparison Chart.

The production volume sensitivities in Figures 6 and 8 show how both per-unit manufacturing costs and facility investment totals change as a function of annual production volume. The baseline assumption for the analysis was 720 units per year based on typical model production volumes. The sensitivity analysis explored the range of 100 to 5000 units per year. In each chart, the left hand axis reflects unit manufacturing cost for the solid line, while the right hand axis displays fixed investment for equipment, tooling, and building space, relating to the dotted line.

Conclusions

In addition to the weight savings gained from the stainless steel design [current numbers show approximately 1000 lb. (based on the 6215 lb. conventional steel tube structure vs. the 5300 lb. roll formed stainless steel structure), plus an additional 850 lbs. accounting for the mass of flooring, skins, and roof already integral to the structure], the manufacturing economics of the stainless steel design are compelling, even more so in this updated analysis than the earlier baseline. The combination of the novel design approach, using roll forming and high-rate spot welding (instead of arc welding), allows for a reduction in assembly labor and fixturing to offset the much greater material price of stainless steel relative to the steel tube stock.

In the updated phase of the analysis, the cost and mass of the stainless design was increased by the addition of the reinforcement elements to the structure pillars. However, this increase (217 lbs.) was more than offset when the comparison is made to the conventional bus including floor, roof, and skins (850 lbs.).

As the program moves into the next phase of demonstrating a working powertrain, the extended benefits of the lightweight structure on reduced power requirements and secondary mass savings can be explored. The economic analysis can also be employed to demonstrate to potential manufacturers the specific capital requirements needed for commercializing the proposed concept.

6. Application of Innovative Materials

A. Carbon Fiber SMC for Class 8 Vehicle Hoods

Principal Investigator: Nicholas A. Rini
Volvo Trucks North America, Inc.
P.O. Box 26115; Greensboro, NC 27402-6115
(366) 393-2771; fax: (336)-393-2773; e-mail: nicholas.rini@consultant.volvo.com

Cliff Eberle, Project Manager
(865) 574-0302; fax: (865) 574-8257; e-mail: eberlecc@ornl.gov

Chief Scientist: James J. Eberhardt
(202) 586-9837; fax: (202) 587-2476; e-mail: James.Eberhardt@ee.doe.gov
Field Technical Manager: Philip S. Sklad
(865) 574-5069; fax:(865) 576-4963; e-mail:skladps@ornl.gov

Contractor: Volvo Trucks North America
Contract No.: 4000010928

Objective

- Develop carbon fiber sheet molding compounds (SMC) and processing techniques which will enable serial production of Class 8 truck hoods with structural integrity, class A surface quality, significantly reduced mass, and competitive in costs with existing glass fiber SMC molded components.

Approach

- Accumulate material property data to establish reliable design properties that can be utilized for engineering design analysis.
- Perform finite element analysis of a carbon fiber SMC based Class 8 hood design.
- Evaluate consistency and repeatability of carbon fiber SMC material properties, processing techniques, and surface quality.
- Evaluate mass savings and costs.
- Confirm predicted results by constructing prototype hoods and performing accelerated endurance tests.
- Determine if a business case can be made for a carbon fiber hood to proceed into serial production.

Accomplishments

- Built twelve (12) prototype hoods using existing production tools to evaluate processing characteristics of various combinations of lightweight materials and successfully processed the hoods through the VTNA production paint process.
- Determined that the cycle time for carbon fiber SMC was comparable to glass fiber SMC (one minute of chemical cure) and exhibited similar flow and mold characteristics as structural grades of glass fiber SMC. This is compared to several hours of effective cure with an epoxy/autoclave system with minimal flow.
- Found from the prototype hoods that the bond strength between carbon fiber SMC components and the lightweight glass fiber SMC components varies substantially, the weakest link being the mid- and low-density

glass fiber SMC components. The interlaminar strength of the low-density fiberglass SMC (loaded with hollow glass microspheres) was considerably lower than expected, leading to poor bond performance.

- Found that the published tensile and flexural strength properties of lightweight glass fiber SMC materials are unreliable due to the methods used in determining and calculating the properties.
- Developed a preliminary carbon fiber SMC material performance specification.
- Developed a preliminary adhesive bond specification for carbon fiber SMC and lightweight fiberglass SMC bonded assemblies.
- Completed the engineering detail and assembly drawings for a lightweight hood assembled from carbon fiber inner reinforcement structures and mid-density fiberglass SMC surface panels.
- Successful Finite Element Analysis of the carbon fiber reinforced lightweight hood assembly.
- Meridian Automotive Systems designed, built, installed, and tested a small scale carbon fiber SMC compounding line to supply materials to support this research and development project.
- Obtained formal quotations for production tools, detail hood parts and hood assembly costs.
- Performed cost and weight evaluations comparing the carbon fiber reinforced hood to the same hood constructed of typical fiberglass SMC.
- Performed a business case analysis for the carbon fiber reinforced hood and determined that the cost premium for the carbon fiber hood was too high and the lightweight hood could not proceed into production.
- Conducted a roundtable discussion to identify barriers and possible solutions to using carbon fiber SMC materials in automotive production applications.

Future Direction

- Encourage and follow the development of new low cost carbon fiber material production processes.
- Evaluate low cost carbon fiber materials and surface treatments as they become available.
- Evaluate the long term supply stability of low cost carbon fiber materials.
- Look for opportunities to utilize low cost, light weight, high strength carbon fiber materials in automotive applications.

Introduction

The mass of light automotive and commercial heavy-duty vehicles can be reduced utilizing modern lightweight, high performance composite materials. The reduction in vehicle mass translates into an increase in fuel efficiency. Currently, polymeric carbon fiber composites are utilized in low volume, high performance applications such as spacecraft, aircraft, and racecars. Carbon fiber reinforced composites can reduce vehicle body mass by 40% to 60%. However, market conditions and technical barriers inhibit their use in high volume automotive applications.

Class 7 and 8 trucks offer a lower production volume, lower technical barriers, and financial incentives that can justify a modest price premium for competent lightweight materials. The aim of this Project is to accelerate the commercial implementation of high performance, lower cost carbon fiber SMC (sheet molding compound) material body components for Class 7 and 8 trucks. As utilization of carbon fiber SMC develops and the technology matures, it is foreseeable that carbon fiber SMC will migrate into the high volume automotive market.

The Project was initiated by performing a comparative finite element analysis of a hood configuration made of glass fiber SMC material that had been validated through modeling, accelerated endurance tests, and field test. Based on expected carbon fiber physical and mechanical properties, hood structural and surface component material thicknesses were reduced through several iterations to determine the effect on hood system stress states and displacements. Modal analyses were performed to determine mode shapes, and complete vehicle models were utilized to obtain dynamic responses in the frequency domain. Fatigue life comparisons were made based on the complete vehicle model transient analyses.

Based on the initial investigation, it was concluded that a competent hood could be produced with a 40% to 60% reduction in hood mass if a carbon fiber SMC material could be produced that would consistently provide the physical and mechanical properties targeted.

Carbon Fiber SMC Material Search and Comparative Testing

A search was initiated to find suppliers of polymers and carbon fibers combined in a useable sheet molding compound (SMC). Materials from Zoltec, SGL, Toray, Grafill, and others were evaluated. Early on, two significant obstacles became evident; completely wetting out the carbon fiber and defilamentizing the fiber bundles. Suppliers were worked with to optimize chemistry and processes to consistently provide carbon fiber SMC material with the targeted material properties. Recent work with carbon fiber supplier Toho utilizing large tow industrial fibers indicated some cost reduction may be reached with minor reductions in some mechanical properties.

Class A Surface Quality Development

Previous work pursuing the development of Class A surface quality carbon fiber SMC indicated that a substantial effort would be required in materials and process development to achieve the desired quality level. Because of the anticipated higher cycle times and additional processing steps, the projected cost of carbon fiber SMC for Class A surface components was estimated to be too high for commercial truck applications. Therefore, development of carbon fiber SMC for exterior Class A surface quality components was held in abeyance in order to pursue lower-cost, lightweight, low and mid-density glass fiber reinforced SMC for Class A surface components. In searching for a lightweight material that would provide Class A surface quality, a low-density, glass microsphere loaded glass fiber SMC was found that showed promise. However, prototype hood parts made from the material did not develop the mechanical properties indicated on the material specification sheet. Hood assembly bond strengths were also significantly lower than expected.

Assembly Process Evaluation

To evaluate the processing characteristics of various combinations of lightweight SMC materials, 12 prototype hoods were built using the production tooling from an existing hood. The prototype hoods were fabricated using low-density and mid-density glass fiber SMC Class A surface quality outer panels, with inner reinforcements constructed of glass or carbon fiber reinforced SMC. The prototype hoods were used to assess manufacturing process variability, dimensional stability, and adhesive bonding characteristics. To evaluate the viability of the lightweight materials in the production environment, the hoods were run through the normal assembly plant production processes and evaluated for surface quality, paint quality, and bond read-through. No unusual production assembly process problems were found.

Cost and Weight Evaluation

Initial concept work concluded that a 40% to 60% weight reduction was within range, as samples in the required reduced material thickness were successfully molded. Preliminary cost estimates of the carbon fiber SMC hood indicated a higher than expected cost premium based on the then current best estimate of CF SMC material costs. Therefore, alternative constructions utilizing carbon fiber only in areas requiring high strength and stiffness were pursued. During the course of the Project, carbon fiber costs continued to rise and are now at a level almost three times their cost at the beginning of the Project. When the formal quotes for the carbon fiber hood were reviewed, it became apparent that a business case for the hood could not be made. It was then decided to cease work on the carbon fiber hood.

Conclusions

The Project has made good progress in identifying materials and processes that could be utilized in automotive body structural applications. Molding and bonding processes are very similar to existing glass fiber SMC processes, requiring only minor adjustments in process variables. Most of the potential weight reduction was achieved. Good progress was made in the development of carbon fiber SMC materials for Class A surface quality applications. However, the lengthened process for Class A surface quality components was projected to be too expensive for commercial vehicle applications, and development was not pursued further.

The main impediments to the utilization of carbon fiber SMC in automotive applications are the cost and supply stability of the carbon fiber material. Compared to the commodity glass fiber, which is a competitively priced, mature, mass produced unspecialized product available in adequate supply, carbon fiber is an emerging specialty product available from few sources in limited supply at market driven prices. Further, much of the carbon fiber currently produced is utilized in government supported applications (aerospace, aviation, military, security, marine, and energy), which to some degree removes competitive pricing pressure. It appears that a breakthrough process for mass producing carbon fiber from a readily available and stable source of raw materials is required to bring carbon fiber costs down to levels that can be utilized in automotive applications.

B. Application of Carbon Fiber for Large Structural Components

Principal Investigator: Kevin L. Simmons
Pacific Northwest National Laboratory
P.O. Box 999, MSIN: K2-44, Richland, WA 99352
Phone 509-375-3651, Fax 509-375-2186, kl.simmons@pnl.gov

Chief Scientist: James J. Eberhardt
(202) 586-9837; fax: (202) 587-2476; e-mail: James.Eberhardt@ee.doe.gov
Field Technical Manager: Philip S. Sklad
(865) 574-5069; fax: (865) 576-4963; e-mail: skladps@ornl.gov

---

Contractor: Pacific Northwest National Laboratory
Contract No.: DE-AC06-76RLO1830

Objective

- To develop selective reinforcement technology that can be applied to large truck components to improve specific stiffness and strength while reducing overall component weight.

Approach

- Determine how well the low-cost carbon fibers can be hybridized with glass fibers to provide substantial weight and cost reductions in large cab components.
- Develop a system for preforming carbon and glass fibers together that will allow components to take maximum advantage of the capabilities of selective reinforcement alignment and property contribution.
- Develop models for the analysis of hybrid chopped fiber preforms and composites that allow the thermal and structural properties to be developed and compared to experimental analysis.
- Perform structural testing to define the limits of applicability of the carbon/glass hybrid reinforcement materials to the large structures and develop guidelines for applications that may be utilized by original equipment manufacturers (OEMs).
- Design and develop critical sub-section components of large structures to use in correlation to the predictive models, and to validate the structural application criteria. Determine the capability of the materials to be fabricated in full-scale components and determine the performance of these full-scale components in real application scenarios.

Accomplishments

- Developed the first Class A structural carbon composite panels for truck applications.
- Developed hybrid carbon composite with improved impact performance over fiberglass composites.
- Demonstrated thin (2.5mm) panel fabrication and resin transfer molding capability.
- Demonstrated panel molding with varying cross-sections from 2.5 mm to 7 mm in a single component.
- Performed panel molding with various filler types and loading, and selected optimum fillers for achieving Class A surface.
- Performed mechanical and impact tests on a range of panels.
- Developed and performed process trials with a new tooling system that allowed system to work together, and improved thermodynamic control for achieving mechanical and impact properties.

- Completed optimization of the resin system using different fillers.
- Tested and validated thickness constraints on panels for achieving structural performance on surface coated thin hybrid panels.
- Tested and validated barrier coat and optimized for surface profile.
- Completed modeling of tooling flows.

Future Direction

- Scale up to test production component as selected by CRADA partner.
- Fabricate test tooling for production level component.
- Verify tooling performance and long-term viability.

Introduction

Current interest in the attractive properties arising from the combination of polyester and urethane resin chemistries has prompted investigation into efficient manufacturing methods using a blended polyester/urethane system. By mating this material to a glass/carbon hybrid fiber preform an optimization of properties from all of the constituents can be achieved at a relatively low cost, especially if the laminate production can occur within a short cycle time. Using combinations of these materials, test panels were manufactured at different lengths to provide specimens and validate the feasibility of molding large (>5ft) and thin (<3mm) components. Close monitoring of developing manufacturing procedures provided valuable data concerning the behavior of both the resin and fiber hybrids in VARTM and closed molding operations.

Two types of flat laminate panels were produced from two different moldsets. Initially, a 12" x 24" glass-top mold (Figure 1) was loaded with the preform and infused with both neat and filled blended resin systems using VARTM. The transparent mold allowed for visual confirmation of the location and flow path of the hybrid resin at any point during the infusion process. In addition, the mold was fitted with inlet and outlet pressure transducers to record pressure gradients during mold filling. The second mold (Figure 2) was constructed of plywood, MDF, and Melamine facing fitted to a hydraulic press operating at 2500 psi. Visual

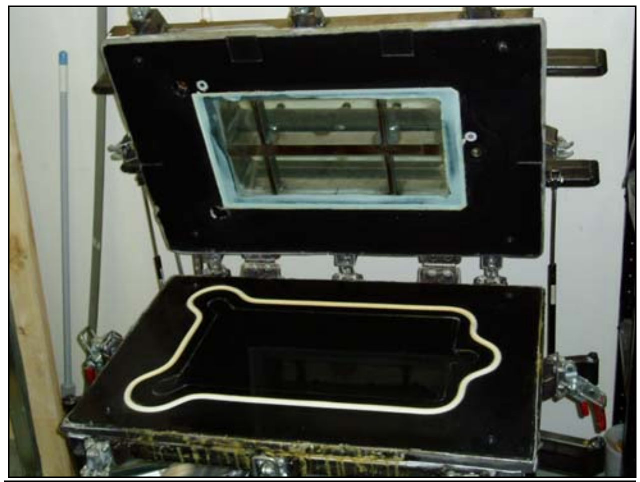

Figure 1. Glass top mold for test trials

confirmation of resin flow was confirmed via short tube ports protruding from the upper mold half. The panel preforms were one of two types of cores, with and without chopped carbon fiber. In all cases, temperature was kept between 100-120ºF and the mold cavity was evacuated to 85 kPa prior to injection of the resin with an 11:1 custom piston pump which kept the unmixed resin components at 104ºF also.

Four cores of different thickness and architecture were examined as possible core materials for use with the highly viscous blended resin. CR-1, FM-1, S&F and "M-03" core materials were compared during initial testing. Only the S&F products were capable of providing fully wet out panels less than

Figure 2. Top of long flow path mold

Fiber Preform Development and Evaluation

The purpose of this investigation was to evaluate the processability of the blended resin and hybrid fiber/mat raw materials and characterize the required production cycle. During the early stages of testing, the S&F mats performed exceptionally allowing the matrix to fill and fully wet the glass and hybrid preforms in less than half the time of competitor's core materials (Table 1). Figures 3 and 4 show the difference between inlet and outlet pressures recorded during the RTM process. Both the S&F and M-03 had equal gate and vent pressures in less than 100 seconds, with the thinner 5mm. S&F and "M-03" are 4mm and 3mm thick fabrics respectively, consisting of glass strand mat stitched to a 'knitted' polypropylene core, which provides loft to create a flow path for the resin and reduce back pressure within the mold. S&F designed these mats specifically for the purpose of injection molding with high viscosity, highly filled resin systems and the fabric has never been tested previously, with the exception of product development at S&F. Discontinuous carbon fibers were chopped from Toray 12k tows directly onto the cores and held in place with polyester binder. In some cases, final placement and consolidation by hand was required to achieve full panel coverage and even fiber distribution. When filler was introduced to the matrix, calcium carbonate, in powder form, was added to the polyester side of the blended resin. The resin itself was supplied as a proprietary chemistry consisting of a polyester component, compatible urethane component, and catalyst.

Table 1. Recorded fill times for core materials.

Material	Time to fill 24" x 12" x 0.12" cavity
CR-1	4:38
FM-1	5:20
S&F	1:43
M-03	0:34

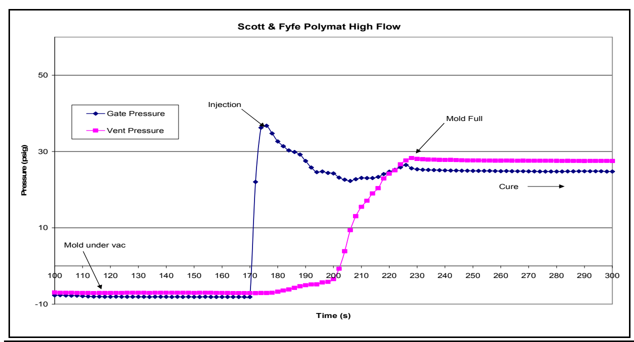

Figure 3. Pressure difference between gate and vent during injection cycle for S&F core material.

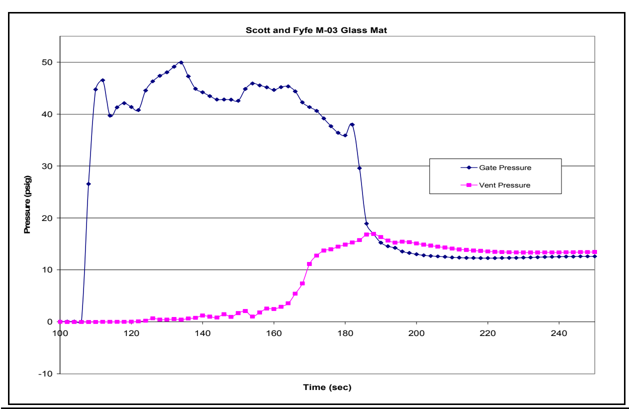

Figure 4. Pressure difference between gate and vent during injection cycle for M-03 core material.

M-03 requiring slightly more time. It is important to note the design of the mold cavity itself is critical to both the fill time and level of filler filtering. Resin must be injected directly into the polypropylene core of the mat, along the material plane. Otherwise the flowrate within the S&F is hindered by a layer of glass strand and it behaves similar to any other core material.

The success of the 6ft panel validates the use of the filled, blended resin system and S&F and M-03 for the production of large components. The injection took less than 4 minutes to complete and the panel was demolded in less than 25 minutes from first injection. Resin ports along the length of the mold indicated an even flow rate along the full length of the panel. When demolded, the preform had been stretched slightly along the inlet width, a problem that was corrected for by pinching the fiber along its edge and cutting a small section away directly in front of the resin gate.

The quality of the final panels was excellent in both the 2ft and 6ft panels. Panel surfaces showed no shrinkage or print through and thickness was as consistent as the molds would allow. Final panel thicknesses were between 2.5 and 3.25 mm when using M-03 and between 3.5 and 4.5 mm when using S&F. The nature of the S&F mat filling from 'behind' the glass mat virtually eliminated washout of carbon fiber during RTM. However, polyester powder was still applied to ease preform handling. Filler improved the shrinkage characteristics slightly, although it would slow the rate of cure, possibly due to absorption of promoter over time. The resin system also performed admirably, wetting and bonding intimately to both types of fibers as well as the polypropylene core. The fast fill rates and high level of promoter reduced cycle times to less than 16 min for the short panels and 25 min for the longer pieces, although the larger mold was frequently at a lower temperature than the glass-top.

Panels produced from the S&F mat and carbon chop were sectioned and subjected to flexural and tensile testing. The results agree quite well with the predicted material properties for hybrid fibers and blended resins. In addition, optical analysis of panel cross sections showed no signs of resin filtering along the length of the panels.

Filler Optimization

Filler optimization is an important part of viscosity minimization for the benefit of lowest achievable fill pressures on large structures. Likewise, maximum filler loading is an important aspect of reducing resin shrinkage for achieving the best possible surface finish (class A).

The results of the design of experiments (DoE) to optimize filler loading with viscosity included four factors of Resin Blend (20/80 to 30/70), Filler Load (25 pphr to 45 pphr). The Filler Ratio (15% to 35% filler A to filler B) measured at 2 and 12 minutes after mixing as a function of viscosity, showed that there is an optimal region of Filler Ratio and Filler Loading within the tested ranges. In Figure 5, the Pareto Chart of the Effects, not including mixing time, shows that the factor of Resin Blend is the largest determinant of viscosity at a given mix time.

Therefore, the most sensitive component of final mix viscosity is the isocyanate to polyester ratios, with some dependence on Filler Load.

The other non-setting factors show fairly narrow ranges of minimum viscosity. The Filler Load seems to have the second largest effect on mix viscosity and, in general, viscosity increases with increasing Filler Load. Filler Load shows a decreased viscosity response between 30 pphr and 40 pphr and a Resin Blend ratio below where an interaction may be occurring with the Filler Ratio.

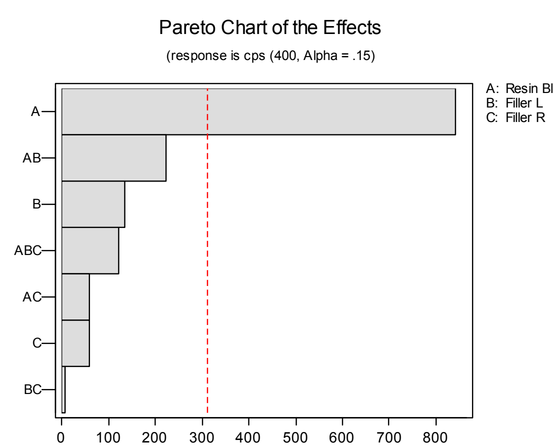

Figure 5. A Pareto chart illustrating the combined and individual effects of the different constituents of the mixes.

Filler Ratio, the percentage of Optifil JS within the blend of Optifil JS and Optifil T, gives a minimum viscosity within the range of 20% to 25% depending on the total Filler Load in the mix and set-time. This interaction results in the viscosity's minimum shifting from 25% to 20% in Filler Ratio as the Filler Load shifts from 30 pphr to 40 pphr. It is also affected by the setting of the resin over time by shifting the optimum Filler Ratio back from 20% to 25%. This same shift with set-time can be seen in the Resin Blend vs. Filler Ratio above. Is this shift an interaction between the surface of one of the fillers and a resin component?

The approach to this screening study was intentionally broad within the area; we now know a more optimal range for the factors tested. The next step needed to verify and improve the data's resolution is a full factorial concentrated around a focal point of: Filler Ratio of 23% JS, Filler Load of 35%, a Resin Blend minimizing isocyanate but controlled for its effects on the final composite properties and mixing times of 2, 7, and 12 minutes.

Flow Modeling

Flow modeling utilized Polyworx software for simulations in the flat plate tools for determining preform permeability based on temperature, pressure and viscosity. Figure 6a and b illustrates the pressure and flow patterns in the long flat plate tool. The flow and pressure patterns were even. The information determined from the flat panels was correlated to experimental data which gave us the information needed for inputting into the more complicated test as well.

The Freightliner test tool was then modeled using the permeability numbers determined from the flat panels and the other resin input variables.

Modeling of the test tool was then used to see the correlation between model and experiment for scaling up complexity in the part. Figure 7, illustrates multiple time snapshots of fill percentages and how that correlates to the actual fill time and flow behavior with partial shots. The correlation of three minute fill times from model to experiment is inline with each other.

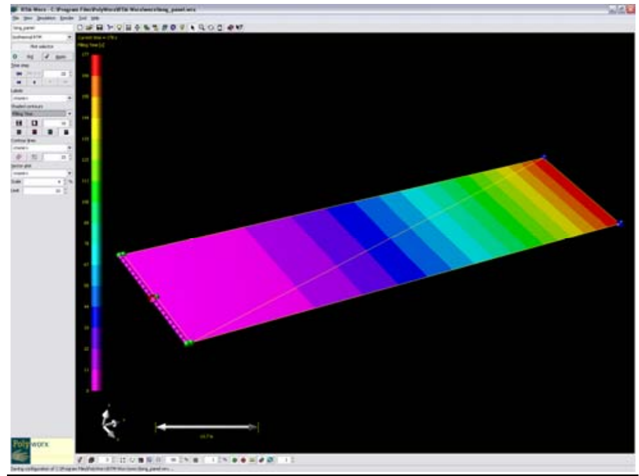

Figure 6a. Modeled flow pattern in 18” x 72” panel mold

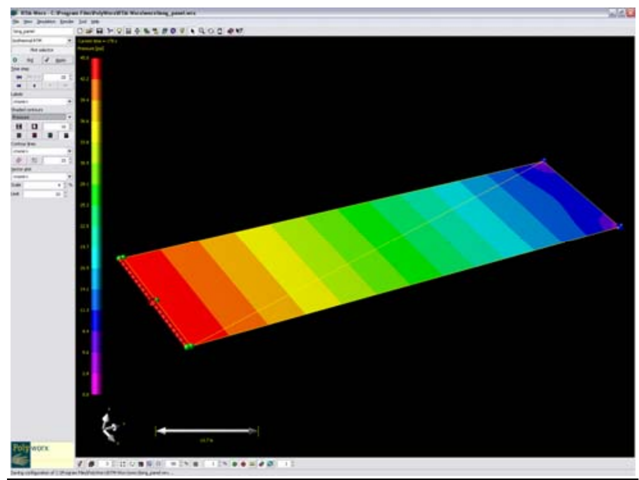

Figure 6b. Modeled pressure pattern in 18” x 72” panel mold

The next task will be to model a large structure that will be fabricated in FY06. These simulations will help us in determining flow patterns and fill times with the current material configuration. This will give confidence that the design will work prior to tool build.

Conclusions

The flow trials gave us valuable insight as to how fast large panels will fill. The rheology studies indicate time sensitivity when the two resin components are mixed and have the largest influence on the viscosity. There is an optimum ratio of the two fillers at 25 pphr that will help in reducing filler cost and viscosity. The viscosity data

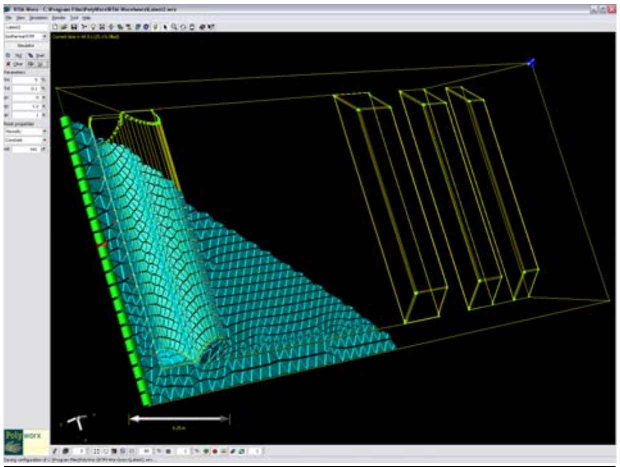

Permeability = 0.008 sq-cm, ~25% Fill, t = 48.5sec.

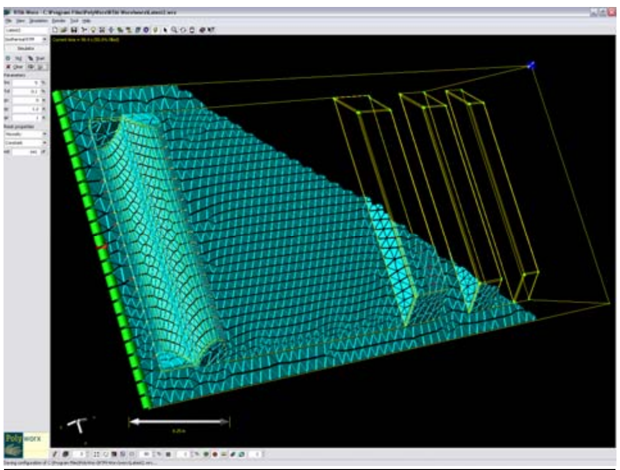

Permeability = 0.008 sq-cm, ~50% Fill, t = 98.4sec.

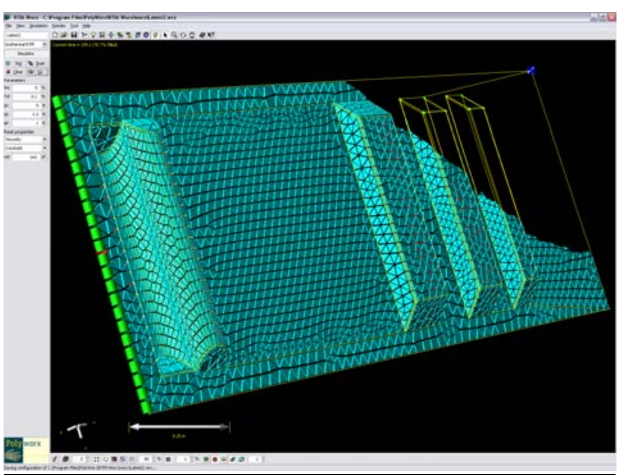

Permeability = 0.008 sq-cm, ~79% Fill, t = 155sec.

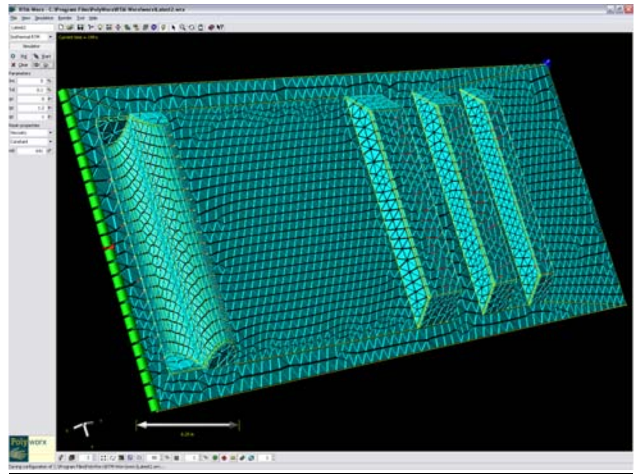

Permeability = 0.008 sq-cm, ~100% Fill, t = 199sec.

Figures 7 a,b,c,d. Illustration of the flow pattern at different fill percentages.

became very useful with the modeling which illustrated the fill time and pressure gradients within the part. These models and the correlation data gave us the information needed to be able to model large structures prior to building the tool. This will help reduce the risk of the unknown with any large, complicated and expensive tool.

Future work will model a large composite structure and build the tooling. Experimental correlation will be evaluated on the large molded parts. A large tool will be fabricated for testing the moldability and mechanical testing of large parts. A series of factors associated with optimizing details of the process technology are being worked, and the CRADA partner is developing an approach to mold full-scale parts that will ultimately go on over-the-road trials. These parts have been chosen to demonstrate the most challenging aspects of the process capability, namely highly structural, Class A surfaces in direct line-of-sight, with some complex process details required for success. Tooling quotes and negotiations are ongoing, and several aspects of the process are anticipated to go forward for patent protection.

C. Hybrid Composite Materials for Weight-Critical Structures

Principal Investigator: Curt A. Lavender
Pacific Northwest National Laboratory
P.O. Box 999, Richland, Washington 99352
(509) 372-6770; fax: (509) 375-4448; e-mail: curt.lavender@pnl.gov

Principal Investigators: Donald Trettin
PACCAR Technical Center
12479 Farm to Market Road, Mount Vernon, Washington 98273
(360) 757-5241; fax: (360) 757-5370; e-mail: don.trettin@paccar.com

Chief Scientist: James J. Eberhardt
(202) 586-9837; fax: (202) 587-2476; e-mail: James.Eberhardt@ee.doe.gov
Field Technical Manager: Philip S. Sklad
(865) 574-5069; fax:(865) 576-4963; e-mail:skladps@ornl.gov

Contractor: Pacific Northwest National Laboratory
Contract No.: DE-AC06-76RLO1830

Objective

- Develop and demonstrate (1) the application of hybrid composites and composite/metal hybrids to heavy-duty vehicles and (2) the capability to integrate these materials choices into moderate-volume production.
- Develop and demonstrate the potential for major weight savings (>50% on a component basis) in critical structures applicable to truck cabs and support components.
- Demonstrate the basis for use of hybrid metal-composite systems to reduce weight via proof-of-principle experimentation.
- Develop full-scale prototype components for vehicle testing and validation.

Approach

- Investigate the potential of new materials and manufacturing technologies to effect major weight reductions for heavy-duty vehicles.
- Assist in demonstrating the applicability of composites and composite/metal hybrids to operational vehicles with little or no cost impact.
- Provide the experience base to develop the design and analysis tools, as well as the scientific understanding of the factors affecting molding and materials performance.
- Provide the materials suppliers with a market that can stimulate demand, leading to an increase in their production capacity. This will help reduce materials costs by creating higher volumes. Develop and assemble full-scale hybrid material prototype door system for heavy vehicle test and evaluation.

Accomplishments

- Completed three sets of prototype hybrid door components, which were delivered to Pacific Northwest National Laboratory (PNNL) by the subcontractors. The key components include sand cast magnesium door inners (Style and Tech) and molded hybrid glass/carbon fiber upper door frames (Profile Composites).
- Developed bonding fixture, bonded the initial hybrid door components, and verified dimensional conformance.

- Assembled the first door and performed static load analysis. Initial results indicate that the hybrid door assembly exceeded the targeted 50% improvement and exhibited a 64% improvement.
- Assembled additional door for cab fit and function, and full-length cab door durability testing.

Future Direction

- Assemble three prototype hybrid material doors for testing by PACCAR. Plans call for cab door durability tests to be conducted in 2005, these tests are currently underway.
- Based on component design and assembly tasks, update door manufacturing cost models for PACCAR (PNNL and Mercia).
- Compile a final report at the conclusion of the prototype demonstration phase.

Introduction

Current materials and manufacturing technologies used for heavy vehicle door systems are often dictated by the high cost of tooling and the relatively low production volumes for Class 8 trucks. Automotive-style stamped door designs, whether of steel or aluminum, require multistage stamping dies that are generally cost-prohibitive at lower production volumes (<50,000 units per year). Alternate materials, such as glass-reinforced sheet molding compound (SMC), require less expensive tooling and can provide a Class A finish; but the relatively poor specific properties of SMC tend to compromise design and result in a heavier door system. For many production truck cabs, a simple aluminum extrusion frame is used with a flat aluminum sheet riveted to the frame. Although this approach does not require expensive tooling, the use of constant cross-section extrusions in the frame is less than optimum, and it requires more assembly labor than other approaches. PACCAR, a world leader in Class 8 truck design and manufacturing, teamed with PNNL to explore alternate “hybrid” door system designs that minimize tooling cost and per/part door cost, while providing a lightweight, structurally stiff, automotive-style door.

Project Approach

The initial approach to development of the hybrid door system was to perform a structural analysis of an existing PACCAR door design and to determine what the design and performance goals should be for new-generation door systems. PACCAR provided a number of weight, cost, and performance parameters that it considered important for future door designs. PNNL was tasked to survey existing and emerging materials and manufacturing approaches that could be applied to a new door design. Following completion of this survey and analysis of existing door designs, PNNL, with design assistance from Mercia, Ltd., developed a series of five door design concepts that included combinations of large die castings, extrusions, carbon- and glass-reinforced composites, and conventional SMC and stamped aluminum exterior panels.

Following a concept review meeting with PACCAR, an optimized hybrid door design concept was selected. The door concept was then defined using computer-aided-design tools and analyzed with finite element models to validate performance, weight, and cost. After determining that the prototype design met or exceeded all performance and projected cost targets, PNNL and PACCAR selected methods to produce prototype components for the full-scale assembly and testing phase of the project. The finite element model of the prototype door system is shown in Figure 1.

Following completion of the design selection phase of the project, full-scale hardware components were developed and shipped to PACCAR Technical Center for assembly and testing. In addition, to the static deflection tests, a complete door was assembled and mounted in a Class 8 truck cab for fit and functional tests (Figure 2). Subsequently, the door was placed into a door durability cab test which is currently being run to completion.

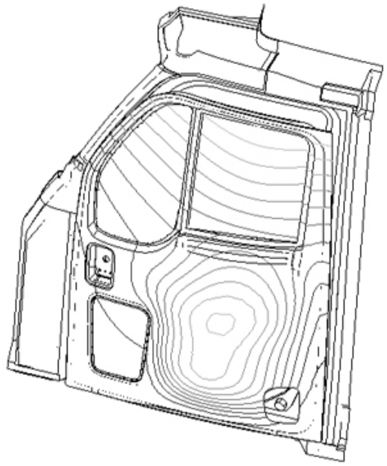

Figure 1. Finite element model of prototype door system under simulated loading conditions.

Figure 2. Prototype door assembled in Class 8 cab for functional testing.

Conclusion

The prototype development of hybrid door components for an advanced heavy truck door was completed by the team and its selected subcontractors. Prototype assembly has been completed by the team, including inspection and assembly fitting, as well as adhesive bonding development. Three prototype doors have been assembled by the team for cab testing and evaluation during calendar year 2005. Static testing and cab functional test and evaluation have been completed. A prototype door is now undergoing cab durability testing. The hybrid door design that will be prototype-tested reduces door weight by 37%. If the hybrid design were to move into production, the use of a stamped aluminum outer panel (cost-prohibitive during the prototype stage) would improve structural performance, reduce cost to project goals, and increase weight savings to 55%.

D. Advanced Composite Structural Cab Components

Principal Investigator: Jay Batten
National Composite Center
2000 Composite Drive
Kettering, OH 45420
(937 -296-5012; fax (937) 297-9440; e-mail: jbatten@compositecenter.org

Chief Scientist: James J. Eberhardt
(202) 586-9837; fax: (202) 587-2476; e-mail: James.Eberhardt@ee.doe.gov
Field Technical Manager: Philip S. Sklad
(865) 574-5069; fax:(865) 576-4963; e-mail:skladps@ornl.gov

Contractor: Oak Ridge National Laboratory
Delphi/ORNL Contract No.: 4000009401

Objective

- Develop an advanced composite cab structural component for a Class 8 tractor:
- Develop the design and the manufacturing process for utilizing continuous-oriented, fiber-reinforced composites for affordable commercialization within 5 years of beginning the project.
- Reduce the existing mass by at least 30% from 22.8 kg to 15.96 kg.
- Meet or exceed the performance of the existing cab structural component.
- Meet customer target cost.

Approach

- Perform a Value Analysis/Value Engineering (VAVE) workshop to generate options for design and manufacturing.
- Perform finite element analysis (FEA) to develop and optimize design options.
- Perform a process cycle study and make prototype panels to develop Class B surface requirements.
- Conduct Design Failure Modes Effects and Analysis (DFMEA).
- Construct prototype parts and verify proposed design using a design validation (DV) test.
- Release final designs, construct production tools, perform Process Failure Mode and Effects Analysis (PFMEA), and undergo Process Validation (PV) of the production phase.
- Commercialize and start of production.

Accomplishments

- Completed "Proof-of-process" study with generic "block" mold, which demonstrates feasibility of infusing thin-walled laminates; then completed " Pre-PV" study with production foam core and prototype composite mold for areas 3&4 of lower B-Pillar.
- Completed DV testing of prototype components in full cab build. (Door slam test had gone through 3 life cycles and sustained no structural issues) Completed fastener torque studies in molded sample blocks.
- Updated the system DFMEA with suppliers and customer.

- Refined FEA models to include material properties from actual material test data, developed local composite reinforcements to improve stiffness, and studied the effect of processing tolerances for an affordable product.
- Simplified construction in air duct area by making air duct a separate, post mold fastened part.
- Reduced metal usage by eliminating large steel plate and using more localized attachments with composite reinforcements.
- Produced assembly drawings, CAD models, design details, and specifications for quote packages.
- Selected production source for final assembly.
- Reduced flange areas to 3mm thick (current production flange varied from 6 to 12 mm thick).
- Performed cure-cycle study, made composite panels, conducted Class B surface activities.
- Made plaques and part skins using conductive gel coat to demonstrate elimination of post mold spray conductive primer. Validated conductive gel coat to replace post mold, spray primer system (resulted in an overall 10% total mfg cost savings).
- Finalized metal hardware material specifications.
- Determined optimal machining process parameters (tool shapes, feeds, and speeds for drill/tap of composite laminate over metal hardware) without any delamination or degradation to the laminate.
- Created 2D lay-flat fabric patterns from 3D part geometry with slits and darts to minimize fabric shear and to optimize the overall fabric blank size.
- Completed environmental testing.
- Finished final design math model and process.

Future Direction: Applicable only after receiving Purchase Order

- Conduct PFMEA with sourced supplier and customer.
- Finalize specifications, assembly and detail drawings.
- Release final design, release remaining production tools, and PPAP validate the production phase.
- Begin production.

Introduction

Significant strides forward were made on the Advanced Composite Structural Cab project. Within Delphi, the project had moved from a development activity to an implementation team and with the progress outlined in this report below, both cost and mass targets were achieved.

To accomplish the project objectives the Delphi-led team had to replace the present production liquid compression molded two component post-bonded assembly made of non-oriented chopped fiberglass with a single RTM processed foam core structure enclosed with a thin-laminate of oriented and continuous length fiberglass.

Design and Process Failure Modes and Effects Analysis

A system-based design failure modes and effects analysis (DFMEA) was initiated in early 2003 and had periodically been updated as the production intent design had been refined. This included a review at Delphi's OEM partner's assembly plant with representation from Engineering, Quality, and Purchasing. Another DFMEA was reviewed in June 2004 with the OEM engineers after the DV tests were completed. The suppliers of individual components and final molder have responsibility for performing the PFMEA and creating process control plans after final sourcing. Delphi participates in each FMEA.

Pre-Production Validation Development: Resin Cure Times and Thin-Walled Infused Laminates

In order to determine the proper tooling and cure cycle, Delphi and Reichhold, a leading resin supplier, conducted multiple cure-cycle studies. The goal was to make a resin recipe that would meet a 22-min full-cure cycle at 120ºF. Initial studies completed in February 2004 indicated that a processing temperature of 120ºF cure cycle was possible.

One of the major design obstacles of this project was the processing of thin (1.0-1.5 mm) laminates with resin transfer molding (RTM) to produce high quality parts. Some of the concerns originated around tolerances and geometric stack-ups of all the components within the molded assembly. Secondary concerns included the response of the foam core, tooling, and hardware during infusion, multiple layers of fabric and the reinforcements that were located between various foam cores.

In order to expedite the "Pre-Production Validation" (production validation = PV hereinafter) development, a small section of the molded assembly was selected rather than working with the complete assembly. The "Pre-PV" development used results from early "Proof-of-Concept" development.

"Proof-of-Concept" development utilized a rectangular box (4"x6"x16"), a cross section of which is shown in Figure 1. This shape closely represents one of the longest infusion sections of the actual component. The tool was designed to infuse the 16" length with an injection and a vacuum port on opposite ends. The cover of the tool was made of clear glass to allow visual inspection and video taping of the resin flow front.

Almost 50 individual infusion runs were conducted with very positive end results. In the course of the "Proof-of-Concept" study, it was determined that laminate thicknesses of less than the 1.5mm were achievable. The limiting factors in achieving thin laminates were the tolerances of the tooling and the foam cores, but even on areas where the fabric was pinched due to irregularities or multiple plies, it was still possible to infuse. In order to maintain regular laminate thicknesses between the top and bottom surfaces due to pressure gradients, special geometries were added to the foam cores. With respect to internal supports and multiple plies, the development showed a process that was able to fully infuse any of the combinations we were able to create. A close-up view of a "Proof-of-Process" through-part reinforcement is shown in Figure 2.

Other notes from this process development were that pressure/vacuum values as well as the foam density were optimized. With a low-density foam core, vacuum assist and low resin pressure, consistent processing results were obtained with few air voids and an infusion time of 1 minute. High pressure resulted in foam compression allowing more resin into the part and did not shorten the injection time. Finally, a modified resin with less inhibitor was used to allow the cure cycle (from mixing to cured part) to meet an acceptable cycle time (<22 minutes) at a heated tool temperature of <120ºdeg F.

The next step in developing the "Pre-PV" molding process was to build a larger tool with actual part geometry (foam core areas 3 & 4) to ensure "Pre-PV" process capability. Two production level foam core tools were made to allow refinement of the process on actual production geometry tool. Figure 3 shows a view of an open Aluminum based RTM "Pre-PV" tool. Figure 4 shows the first part made out of the Aluminum based "Pre-PV" tool and Figure 5 shows a cutout portion view of a molded part section from the Aluminum "Pre-PV" tool. The part was made using production intent resin with low inhibitor level and production intent foam. The resulting composite part was very close to the targeted weight.

Hardware: Secondary Machining Operations

A key design element to minimize cost was insert molding of the metal fasteners into the foam cores. Another factor for affordability was to ensure that drilling and tapping time were optimized. To ensure optimal drill & tap cycle time after parts were made, a study was conducted. Figure 6 shows a robotic machine cell that was utilized to optimize drilling method. Various drill bits and speeds were determined to help remove chips, and countersink

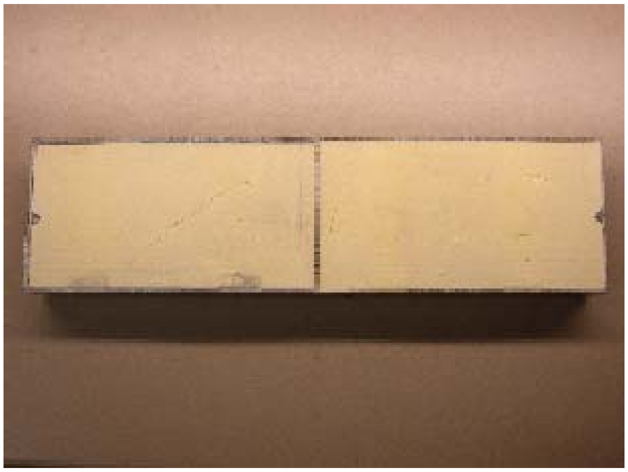

Figure 1. "Proof-of-Process" Mold Block.

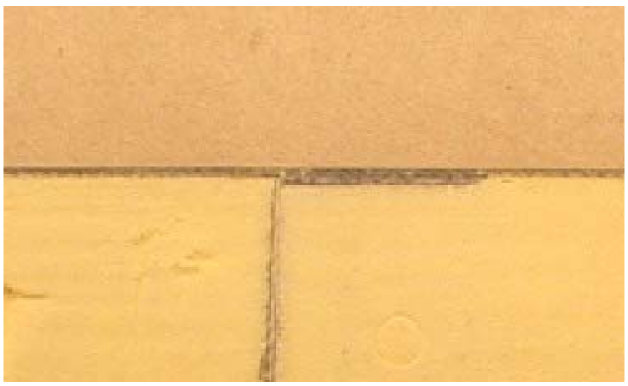

Figure 2. Close-up view of "Proof-of-Process" composite block with reinforcement.

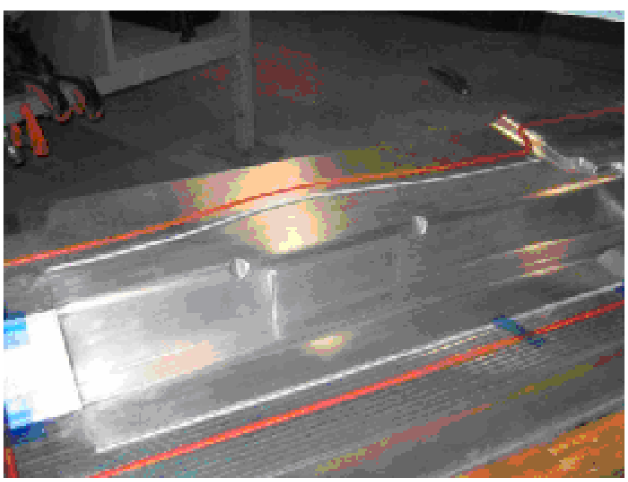

Figure 3. Open view of Aluminum based RTM "Pre-PV" tool for sections 3&4

Figure 4. First "Pre-PV" part made out of Aluminum based RTM tool.

Figure 5. A cutout portion of molded "Pre-PV" part from Aluminum tool.

Figure 6. Drill & tap time study fixture for hardware molded test block.

methods were developed to avoid composite damage during tapping.

Analytical Work - Finite Element Analysis and Fabric Pattern Development

The production design direction has been finalized, and FEA and CAD data files are undergoing final updates before production release. FEA indicates that all performance requirements will meet or exceed requirements.

Fifteen individual fabric pieces are required in the molding operation. The initial lay-flat patterns developed did not drape well over the foam cores or into the molding tool. Alternative lay-flat software is being investigated.

Cost Reduction: Conductive Gel Coat

A systematic review of the final assembly cost indicated that masking; conductive spray primer and finish were areas with great cost reduction potential. By implementing a conductive gel coating in the composite molding, preliminary estimates showed that finished assembly cost could be reduced by up to 10%. Delphi identified a conductive gel coat system that had already been approved by the OEM partner in other applications and fabricated flat panels production representing exterior part surfaces (see Figure 7) with this conductive gel coat. These samples were forwarded to the OEM partner for oven and environmental conditioning. Following this conditioning, surface finish and resistivity will be evaluated.

Testing Activities

Fastener testing - Tests for torque and pullout load had been conducted on several M5 and M6 threaded fastener designs in composite panels with steel plates. Other sizes were also tested per their application category (e.g., FMVSS, heavy load bearing, interior to the door seal, exterior to the door seal).

The foam block with hardware after drilling and tapping can be seen in Figure 8. To ensure that new hardware will work, a hardware bonding study and corrosion resistance were conducted.

Figure 7. Exterior surface showing conductive Gel- coat.

Figure 8. Hardware molded block after drilling & tapping

Torque and pullout load between composite and metal hardware embedded in foam was determined using various surface preparations for metal hardware. The torque fixture used for the study is shown in Figure 9. The purpose was to determine that threaded fasteners meet FMVSS requirements. The results showed that all various surface

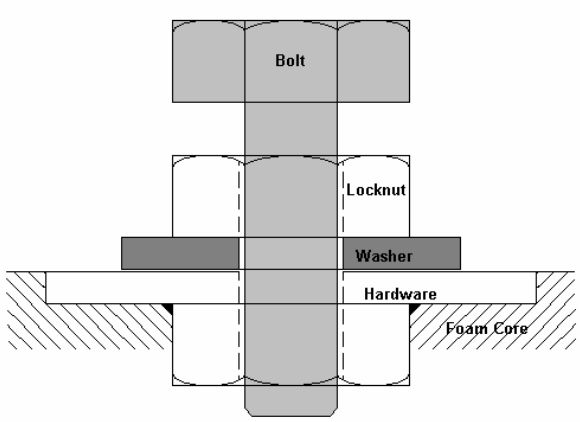

Figure 9. Torque test fixture for hardware molded test block.

preparations were acceptable for bonding with the proposed composite materials.

Expansion testing - Blocks of the same composition of composite and foam design have been heated to process temperatures of 225ºF for one hour with no effects to the part due to differences in expansion rates of the differing materials.

Environmental testing – Environmental testing was conducted on both composite test blocks and cut-away sections of prototype parts. The effect on the foam, the hardware, and the laminate was determined. The results, as expected, verified that the foam and composite laminate construction protect the hardware from the environment and resisted moisture penetration into the structure.

To meet the corrosion requirement it was decided, and approved by the customer, that we use SS material for machined and tapped holes outside the seal and carbon steel material in areas inside the seal. The corrosion resistance test was performed per OEM's standard practice on drilled metal fasteners (Fig. 10). The results showed that Dupont's E-Coated steel exhibited similar results as current production parts. Since the cost difference was minimal, the team decided to use E-coat to keep within the customer specifications.

Figure 10. Hardware molded block after corrosion.

Summary

These are the highlights for the progress during the first three years of this project (FY02-FY04).

1. Reduced laminate thickness from 3.0mm to 1.5mm using 30% fiber volume with production intent resin and process. The visual inspection looked good. Mechanical testing of the panels was performed and the test properties were used to refine the FEA model of the Cab Structure.
2. Reduced component mass by 32% over current composite technology.
3. In-molded hardware met process requirements.
4. Proved 1.5mm thick process capability in a portion of the cab structure by molding just area 3&4 with "Pre-PV" tools, including the use of foam cores from production sections 3&4 foam core tools.
5. Used in-mold conductive gel coating to reduce process steps and material cost of a post-mold conductive spray primer.
6. The cab structure using VARTM thin-walled laminates over foam cores with embedded metal hardware has successfully completed cab shake testing. This same cab structure completed the final stages of Design Validation testing, again with no failures. Also, torsion and pullout testing have met specifications.

7. Met all mass, performance, and cost objectives.

The advanced cab component technology demonstrated a 32% weight savings while maintaining superior structural performance and cost competitiveness. The customer successfully completed all verification testing. However, due to commercial concerns with the Tier 2 supplier, production plans were halted. In FY2005, the project was novated from Delphi to the National Composites Center. During FY2005, the customer also completed laboratory tests simulating a lifetime of opening the cab door against its stops. The test component exceeded requirements. Discussions continue with the customer on potential application of the technology for new products. The customer is also considering bringing the molding of this cab structure in-house, instead of using a Tier 1 or Tier 2 molder. Without renewed DOE funding this project is being closed out. Currently, this customer is unable to resource this development on its own.

E. Advanced Composite Structural Chassis Components

Principal Investigator: Jay Batten
National Composite Center.
2000 Composite Drive
Kettering, OH 45420
(937 -296-5012; fax (937) 297-9440; e-mail: jbatten@compositecenter.org

Chief Scientist: James J. Eberhardt
(202) 586-9837; fax: (202) 587-2476; e-mail: James.Eberhardt@ee.doe.gov
Field Technical Manager: Philip S. Sklad
(865) 574-5069; fax:(865) 576-4963; e-mail:skladps@ornl.gov

Contractor: Oak Ridge National Laboratory
Contract No.: DE-AC05-00OR22725

Objectives

- Develop an economical, long-fiber-reinforced manufacturing procedure utilizing continuous and/or oriented chopped fibers for structural chassis components for Class 7 and 8 trucks.
- Reduce mass of these components by 30% minimum.
- Commercialize and annually produce these components, reducing vehicle mass by about 50 kg/vehicle and significantly increasing North American carbon fiber demand annually, within 5 years of beginning the project.

Approach

- Conduct Value Analysis/Value Engineering workshop(s) to conduct function analysis and brainstorm solutions using composites for each component function.
- Develop Finite Element Analysis (FEA) models at both the component and system level. Conduct structural optimization (topology and shape/sizing) on components for "material efficient" designs.
- Build and test prototypes.
- Develop production viable product along with processes for required cost and volumes.
- Secure production orders for the components developed within the scope of the project.

Accomplishments

- Received customer production part approval of two different models of lateral links. Completed first order of more than 1000 lateral links. Submitted samples and obtained initial order from second commercial vehicle customer. Composite lateral links are 66% lighter than current steel, resulting in almost 5 kg/system mass savings.
- A new lower cost version of lateral link has been designed and performed favorably in initial testing. Additional testing and product validation testing is currently ongoing.
- Proof-of-concept composite-reinforced, thin-wall steel tube main support successfully completed all cycles in the side load testing and brake load testing.
- Tier 1 partner used team's composites research and design concepts to develop and commercialize an aluminum z-beam, which resulted in over 27 kg mass savings per system. Combined with the mass savings of the lateral link, this project has realized 32 kg of the 50 kg target for system mass reduction at the end of FY 2003.

- Completed testing the proof-of-concept reinforced main support. This product has the potential for over 20 kg additional mass savings.

Future Direction

- Complete the cost model for reinforced main supports.
  - Select the appropriate partner for commercialization.
- Investigate and validate lower cost lateral link designs and processes.
  - Select the appropriate partner for commercialization.

Introduction

In response to a request for proposals from Oak Ridge National Laboratory (ORNL) in February 2001, a submission from Delphi Corporation led to the award of a subcontract for the development of advanced composite structural chassis components with the objectives listed above.

Sponsored by the DOE, the subcontract was initially scheduled to run for three years with an estimated cost of $2.5M. This project is a 50/50 cost share between ORNL and industry. In this project, Delphi Corporation, the world's largest automotive Tier 1 supplier, partnered with an industry-leading Tier 1 supplier to the truck and trailer industry and focused on three components in a chassis/suspension system: lateral links, main supports and z-beams.

Lateral Link Status

A key project milestone (limited-volume commercialization) for the lateral link was realized in FY 2003 with the acceptance by Delphi of the first 1000-piece order from its Tier 1 partner. Two different models of the link (different lengths for different applications) were approved through the production part approval process (PPAP), and several hundred are in use in the field.

Glass and standard modulus carbon-fiber-reinforced prepreg are the materials utilized in the manufacture of the links. The bulk of the material is carbon-fiber reinforced to obtain the buckling stiffness required. Tubes are mandrel roll-wrapped, cured, and threaded. Metal inserts are then bonded in each end. The glass prepreg is employed for the threading operation and as protective outer layer.

Current composite links offer a 67% mass reduction and outperform the mainstream steel in buckling load capacity and three-point bending, and they also have a significantly higher natural frequency. Examples of both link assemblies are shown in Figure 1.

Figure 1. Typical steel and composite lateral link assemblies.

Although the lateral link can be deemed a success both technically and commercially, costs are still somewhat prohibitive for applications other than lower-volume niche markets. Beginning in 2003, efforts were made to develop lower-cost designs and processes to broaden the market potential and increase the impact on fleet fuel efficiency. Two options that were built as prototypes were hybrids (thin-walled steel overwrapped with composite) and pultrusion. Cost models for the hybrid design were not favorable, and costs for pultruded designs are still being analyzed. Initial pultruded test samples failed to satisfy the test requirements.

Because many of the properties of the composite tube are significantly superior to those of the steel, a lower-cost roll-wrapped option has been investigated. In this option, the number of carbon fiber unidirectional layers will be reduced as well as strategically placed to be in the most effective location for the required load cases. The glass fabric on the inner diameter will be placed only at the ends instead of along the entire length. It is anticipated that this will yield up to a 20% cost reduction.

Preliminary test results demonstrate favorable results.

The team attempted to validate lower-cost lateral links for a second Tier 1 partner through building and testing the prototypes. This second Tier 1 tested to higher standards than did the first Tier 1. As a result, the design did not pass its DV testing. A redesign would have been required, but a costly and high-risk development program would have been required to achieve the target piece price. Thus, the development was stopped.

Main Support Status

A significant amount of design effort was spent on the main support. The main thrust of this design was toward carbon-fiber reinforcement of a relatively thin-walled steel tube. Although the design of the tube reinforcement remained stable, much difficulty was encountered in obtaining a solution for the interface between the tube and the mounting hardware and brackets.

The initial all-composite interface design was not cost-effective. When all steel hardware was used in the design, mass targets were not met. As a compromise, a hybrid interface was designed in which thin steel brackets were welded to the tube (see Figure 2). These brackets were then reinforced with composites with the rest of the tube.

The current prototype design yields a mass savings of approximately 30% or 23 kg per system.

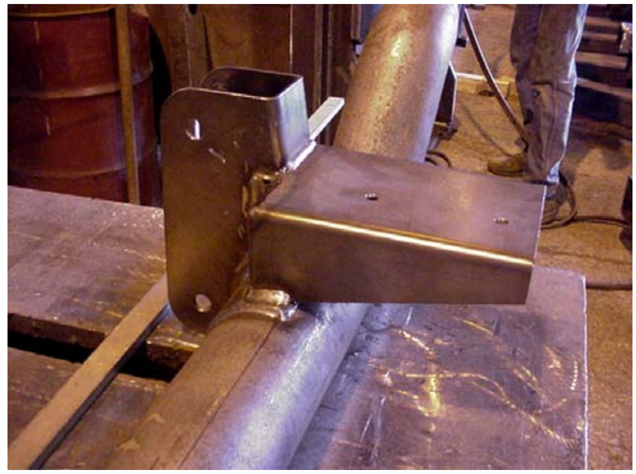

Figure 2. Steel interface-bracket assembly on subplate welded to tube.

Six steel framework subassemblies (Figure 3) were fabricated. The first composite-reinforced assembly is shown in Figure 4 prior to any finishing work.

These prototypes are fabricated by placing dry fabrics with specific fiber orientations around the tube and brackets. The entire support is then enclosed and infused with epoxy resin. For production, mold tooling would be used for application of the reinforcement material.

Figure 3. Prototype steel framework ready for composite fabrication.

Figure 4. First composite-reinforced main support just out of cure oven, prior to any finishing work.

The prototype reinforced main supports satisfied or exceeded all test goals. Commercialization of this component in the chosen application was stopped when Delphi's Tier 1 partner expressed interest in a multi-piece design for its next generation of products. Unfortunately, these designs were not affordable for development with the use of advanced composites. Alternative applications were investigated and pursued by Delphi with other potential Tier 1 partners.

Z-Beam Status

At the beginning of FY 2003, Delphi's Tier 1 partner announced its intention to commercialize an aluminum version of the z-beam based on FEA topology optimization completed for a composite design. The cast aluminum solution reduced the mass by approximately 7 kg and was at cost parity with or below the current cost of welded steel designs. Because four z-beams are used in each system, total system mass was reduced by 28 kg.

Based on the success of the aluminum, work was suspended on composites. Composites were considered again for a heavy-duty application, but cost models were not favorable, and work was suspended.

In FY 2005, this program was novated to the National Composite Center in anticipation of finding new Tier 1 partners for main support commercialization. The National Composite Center has found a couple of other Tier 1 partners ready to carry forward commercialization of a main support. In fact, one came to the National Composite Center on September 15, 2005 for a workshop to narrow down which product to propose. Thus, we had requested to keep this project open for re-initiation of activities to start when a new project could be defined with this new Tier 1. However, the DOE budget could not be realized. As such, this project is being closed out.

Summary

Three polymer composite-intensive components were investigated for a heavy truck auxiliary axle system. Lateral links were developed and commercialized in low volumes, saving approximately 5 kg or 66% of incumbent steel member's mass. High carbon fiber prices have prevented their widespread adoption. The initial composite design for z-beams (trailing arms) morphed into an aluminum member that was commercialized at a cost lower than the incumbent steel member, while reducing mass by approximately 27 kg per vehicle. A proof-of-concept main support was developed, with potential mass savings around 20 kg.

This document highlights work sponsored by agencies of the U.S. Government. Neither the U.S. Government nor any agency thereof, nor any of their employees, makes any warranty, express or implied, or assumes any legal liability or responsibility for the accuracy, completeness, or usefulness of any information, apparatus, product, or process disclosed, or represents that its use would not infringe privately owned rights. Reference herein to any specific commercial product, process, or service by trade name, trademark, manufacturer, or otherwise does not necessarily constitute or imply its endorsement, recommendation, or favoring by the U.S. Government or any agency thereof. The views and opinions of authors expressed herein do not necessarily state or reflect those of the U.S. Government or any agency thereof.

Printed on
recycled
paper

A Strong Energy Portfolio for a Strong America

Energy efficiency and clean, renewable energy will mean a stronger economy, a cleaner environment, and greater energy independence for America. Working with a wide array of state, community, industry, and university partners, the U.S. Department of Energy's Office of Energy Efficiency and Renewable Energy invests in a diverse portfolio of energy technologies.

For more information contact:
EERE Information Center
1-877-EERE-INF (1-877-337-3463)
www.eere.energy.gov